Cosmochimie isotopique du molybdène

Nicolas Dauphas

Institut National
Polytechnique de Lorraine

CRPG

CNRS UPR 2300

Cosmochimie Isotopique du Molybdène

THÈSE

présentée et soutenue publiquement le 24 janvier 2002

pour l'obtention du

Doctorat de l'Institut National Polytechnique de Lorraine
(spécialité géosciences)

par

Nicolas Dauphas

Composition du jury

Rapporteurs :	Jean-Louis Birck	Institut de Physique du Globe de Paris (Paris)
	François Robert	Muséum National d'Histoire Naturelle (Paris)
Examinateurs :	Francis Albarède	École Normale Supérieure de Lyon (Lyon)
	Günter W. Lugmair	Max-Planck-Institut für Chemie (Mainz)
	Thomas Rauscher	Departement für Physik und Astronomie (Basel)
Directeurs :	Bernard Marty	École Nationale Supérieure de Géologie (Nancy)
	Laurie Reisberg	Centre de Recherches Pétrographiques et Géochimiques (Nancy)

Centre de Recherches Pétrographiques et Géochimiques — UPR 2300

CENTRE NATIONAL
DE LA RECHERCHE
SCIENTIFIQUE

Remerciements

Ce travail scientifique représente également une construction sociale riche de la contribution et du soutien de nombreuses personnes. Je tiens à remercier particulièrement,

Bernard Marty pour la richesse des échanges que nous avons eus. Il a su le premier me transmettre son enthousiasme pour le métier de découvreur.

Laurie Reisberg pour son humilité et sa probité scientifique. Les idées que j'ai pu avoir au cours de cette thèse ont toujours bénéficié de son examen critique.

Thomas (Tommy) Rauscher pour m'avoir accueilli à Bâle et avoir fait montre d'une très grande ouverture d'esprit en acceptant de collaborer sur une partie de cette étude. Lors de mon séjour à Bâle, j'ai également bénéficié d'échanges fertiles avec F.-K. Thielemann.

François Robert pour sa grande patience et son enthousiasme. Sa vitalité scientifique se manifeste par le grand nombre d'idées iconoclastes dont il se fait l'ardent avocat.

Michèle Denise pour avoir toujours accueilli avec attention et traité avec diligence les nombreuses demandes d'échantillons que j'ai faites au cours de cette thèse. J'ai également apprécié les discussions informelles que j'ai pu avoir avec Claude Perron.

Gero Kurat pour la confiance qu'il m'a témoigné en me confiant des échantillons précieux.

Laurent et Catherine Zimmermann pour leur expertise technique et leur joie de vivre communicative.

Je remercie Jean-Louis Birck et François Robert d'avoir accepté d'être rapporteurs de ce mémoire et suis reconnaissant à Francis Albarède, Günter Lugmair, et Thomas Rauscher d'avoir bien voulu former le jury de cette thèse.

Je remercie John Ludden pour m'avoir accueilli au centre et s'être efforcé de faire de ce lieu un endroit agréable à vivre. Je suis également reconnaissant envers toutes les personnes avec qui j'ai eu l'occasion d'intéragir et qui ont nourri ma réflexion (Marc Chaussidon, Ko Hashizume, Jean Carignan, Luc Marin, Béatrice Luais, Guy Libourel, Jean-Claude Demange, et Delphine Yeghicheyan). Je remercie tous les étudiants (Jérôme Aléon, Éric Gayer, Gilles Levresse, Anne-Catherine Pierson-Wickmann, Claire Rollion-Bard, Estelle Rose, Mathieu Roskosz, Olivier Rouxel, Mustapha Souhassou, Laurent Tissandier, et Alice Toppani) et acteurs du centre (Jean-Marc Chaffaut, Michel Champenois, Emmanuel Davy, Xavier Framboisier, Isabelle Geoffroy, Pascal Hild, Jacques Morel, Catherine Negre y Rossello, Martine Noel, Christiane Parmentier, Raphael Pik, Bruno Porcu, Pascal Robert, Larry Shengold, Valérie Sourlier, et Caroline Zimmer) avec qui j'ai partagé un peu plus que de l'espace vital. Je suis reconnaissant envers mon frère Éric Dauphas et mes amis Anne-Sophie et Jean-Charles Royant, Antoine Breuil, Yannick Dubouloz, et Olivier Marionneau pour leurs soutiens.

Enfin, j'ai une pensée émue pour Stuart Boyd et ses proches.

Quand tu regarderas le ciel, la nuit, puisque j'habiterai dans l'une d'elles, puisque je rirai dans l'une d'elles, alors ce sera pour toi comme si riaient toutes les étoiles. Tu auras, toi, des étoiles qui savent rire !

Antoine de Saint-Exupéry

Je dédie cette thèse
à mes parents,
François et Marie-Louise Dauphas.

Table des matières

Introduction

L'algèbre s'applique aux nuages ; l'irradiation de l'astre profite à la rose ; aucun penseur n'oserait dire que le parfum de l'aubépine est inutile aux constellations.

Victor Hugo

Les phénomènes qui ont contribué à façonner notre univers ont évolué avec le temps. C'est ce changement qui donne au monde tangible une histoire que les sciences de l'univers tentent d'appréhender. Il est rare de reconnaître dans un phénomène actuel un modèle qui permette de rendre compte d'une observation. Dès lors, les scientifiques qui s'intéressent aux phénomènes qui ne sont pas répétables ou dont l'intervalle de répétabilité est supérieur à l'histoire de l'humanité doivent avoir recours à une lecture indirecte du monde. Cette lecture procède d'une observation attentive de la matière qui porte les stigmates laissés par les phénomènes qui ont contribué à façonner notre environnement. A l'instar des autres disciplines naturalistes, cette démarche n'offre pas une compréhension univoque mais permet de construire un modèle d'évolution cohérent de notre univers en accord avec le monde tel que nous l'observons.

Un des aspects importants de notre compréhension de l'univers se rapporte à la formation des systèmes planétaires. Le soleil est une étoile banale beaucoup mieux caractérisée que les autres astres et dont l'étude permet d'aborder la question plus générale de l'origine des corps stellaires. Cette question n'est pas anecdotique car l'effondrement d'un nuage moléculaire pour former un système planétaire susceptible d'accueillir la vie est une articulation clé dans notre histoire, depuis le Big-Bang jusqu'à l'essor de l'humanité.

Deux approches sont envisageables pour comprendre la formation du système solaire. L'une consiste à étudier des analogues actuels du système solaire dans ses premiers instants. Cette approche se heurte à la distance spatiale mais jouit d'une grande proximité temporelle. L'autre approche consiste à décrypter la matière pour dénouer le fil de nos origines. Cette approche se heurte à la distance temporelle qui nous sépare de la formation du système solaire mais jouit d'une plus grande proximité spatiale. Ces deux approches loin d'être antagonistes sont complémentaires.

Les météorites constituent un échantillonnage précieux pour aborder la question de l'origine du système solaire. En effet, ces objets se sont formés en même temps que le soleil et n'ont pratiquement pas subi d'altération depuis leur formation, il y a 4.566 milliards d'années. Ainsi, les météorites constituent des témoins fidèles des événements qui ont contribué à façonner le système solaire dans ses premiers instants. Les éléments peuvent être étudiés de deux points de vues. Il est possible d'analyser leur environnement moléculaire ainsi que leurs constituants nucléaires. La difficulté de comprendre le message chimique porté par la matière est à la mesure

de la complexité des processus chimiques mis en jeu dans la nébuleuse protosolaire. A l'opposé, l'évolution de la matière nucléaire, et plus spécifiquement de sa composition isotopique, est gouvernée par des processus physiques simples.

Dans le système solaire, la composition isotopique d'un élément peut varier en fonction de plusieurs processus. (*i*) La masse est un paramètre qui contrôle en partie les transferts chimiques et physiques des nucléides. Ainsi, la composition isotopique d'un élément peut varier en fonction de la masse selon un formalisme simple. De telles variations sont regroupées sous le vocable *fractionnement de masse.* (*ii*) Certains transferts isotopiques conduisent à des variations qui ne dépendent pas de la masse selon une loi simple. L'assise théorique de ces phénomènes est très fragile. On désigne ces variations qui sont très rares dans la nature par le terme *nomade* pour non mass-dependent effect. (*iii*) Toutes les *réactions nucléaires* qui mettent en jeu le noyau des atomes sont susceptibles d'induire des variations de composition isotopique. (*iv*) Le système solaire s'est formé à partir d'un assemblage hétéroclite de solides et de gaz hérité du milieu interstellaire. Ces différents composants ne se sont pas complètement homogénéisés dans la nébuleuse protosolaire comme en témoignent les grains présolaires retrouvés intacts dans les météorites primitives. Cette hétérogénéité de la nébuleuse se manifeste isotopiquement sous la forme d'un *héritage présolaire.* Ces quatre phénomènes (fractionnement de masse, nomade, réaction nucléaire, et héritage présolaire) portent des informations importantes sur l'origine et l'évolution du système solaire.

La cosmochimie est une science des origines qui est par nature exploratoire. Les progrès avérés dans notre compréhension du système solaire sont souvent le fait des avancées technologiques qui permettent au scientifique de sonder la matière dans ses plus infimes détails. L'avènement récent de nouveaux instruments de mesure a suscité un regain d'intérêt pour des thématiques anciennes qui sont abordées maintenant sous un jour nouveau [1].

Le molybdène (Z=42) est un élément du groupe VIA de la classification périodique des éléments qui comprend également le chrome et le tungstène. Le molybdène peut prendre les valences +2, +3, +4, +5, ou +6. C'est un élément hautement réfractaire et modérément sidérophile [2]. Cet élément possède six isotopes stables (92, 94, 95, 96, 97, 98) et un isotope très faiblement radioactif (100) produits par les processus *p* (92 et 94), *r* (95, 97, 98, et 100), et *s* (95, 96, 97, et 98) de nucléosynthèse [3]. Les abondances respectives des isotopes 92, 94, 95, 96, 97, 98, et 100 sont 14.84, 9.25, 15.93, 16.68, 9.55, 24.13, et 9.61 %, ce qui correspond à une masse atomique de 95.93 [4].

Les problématiques auxquelles répondent les mesures de composition isotopique dans des objets naturels et spécifiquement dans des météorites sont nombreuses. (*i*) Des grains de graphite et de carbure de silicium ont été isolés dans des météorites primitives [5]. La composition isotopique du molybdène dans ces grains a été héritée de l'environnement stellaire où ces objets se sont formés [6, 7, 8, 9]. Des anomalies isotopiques ont été également observées dans des objets macroscopiques [10]. Ainsi, il est important de documenter la composition isotopique du molybdène pour caractériser l'hétérogénéité isotopique héritée de la nébuleuse protosolaire, ce qui a des implications directes sur les relations génétiques qu'entretiennent les différents corps planétaires du système solaire entre eux. (*ii*) Un certain nombre de radionucléides à courtes demi-vies ont été observés dans le système solaire [11, 12]. Ces radionucléides ont des demi-vies trop courtes pour pouvoir être detectés directement mais leur présence antérieure peut être déduite des variations de compositions isotopiques des isotopes fils. Ainsi, le *p*-nucléide ^{97}Tc décroît par capture électronique en ^{97}Mo avec une vie moyenne de 3.7 millions d'années. A l'instar d'autres radioactivités éteintes, ce radionucléide a pu être présent dans le système solaire au début de son histoire [13]. La mise en évidence du ^{97}Tc, ou à l'inverse son absence, permettrait de discuter la chronologie du système solaire dans ses premiers instants (depuis l'effondrement du noyau pré-

solaire jusqu'à la différentiation des premiers objets dans le système solaire) ainsi que l'origine des radioactiviés éteintes dans le système solaire. (*iii*) Les météorites de fer sont pour la plupart issues d'un magma métallique par cristallisation fractionnée [14]. Cette cristallisation du métal a pu induire un fractionnement du molybdène qui ne se partage pas également entre le métal solide et liquide [15]. Par ailleurs, les inclusions réfractaires qui sont parmi les premiers condensats à s'être formés dans le système solaire, sont très appauvries en molybdène [16]. Cet appauvrissement résulte vraisemblablement d'une condensation partielle sous forte fugacité en oxygène. La déficience observée en molybdène a dû s'accompagner d'un fractionnement de masse des isotopes du molybdène. Couplé à un travail expérimental, l'analyse de fractionnements isotopiques du molybdène dans des inclusions réfractaires permettrait de mieux caractériser l'environnement nébulaire qui a présidé à la formation de ces objets énigmatiques.

Au total, les problématiques cosmochimiques auxquelles répondent les mesures de composition isotopique du molybdène dans des objets extraterrestres sont nombreuses. Ces mesures ont été abordées par les pionniers [17, 18] avec des outils qui n'offraient pas une précision suffisante. L'avènement récent des spectromètres de masse à source plasma et multicollection [1] ouvre ainsi de larges perspectives scientifiques.

Cette thèse s'articule autour de trois parties. La séparation du molybdène et son analyse au spectromètre de masse est un prérequis avant de discuter les variations naturelles de composition isotopique [4]. La présence d'anomalies nucléosynthétiques à grande échelle dans le système solaire est ensuite discutée dans une seconde partie en terme de sources et de relations génétiques [19, 20, 21]. Enfin, la recherche de téchnétium dans le système solaire naissant est détaillée. Ce point est mis en perspective avec ce que l'on sait des autres radioactivités éteintes de type p et de l'évolution chimique de la Galaxie dans le voisinage du système solaire [22].

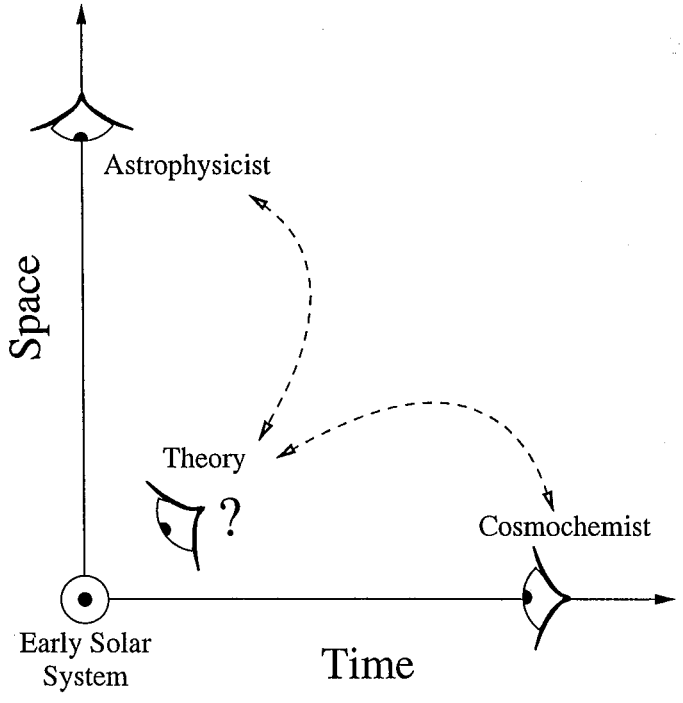

Table des figures

Protocole Analytique

L'éternel mystère du monde est son intelligibilité. (...) Le fait qu'il soit intelligible est un miracle.

Albert Einstein

La composition isotopique du molybdène est mesurée par spectrométrie de masse. Ces instruments permettent une séparation des ions en fonction du rapport masse sur charge. Certains ions peuvent ainsi interférer avec le molybdène. On qualifie de telles interférences d'isobariques. Les isotopes 92, 94, et 96 du zirconium ainsi que les isotopes 96, 98, et 100 du ruthénium sont des interférents isobariques directs du molybdène (figure 1). Ces interférences simples peuvent être corrigées en mesurant des isotopes libres du zirconium (91) et du ruthénium (99) lors de l'analyse. D'autres composés plus complexes peuvent également former des interférences isobariques mais ne peuvent pas être corrigés en cours d'analyse. Il est ainsi nécessaire de séparer le molybdène des nucléides isobares et de la matrice avant de réaliser son analyse isotopique.

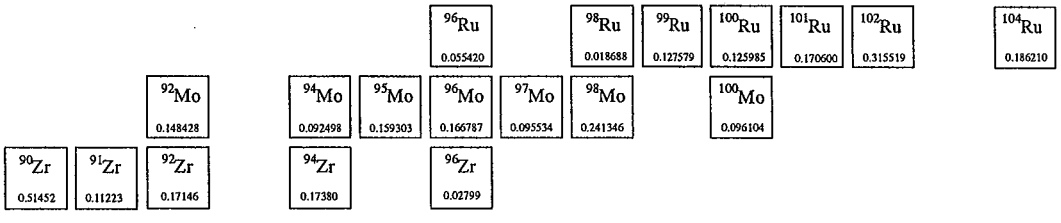

FIG. 1 – Répartition en masse des isotopes du molybdène, du zirconium, et du ruthénium. Les abondances relatives des différents nucléides sont indiquées au-dessous des symboles [4, 23, 24].

La matrice des météorites est très variable et complexe. Rubin [46] rapporte ainsi que 275 espèces minérales ont été reconnues jusqu'à présent dans ces objets. Les phases les plus communes sont l'olivine, le pyroxène, le plagioglace, les alliages Fe-Ni kamacite et taenite, la troilite, la chromite, la silice libre, les nitrures, les siliciures, les phyllosilicates hydratés, les composés organiques complexes, la magnetite, les sulphates, et les carbonates. Les objets différenciés peuvent être constitués uniquement de phases silicatées ou métalliques. Face à une telle diversité de matrice, il est important de développer une chimie de séparation qui soit flexible. La concentration en molybdène dans les météorites est relativement faible, de l'ordre de 1 ppm dans les météorites

indifférenciées [47]. Ainsi, les éléments majeurs qui pourraient former des interférences inattendues doivent être complètement séparés du molybdène. L'analyse du molybdène à l'aide d'un spectromètre de masse à source plasma complique encore la chimie de séparation. Compte-tenu de la température de la torche plasma, la plupart des éléments sont ionisés ce qui impose une séparation complète du molybdène des composés isobares. En thermo-ionisation, les éléments sont émis dans une fenêtre de ionisation ce qui assouplit l'exigence qui porte sur la chimie.

De nombreux schémas ont été envisagés et testés pour séparer le molybdène des interférents isobares et de la matrice (TOPO sur laine de carbone, extraction en ampoule à décanter TBP et TOPO, fixation sur résine AG1-X8 en H_2SO_4, élution du molybdène en HNO_3, *etc.*). La solution retenue est très proche de celle développée par Qi-Lu et Masuda [48, 49, 50] qui consiste à fixer le molybdène sur un extractant organique de type di(2-ethylhexyl) phosphate [25], de le purifier par une série de lavages du solvent organique avec des acides variés, de l'extraire de l'HDEHP par complexation avec du peroxyde, et ensuite de raffiner sa séparation sur résine échangeuse d'ions AG1-X8 [29]. Cette méthode permet une séparation complète du molybdène des espèces isobares avec des rendements de 60-100 % et des blancs de 6 ± 3 ng.

1 Digestion des échantillons

La digestion des échantillons est réalisée suivant deux protocoles standards [51]. Les météorites de fer (0.5-1 g) ont été dissoutes dans des récipients hermétiques en téflon PTFE dans un mélange 15 ml HCl 12 M- 1 ml HF 28 M à 130 °C pendant 2-3 jours. La dissolution suit un mécanisme d'oxydoréduction. Le fer métal est oxydé pour former des chlorures et des fluorures tandis que du dihydrogène est libéré (dégagement gazeux). La présence d'acide fluorhydrique permet d'attaquer les éventuelles inclusions silicatées présentes. La troilite, un monosulfure, est également entièrement dissoute. Les échantillons plus complexes (0.5-1 g) qui peuvent contenir des phases résistantes sont dissous dans des récipients hermétiques en téflon PTFE dans un mélange 10 ml HNO_3 15 M-5 ml HF 28 M-1 ml $HClO_4$ 12 M à 130 °C pendant 3-15 jours. Les phases les plus réfractaires ne sont pas entièrement digérées. La présence de $HClO_4$ prévient la formation d'un gel hydraté de silice et de magnésium lors de l'évaporation et permet une oxydation partielle des composés organiques complexes.

2 Extraction par solvent di(2-ethylhexyl) phosphate

Des essais préliminaires ont été effectués sur ICP-MS (inductively coupled plasma mass spectrometer) et TIMS (thermal ionization mass spectrometer) qui ont indiqué que, au minimum, 1 μg de molybdène était nécessaire pour réaliser une mesure au niveau de précision nécessaire pour observer d'éventuelles variations. La concentration du molybdène dans les météorites indifférenciées est de l'ordre de 1 ppm [47], de sorte qu'il s'est avéré nécessaire de développer un protocole capable de traiter environ 1 g d'échantillon. La fixation sur extractant organique (figure 2) est apparue comme étant la méthode la plus adaptée pour traiter une masse aussi importante de matrice.

2.1 Principe

L'utilisation de l'HDEHP repose sur le principe des extractions par solvants où deux phases immiscibles sont mises en contact. Ce composé est intensivement utilisé dans l'industrie nucléaire, ce qui explique que les coefficients de partage de nombreux métaux aient été documentés

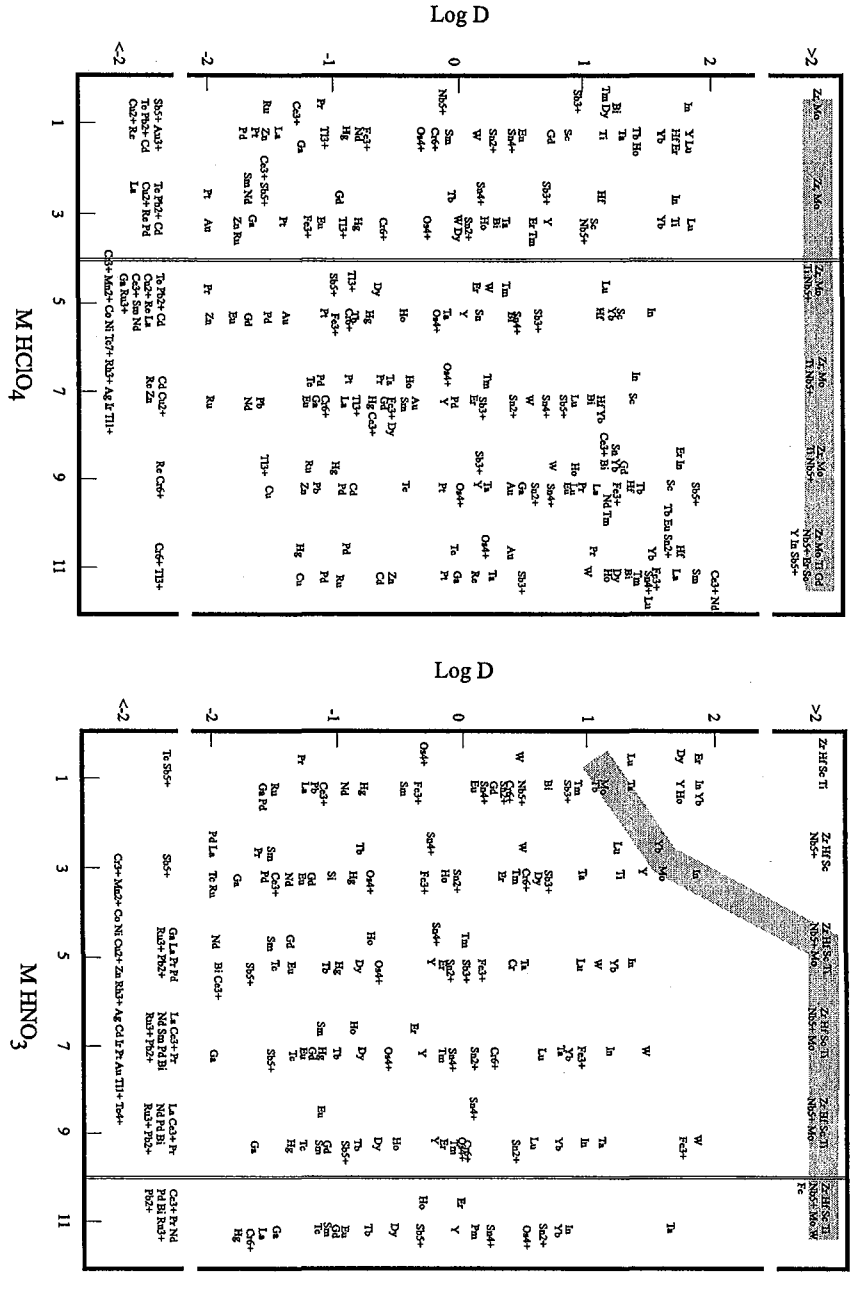

FIG. 2 – Coefficients de partage entre du di(2-ethylhexyl) phosphate dissous à 0.75 M dans du cyclohexane et une solution aqueuse d'acide perchlorique ou d'acide nitrique [25].

[25]. L'extraction du molybdène dans le di(2-ethylhexyl) phosphate procède selon un mécanisme d'échange cationique [52],

$$MoX^{2+} + 2HDEHP \rightleftharpoons MoX(DEHP)_2 + 2H^+. \quad (1)$$

Le principe général de fonctionnement du HDEHP repose sur la formation de dimères. Chaque dimère s'attache au métal extrait en libérant un ou deux protons. D'après cette réaction, l'extraction du molybdène est favorisée par un pH élevé. Cependant, seule la forme cationique du molybdène est susceptible d'être extraite. Cette forme est uniquement présente à pH bas. Il se produit ainsi une compétition entre la spéciation du molybdène et la disponibilité en protons qui complique l'interpétation des courbes de partage pour le molybdène. Dans le cas où le solvent organique n'est pas saturé et où le comportement est idéal, le rapport entre la concentration dans la phase organique et la concentration dans la phase aqueuse est constant. On définit ainsi le coefficient de partage, $D = [X]_o/[X]_a$. Soit R le rapport de volume entre la phase organique et la phase aqueuse. On montre simplement qu'après équilibration, la fraction de X présente dans la phase organique et la phase aqueuse sont respectivement, $x_o = RD/(1 + RD)$ et $x_a = 1/(1 + RD)$. Connaissant les coefficients de partage [25], il est aisé de déterminer le rendement théorique pour une série d'extractions.

2.2 Application

Les matrices des objets extraterrestres sont souvent très riches en fer. Le molybdène présente une très forte affinité pour le HDEHP pour toutes les molarités d'acide perchlorique (figure 2). En $HClO_4$ 4 M, le fer présente à l'opposé une préférence pour la phase aqueuse. Le ruthénium n'est pas du tout extrait non plus dans un tel milieu. Après digestion des échantillons, ceux-ci ont d'abord été évaporés puis repris en $HClO_4$ 4 M afin de permettre la fixation du molybdène sur le HDEHP et l'élimination d'une part importante de la matrice et du ruthénium. Afin de renforcer le bénéfice des coefficients de partage du HDEHP pour le molybdène, la fraction organique a été lavée trois fois par équilibration avec du $HClO_4$ 4 M. De nombreux éléments ont une affinité modérée pour le HDEHP en acide nitrique. Il a donc été décidé de laver deux fois la phase organique avec du HNO_3 10 M dans l'intention de croiser les sélectivités et de préparer la récupération du molybdène. Enfin, les propriétés complexantes du peroxyde d'hydrogène ont été mises à profit pour cacher le molybdène des dimères de HDEHP et permettre ainsi de le récupérer dans une phase aqueuse susceptible d'être évaporée. Deux étapes sont nécessaire pour récupérer entièrement le molybdène précedemment fixé. En utilisant les équations de partage, il est possible de calculer le rendement théorique d'une telle procèdure. Pour des raisons pratiques, il est difficile de procéder à une extraction liquide liquide avec un volume organique très différent du volume aqueux (R$\sim$ 1). Il est impossible de déterminer avec certitude le rendement du molybdène lors d'un tel traitement car l'effet complexant du peroxyde d'hydrogène sur les coefficients de partage n'est pas connu. Un petit calcul simple permet néanmoins de s'assurer que dans le cas le plus favorable, le rendement du molybène devrait être supérieur à ~ 0.93. L'utilisation d'ampoules à décanter est longue et fastidieuse. Il a été décidé d'effectuer les différentes étapes de l'extraction dans des tubes à centrifugation afin de permettre un traitement plus rapide des échantillons, ce qui autorise un plus grand nombre de mesures. A chaque étape, la phase aqueuse (5 cc) est ajoutée à la phase organique (5 cc), le tube est agité pendant 1-4 minutes selon l'étape considérée, et est ensuite centifugé. Il suffit ensuite de pipetter le surnageant (HDEHP) pour le transférer dans un autre tube à centrifugation et de poursuivre ainsi le traitement (figure 3).

Le rendement de cette étape a été étudié. Dans le cas d'une solution monoélémentaire de molybdène, le rendement total est très proche de 1. Dans le cas d'un échantillon naturel, le

rendement de la séquence est largement contrôlé par le rendement à la fixation qui est moins bon que dans le cas d'une solution mono-élémentaire (0.4-0.8). Ces rendements sont explicables par le rapport échantillon/extractant élevé lors de la fixation ($\sim$ 1/5). En dépit de ce défaut, l'extraction par solvent a été retenue car elle permet de traiter une masse importante d'échantillon et assure une bonne séparation du molybdène par rapport aux éléments de la matrice et aux interférents isobariques (figure 4). En outre, l'usage de tubes à centrifugation jetables allège considérablement le protocole (par rapport à l'utilisation d'ampoules à décanter), ce qui permet de traiter rapidement un grand nombre d'échantillons.

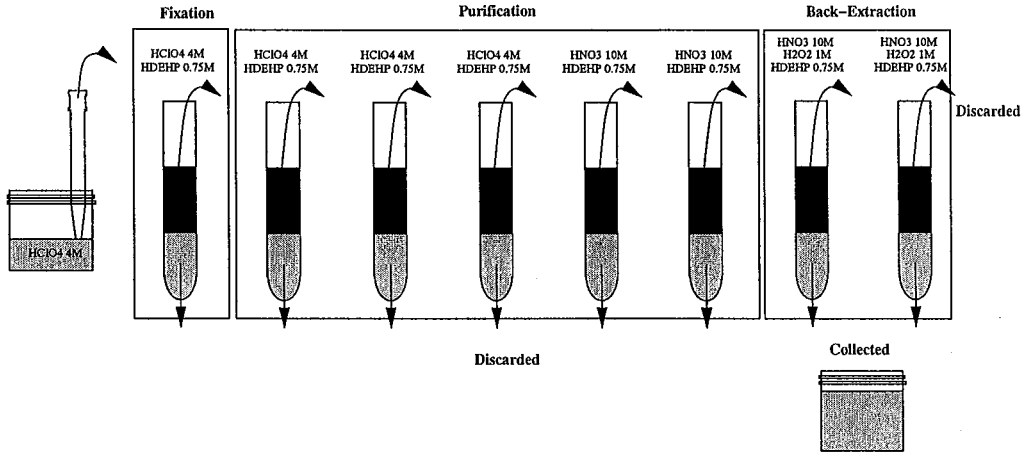

FIG. 3 – Schéma d'extraction du molybdène par extraction par solvent. Après digestion des échantillons, la solution est évaporée puis reprise dans 5 ml d'acide perchlorique. Le molybdène est ensuite purifié par une succession d'échanges liquide-liquide pour être finalement récupéré dans un mélange de HNO_3 et de H_2O_2.

Le comportement du molybdène et des nucléides directement interférents a été suivi lors de la séquence d'extraction pour une solution standard Zr-Mo-Ru (figure 4). Lors de la première étape, le molybdène et le zirconium sont complètement extraits dans le solvent organique tandis que le ruthénium reste dans la phase aqueuse. Lors des étapes suivantes de purification, le zirconium et le molybdène restent liés au HDEHP. L'ajout de peroxyde d'hydrogène aux deux dernières étapes permet de complexer le molybdène ce qui le masque vis-à-vis du solvent organique et permet son extraction dans la phase aqueuse. Au contraire, le zirconium ne semble pas être affecté par l'ajout de H_2O_2 et reste fixé. Ce protocole permet dans une large mesure de séparer le molybdène du zirconium et du ruthénium et de s'affranchir des éléments de la matrice.

3 Chromatographie ionique sur résine AG1-X8

L'étape d'extraction liquide-liquide peut être assimilée à une étape de pré-traitement car la solution de molybdène obtenue n'est pas suffisamment pure pour pouvoir être mesurée directement sur un spectromètre de masse à source plasma. Il est donc nécessaire d'affiner la séparation du molybdène. La fraction obtenue après extraction liquide-liquide a été évaporée pour être ensuite traitée par chromatographie échangeuse d'ions. L'utilisation couplée de deux méthodes de séparation dont les principes de séparation sont complètement indépendants permet de croiser les

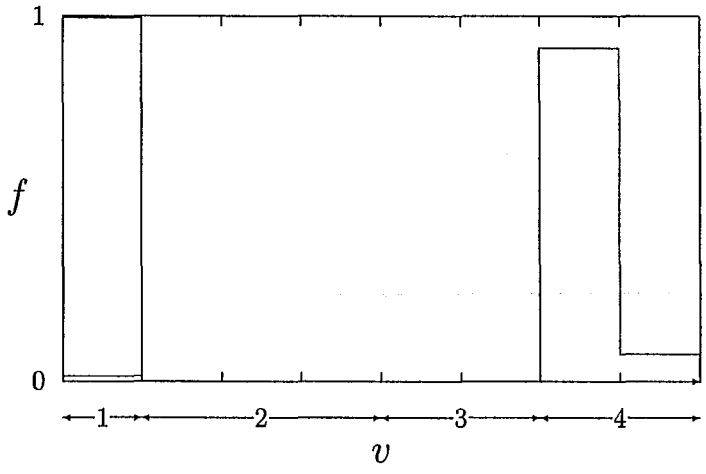

FIG. 4 – Séquence d'extraction dans le cas d'une solution standard Zr/Mo/Ru. f est la fraction en masse de zirconium, molybdène, et ruthénium dans chaque volume échantillonné de la phase aqueuse. *1.* 5 ml $HClO_4$ 4 M- 5 ml HDEHP 0.72 M, le ruthénium n'est pas fixé, tandis que le molybdène et une large fraction du zirconium sont extraits. *2.* 3*5 ml $HClO_4$ 4 M-5 ml HDEHP 0.72 M, la matrice est éliminée. *3.* 2*5 ml HNO_3 10 M-5 ml HDEHP 0.72 M, la matrice est éliminée. *4.* 2*5 ml HNO_3 - H_2O_2 1M - 5 ml HDEHP 0.72 M, le molybdène est complexé par le peroxyde ce qui permet son extraction tandis que le zirconium reste fixé sur le solvent organique.

sélectivités et d'obtenir une solution libre non seulement d'interférents isobariques directs (zirconium et ruthénium) mais également de nombreux éléments susceptibles de former des composés inattendus dans la gamme de masse des isotopes du molybdène.

3.1 Principe

Description microscopique

Les résines échangeuses d'ions sont constituées d'un support inerte sur lequel sont liés de manière covalente des groupes fonctionnels chargés (figure 5). Des contre-ions sont fixés aux groupes fonctionnels pour assurer l'électroneutralité de l'ensemble. Lorsque un échantillon est élué à travers la colonne, les ions chargés à l'opposé du groupe fonctionnel entrent en compétition avec le contre-ion et peuvent éventuellement se substituer. Les molécules neutres ou qui portent la même charge que le groupement fonctionnel n'intéragissent pas avec la résine.

$$n - \mathrm{N(CH_3)_3^+Cl^-} + \mathrm{MoX^{n-}} \rightleftharpoons -[\mathrm{N(CH_3)_3^+}]_n\mathrm{MoX^{n-}} + n\mathrm{Cl^-}. \quad (2)$$

La résine AG1-X8 200-400 Cl^- est une résine Bio-Rad de degré AG (analytical grade), de type 1 (échangeur d'anions contenant des groupes ammonium quaternaire), de polymérisation X8 (8% de liaisons divinylbenzene du polymère styrène divinylbenzene), de granulométrie 200-400 (désigne la taille des particules sphériques de résine selon un code standardisé), et conditionnée en chlorure (le contre-ion est Cl^-).

Description macroscopique

Modèle continu

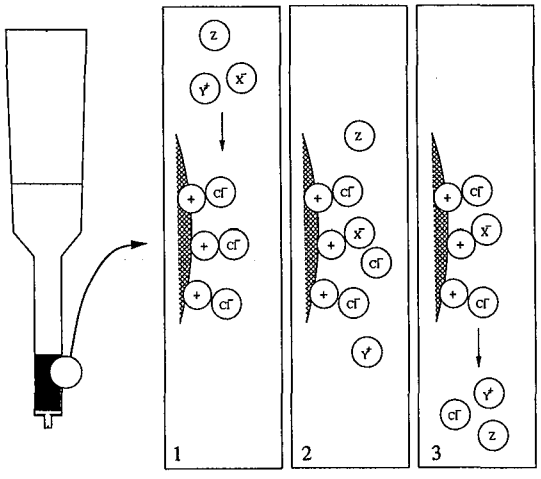

FIG. 5 – Modèle de fonctionnement d'une résine échangeuse d'anions [26]. La résine est constituée d'un support inerte sur lequel sont fixés des groupes fonctionnels chargés. Sur ces goupes sont liés des anions échangeables.

Une résine échangeuse d'ions est constituée de l'association de sphères. Ce milieu par essence discret est néanmoins décrit suivant un modèle continu [53, 54, 55]. On considère un volume élémentaire macroscopique. C'est un volume suffisamment petit pour que puisse être appliqué le calcul élémentaire et suffisament grand pour pouvoir définir des grandeurs macroscopiques comme la porosité. Dans ce cadre, il est possible de développer un modèle continu des résines échangeuses d'ions. On convient de noter,

Ω	volume arbitraire
Σ	surface du volume arbitraire Ω
Mi	masse du composé i comprise dans le volume arbitraire Ω
t	temps
ϕ	fraction volumique de la phase 1
ρ_1,ρ_2	densités des phases 1 et 2
C_1^i,C_2^i	concentrations en poids du composé i dans les phases 1 et 2
$\vec{V}_1$,$\vec{V}_2$	vitesses des phases 1 et 2
$\vec{V}_1^i$,$\vec{V}_2^i$	vitesses du composé i dans les phases 1 et 2
$\mathcal{D}_1^i$,$\mathcal{D}_2^i$	diffusivités du composé i dans les phases 1 et 2

Le taux de variation de ρC_i s'écrit,

$$\frac{\mathrm{d}\rho C_i}{\mathrm{d}t} = \frac{\mathrm{d}}{\mathrm{d}t}\iiint_\Omega \phi\rho_m C_m^i + (1-\phi)\rho_s C_s^i \,\mathrm{d}\Omega, \tag{3}$$

soit,

$$\frac{\mathrm{d}\rho C_i}{\mathrm{d}t} = \iiint_\Omega \frac{\partial}{\partial t}\phi\rho_m C_m^i + (1-\phi)\rho_s C_s^i \,\mathrm{d}\Omega. \tag{4}$$

Le flux entrant étant compté négativement, le taux de variation de ρC^i peut également s'écrire,

$$\frac{\mathrm{d}\rho C_i}{\mathrm{d}t} = -\iint_\Sigma \vec{J^i}\,\mathrm{d}\vec{\Sigma}. \tag{5}$$

D'après le théorème de la divergence de Gauss,

$$\frac{\mathrm{d}\rho C_i}{\mathrm{d}t} = -\iiint_\Omega \nabla \vec{J^i}\ \mathrm{d}\Omega, \tag{6}$$

soit,

$$\frac{\partial}{\partial t}[\phi\rho_m C_m^i + (1-\phi)\rho_s C_s^i] + \nabla \vec{J^i} = 0. \tag{7}$$

En décomposant le transport de i en termes advectif, dispersif, et diffusif, il vient,

$$\vec{J^i} = \vec{J^i}_{advection} + \vec{J^i}_{dispersion} + \vec{J^i}_{diffusion}, \tag{8}$$

$$\vec{J^i} = \phi\rho_m C_m^i \vec{V}_m - \phi \sum_{j=1}^{n} \mathcal{D}_{ij} \nabla \rho_m C_m^j - \phi\alpha\nabla\rho_m C_m^i, \tag{9}$$

soit,

$$\frac{\partial}{\partial t}[\phi\rho_m C_m^i + (1-\phi)\rho_s C_s^i] + \nabla[\phi\rho_m C_m^i \vec{V}_m - \phi \sum_{j=1}^{n} \mathcal{D}_{ij} \nabla \rho_m C_m^j - \phi\alpha\nabla\rho_m C_m^i] = 0. \tag{10}$$

Dans le cas de la chromatographie ionique sur colonne, une phase fluide incompressible est en mouvement (m) au sein du réseau poreux d'une phase solide stationnaire (s). L'équation (10) se résume alors (en négligeant le transport diffusif du soluté) à,

$$\phi\rho_m \frac{\partial C_m^i}{\partial t} + (1-\phi)\rho_s \frac{\partial C_s^i}{\partial t} + \phi\rho_m \vec{V}_m \nabla C_m^i = 0. \tag{11}$$

On peut alors introduire la loi de partage entre phase mobile et phase stationnaire,

$$K^i = \frac{C_s^i}{C_m^i}. \tag{12}$$

On convient de noter $\mathcal{X}_m^i$ la fraction (en masse) de i présente dans m,

$$\mathcal{X}_m^i = \frac{\phi\rho_m}{\phi\rho_m + (1-\phi)\rho_s K^i}. \tag{13}$$

Par suite,

$$\frac{\partial C_m^i}{\partial t} + \mathcal{X}_m^i V_m \frac{\partial C_m^i}{\partial x} = 0. \tag{14}$$

Ce modèle est fondé sur l'hypothèse que pour chaque volume élémentaire la phase stationnaire est en équilibre avec la phase mobile. Cette hypothèse n'est pas réalisée dans la pratique car l'éluant n'est pas en équilibre avec la résine. Ce formalisme est donc d'un intérêt pratique limité et on lui préfère une description discrète.

Modèle discret

La colonne est assimilée à une succession de plateaux (figure 6) pour lesquels l'équilibre entre la résine et l'éluant est réalisé [27, 28, 26]. Ce modèle semi-empirique permet de rendre compte de la non idéalité de l'ensemble résine-éluant. La hauteur du plateau théorique est déterminée expérimentalement.

Ce modèle permet d'anticiper le comportement d'une résine et de tester ainsi divers protocoles d'élution. Un programme a été développé en *C* qui permet de simuler des chromatogrammes sur résines échangeuses d'ions. Des formules simples permettent en outre de calculer directement les caractéristiques fondamentales de l'élution comme la position des pics et leur largeur qui permettent d'appréhender la qualité de la séparation [28, 26].

```
/* Chromatography Simulation */

#include <stdio.h>
#include <stdlib.h>
#include <time.h>
#include <math.h>
#include <fcntl.h>

const float HETP=0.002; /* Height Equivalent Theoretical Plate m */
const float CH=0.01; /* Column Height m */
const float CR=0.005; /* Column Radius m */
const float P=0.3; /* Porosity */

float V; /* injection volume */
float K; /* partition coefficient */
float C; /* concentration */

typedef struct
{
 float K; /* partition coefficient */
 float C; /* concentration */
} liquid; /* type of liquid array */

typedef struct
{
 float C; /* concentration */
} solid; /* type of solid array */

typedef struct
{
 float V; /* volume eluted */
 float C; /* concentration */
} eluate; /* type of eluate array */

liquid L[10000];
solid S[10000];
eluate E[10000];
int i,j,k,n,N; /* N number of theoretical plates */
FILE *fichier;

main()
{
fcloseall();
k=0;
fichier=NULL;
fichier=fopen("elutionZr.txt","w+t");
for (j=0;j<=9999;j++)
  {
   L[j].K=0;
   L[j].C=0;
   S[j].C=0;
   E[j].V=0;
   E[j].C=0;
  }
N=(int)(CH/HETP);
printf("Injection Volume ml (0 for end) ");
scanf("%f", &V);
while(V!=0)
  {
    printf("Partition coefficient ");
    scanf("%f",&K);
    printf("Concentration mol/ml ");
    scanf("%f",&C);
    n=(int)(V*1e-6/(HETP*3.14159*CR*CR*P));
    for(i=1;i<=n;i++)
      {
       k++;
       E[k].V=HETP*3.14159*k*CR*CR*P;
       E[k].C=L[N].C;
       fprintf(fichier,"\n %e %e ",E[k].V*1e6,E[k].C);
       for(j=N;j>=2;j--)
 {
          L[j].K=L[j-1].K;
          L[j].C=L[j-1].C;
        }
       L[1].K=K;
       L[1].C=C;
       for(j=1;j<=N;j++)
          {
            L[j].C=(S[j].C*(1-P)+L[j].C*P)/(P+L[j].K*(1-P));
            S[j].C=L[j].C*L[j].K;
          }
      }
    printf("Injection Volume ml (0 for end) :");
    scanf("%f", &V);
    }
fcloseall();
}
```

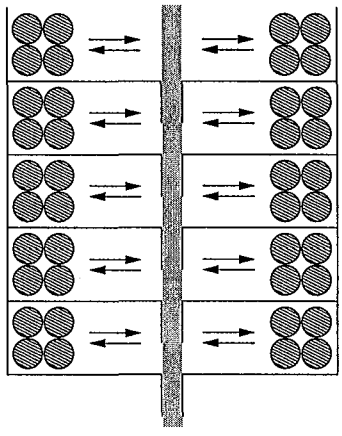

FIG. 6 – Modèle discret des plateaux théoriques. Pour chaque plateau de dimension finie, l'équilibre est réalisé entre l'éluant mobile et la résine stationnaire [27, 28, 26].

3.2 Application

La solution obtenue après l'étape d'extraction liquide-liquide n'est pas suffisament propre pour pouvoir être mesurée directement au spectromètre de masse. Il s'est donc avéré nécessaire d'affiner la séparation du molybdène sur résine échangeuse d'anions. La solution obtenue après la première étape de séparation a été dopée avec 2 ml de H_2O_2 puis chauffée à 400 K pendant une nuit afin d'oxyder le solvent organique solubilisé dans l'acide ainsi que le ruthénium résiduel et ainsi de les éliminer lors de l'évaporation à sec.

Compte-tenu du protocole d'élution choisi [29, 48, 49, 50, 4], la résine a été lavée directement sur colonne par passage de 5 ml H_2O, 5 ml HCl 6 M, 5 ml H_2O, 5 ml HCl 1 M, 5 ml H_2O, et finalement 5 ml de HF/HCl 1 M/0.5 M. Les particules les plus fines de la résine ont été au préalable éliminées par quelques lavages dans de grands volumes d'eau. La quantité de matière résiduelle après l'étape d'extraction liquide-liquide étant très faible, un volume limité (0.6 ml = l 1.2 cm × d 0.8 cm) de résine a été utilisé.

Le résidu sec a ensuite été repris dans 1 ml de HF 1 M-HCl 0.5 M car dans ces conditions (figure 7), le molybdène reste fortement fixé tandis que le fer est élué. Afin de s'assurer que le fer est complètement éliminé, 6 ml de HF 1 M/HCl 0.5 M sont élués à travers la colonne. Le zirconium est ensuite éliminé de la résine par l'élution de 4 ml HCl 6 M. A une telle acidité, le molybdène reste fixé alors que le zirconium est élué. Le molybdène est ensuite recueilli dans 6 ml de HCl 1 M. Dans cette fraction, seul le molybdène est élué car le zirconium a déjà été éliminé dans l'élution précedente. La solution résultante est évaporée pour être ensuite mesurée au spectromètre de masse.

La mise au point de ce protocole d'élution est le résultat d'allers-retours constants entre la simulation sur ordinateur et la détermination experimentale des courbes d'élution. Différents protocoles ont pu ainsi être rapidement testés. Le résultat d'une telle simulation est illustré dans la figure 8 où l'on observe que les pics d'élution du zirconium et du molybdène sont complètement séparés. On peut en outre remarquer que les pics d'élution sont très disymétriques. Cela résulte normalement du faible nombre de plateaux théoriques de la colonne employée. Le chromatogramme simulé peut être comparé avec une détermination expérimentale (figure 9) qui corrobore les résultats de la modélisation. Il convient de souligner que le protocole d'élution employé fonc-

tionne selon un mode binaire (les éléments sont fixés ou ne le sont pas) de sorte que l'ultilité du modèle théorique est limitée dans ce cas.

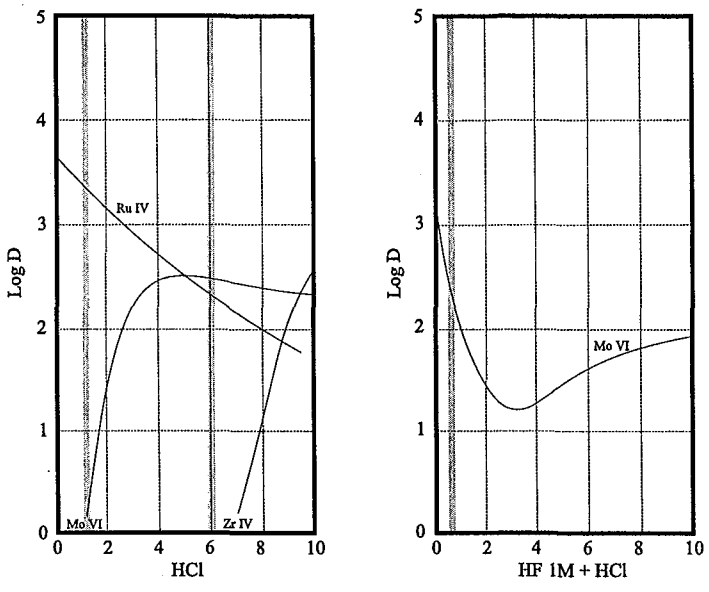

FIG. 7 – Coefficients de partage du molybdène et des nucléides isobares sur résine anionique [29].

4 Mesure isotopique sur MC-ICP-Hex-MS

Pendant très longtemps, la méthode de prédilection pour effectuer des mesures précises de composition isotopique a été la spectrométrie par thermo-ionisation (TIMS). Cette technique repose sur l'émission des ions par chauffage d'un filament sur lequel a été préalablement déposé l'élément à analyser ainsi qu'un éventuel activateur. L'émission des ions en TIMS est dépendante de la température et du type de dépôt effectué. Ainsi, deux nucléides isobares peuvent ne pas interférer lors de la mesure si leurs comportements vis-à-vis de la ionisation sont différents. Il est par exemple commode d'émettre une partie du rubidium résiduel vanne fermée à basse température avant d'effectuer la mesure isotopique de strontium. Cette sélectivité du TIMS constitue à la fois une qualité et un défaut. C'est un défaut en ce sens où il n'existe pas de méthode d'ionisation satisfaisante pour certains éléments. Même si le domaine des nucléides accessibles en TIMS a été largement étendu avec la mise au point du spectromètre de masse à thermo ionisation négative, certains éléments restent difficilement mesurables avec une telle machine. Ceci est particulièrement vrai pour les éléments comme le molybdène dont l'énergie de première ionisation est particulièrement élevée (7.1 eV). En outre, le TIMS est particulièrement adapté à la mesure des variations isotopiques qui ne dépendent pas de la masse (productions radiogéniques, héritages présolaires, *etc.*) car le fractionnement de masse entre deux échantillons successifs est difficilement reproductible. Cette difficulté peut être résolue par l'emploi de spikes multiples qui permet de s'affranchir du fractionnement de masse instrumental.

L'avènement récent de spectromètres de masse à source plasma [1] permet de s'affranchir de ces deux difficultés (ionisation sélective et contrôle incertain du fractionnement de masse). Les spectromètres de masse à source plasma ne sont pas sélectifs vis-à-vis de la ionisation des

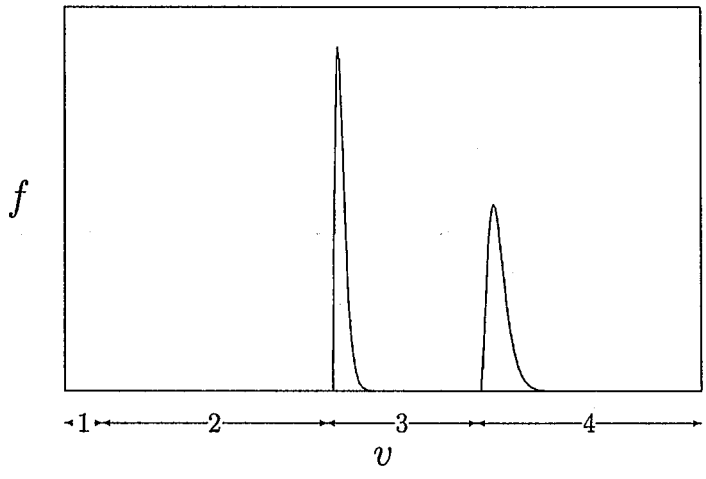

FIG. 8 – Simulation de l'élution du zirconium et du molybdène sur résine anionique AG1-X8 200-400 Cl-. f est la fraction en masse de ziconium et de molybdène dans chaque volume élémentaire. *1.* 1ml HF 1 M-HCl 0.5 M, élution d'une large fraction de la matrice et fixation du molybdène et du zirconium sur la résine. *2.* 6 ml HF 1 M-HCl 0.5 M, élution de la matrice. *3.* 4 ml HCl 6 M, élution du zirconium. *4.* 6 ml HCl 1 M, élution du molybdène.

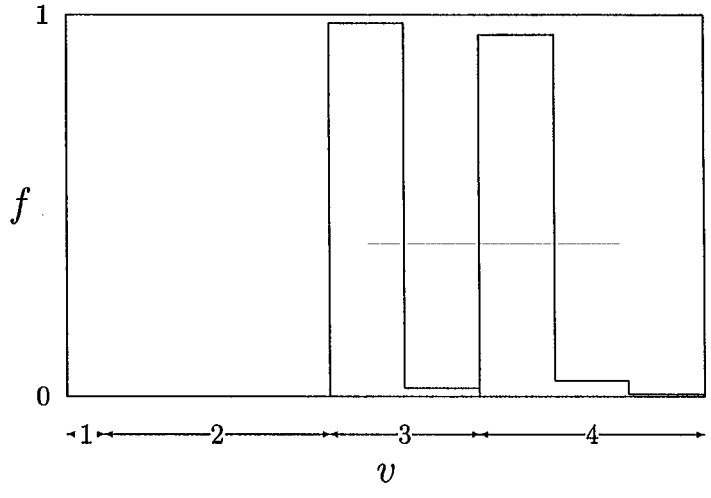

FIG. 9 – Elution du zirconium et du molybdène sur résine anionique AG1-X8 200-400 Cl-. f est la fraction en masse de ziconium et de molybdène dans chaque volume échantillonné. *1.* 1ml HF 1 M-HCl 0.5 M, élution d'une large fraction de la matrice et fixation du molybdène et du zirconium sur la résine. *2.* 6 ml HF 1 M-HCl 0.5 M, élution de la matrice. *3.* 4 ml HCl 6 M, élution du zirconium. *4.* 6 ml HCl 1 M, élution du molybdène.

Digestion

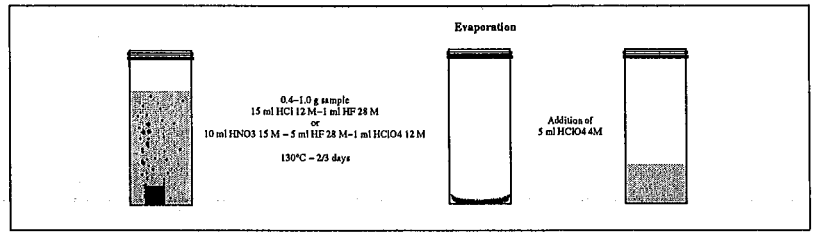

Solvent extraction di(2–ethylhexyl) phosphate

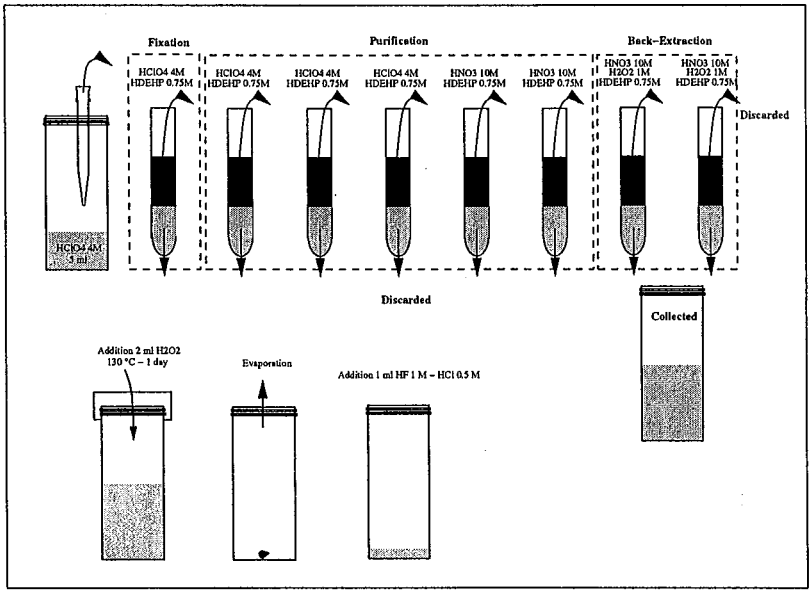

Ion chromatography AG1–X8

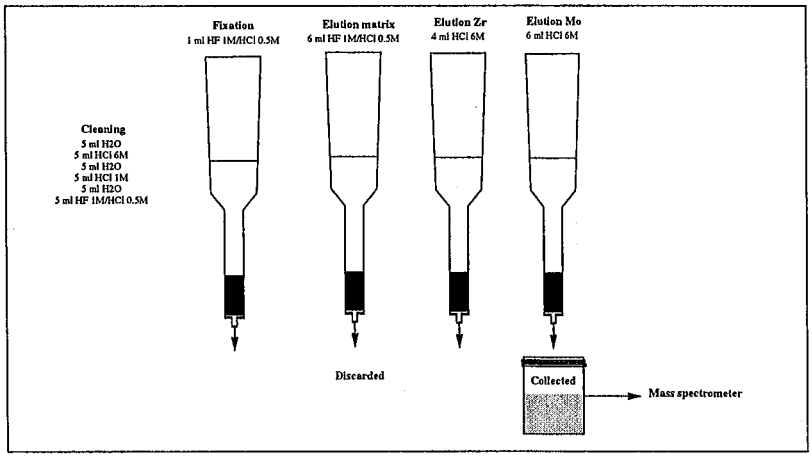

FIG. 10 – Synthèse du protocole de séparation.

éléments [56]. Cela implique que l'élément analysé doit être préalablement séparé des nucléides isobares et des composés complexes susceptibles d'interférer lors de l'analyse isotopique. De nombreux éléments qui étaient inaccessibles à l'analyse en thermo ionisation peuvent être maintenant mesurés. Ceci a ouvert de larges perspectives de recherche en cosmochimie. Un aspect important des spectromètres de masse à source plasma est la très bonne reproductibilité du fractionnement de masse d'un échantillon à l'autre et l'indépendance en première approximation du biais de masse vis-à-vis de l'élément analysé. Il est ainsi aisé de corriger les mesures du fractionnement instrumental et d'estimer ainsi les variations naturelles d'abondances isotopiques. La principale différence entre les spectromètres de masse à thermo-ionisation et spectromètres de masse à source plasma réside dans le processus de ionisation.

4.1 Source plasma

Les échantillons analysés en ICPMS sont généralement introduits sous forme de solution en milieu nitrique. Des aérosols sont ensuite formés et transportés par un gaz vecteur jusqu'à la torche plasma où les atomes sont ionisés. Une partie des aérosols est éliminée dans une chambre de vaporisation. Le rendement lié au transport dans une configuration standard de source est de l'ordre de 0.03. Des systèmes complexes d'introduction ont été développés qui permettent d'augmenter l'efficacité du transport. Seuls seront explicités les fonctionnements du système standard fourni avec le spectromètre de masse (nébuliseur Meinhard, chambre de vaporization de type Scott) ainsi que le système de désolvatation Aridus.

Introduction et nébulisation de l'échantillon

Nébuliseur Meinhard et chambre de Scott

Le système d'introduction des échantillons est conditionné aux possibilités de la source plasma [57]. Les échantillons introduits dans la torche doivent être sous forme gazeuse ou liquide et dans le cas d'une introduction liquide, la taille des aérosols ne doit pas dépasser quelques dizaines de micromètres. Le nébuliseur le plus répandu est un nébuliseur pneumatique concentrique en quartz de type Meinhard (figure 11). Le flux d'argon à l'entrée du capillaire crée une dépression qui draine la solution vers la chambre de nébulisation et qui permet sa nébulisation. La chambre de Scott est une chambre à décantation ou sédimentation (figure 11). Les aérosols doivent parcourir un trajet tortueux avant d'être dirigés vers la torche. Les plus gros d'entre eux, dont la vitesse de chute est la plus élevée, tombent au fond de la chambre avant d'avoir réussi à s'en sortir et sont ensuite éliminés par un drain situé à la base de la chambre. Ce système d'introduction est efficace du point de vue du transport des échantillons mais souffre d'une grande mémoire. Dans le cas du molybdène et plus spécifiquement de la recherche d'anomalies non dépendantes de la masse, cela n'a pas constitué un véritable problème. Il convient de noter qu'il existe un autre type de chambre qui repose sur le même principe de sédimentation que la chambre de Scott et dont la mémoire est beaucoup plus faible (chambre cyclonique), ce qui réduit d'autant le temps de lavage entre deux échantillons. Le débit d'argon est ajusté afin d'optimiser le signal mesuré. Le débit ne croît pas simplement avec le débit d'argon car lorsque celui-ci augmente beaucoup, la taille de coupure de la chambre de nébulisation augmente, et la quantité d'aérosols qui réussissent à sortir de la chambre diminue. L'ajustement du débit est donc un compromis entre efficacité de nébulisation et efficacité de transport.

Désolvateur Aridus

Dans le cas d'une introduction standard d'échantillons, les aérosols qui portent l'élément à analyser sont aqueux. Le système de désolvatation Aridus permet d'éliminer une partie du solvent

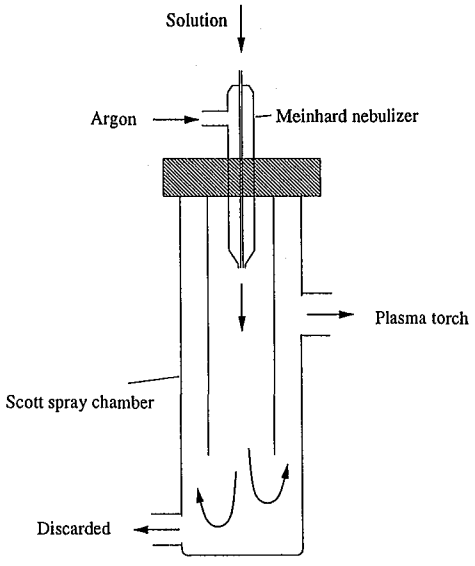

FIG. 11 – Système d'introduction nébuliseur Meinhard – chambre de nébulisation Scott.

et d'introduire ainsi des aérosols secs dans le plasma. Cette désolvation des aérosols permet d'augmenter l'efficacité du transport et de diminuer la charge de solvent dans le plasma. Avec les systèmes conventionnels d'introduction, la vapeur d'eau injectée provoque la formation d'espèces polyatomiques d'hydrures et d'oxydes qui peuvent interférer lors des mesures iostopiques. En dépit de ses nombreux avantages, ce système d'introduction a été très peu utilisé car il ne constitue pas un équipement standard de la machine et a été acquis tardivement.

Ionisation dans la torche plasma et interface

Un plasma est un état de la matière caractérisé par la présence de charges libres mais qui reste macroscopiquement neutre. Son comportement se rapproche de celui d'un gaz mais les interactions sont principalement coulombiennes. Un courant alternatif haute-fréquence circule dans les spires d'une bobine. Ce courant induit la presence d'un champ magnétique variable à l'intérieur de la bobine, dont les caractéristiques répondent à la loi de Biot et Savart. Si un plasma coupe la section de la bobine, alors les particules chargées du plasma vont se mettre en mouvement suivant la loi de Lenz pour modérer cette variation du champ. Ce mouvement provoque un chauffage du plasma qui permet de maintenir l'état ionisé du gaz. L'intéraction du courant haute fréquence dans la bobine et du gaz ionisé permet ainsi d'entretenir naturellement la stabilité du plasma. Pour initier la conductibilité électrique du gaz, un arc est utilisé.

La température cinétique de fonctionnement de la torche plasma est de l'ordre de 5000 K et la pression est de 1 bar. La torche en quartz est constituée de tubes concentriques. Le tube le plus externe est celui qui enserre le gaz de refroidissement (cool). Le tube le plus interne porte les aérosols depuis le nébuliseur vers la torche (nebulizer). Le tube intermédiaire a un rôle de confinement du plasma (intermediate). L'énergie de première ionisation de l'argon est 16 eV. Le degré de ionisation du molybdène dans un plasma HF est proche de 100 % [56]. Ainsi, les spectromètres de masse à source plasma permettent une ionisation quasiment complète de l'analyte étudié, en l'occurence du molybdène.

La torche plasma travaille à pression atmosphérique. Cependant, la séparation des ions en fonction du rapport masse/charge n'est possible que dans un environnement à faible pression. Dans la pratique, il est donc nécessaire d'utiliser un système qui permet le passage de 1 bar à 10^{-8} mbar tout en conservant une bonne transmission de l'ion que l'on cherche à analyser. Ceci est réalisé dans l'interface qui consiste en une succession de cônes qui séparent des zones dans lesquelles la pression va en décroissant (figure 12). Cette interface est constituée d'un cône échantillonneur qui peut être en platine ou en nickel (nickel dans notre cas), d'un cône écrémeur, et d'un cône collimateur. Après passage dans cette interface, les ions sont injectés dans un système de collision hexapole.

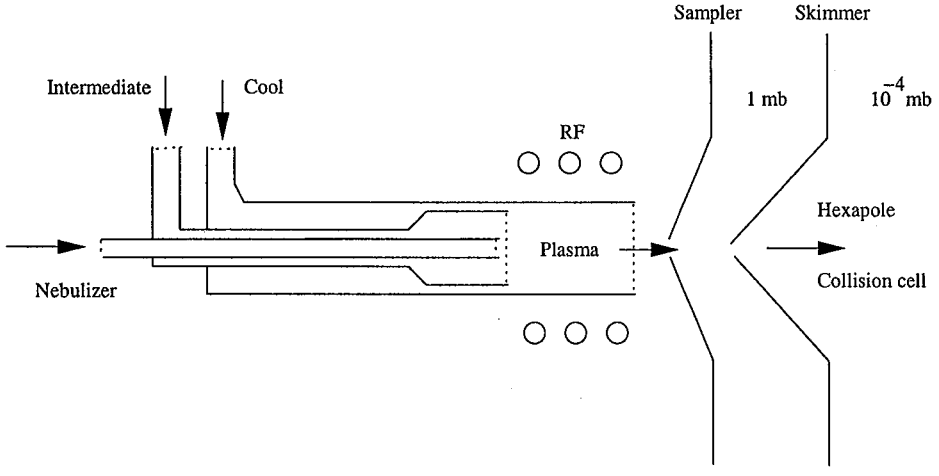

FIG. 12 – Torche plasma et interface.

4.2 Cellule de collision hexapole

A l'entrée de la cellule de collision hexapole, la dispersion en énergie des ions est très large (30 eV). Avec une telle dispersion, il est impossible de séparer directement les ions en fonction du rapport masse sur charge dans une secteur magnétique car la forme des pics est très dégradée. Il importe donc de réduire la dispersion en énergie des ions avant de les analyser. Cela peut être réalisé grâce à un secteur électrostatique. Historiquement, c'est cette solution qui a été retenue sur les premiers spectromètres de masse à source plasma et multicollection. La solution mise en oeuvre sur l'Isoprobe fabriqué par Micromass est différente. Elle consiste en l'utilisation d'un système de focalisation hexapole couplé à une cellule de collision [58]. Cette cellule présente deux intérêts. Elle permet d'abord une réduction de la dispersion en énergie des ions par interaction avec le gaz de collision [59, 58]. Elle permet également de filtrer certains ions qui pourraient interférer lors de la collection des ions [60, 61, 58]. Les cellules de collision dans lesquelles sont introduits des gaz non inertes sont désignées sous le vocable de cellule de réaction. Le principe de ces cellules de réaction est identique au principe des cellules de collision.

La cellule hexapole est constituée de six pôles sur lesquels sont appliqués des potentiels $\Phi_0/2$ et $-\Phi_0/2$ suivant la configuration décrite dans la figure 13,

$$\Phi_0 = U - V\cos\omega(t - t_0). \tag{15}$$

L'ion ne subissant aucune force selon l'axe optique z, seules les trajectoires suivant les axes X et Y sont décrites. La position des ions en notation complexe est $Z = X + iY$. Szabo [30] et Hägg and Szabo [62] ont dérivé l'équation différentielle qui gouverne la trajectoire des ions dans un champ électrique hexapolaire (n représente le nombre de pôles, 3 dans le cas d'un hexapole),

$$\frac{\mathrm{d}^2 Z}{\mathrm{d}T^2} + [a_n - 2q_n \cos n(T - T_0)]\overline{Z}^{n-1} = 0, \tag{16}$$

où le temps T est adimensionnel, et a_n et q_n sont des constantes. Cette équation peut être intérprétée en termes physiques après un simple réarrangement,

$$m\frac{\mathrm{d}^2 Z}{\mathrm{d}T^2} = -ma_n\overline{Z}^{n-1} + 2q_n[\cos n(T - T_0)]\overline{Z}^{n-1}. \tag{17}$$

Cette équation régit un mouvement d'oscillation non linéaire, non atténué, et forcé. Le terme $m\mathrm{d}^2Z/\mathrm{d}T^2$représente l'inertie de la particule ($m\mathbf{a}$). Le terme $-ma_n\overline{Z}^{n-1}$ représente une force de rappel (équivalent à la force de rappel d'un ressort). Le terme $2q_n[\cos n(T - T_0)]\overline{Z}^{n-1}$ représente une force extérieure appliquée ; c'est l'expression formelle d'une excitation. Le mouvement d'une particule chargée dans un champ multipolaire peut ainsi être décrit selon le même formalisme qu'un solide autoporteur attaché au bout d'un ressort (figure 14).

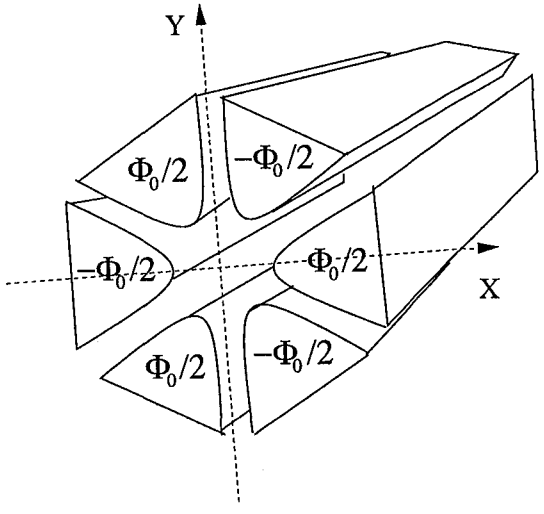

FIG. 13 – Configuration du système hexapole.

La présence d'un champ électrique hexapolaire permet donc de confiner le mouvement des ions le long de l'axe optique. La réduction de la dispersion en énergie des ions est réalisée par l'introduction dans la cellule hexapole d'un gaz de collision avec lequel les ions incidents vont entrer en collision. A chaque choc, les ions échangent de l'énergie avec le gaz. Après un certain nombre de collisions, les ions sont thermalisés (la dispersion en énergie des ions se rapproche de celle qui correspond à la température du gaz). On considère que les ions de masse m_1 entrent dans la cellule hexapole avec un énergie initiale E_0. Les ions entrent en collision avec des atomes immobiles de masse m_2. On covient de noter $k=m_1/m_2$ et λ le libre parcours moyen. On montre ainsi [58] simplement que,

$$E = E_0 \exp \frac{-4kx}{\lambda(1+k)^2}, \tag{18}$$

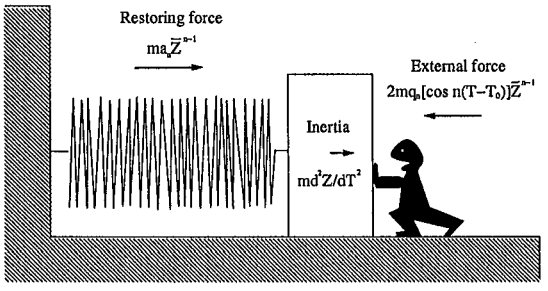

FIG. 14 – Analogie entre le mouvement d'une particule chargée dans un champ hexapolaire et le mouvement d'un solide autoporteur fixé à un ressort [30].

où x est la distance parcourue au total par les ions. Une application numérique permet d'estimer la dispersion en énergie des ions à la sortie de la cellule de collision hexapole qui est de 0.1 eV environ. Ce simple modèle ne permet pas d'appréhender le phénomène dans son détail. Il est impossible de dériver analytiquement le comportement des ions dans un système hexapolaire empli de gaz. Seules des simulation numériques permettent de rendre compte du processus dans sa réalité. Krutchinsky *et al.* [31] ont ainsi simulé par méthode de Monte-Carlo le mouvement des ions dans une cellule de collision quadrupolaire pour des molécules de myoglobine. A l'entrée de la cellule de collision, des ions sont simulés avec des vecteurs vitesse et des positions aléatoires. Le mouvement de chaque ion est ensuite suivi avec un certain nombre de collisions aléatoires (figure 15).

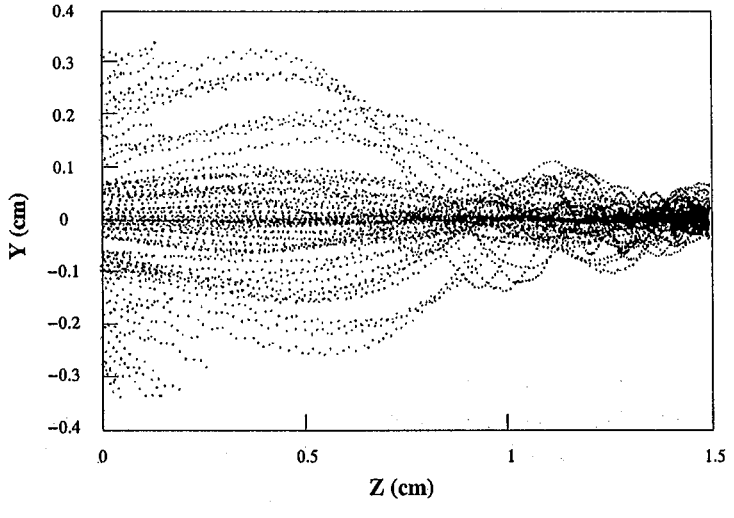

FIG. 15 – Simulation de Monte-Carlo des trajectoires d'ions de myoglobine dans un champ quadrupolaire empli d'un gaz de collision [31].

Dans le cas du molybdène, le gaz de collision introduit est de l'argon. La fonction de l'argon est alors de réduire la dispersion en énergie des ions incidents et d'assurer une transmission

efficace entre l'interface et le secteur magnétique.

4.3 Secteur magnétique

Le principe des spectromètres de masse dédiés à l'analyse isotopique repose sur la séparation en masse des ions dans un champ magnétique (figure 16). Avant d'entrer dans le champ magnétique orthogonal au mouvement des ions, ceux-ci sont accélérés dans un champ électrostatique. Le plus souvent l'analyseur est à la masse. L'Isoprobe construit par Micromass présente là aussi une spécificité en ce sens où l'analyseur est à un potentiel non nul. Les raisons de ce choix technologique n'ont jamais été exprimées clairement mais il pourrait s'agir d'éviter la formation de charges statiques sur l'analyseur qui pourraient perturber le mouvement des ions. Après cette accélération, les ions sont séparés dans un secteur magnétique. Les équations qui gouvernent le mouvement des ions dans l'analyseur sont simples et leur démonstration ne présente aucune difficulté. On se limitera donc à donner le résultat final de ce calcul formel qui indique que le rayon de courbure de la trajectoire circulaire des ions dans l'analyseur est proportionnel au rapport masse sur charge.

$$R = \sqrt{\frac{2U}{B^2}\frac{m}{q}}, \tag{19}$$

où U est la tension d'accélération, B est l'intensité du champ magnétique orthogonal, m est la charge d'un ion, et q est sa charge. Deux nucléides simplement ionisés pourront être séparés en fonction de leur masse. Ce résultat implique également que des espèces plusieurs fois ionisées (W, Os, Pt, et Hg) peuvent interférer sur le molybdène simplement ionisé. Il importe donc de séparer le molybdène des nucléides même lorsque ceux ci ne sont pas directement isobares car ils peuvent former des ions multiples qui peuvent interférer lors de l'analyse avec les masses du molybdène.

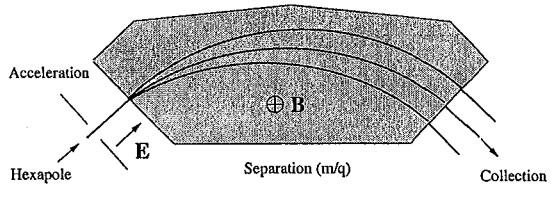

FIG. 16 – Séparation en masse des ions dans un champ magnétique orthonormal à la trajectoire de ions après application d'une tension d'accélération.

4.4 Collection

Les courants ioniques qui ont été séparés en fonction du rapport masse sur charge sont ensuite mesurés grâce à des cages de Faraday recouvertes de carbone (ce qui augmente leur durée de vie). Le flux ionique est quantifié indirectement par la mesure de la tension aux bornes d'une résistance de très grande valeur. L'Isoprobe de Micromass est équipé de neuf cages de Faraday mobiles (figure 17). Le molybène possède sept isotopes. Deux cages de Faraday restent donc libre pour mesurer des nucléides du zirconium et du ruthénium, ce qui permet de corriger les analyses isotopiques pour les interférences isobares qui peuvent rester après séparation chimique.

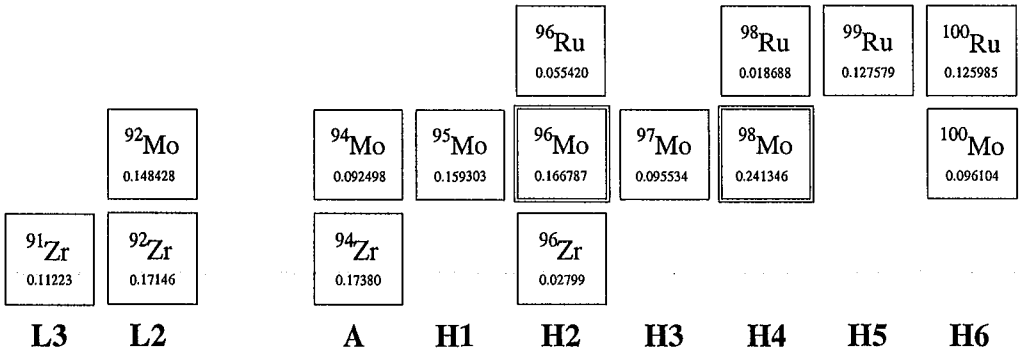

FIG. 17 – Schéma d'acquisition du molybdène.

5 Acquisition et traitement des données

5.1 Fractionnement de masse et interférences isobariques

La composition isotopique du molybdène mesurée au spectromètre de masse peut varier en fonction du fractionnement de masse instrumental et naturel. Le fractionnement de masse peut être corrigé en supposant un rapport fixe et en calculant le biais de masse sur ce rapport pour le propager ensuite sur tous les isotopes. Ce type de correction est appelé normalisation interne. La correction du fractionnement de masse s'appuie sur une description formelle du biais de masse. Plusieurs lois sont envisagées pour décrire le fractionnement de masse (loi linéaire, exponentielle, puissance, et puissance généralisée). Il semble que le fractionnement de masse dans de nombreux instruments suive un formalisme proche de la loi exponentielle [63] qui relie la variation de composition isotopique à la différence de masse suivant l'expression,

$$r = R(1 + \Delta M/M)^{\beta}, \tag{20}$$

où r est le rapport mesuré, R est le rapport "vrai", ΔM est la différence de masse, et β est le biais de masse. Pour corriger du biais de masse dans le cas du molybdène on procède comme suit. Le rapport $^{98}Mo/^{96}Mo$ est mesuré après correction des interférences possibles du zirconium et du ruthénium. On suppose la valeur du rapport vrai connu ($^{98}Mo/^{96}Mo = 1.4470$) [4], ce qui permet de calculer le biais de masse β. Cette valeur du biais de masse est ensuite appliquée sur l'ensemble des rapports fractionnés afin de les corriger.

La correction des interférences isobariques et du biais de masse doit procéder en fait par itérations. En effet, les compositions isotopiques du zirconium et du ruthénium (isobares du molybdène) sont elles aussi fractionnées. La configuration de la collection ne permet de mesurer qu'un seul isotope du zirconium et du ruthénium. Il est ainsi impossible de calculer le biais de masse sur ces deux éléments. Des études antérieures ont montré que dans une fenêtre de masse restreinte, les éléments présentaient un fractionnement de masse par unité de masse atomique proche. Il est donc possible d'appliquer la valeur du biais de masse calculé sur le molybdène au zirconium et au ruthénium afin de déterminer les abondances fractionnées de ces éléments. Le zirconium et le ruthénium interférent sur le rapport de normalisation, ce qui fausse le biais de masse. Pour corriger à la fois du fractionnement de masse et des interférences isobariques on procède donc selon un schéma itératif. Le biais de masse est d'abord calculé sur les données brutes du molybdène. Ce biais de masse est appliqué au zirconium et au ruthénium afin de

corriger leurs contributions sur les isotopes du molybdène. Un nouveau biais de masse est calculé sur ces abondances corrigées qui est ensuite utilisé pour corriger plus justement les abondances du molybdène des interférences du zirconium et du ruthénium. Ce schéma de correction peut être reproduit jusqu'à convergence de la composition isotopique du molybdène. Dans la pratique, cet algorithme de correction n'est utile que pour des niveaux d'interférences très élevés. Il offre dans ce cas une correction très efficace (figure 18). La composition isotopique du molybdène est exprimée en notation ϵ,

$$\epsilon^i = [(^iMo/^{96}Mo)/(^iMo/^{96}Mo)_{STD} - 1] \times 10^4, \tag{21}$$

où STD représente une solution standard Alfa Aesar d'origine inconnue.

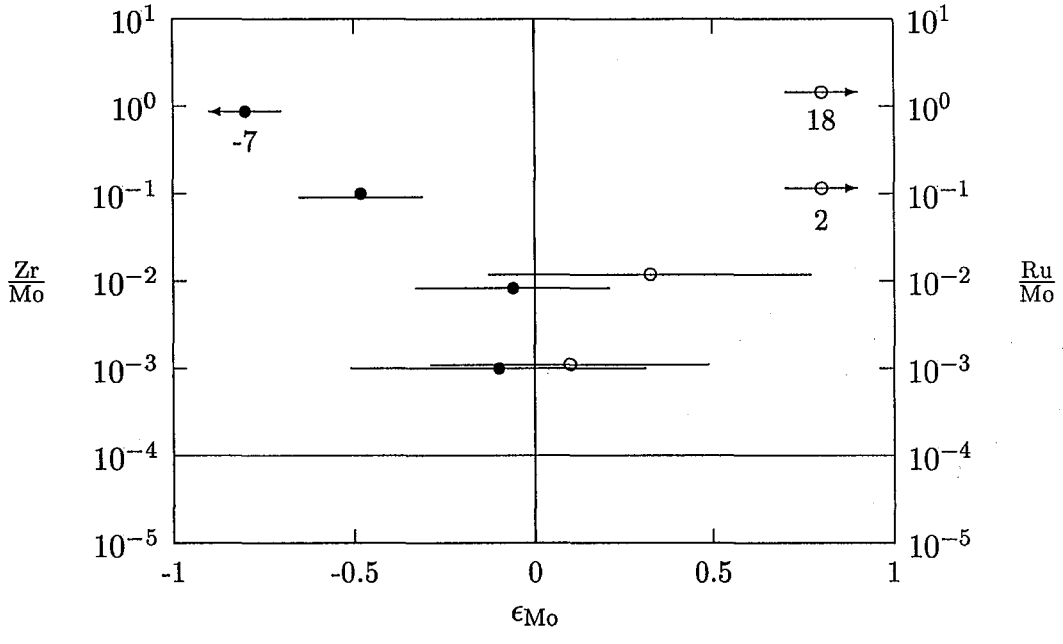

FIG. 18 – Test de l'influence des interférences isobares du zirconium et du ruthénium sur la composition isotopique du molybdène. Différents standards ont été dopés en Zr et Ru afin d'apprécier l'efficacité du processus itératif de correction des interférences et du fractionnement sur la composition isotopique de Mo. Les standards dopés ont été comparés à des standards non dopés. Le niveau d'interférence des standards non dopés correspond à des rapports Zr/Mo et Ru/Mo de 10^{-4}. Comme l'ilustre cette figure, la composition isotopique du molybdène (à la masse 97) peut être justement mesurée jusqu'à des niveaux d'interférences aussi élevés que 10^{-2} avec un niveau de précision inférieur à 1ϵ. Dans le cas des échantillons naturels, les niveaux d'interférences étaient toujours inférieurs à 10^{-4}.

5.2 Acquisition des données

Avant toutes les analyses, le champ magnétique est automatiquement ajusté pour centrer en masse le pic de contrôle 94. Chaque mesure dure de 10 à 15 minutes et consiste en un bloc de 20 cycles, chaque cycle étant composé de la mesure des zéros pendant 14 secondes (7 secondes pour chacun) et de la mesure de l'intensité du pic pendant 14 secondes également. Les zéros

sont mesurés à 0.3 amu de part et d'autre du pic et pas à 0.5 amu afin d'éviter la contribution éventuelle de double-chargés sur le niveau de base. En plus de la normalisation interne, les échantillons sont normalisés en externe par rapport à des standards encadrant l'échantillon et dont les concentrations ont été ajustées à la concentration de l'échantillon analysé (±10 %). Cette procédure permet de s'affranchir des éventuelles fluctuations du niveau de fond des interférences non résolues. Pour les échantillons qui contenaient peu de molybdène (les lessivages en particulier), le blanc est mesuré avant une série standards-échantillon et sa valeur est ensuite soustraite en intensité aux mesures subséquentes. Toutes ces corrections permettent d'obtenir une très bonne justesse sur les rapports isotopiques mesurés en dépit de la présence d'éventuelles interférences non résolues issues du spectromètre de masse à source plasma.

5.3 Estimation des incertitudes

La justesse n'est rien sans une robuste estimation de la précision. On considère que chaque mesure est la réalisation v d'une variable aléatoire parente V de moyenne μ_V et d'écartype σ_V. Pour des raisons qui demeurent obscures, la reproductibilité externe des mesures est systématiquement très supérieure à l'erreur interne. Il est donc impossible de simplement assigner l'erreur interne comme incertitude sur la mesure; d'autres sources de fluctuations doivent intervenir. Compte-tenu de la faible concentration en molybdène des météorites et de la précision requise, il est impossible de répliquer plus de deux ou trois fois la mesure au cours d'une session. La moyenne des analyses suit une loi de Student dont l'étalement augmente avec la diminution du nombre de degrés de liberté. Pour deux ou trois analyses, cette étalement devient rédhibitoire pour discuter de très faibles anomalies. De plus, de nombreux échantillons n'ont été mesurés qu'une seule fois au cours d'une session, ce qui interdit une estimation de l'incertitude basée sur des réplicats. Pour toutes ces raisons, une autre méthode d'estimation des incertitudes a été adoptée. Elle consiste à supposer que les variables aléatoires parentes des standards (Y) et des échantillons (Z) suivent des lois de moyennes μ_Y et μ_Z mais que les dispersions de ces deux variable aléatoires sont identiques, $\sigma_Y = \sigma_Z$. Il est ainsi possible d'estimer l'incertitude sur la mesure de l'échantillon en répliquant de nombreuses fois les standards et en analysant la distribution statistique de ces mesures. On note $\hat{\mu}$ et $\hat{\sigma}$ des estimateurs convergents non biaisés de μ et σ. Les mesures sont effectuées suivant une séquence

$$(x, y_1, y_2, y_3, y_4, y_5, z_1, y_6, \ldots, y_{m-5}, z_n, y_{m-4}, y_{m-3}, y_{m-2}, y_{m-1}, y_m),$$

avec x la mesure du bruit de fond (variable aléatoire parente X), m le nombre de réalisations de Y, et n le nombre de réalisations de Z. On définit la variable $W^* = W - X$ (soustraction du bruit de fond). La composition isotopique de l'échantillon est exprimée en notation ϵ selon,

$$\epsilon = [\hat{\mu}_{Z^*} \,/\, \hat{\mu}_{Y^*} - 1] \times 10^4. \tag{22}$$

L'incertitude qui pèse sur ϵ est basée sur les réplicats de standards,

$$\sigma_\epsilon = \sqrt{1/m + 1/n}\ \hat{\sigma}_{Y^*} \,/\, \hat{\mu}_{Y^*} \times 10^4. \tag{23}$$

6 Anal. Chem. 73, 2613-2616

Solvent Extraction, Ion Chromatography, and Mass Spectrometry of Molybdenum Isotopes

Dauphas, N., Reisberg, L., and Marty, B.

Analytical Chemistry (2001) **73**, 2613-2616

Anal. Chem. **2001**, *73*, 2613–2616

Solvent Extraction, Ion Chromatography, and Mass Spectrometry of Molybdenum Isotopes

Nicolas Dauphas,*,† Laurie Reisberg,† and Bernard Marty†,‡

Centre de Recherches Pétrographiques et Géochimiques, CNRS UPR 2300, 15 rue Notre-Dame des Pauvres, BP 20, 54501 Vandoeuvre-lès-Nancy Cedex, France, and École Nationale Supérieure de Géologie, rue du doyen Marcel Roubault, BP 40, 54501 Vandoeuvre-lès-Nancy Cedex, France

A procedure was developed that allows precise determination of molybdenum isotope abundances in natural samples. Purification of molybdenum was first achieved by solvent extraction using di(2-ethylhexyl) phosphate. Further separation of molybdenum from isobar nuclides was obtained by ion chromatography using AG1-X8 strongly basic anion exchanger. Finally, molybdenum isotopic composition was measured using a multiple collector inductively coupled plasma hexapole mass spectrometer. The abundances of molybdenum isotopes 92, 94, 95, 96, 97, 98, and 100 are 14.8428(510), 9.2498(157), 15.9303(133), 16.6787(37), 9.5534(83), 24.1346(394), and 9.6104(312) respectively, resulting in an atomic mass of 95.9304(45). After internal normalization for mass fractionation, no variation of the molybdenum isotopic composition is observed among terrestrial samples within a relative precision on the order of 0.00001–0.0001. This demonstrates the reliability of the method, which can be applied to searching for possible isotopic anomalies and mass fractionation.

Molybdenum ($Z = 42$) has seven stable ($A = 92$, 94, 95, 96, 97, and 98) and long-lived ($A = 100$) isotopes produced by the *p* (92 and 94), *r* (95, 97, 98, and 100), and *s* (95, 96, 97, and 98) nucleosynthetic processes.[1] The abundances of molybdenum isotopes corrected for natural and instrumental mass fractionation are known to vary in the solar system as a result of (i) inheritance of nucleosynthetic anomalies,[2,3] presumably carried by unprocessed presolar dust grains which survived homogenization of the protosolar nebula;[4,5] (ii) electron capture of the *p*-process nuclide ^{97}Tc to form ^{97}Mo, with a mean life of 3.7 Ma early in the solar system;[6,7] (iii) spontaneous fission of uranium;[8,9] (iv) double β decay of ^{96}Zr to form ^{96}Mo;[8] and (v) anomalous isotope effects.[10]

During the past decade,[2-17] great efforts have been made to measure molybdenum isotope abundances accurately and precisely. Such measurements have long been hampered by zirconium ($Z = 40$) and ruthenium ($Z = 44$) isobaric interferences and the high first ionization potential of molybdenum (7.1 eV). We have developed a separation procedure for molybdenum that is based on solvent extraction and ion chromatography which efficiently removes matrix elements and isobar nuclides. Isotopic analyses were performed using a Micromass Isoprobe multiple collector inductively coupled plasma hexapole mass spectrometer (MC-ICP-Hex-MS) equipped with nine Faraday collectors. This instrument allows high ionization yields of molybdenum to be achieved and permits the correction of zirconium and ruthenium isobaric interferences so that the isotopic composition of molybdenum can be measured with high accuracy and precision.

1. EXPERIMENTAL SECTION

Separation Chemistry. The procedure we developed was inspired by the work of Qi-Lu and Masuda,[11,12,15] who took advantage of the affinity of molybdenum for di(2-ethylhexyl) phosphate ($C_{16}H_{35}O_4P$, HDEHP)[18] and used a strongly basic anion exchanger (AG1-X8, 100–200 mesh, chloride form)[19] in order to achieve fine separation of molybdenum from potential interfering species. We made several modifications to the Qi-Lu and Masuda separation procedure on the basis of computer simulations. After

* To whom correspondence should be addressed. E-mail: dauphas@crpg.cnrs-nancy.fr.

† Centre de Recherches Pétrographiques et Géochimiques.

‡ École Nationale Supérieure de Géologie.

(1) Anders, E.; Grevesse, N. *Geochim. Cosmochim. Acta* **1989**, *53*, 197–214.
(2) Masuda, A.; Qi-Lu *Proc. Jpn. Acad.* **1991**, *67*(B), 134–139.
(3) Yin, Q. Z.; Yamashita, K.; Jacobsen, S. B. *Lunar Planet. Sci.* **2000**, *31*, no. 1920.
(4) Nicolussi, G. K.; Pellin, M. J.; Lewis, R. S.; Davis, A. M.; Amari, S.; Clayton, R. N. *Geochim. Cosmochim. Acta* **1998**, *62*, 1093–1104.
(5) Nicolussi, G. K.; Pellin, M. J.; Lewis, R. S.; Davis, A. M.; Clayton, R. N.; Amari S. *Astrophys. J.* **1998**, *504*, 492–499.
(6) Yin, Q. Z.; Jacobsen, S. B. *Lunar Planet. Sci.* **1998**, *29*, no. 1802.
(7) Yin, Q. Z.; Yamashita, K.; Jacobsen, S. B. *Ninth Annual V. M. Goldschmidt Conference*; Lunar and Planetary Institute: Houston, 1999; LPI contribution no. 971, pp 335–336.
(8) Kawashima, A.; Takahashi, K.; Masuda, A. *Phys. Rev. C* **1993**, *47*, R2452–R2456.
(9) Kawashima, A.; Masuda, A.; Takahashi, K. *Naturwissenschaften* **1995**, *82*, 235–237.
(10) Fujii, T.; Inagawa, J.; Nishizawa, K. *Bull. Chem. Soc. Jpn.* **1999**, *72*, 1219–1223.
(11) Qi-Lu; Masuda, A. *J. Am. Soc. Mass Spectrom.* **1992**, *3*, 10–17.
(12) Qi-Lu; Masuda, A. *Analyst* **1992**, *117*, 869–872.
(13) Kawashima, A.; Takahashi, K.; Masuda, A. *Int. J. Mass Spectrom. Ion. Proc.* **1993**, *128*, 115–121.
(14) Turnlund, J. R.; Keyes, W. R.; Peiffer, G. L. *Anal. Chem.* **1993**, *65*, 1717–1722.
(15) Qi-Lu; Masuda, A. *Int. J. Mass Spectrom. Ion Proc.* **1994**, *130*, 65–72.
(16) Lee, D.-C.; Halliday, A. N. *Int. J. Mass Spectrom. Ion Proc.* **1995**, *146/147*, 35–46.
(17) Wieser, M. E.; De Laeter, J. R. *Int. J. Mass Spectrom.* **2000**, *197*, 253–261.
(18) Qureshi, I. H.; McClendon, L. T.; Lafleur, P. D. *Radiochim. Acta* **1969**, *12*, 107–111.
(19) Kraus, K. A.; Nelson, F.; Moore, G. E. *J. Am. Chem. Soc.* **1955**, *77*, 3972–3977.

10.1021/ac000998g CCC: $20.00
Published on Web 04/26/2001

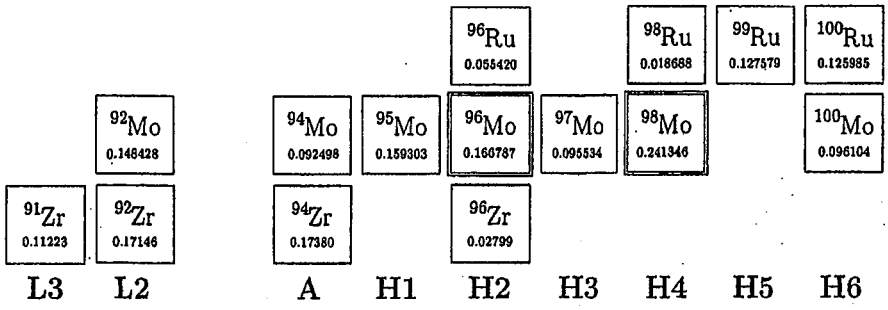

Figure 1. Molybdenum data acquisition scheme. Configuration of the nine Faraday collectors L3, L2, A, and H1–H6 made it possible to measure seven molybdenum isotopes at masses 92, 94–98, and 100 and to monitor zirconium and ruthenium isobaric interferences at masses 91 and 99. Precisely determined isotope abundances[31,32] are reported under nuclide symbols and were used to correct iteratively for interference contributions at masses 92, 94, 96, 98, and 100 and for exponential[26–28] mass fractionation by normalization to $^{98}Mo/^{96}Mo = 1.4470$.

digestion of the samples in a suitable medium,[20] the solution was evaporated to dryness and taken up in 5 mL of perchloric acid ($HClO_4$), 4 M. The solution was poured into a 10-mL polypropylene centrifuge tube where it was equilibrated with 5 mL of HDEHP diluted to 0.72 M with cyclohexane (C_6H_{12}). During this step, the molybdenum was strongly partitioned into the organic phase, while most matrix elements remained in the aqueous phase. The supernatant was hand-pipetted and washed three times with 5 mL $HClO_4$, 4 M, and two times with 5 mL nitric acid (HNO_3), 10 M. Next, molybdenum was back-extracted from the organic phase by two equilibrations with 5 mL HNO_3/hydrogen peroxide (H_2O_2), 10 M/1 M. The back extractant was transferred into a 15-mL Teflon PFA vessel. The solution was doped with 2 mL of H_2O_2, 9.9 M, and baked overnight at 400 K in order to ensure oxidation and subsequent loss of ruthenium and trace organic phases. The back extractant was evaporated to dryness and taken up in 1 mL of hydrofluoric acid (HF)/hydrochloric acid (HCl), 1 M/0.5 M, which was then loaded onto a Bio-Rad Poly-Prep column filled with 0.6 mL (l, 1.2 cm × Ø 0.8 cm) of AG1-X8, 200–400 mesh, chloride-form resin previously washed and conditioned with 5 mL of H_2O; 5 mL of HCl, 6 M; 5 mL of H_2O; 5 mL of HCl, 1 M; 5 mL of H_2O; and finally, 5 mL of HF/HCl, 1 M/0.5 M. Matrix elements were removed using 6 mL of HF/HCl 1 M/0.5 M. Zirconium was eluted with 4 mL of HCl, 6 M. Finally, molybdenum was stripped from the column using 6 mL of HCl, 1 M. The ion exchange step was repeated twice. Molybdenum was then ready for mass spectrometric analysis. The yields were adequate (0.4–1) and the blanks, negligibly small ($<10^{-10}$ mol).

Mass Spectrometry. Molybdenum isotopic analyses were performed on the MC-ICP-Hex-MS operated at the Centre de Recherches Pétrographiques et Géochimiques, Nancy, France. The dry residue that was obtained after chemical treatment was dissolved in HNO_3, 0.15 M, to a molybdenum concentration of 10^{-8} mol·g^{-1}. The solution was drawn into the source through a Teflon TFE tube (l, 75 cm × Ø 0.018 cm) at an uptake rate of 0.07–0.1 mL·min^{-1}, requiring 1 mL of solution per analysis. Aerosols produced in the Meinhard nebulizer (argon flow rate, 1.0 L·min^{-1}) were transferred through a Scott spray chamber to the plasma torch (intermediate argon flow rate; 0.8 L·min^{-1}, cool gas argon flow rate, 13.5 L·min^{-1}; and forward power, 1450 W). Ionized atoms and molecules were extracted into the hexapole cell through a nickel sample cone (Ø 1.1 mm), a nickel skimmer cone (Ø 0.8 mm), and a collimator cone (Ø 2.0 mm). The hexapole lens[21] was a gas-filled (argon flow rate, 1.3 mL·min^{-1}) radio-frequency collision cell that serves to reduce the energy spread of the incident ions[22] and to diminish certain isobaric interferences.[23,24] After passage through the hexapole cell, the ion beam was transferred through a lens system to the analyzer (−6 kV) where the ions were separated according to their mass-to-charge ratios in a field generated by a fast-scanning laminated magnet ($M/\Delta M = 420$). Ion beam intensities were measured on nine carbon-coated Faraday collectors (two on the low-mass side, one in the axis, and six on the high-mass side). Molybdenum isotope (92, 94–98, and 100) abundances were measured on the L2, A, H1, H2, H3, H4, and H6 detectors, and zirconium (90–92, 94, and 96) and ruthenium (96, 98–102, and 104) isobaric interferences were monitored at masses 91 and 99 on the L3 and H5 collectors, respectively (Figure 1). Each measurement (10–15 min) consisted of one block of 20 cycles. Before each run, the magnetic field was adjusted by centering the monitor peak. The ion beam was automatically focused at the beginning of the analysis. Peak intensities were integrated over 14 s. Background intensity was measured during 14 s (7 + 7) at masses free of potential doubly charged interferences (±0.3 amu). Before and after each sample measurement, many Alfa Aesar standard solutions were analyzed at concentrations that were adjusted to match that of the sample within 10%. The mass spectrometer sensitivity was approximately 7×10^{-5} ions analyzed/atom injected.

REFERENCE MATERIAL

External normalization was used in order to determine the composition and atomic mass of molybdenum. An Alfa Aesar solution was doped with the strontium standard reference material SRM 987 from the National Institute of Standards and Technology.[25] Strontium and molybdenum measurements were performed sequentially. In the first instance, strontium isotopes 86 and 88 were measured on H1 and H3 collectors, while krypton interferences were monitored at mass 83 on the L2 collector. Then molybdenum isotopes 96 and 98 were measured on H2 and H4 collectors while zirconium and ruthenium interferences were

(20) Sulcek, Z.; Povondra, P. *Methods of Decomposition in Inorganic Analysis*; CRC Press: Boca Raton, 1989.

(21) Szabo, I. *Int. J. Mass Spectrom. Ion Proc.* **1986**, *73*, 197–235.
(22) Douglas, D. J.; French, J. B. *J. Am. Soc. Mass Spectrom.* **1992**, *3*, 398–408.
(23) Douglas, D. J. *Can. J. Spectrosc.* **1989**, *34*, 38–49.
(24) Rowan, J. T.; Houk, R. S. *Appl. Spectrosc.* **1989**, *43*, 976–980.
(25) Moore, L. J.; Murphy, T. J.; Barnes, I. L.; Paulsen, P. J. *J. Res. Natl. Bur. Stand.* **1982**, *87*, 1–8.

Table 1. Molybdenum Isotope Abundances and Atomic Masses[a]

Audi & Wapstra[34]	92 91.906810	94 93.905087	95 94.905841	96 95.904678	97 96.906021	98 97.905407	100 99.907477	*M*
IUPAC[29,30]	14.84(35)	9.25(12)	15.92(13)	16.68(2)	9.55(8)	24.13(31)	9.63(23)	95.94(1)
Turnlund et al.[14]	14.852(6)	9.266(5)	15.921(3)	16.663(4)	9.565(7)	24.115(5)	9.618(5)	95.930(13)
Qi-Lu & Masuda[15]	14.7287(10)	9.2118(6)	15.8935(11)	16.6731(11)	9.5692(7)	24.2289(17)	9.6950(7)	95.9415(1)
Lee & Halliday[16]	14.8389(5)	9.2484(1)	15.9269(3)	16.6770(4)	9.5528(3)	24.1376(4)	9.6184(2)	95.93101(3)
Wieser & De Laeter[17]	14.769(1)	9.228(1)	15.9022(4)	16.676(7)	9.5618(7)	24.1959(6)	9.6671(4)	95.9377(1)
Dauphas et al.	14.8428(510)	9.2498(157)	15.9303(133)	16.6787(37)	9.5534(83)	24.1346(394)	9.6104(312)	95.9304(45)

[a] A standard solution was doped with the strontium reference material SRM 987 to correct the $^{98}Mo/^{96}Mo$ ratio for exponential mass fractionation by normalizing the $^{88}Sr/^{86}Sr$ ratio to 8.37861(325)[25] and assuming that $\beta_{Mo} = 1(0.1)\beta_{Sr}$. The $^{98}Mo/^{96}Mo$ ratio obtained, 1.4470(17), was then used to correct molybdenum analyses for mass discrimination.[26-28] Uncertainties are 2σ.

monitored at masses 91 and 99 on L3 and H5 collectors, respectively. The certified $^{88}Sr/^{86}Sr$ ratio[25] was used in order to correct the observed $^{98}Mo/^{96}Mo$ ratio for instrumental mass fractionation.[26-28] This ratio was then used as a normalization pair in order to correct molybdenum analyses for mass discrimination. Thus, the abundances of molybdenum isotopes 92, 94–98, and 100 are 14.8428(510), 9.2498(157), 15.9303(133), 16.6787(37), 9.5534(83), 24.1346(394), and 9.6104(312) respectively, resulting in an atomic mass of 95.9304(45). Note that error bars include all sources of uncertainties. These estimates are in agreement with those recommended by the International Union of Pure and Applied Chemistry[29,30] (Table 1).

DATA PROCESSING

Isobaric interferences and mass fractionation were corrected for in an iterative manner. It has been shown that mass fractionation in SIMS, TIMS, and PIMS follows to first order the exponential law,[26-28] which relates the measured ratio (r) to the true value (R) and the relative mass difference ($\Delta M/M$)

$$r = R\,(1 + \Delta M/M)^{\beta}$$

The β factor that was required to normalize the measured $^{98}Mo/^{96}Mo$ ratio to 1.4470 was calculated. This value was used to compute the corresponding fractionated zirconium and ruthenium isotopic ratios using precisely determined literature isotope abundances[31,32] for the unfractionated ratios. Then zirconium and ruthenium interferences on molybdenum isotopes were estimated on the basis of the measured intensities at masses 91 and 99 and the calculated fractionated isotopic ratios. After subtraction of isobaric interferences, molybdenum isotope abundances were corrected for mass fractionation. The new β factor was used in order to recalculate the fractionated zirconium and ruthenium isotopic ratios and the resulting interferences. This correction procedure was iterated until convergence of the molybdenum isotopic composition was attained.

Sample (x) and standard (y) solutions were measured sequentially (5y-x-...-y-x-y-...-x-5y). For each isotope, i, the average ($^i\bar{X}$) of the m sample ratios (^iX) was normalized (ϵ^i) to the average ($^i\bar{Y}$) of the n surrounding standard ratios (^iY). Uncertainties were based on standard replicates and propagated accordingly,

$$\epsilon^i = [{}^i\bar{X}/{}^i\bar{Y} - 1] \times 10^4,$$
$$\sigma(\epsilon^i) = \sqrt{1/m + 1/n}\;\sigma({}^iY)/{}^i\bar{Y} \times 10^4.$$

2. RESULTS AND DISCUSSION

To test the ability of the data reduction program to correct adequately for isobaric interferences, molybdenum standard solutions (10^{-8} mol·g^{-1}) were doped with zirconium and ruthenium at Zr/Mo and Ru/Mo ratios ranging from 0.0001 to 1, approximately. Each interference analysis ($I_0 - I_8$) was bracketed by standard measurements at interference levels close to that of the mass spectrometer background (I_0). The iterative procedure is able to successfully correct for isobaric contributions and mass fractionation up to interference levels as high as 0.01–0.1 (Table 2), which is a major and unexpected result of this work. These levels are much higher than the Zr/Mo and Ru/Mo ratios obtained after chemical treatment. For interference levels higher than 0.01–0.1, the correction procedure breaks down, which may suggest that the exponential law does not adequately correct for mass fractionation or that there are natural isotopic variations of zirconium, molybdenum, or ruthenium.

We measured standard rocks[33] GSD-11 (stream sediment collected from the Shizhuyuan ore field in Binzhou, Hunan province, China), GSD-6 (stream sediment collected from mountainous terrain in Qinghai province, China), GSD-12 (stream sediment sampled from a tributary draining the Yangchun ore field, Guangdong, China), GXR-5 (soil, B zone from Somerset, County, ME), GXR-4 (porphyry copper millhead, Utah), and VS-N (synthetic glass standard, France). If the molybdenum isotopic compositions of terrestrial rocks differ from one another by only mass fractionation, then the isotopic compositions of these samples should be identical when corrected for interference contributions and mass fractionation. This is exactly what is observed (Table 2), which demonstrates that the molybdenum isotopic composition can be measured with high precision in natural samples.

3. CONCLUSIONS

Solvent extraction of molybdenum allows large quantities of sample to be treated. Ion exchange chromatography makes it

(26) Fahey, A. J.; Goswami, J. N.; McKeegan, K. D.; Zinner, E. *Geochim. Cosmochim. Acta* **1987**, *51*, 329–350.
(27) Hart, S. R.; Zindler, A. *Int. J. Mass Spectrom. Ion Proc.* **1989**, *89*, 287–301.
(28) Maréchal, C. N.; Télouk, P.; Albarède, F. *Chem. Geol.* **1999**, *156*, 251–273.
(29) Rosman, K. J. R.; Taylor, P. D. P. *Pure Appl. Chem.* **1998**, *70*, 217–236.
(30) Moore, L. J.; Machlan, L. A.; Shields, W. R.; Garner, E. L. *Anal. Chem.* **1974**, *46*, 1082–1089.
(31) Nomura, M.; Kogure, K.; Okamoto, M. *Int. J. Mass Spectrom. Ion Phys.* **1983**, *50*, 219–227.
(32) Huang, M.; Masuda, A. *Anal. Chem.* **1997**, *69*, 1135–1139.
(33) Govindaraju, K. *Geostand. Newslett.* **1994**, *18*, 1–158.
(34) Audi, G.; Wapstra, A. H. *Nucl. Phys.* **1995**, *A595*, 409–480.

Table 2. Molybdenum Isotope Measurements[a]

			ϵ^i						
	Zr/Mo	Ru/Mo	92	94	95	96	97	98	100
I_0	1.2×1.0^{-4}	6.9×10^{-5}	−0.66 ± 0.83	2.67 ± 3.51	0.52 ± 0.87	0	−0.24 ± 0.33	0	1.79 ± 2.28
I_1	1.0×10^{-3}	6.8×10^{-5}	4.93 ± 6.54	2.32 ± 4.31	0.13 ± 2.97	0	−0.10 ± 0.41	0	1.00 ± 0.48
I_2	2.7×1.0^{-4}	1.1×10^{-3}	1.01 ± 3.35	0.34 ± 1.16	−0.19 ± 0.48	0	0.10 ± 0.39	0	−0.95 ± 1.85
I_3	8.3×10^{-3}	6.3×10^{-5}	3.34 ± 5.11	2.09 ± 1.08	0.12 ± 0.45	0	−0.06 ± 0.27	0	−0.03 ± 0.60
I_4	1.8×1.0^{-4}	1.2×10^{-2}	1.63 ± 3.29	1.65 ± 0.84	0.91 ± 0.50	0	0.32 ± 0.45	0	0.38 ± 1.66
I_5	9.0×10^{-2}	5.6×10^{-5}	−4	8	−1	0	0	0	2
I_6	1.5×1.0^{-4}	1.2×10^{-1}	9	7	6	0	2	0	1
I_7	8.7×10^{-1}	5.7×10^{-5}	−13	106	−23	0	−7	0	16
I_8	1.6×1.0^{-4}	1.5×10^{0}	97	64	49	0	18	0	11
	C, mol·g^{-1}	yield							
GSD-11	6.1×10^{-8}	1	0.34 ± 2.73	−1.40 ± 2.45	0.55 ± 0.54	0	0.47 ± 0.54	0	0.85 ± 0.74
GSD-11	6.1×10^{-8}	0.6	−1.87 ± 3.43	−1.28 ± 1.40	0.14 ± 0.51	0	0.12 ± 0.30	0	0.97 ± 0.85
GSD-6	8.0×10^{-8}	0.8	2.33 ± 5.33	1.00 ± 2.59	0.04 ± 0.66	0	0.00 ± 0.48	0	0.12 ± 1.83
GSD-6	8.0×10^{-8}	0.6	−0.36 ± 1.39	0.11 ± 1.09	0.18 ± 0.49	0	0.00 ± 0.23	0	−0.19 ± 1.40
GSD-12	8.8×10^{-8}	0.6	−1.83 ± 1.35	1.22 ± 2.04	0.13 ± 0.33	0	−0.13 ± 0.70	0	0.03 ± 1.22
GSD-12	8.8×10^{-8}	0.4	−1.97 ± 1.30	−1.05 ± 0.60	0.03 ± 0.31	0	0.31 ± 0.28	0	0.46 ± 1.27
GXR-5	3.2×10^{-7}	0.7	−0.64 ± 0.92	0.24 ± 0.50	0.02 ± 0.36	0	0.07 ± 0.10	0	0.69 ± 0.44
GXR-5	3.2×10^{-7}	0.5	−0.79 ± 1.31	−0.48 ± 0.87	−0.16 ± 0.31	0	0.19 ± 0.23	0	−0.10 ± 0.47
GXR-4	3.2×10^{-6}	0.6	−1.20 ± 5.49	0.69 ± 1.38	0.20 ± 0.59	0	−0.03 ± 0.42	0	0.64 ± 1.91
GXR-4	3.2×10^{-6}	0.6	−0.81 ± 0.75	−0.62 ± 0.44	−0.07 ± 0.27	0	−0.07 ± 0.20	0	0.05 ± 0.46
VS-N	7.3×10^{-6}	0.5	−2.12 ± 2.17	0.18 ± 0.44	−0.21 ± 0.33	0	−0.11 ± 0.16	0	0.95 ± 0.93
VS-N	7.3×10^{-6}	0.6	−1.26 ± 2.04	−0.69 ± 0.94	−0.16 ± 0.43	0	0.04 ± 0.19	0	−0.07 ± 0.32

[a] ϵ^i is defined as $[(^iMo/^{96}Mo)_{sample}/(^iMo/^{96}Mo)_{standard} - 1] \times 10^4$. Molybdenum isotope abundances were corrected for zirconium[31] and ruthenium[32] isobaric interferences by monitoring the ion beam signal at masses 91 and 99 and for exponential mass fractionation[26-28] by normalization to $^{98}Mo/^{96}Mo = 1.4470$. I_0–I_8 correspond to interference analyses. GSD-11, GSD-6, and GSD-12 are stream sediments, GXR-5 is a soil, GXR-4 is a porphyry copper millhead, and VS-N is a synthetic glass standard.[33] Uncertainties are 2σ.

possible to separate molybdenum completely from interfering species. The recent advent of MC-ICP-Hex-MS offers high sensitivity and efficient correction of isobaric interferences. These advances permit natural molybdenum isotope variations to be investigated with unprecedented precision. Important subjects such as inheritance of molybdenum nucleosynthetic anomalies in the solar system, isotope mass fractionation by use of the multiple spike technique, electron capture of the possible extinct radionuclide ^{97}Tc to form ^{97}Mo, production of molybdenum isotopes from fission, anomalous isotope effects, double β decay of ^{96}Zr to form ^{96}Mo, and molybdenum isotope variations resulting from cosmic ray exposure in space can be addressed confidently with this method.

ACKNOWLEDGMENT

We acknowledge an anonymous referee for insightful comments on the manuscript. We thank C. Spatz and X. Frambolsier for technical assistance. This work benefitted from many fruitful discussions with O. Rouxel, J. Carignan, L. Marin, B. Luais, and J. Ludden. D. Yeghicheyan and P. Hild provided analytical support. This work was funded by grants from the PNP (CNES/INSU) and PRISMS SMT4-CT98-2220 (EC). This is CRPG contribution no. 1503.

Received for review August 21, 2000. Accepted March 7, 2001.

AC000998G

Anomalies Héritées et Relations Génétiques

Le monde visible n'est qu'un gigantesque trésor de paraboles, un livre d'images à déchiffrer.

Théodore Monod

L'univers tel que nous le percevons est le résultat d'une maturation lente et complexe de la matière et des structures. Depuis l'atome jusqu'aux super-amas, des motifs sont identifiables qui, répétés à l'infini, rendent compte de l'organisation à grande échelle du monde (figure 1). A une échelle mégascopique, l'espace est organisé en Galaxies qui sont elles mêmes divisées en systèmes stellaires similaires à celui qui nous abrite, le système solaire. Comprendre comment le système solaire s'est formé c'est également comprendre comment et pourquoi la matière s'organise.

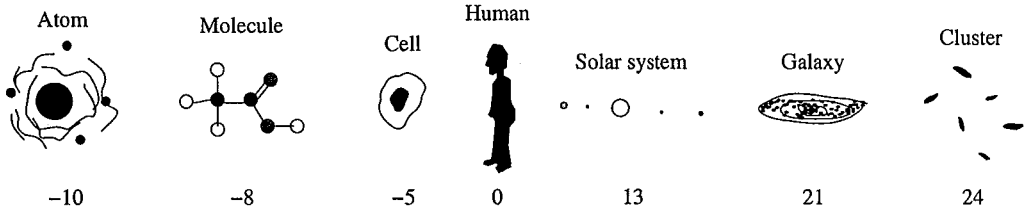

FIG. 1 – Echelles d'organisation de la matière. La dimension est indiquée en puissance de 10 mètres.

Le système solaire s'est vraisemblablement formé dans un nuage moléculaire par effondrement gravitationnel. La composition du milieu interstellaire à partir duquel le système solaire s'est constitué résulte d'une évolution lente et complexe de la matière. Lors du Big-Bang, seuls l'hydrogène et l'hélium ont été synthétisés (*nucléosynthèse cosmologique*), la plupart des *métaux* (dans l'acception astrophysique Z>2) ont été synthétisés au coeur des étoiles (*nucléosynthèse stellaire*). Les générations successives d'étoiles ont ainsi fourni les ingrédients qui ont servi à la formation du système solaire. Cette lente maturation est désignée sous le vocable d'*évolution chimique de la Galaxie*. La formation du système solaire constitue un instantané et intègre dans sa composition l'évolution chimique de la Galaxie dans le voisinage solaire. Une des questions clés de la cosmochimie à l'heure actuelle se rapporte à l'hétérogénéité chimique et isotopique de la nébuleuse protosolaire. Dans quelle mesure la nébuleuse était-elle hétérogène ? Cette hétéro-

généité resulte-t-elle d'un héritage présolaire (hétérogénéité du nuage moléculaire dans lequel le système solaire s'est formé) ou de processus nébulaires (tri granulométrique ou découplage gaz-poussière) ? Le molybdène est particulièrement adapté pour discuter la question de l'héritage présolaire de la nébuleuse et de son hétérogénéité. En effet, des anomalies nucléosynthétiques ont été observées dans des grains présolaires qui se sont vraisemblablement condensés dans les enveloppes d'étoiles massives de type AGB au sein desquelles se développe une nucléosynthèse de type *s*.

1 Hétérogénéité de la nébuleuse

La planète sur laquelle nous vivons est un objet différencié. Sa composition ne reflète pas fidèlement les propriétés physiques et chimiques des planétésimaux précurseurs. En effet, la composition élémentaire de la terre a été largement modifiée par la ségrégation du noyau et l'extraction crustale. Les météorites sont de ce point de vue des objets précieux pour discuter l'hétérogénéité de la nébuleuse. Les datations effectuées sur ces objets indiquent un âge de 4.56 Ga, contemporain de la formation du système solaire. Les météorites représentent donc des sondes temporelles qui nous permettent d'explorer les propriétés de la nébuleuse protosolaire pour une large gamme de distances héliocentriques.

1.1 Structurale

La plupart des météorites indifférenciées contiennent des chondres qui sont des petites billes silicatées [32, 33]. C'est la présence de ces sphères qui confère aux météorites primitives le nom de chondrites. Le schéma de formation des chondres est débattu et plusieurs modèles coexistent pour rendre compte de la présence de ce composant dans les météorites. La dimension des chondres [33] varie d'un groupe de météorites à un autre de 0.1 à 1 mm en moyenne (tableau 1). La distribution en taille des chondres peut être contrôlée par (*i*) des mécanismes directement liés aux processus de formation ou (*ii*) des processus de tri par transport posterieurs à la formation. Dans tous les cas, la variabilité du diamètre des chondres manifeste une hétérogénéité structurale de la nébuleuse protosolaire.

1.2 Chimique

Le message porté par les météorites est en partie obscurci par les processus secondaires qui les ont affectés comme le métamorphisme thermique, l'altération aqueuse sur le corps parent, les chocs, et l'altération sur terre. Des critères permettent de reconnaître et de quantifier ces processus secondaires et constituent ainsi des outils de taxonomie. Le degré de métamorphisme qu'ont subi les météorites est représenté par un indice croissant de 3 à 6 [64, 32]. Le degré d'altération aqueuse sur le corps parent est quantifié par chiffre décroissant de 1 à 3 [32]. Le degré de choc est décrit par un indice S croissant de 0 à 5 [65]. Le degré d'altération terrestre W est indicé sur une échelle croissante de 0 à 6 [66]. L'ensemble de ces critères ne permet pas de rendre compte de la diversité des assemblages observés. Une part importante de l'hétérogénéité provient de l'environnement et des mécanismes qui ont présidé à la formation des premiers solides dans la nébuleuse [64, 32]. La position des différents groupes de météorites dans un diagramme de Urey-Craig (% Fe dans Fe^0+FeS en fonction de % Fe dans FeO ; figure 2) permet d'apprécier l'hétérogénéité chimique de la nébuleuse [32, 33]. Dans une telle représentation, les objets qui contiennent la même quantité de fer s'alignent sur des droites de pentes -1 en fonction de la spéciation plus ou moins réduite du fer. Les météorites forment dans ce diagramme des groupes

distincts illustrant l'hétérogénéité des régions sources du point de vue de la composition (teneur en fer) et de la fugacité en oxygène (spéciation du fer). Les mécanismes qui sont intervenus dans la différentiation chimique de la nébuleuse ne sont pas complètement compris. Cette hétérogénéité chimique est accompagnée d'une hétérogénéité isotopique qui suit une dépendance à la masse et que nous n'aborderons pas.

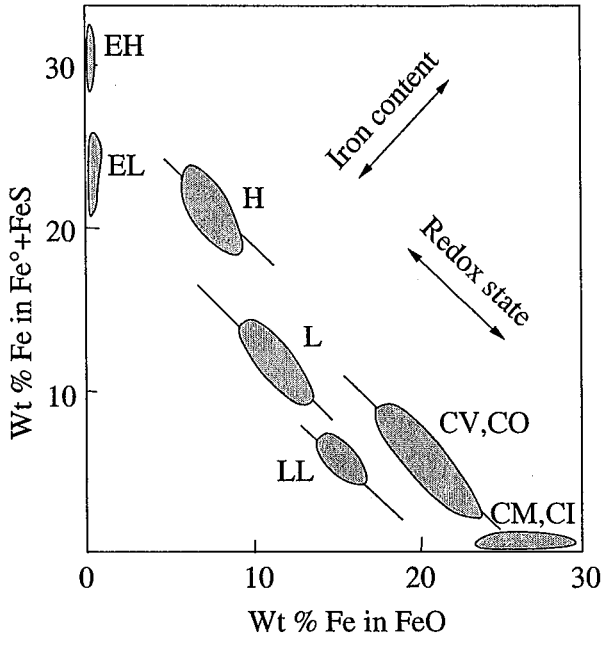

FIG. 2 – Diagramme de Urey-Craig permettant la classification des météorites selon un critère chimique. Les points qui s'alignent sur des droites de pentes -1 ont une concentration identique en fer. La position selon ces segments dépend de la spéciation du fer (oxydé ou réduit) et permet ainsi de discuter l'état redox des météorites [32, 33].

1.3 Isotopique

Après correction des effets nucléaires et du fractionnement de masse, il subsiste des variations de composition isotopique pour un nombre d'éléments restreint. Ces variations sont relativement rares dans la nature et sont qualifiées d'*anomalies*. La meilleure illutration est fournie par l'oxygène qui possède trois isotopes (16, 17, et 18) et est très abundant. Si seule une dépendance à la masse contrôlait la composition isotopique de l'oxygène, alors dans un diagramme $\delta^{17}O$ en fonction de $\delta^{18}O$, les points représentatifs des météorites devraient s'aligner sur une droite de pente 0.5 car l'écart de masse entre les isotopes 18 et 16 dont le rapport sert à former $\delta^{18}O$ est le double de l'écart de masse entre les isotopes 17 et 16. A l'exception de quelques très rares cas, tous les échantillons terrestres s'alignent sur une telle droite ; la droite de fractionnement terrestre. En fait, certaines météorites primitives ne s'alignent pas sur une droite de fractionnement (figure 3) mais plutôt sur une droite de pente 1 dont l'un des termes est l'oxygène 16 pur [34]. Deux écoles s'affrontent pour expliquer ces anomalies. L'une invoque un héritage présolaire [34] tandis que l'autre fait appel à des phénomènes de fractionnement non dépendants de la masse [67, 68].

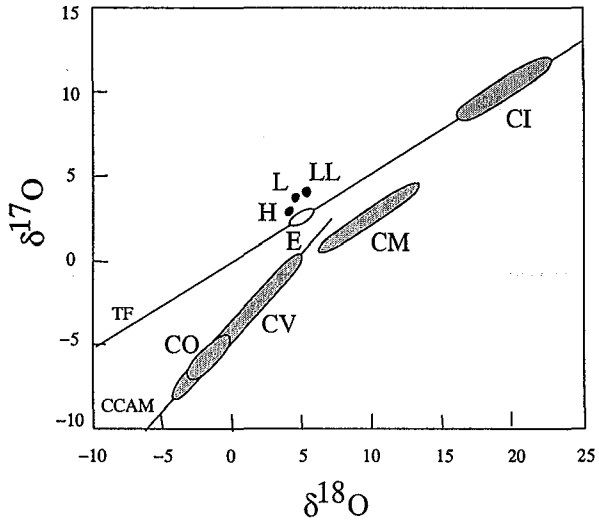

FIG. 3 – Composition isotopique de l'oxygène dans les différents types de chondrites [34, 33]. La droite de fractionnement terrestre (TF) et la droite de pente 1 (CCAM) sont indiquées. Si tous les échantillons dérivaient entre eux par simple fractionnement de masse, alors les points représentatifs de ces objets devraient s'aligner sur une doite de pente 0.5 (parallèle à la droite de fractionnement terrestre).

Le modèle d'héritage défendu en particulier par le découvreur des anomalies [34] postule qu'un composant très enrichi en ^{16}O a été incorporé dans le système solaire au moment de sa formation qui ne s'est par la suite jamais homogénéisé avec le reste de la nébuleuse. Le composant enrichi en ^{16}O issu d'une nucléosynthèse stellaire aurait été porté par la poussière tandis que le gaz aurait eu une composition uniforme. Le mélange de ces deux composants dans des proportions variables expliquerait la dispersion suivant la droite de pente 1 des météorites.

Le modèle des fractionnements non dépendants de la masse repose sur l'observation que certaines réactions chimiques sur terre comme $O + O_2 \rightarrow O_3$ conduisent à des fractionnements non dépendants de la masse qui s'alignent selon une droite de pente 1 [67]. L'assise théorique de ces effets est incertaine mais certains modèles récents semblent pouvoir rendre compte de tels effets [69, 70, 68]. Même s'il est acquis que dans certaines conditions, des réactions d'échange isotopique induisent un fractionnement non dependant de la masse (ou *nomade* pour non-mass dependent effect), il reste à identifier un environnement dans la nébuleuse où de telles réactions auraient pu se développer.

1.4 Taxonomie

L'hétérogénéité intrinsèque ou héritée de la nébuleuse qui se manifeste dans les caractéristiques physiques et chimiques des météorites permet de discuter les relations génétiques des différents objets planétaires et de mettre en place une taxonomie. Les critères qui permettent de classer les météorites sont regroupés dans le tableau 1.

Cette taxonomie doit avoir des raisons génétiques et chaque groupe représente vraisemblablement un corps parent distinct (figure 4). La plupart des critères de classification sont effacés par les processus secondaires qui ont pu affecter les planétésimaux. Dans le cas le plus extrême d'une

	Chondrule (vol%)	Matrix (vol%)	Refractory inclusion (vol%)	Metal (vol%)	Chondrule diameter (mm)	Mg/Si (a/a)	Ca/Si (a/a)	Fe/Si (a/a)	Fa (mol%)	Co kamacite (mg/g)	Fe_{met}/Fe_{tot}	$\delta^{18}O$ (‰)	$\delta^{17}O$ (‰)
CI	<< 1	> 99	<< 1	0	-	1.05	0.064	0.86	-	-	0	16.4	8.8
CM	20	70	5	0.1	0.3	1.05	0.068	0.80	-	-	0	12.2	4.0
CO	48	34	13	1-5	0.15	1.05	0.067	0.77	-	-	0-0.2	-1.1	-5.1
CV	45	40	10	0-5	1.0	1.07	0.084	0.76	-	-	0-0.3	0	-4
H	60-80	10-15	0.1-1 ?	10	0.3	0.96	0.05	0.81	16-20	5.2	0.58	4.1	2.9
L	60-80	10-15	0.1-1 ?	5	0.7	0.93	0.046	0.57	23-26	10.6	0.29	4.6	3.5
LL	60-80	10-15	0.1-1 ?	2	0.9	0.94	0.049	0.52	27-32	22.9	0.11	4.9	3.9
EH	60-80	<2-15 ?	0.1-1 ?	8	0.2	0.77	0.035	0.95	-	-	0.76	5.6	3.0
EL	60-80	<2-15 ?	0.1-1 ?	15	0.6	0.83	0.038	0.62	-	-	0.83	5.3	2.7

TAB. 1 – Caractéristiques physiques, chimiques, et isotopiques des principaux types de chondrites [32, 33].

planète différenciée comme la terre, les structures ont été complètement effacées par les processus de fusion et d'altération, les éléments sidérophiles ont été extraits dans le noyau, les éléments atmophiles ont été dégazés puis perdus dans l'espace, la composition des éléments réfractaires a été brouillée par les processus magmatiques comme l'extraction crustale. Au total, tous les critères structuraux et chimiques ont été effacés et seuls subsistent les traceurs isotopiques. La composante des variations isotopiques qui revient au fractionnement de masse n'est pas utile car elle peut être modifiée également par les processus secondaires sus-cités. Ainsi, les anomalies isotopiques consitituent un matériau de choix pour discuter des éventuelles relations génétiques entre les différents objets planétaires. De ce point de vue, l'oxygène a joué un rôle très important [34, 32, 33, 14]. Malheureusement, il ne permet pas d'apprécier les filiations avec, et entre, les objets qui ne portent pas d'oxygène comme les météorites de fer [14].

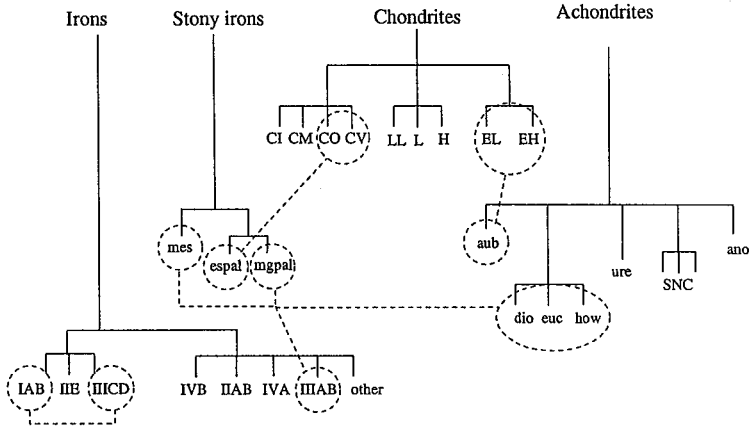

FIG. 4 – Classification des météorites. Les relations structurales et chimiques sont indiquées en traits pleins. Les relations génétiques supplémentaires entre groupes distincts sont indiquées en traits discontinus. mes- mésosidérite, espal- pallasite du groupe eagle station, mgpal- pallasite du groupe principal, aub- aubrite, dio- diogénite, euc- eucrite, how- howardite, ure-ureilite, snc-mars, ano- lune [32, 14].

2 Nucléosynthèse stellaire et grains présolaires

Les *métaux* ont été synthétisés pour la plupart au coeur des étoiles dans notre Galaxie. La formation d'une étoile soustrait de la matière au milieu interstellaire. A la fin de son évolution, l'étoile éjecte la matière nucléaire qui a été modifiée en son sein. Ce processus a permis la synthèse des éléments lourds constitutifs des planètes et des êtres animés. La nucléosynthèse qui se développe dans les étoiles peut être examinée à distance par spectroscopie. Ainsi, la preuve la plus évidente d'une nucléosynthèse stellaire active nous est donnée par l'observation de la raie du technetium dans le spectre de certaines étoiles [71]. Le ^{99}Tc est radioactif à courte période et devrait être absent des spectres s'il n'était pas produit *in situ*. Les mesures spectroscopiques bien que précieuses n'offrent cependant pas une résolution suffisante pour apprécier les subtilités de la nucléosynthèse stellaire. Les grains présolaires isolés dans les météorites primitives constituent ainsi des témoins privilégiés de cette nucléosynthèse.

2.1 Nucléosynthèse stellaire du molybdène

Depuis le travail inaugural de B^{2}FH [72] et Cameron [73], il semble acquis que trois mécanismes ont contribué à la nucléosynthèse des éléments lourds ; les processus s, r, et p (figure 5).

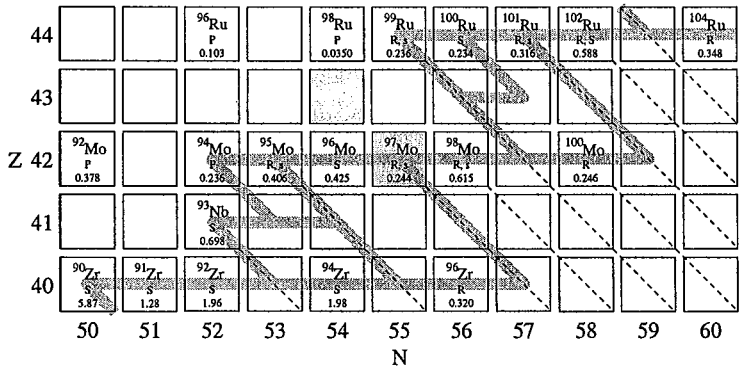

FIG. 5 – Table des nucléides dans la région du molybdène. Le chemin de la nucléosynthèse de type s est indiqué en grisé [35]. Les chemins de décroissance β des progéniteurs du processus r sont représentés en traits discontinus. Les nucléides qui ne sont produits ni par le processus s ni par le processus r (à gauche de la vallée de stabilité β) sont produits par le processus p.

Processus s

Depuis la découverte du technétium [71, 74, 75, 76, 36, 77] dans les enveloppes de géantes rouges pulsantes (thermally pulsing asymptotic giant branch, TP-AGB), ces étoiles ont été identifiées comme étant le site principal de la nucléosynthèse de type s [72, 73, 78, 37, 79, 35]. Le processus s (où s désigne *slow*) est un processus de capture neutronique lente. Dans la couche helium des étoiles TP-AGB, des instabilités appelées *pulsations thermiques* se développent périodiquement qui fournissent un environnement propice à la nucléosynthèse des nucléides de type s. Les éléments au delà du fer captent les neutrons pourvus par les réactions ^{22}Ne$(\alpha,\mathrm{n})^{25}$Mg et ^{13}C$(\alpha,\mathrm{n})^{16}$O. Le taux de capture est faible en regard du taux de décroissance β, de sorte que le chemin de la nucléosynthèse suit étroitement la vallée de stabilité β ; $\beta > (n,\gamma)$. Ceci

implique que la densité neutronique a dû être relativement faible, de l'ordre de 10^8 cm^{-3} pour une température de 4×10^8 K [79].

Il est intéressant de noter que la présence ou l'absence de technétium constitue un critère pour distinguer les étoiles qui sont intrinsèquement ou extrinsèquement enrichies en nucléides s [74, 75, 76, 36, 77]. Les étoiles de type S sont les étoiles qui présentent dans leur spectre un enrichissement en éléments produits par le processus s de nucléosynthèse. Certaines de ces étoiles sont le siège d'une nucléosynthèse active (intrinsèque) tandis que d'autres correspondent à des systèmes binaires où l'étoile observée a reçu une contribution de l'étoile compagne (une ancienne étoile de type TP-AGB devenue une naine blanche indétectable). Comme le ^{99}Tc est un radionucléide à courte demi-vie ($T_{1/2} = 2.13 \times 10^5$ a dans les conditions de laboratoire), il est absent des systèmes binaires mais est présent dans les étoiles où se développe une nucléosynthèse active. Il permet ainsi de reconnaitre les étoiles qui sont intrinsèquement ou extrinsèquement riches en éléments produits par le processus s (figure 6).

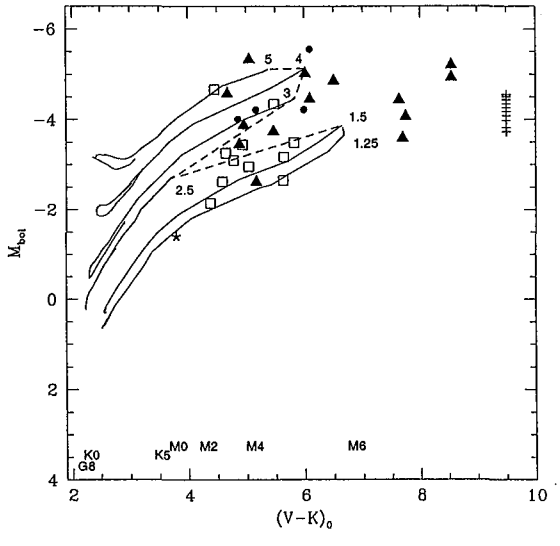

FIG. 6 – Diagramme de Hertzsprung-Russel (magnitude bolométrique en fonction d'un indice de couleur) des étoiles de type S. Les triangles pleins correspondent aux étoiles riches en technétium tandis que les carrés vides correspondent aux étoiles pauvres en technétium. Les courbes représentent le chemin des étoiles AGB jusqu'à la première pulsation thermique. Pour guider les yeux, un trait en pointillés connecte les lieux du début de la phase TP-AGB sur les différents chemins [36].

Des modèles simples ont été employés pour décrire le processus-s qui gardent toujours un intérêt heuristique. Le plus simple d'entre eux est l'approximation locale [37, 79, 80]. On suppose qu'il n'existe pas de compétition entre le taux de décroissance β et le taux capture neutronique (pas de branchement) ; $\beta > (n, \gamma)$. Dans ces conditions on a simplement,

$$\frac{\mathrm{d}N_i}{\mathrm{d}t} = -n_n < \sigma_i v >_{\mathrm{T}} N_i + n_n < \sigma_{\mathrm{i}-1} v >_{\mathrm{T}} N_{i-1}, \qquad (1)$$

où N_i est l'abondance d'un nucléide de masse i, n_n est la densité neutronique, $< \sigma_i v >_{\mathrm{T}}$ est la section de capture neutronique pour i intégrée sur une distribution maxwellienne des vitesses

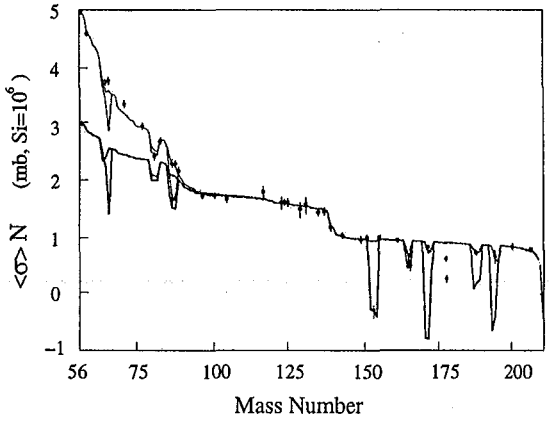

FIG. 7 – Abondances des nucléides produits par le *s*-process. La superposition des composants *principal* (*main*, trait épais) et *mineur* (*weak*, trait fin) permet de rendre compte des abondances observées.

thermiques v. On définit la grandeur $< \sigma_i >=< \sigma_i v >_T / v_T$ qui est indépendante de la température pour les nucléides non magiques. On introduit alors l'exposition neutronique (τ) définie comme,

$$\tau = \int v_T n_n \, dt. \tag{2}$$

Il vient alors,

$$\frac{dN_i}{d\tau} = - < \sigma_i > N_i + < \sigma_{i-1} > N_{i-1}, \tag{3}$$

Lorsque l'équilibre entre production et destruction est atteint, on perd la dépendance au temps et il vient,

$$< \sigma_i > N_i \simeq < \sigma_{i-1} > N_{i-1}. \tag{4}$$

Cette relation est vraie pour une gamme de masse restreinte et porte donc le nom d'approximation locale. On peut ainsi facilement estimer la contribution du processus *s* sur chacun des isotopes du molybdène en utilisant les sections de capture [79] et le fait que le ^{96}Mo est un pur nucléide *s* ($< \sigma_i > N_i =< \sigma_{96} > N_{96}$; tableau 2). Un modèle plus réaliste [78, 37, 79] tient compte d'une exposition neutronique exponentielle donnée par la distribution de probabilité,

$$p(\tau) = e^{-\tau/\tau_0} \, d\tau/\tau_0. \tag{5}$$

L'abondance d'un nucléide pour une telle exposition est simplement,

$$\overline{N}_i = \int_0^\infty N_i(\tau) p(\tau) \, d\tau. \tag{6}$$

A partir de l'équation différentielle initiale (3), il vient,

$$\int_0^\infty \frac{dN_i}{d\tau} \frac{e^{-\tau/\tau_0}}{\tau_0} d\tau = - < \sigma_i > \overline{N}_i + < \sigma_{i-1} > \overline{N}_{i-1}. \tag{7}$$

En intégrant le terme de gauche par parties, on montre,

$$-N_i(0)/\tau_0 + \overline{N}_i/\tau_0 = - < \sigma_i > \overline{N}_i + < \sigma_{i-1} > \overline{N}_{i-1}. \tag{8}$$

En fixant $N_{56}(0) = 1$ et $N_{i\neq 56}(0) = 0$, il vient simplement,

$$< \sigma_k > \overline{N}_k = \frac{1}{\tau_0} \prod_{i=56}^{k} \left(\frac{1}{\tau_0 < \sigma_i >} + 1 \right)^{-1}. \quad (9)$$

Ce développement constitue la base de ce que l'on appelle l'approche classique [78, 37, 79]. Les abondances de la majeure partie des nucléides s peuvent être reproduites dans le cadre d'un tel modèle pour une température T_8 de 2.8-3.9 (T_k est la température en 10^k K) et une densité neutronique n_n de $2.3 - 4.5 \times 10^8$ cm^{-3} [79]. En fait, deux expositions sont nécessaires pour rendre compte des abondances des s-nucléides sur l'ensemble du spectre de masse (figure 7). Ces deux expositions sont appelées *principale* (*main*) et *mineure* (*weak*). La contribution de la composante mineure sur les isotopes du molybdène est faible [79].

Les calculs les plus récents intégrent la nucléosynthèse de type s dans un modèle d'évolution stellaire qui définit plutôt un chemin temps-densité neutronique-température-composition [35, 42]. Les abondances du processus s dérivées à partir de l'approximation locale et du modèle classique sont compilées dans le tableau 2 et ne sont pas très différentes de celles obtenues dans le cadre d'un modèle d'évolution stellaire. Ces estimations sont également en parfait accord avec les abondances dérivées des mesures de grains présolaires de carbure de silicium et de graphite [6, 7, 22].

	92	94	95	96	97	98	100
Process	*P*	*P*	*R, s*	*S*	*R, s*	*R, s*	*R*
$< \sigma >$ (mb)	-	-	333 ± 14	128 ± 9	387 ± 16	113 ± 8	
Solar (atoms/10^6Si)	0.378	0.236	0.406	0.425	0.244	0.615	0.246
s (local approximation)	0	0	0.163 ± 0.013	**0.425**	0.141 ± 0.011	0.481 ± 0.048	0
s (classical approach)	0	0	0.189 ± 0.008	0.475 ± 0.033	0.156 ± 0.006	0.514 ± 0.036	0
s (stellar model)	0.000	0.002	0.225	0.451	0.143	0.466	0.009
s (circumstellar grains)	0	0.014 ± 0.002	0.169 ± 0.05	**0.425**	0.134 ± 0.004	0.446 ± 0.009	0.001 ± 0.002
p (residuals)	0.378	0.222	0	0	0	0	0
r (residuals)	0	0	0.237	0	0.110	0.169	0.245

TAB. 2 – Contribution des processus s, p, et r aux abondances cosmiques des isotopes du molybdène. Les sections de capture neutronique sont extraites de [79]. Les abondances solaires sont compilées par [3]. Dans le cas du molybdène, les abondances estimées à partir de l'approximation locale [79], de l'approche classique [79], et du modèle d'évolution stellaire [35] sont en parfait accord avec les abondances dérivées des grains circumstellaires [6, 7]. Les abondances des processus p et r (residuals) sont obtenues par soustraction des abondances du processus s (circumstellar grains) à la composition solaire (solar).

Processus r

Les nucléides produits par le processus r de nucléosynthèse jouissent d'une position particulière car la plupart des chronomètres utilisés pour discuter l'âge de la Galaxie sont des nucléides r [81, 82, 83]. Certains isotopes riches en neutrons ne sont pas sur le chemin du processus s (figure 8). Ces nucléides ainsi que les espèces nucléaires au delà de ^{209}Bi sont produits par un processus de capture neutronique rapide (processus r). Les abondances des produits du processus r sont obtenues par soustraction des produits du processus s aux abondances solaires (tableau 2). Contrairement au processus s, on considère que les taux de capture ou de photoejection sont très supérieurs au taux de décroissance β ; $\beta < (n,\gamma), (\gamma,n)$. Ainsi, le chemin du process r est décalé

à droite de la vallée de stabilité β (figure 8). Les densités neutroniques et températures mises en jeu sont de l'ordre de $n_n = 10^{24}$ cm^{-3} et $T_9 = 1$ [37]. A mesure que les nucléides captent des neutrons (pour Z fixé), l'énergie de liaison diminue et la réaction inverse entre en compétition. L'énergie de liaison des neutrons est ainsi réduite jusqu'au point d'attente (*waiting – point*) où la photoéjection compense la capture neutronique $(n,\gamma) \rightleftharpoons (\gamma,n)$. Le lieu des nucléides pour lesquels il y a compensation correspond à une énergie de liaison donnée et définit le chemin du processus r. Le r-process pourrait se développer dans (*i*) les supernovae de type II (SNII) ou (*ii*) les étoiles à neutrons coalescentes (neutron star mergers). Les radioactivités éteintes semblent indiquer que plusieurs sources ont contribué à la synthèse des nucléides r du système solaire [84, 85]. En effet, les abondances du ^{129}I et du ^{182}Hf mesurées ne sont réconciliables avec ce que l'on comprend de l'évolution chimique de la Galaxie que si ces deux radionucléides ont été synthétisés dans des environnements stellaires distincts.

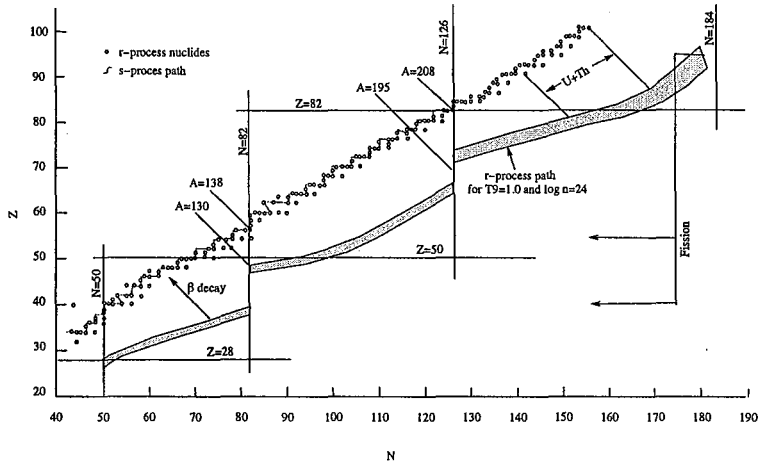

FIG. 8 – Chemin de capture neutronique des processus s et r. Le processus s suit un chemin dans le plan NZ selon la ligne de stabilité β. Les progéniteurs des nucléides r sont formés dans une bande située dans la région riche en neutrons de l'espace NZ. Le chemin du processus r indiqué a été calculé pour $T_9 = 1.0$ et log $n_n = 24$. Après synthèse dans cette bande, les nucléides décroissent pour retourner sur la vallée de β-stabilité. Les pics d'abondance à A=80, 130, et 195 sont attribués à la présence de pics d'abondance pour les progéniteurs à N=50, 82, et 126 [37].

Processus p

Certains nucléides qui se trouvent à gauche de la vallée de stabilité β (figure 5) ne sont produits ni par le processus s ni par le processus r mais pas un processus rare appelé p pour proton car les nucléides qui sont synthétisés par ce processus sont riches en protons. La nucléosynthèse de type p ne procède pas par captures protoniques (p,γ) [72, 86, 87] mais plutôt par photodésintégrations (γ,n) [88, 89, 90, 91, 92, 93, 94, 38] à partir de nucléides germes produits par le processus s de nucléosynthèse. Les conditions favorables au développement des réactions de photodésintégrations (γ-process) semblent être réunies dans les couches O-Ne des supernovae de type II où la température T_9 est de l'ordre de 2-3. Les modèles les plus récents intégrent la synthèse de type p dans un modèle d'évolution stellaire et prennent en compte l'ensemble des réactions impliquées dans un réseau composé de plusieurs milliers de nucléides [38]. Ces modèles

réussissent à rendre compte des abondances solaires pour la plupart des nucléides excepté ceux de la région du molybdène. Dans tous les modèles de SNII, les isotopes du molybdène et du ruthénium produits par le processus p de nucléosynthèse (^{92}Mo, ^{94}Mo, ^{96}Ru, et ^{98}Ru) sont déficients. Il a été proposé par Costa *et al.* [95] que cet échec résultait des incertitudes qui pèsent sur le taux de la réaction ^{22}Ne$(\alpha, n)^{25}$Mg. Le taux de cette réaction source de neutrons a en effet une grande influence sur les abondances des nucléides germes produits par le processus s. Les études récentes de nucléosynthèse dans les SNII [38] ne semblent pas corroborer cette possibilité car d'autres nucléides plus légers sont alors produits dans des abondances qui ne sont plus solaires (figure 9). Les supernovae de type Ia ne semblent pas être capables de résoudre le problème du déficit des isotopes de Mo et Ru.

Dans les systèmes binaires X, une étoile à neutron capte de l'hydrogène et de l'hélium de l'enveloppe d'une étoile compagne. A la surface des étoiles à neutrons, l'hydrogène présent peut fusionner pour former des nucléides plus lourds par captures protoniques rapides (processus *rp* pour *rapid proton capture*). Les binaires X sont ainsi susceptibles de synthétiser les éléments [96] jusqu'au cycle SnSbTe qui termine le processus *rp* [97]. Ils pourraient donc rendre compte des abondances des isotopes du molybdène et du ruthénium sans modifier les abondances des éléments plus lourds. La principale difficulté qui pèse sur ce scénario est de savoir comment la matière synthétisée dans les binaires X peut être rendue au milieu interstellaire. En somme, la synthèse des isotopes p du molybdène et du ruthénium (^{92}Mo, ^{94}Mo, ^{96}Ru, et ^{98}Ru) demeure un mystère et représente une des grandes questions qui reste posée aux astrophysiciens nucléaires.

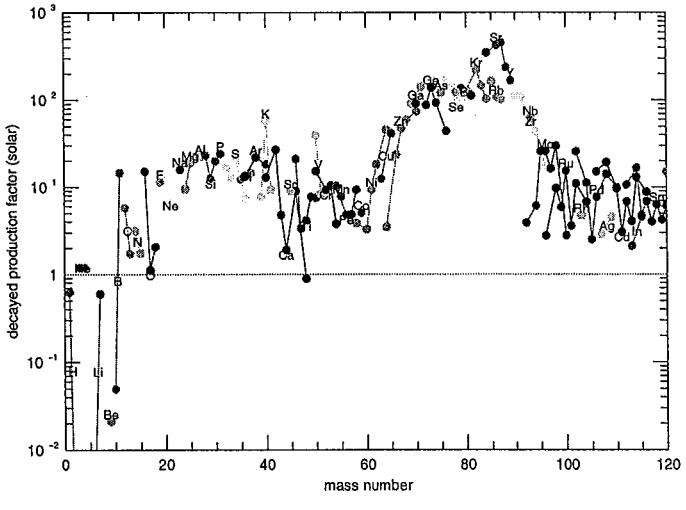

FIG. 9 – Facteurs de production par rapport aux abondances solaires dans une étoile de 25 $M_\odot$ pour un taux de réaction ^{22}Ne$(\alpha, n)^{25}$Mg pris à la marge supérieure de l'intervalle admis [38]. Les nucléides ^{92}Mo, ^{94}Mo, ^{96}Ru, et ^{98}Ru sont produits dans les bonnes proportions par rapport à ^{16}O mais d'autres espèces nucléaires sont co-produites en trop grande quantité.

2.2 Grains circumstellaires

Le spectre des étoiles porte des informations sur leur composition et donc sur la nucléosynthèse qui s'y développe. Deux limitations importantes s'imposent pour discuter des processus nucléosynthétiques à partir de spectres lumineux. D'abord, l'observation à distance des étoiles n'offre des renseignements que sur la composition de surface des astres. Ensuite, les précisions des mesures isotopiques et élémentaires sont très limitées. Des informations complémentaires sont offertes par les grains circumstellaires isolés dans les météorites primitives [98].

Caractérisation

Les grains présolaires sont définis comme étant des solides du milieu interstellaire qui ont été incorporés au système solaire sans subir de modifications. Certains de ces grains ont pu se former dans le nuage moléculaire parent du système solaire à partir d'un gaz homogène. D'autres se sont formés dans les enveloppes d'étoiles et on parle alors de grains circumstellaires [39, 5, 99, 40]. La présence de grains circumstellaires (figure 10) dans les météorites a été mise en évidence historiquement par l'analyse de la composition isotopique des gaz rares dans les météorites primitives. La séparation des grains présolaires a procédé d'abord par attaque sélective des météorites pour ne retenir que les phases les plus résistantes aux acides. Certaines de ces phases se sont révélées être des condensats circumstellaires porteurs des anomalies observées pour les gaz rares. Cette approche a permis de mettre en évidence trois phases circumstellaires, les nanodiamants, les carbures de silicium, et les grains de graphite [5, 99]. Plus récemment, les outils d'imagerie isotopique ont permis de révéler la présence d'autres phases comme le corindon [100] et un nitrure de silicium [101]. En fonction de leurs compositions, il est possible de reconnaître la nature de l'astre au sein duquel les grains circumstellaires se sont condensés. Les grains de carbure de silicium et de graphite contiennent en inclusions des carbures de titane, zirconium, et molybdène [41].

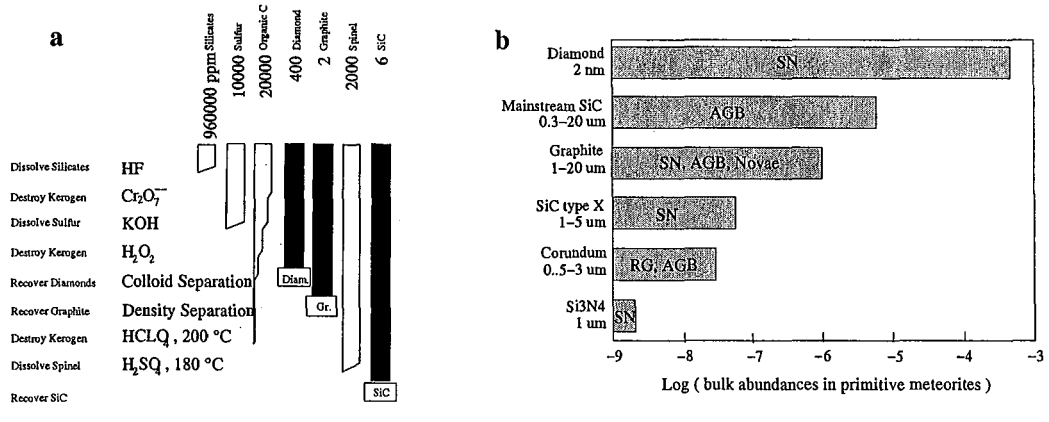

FIG. 10 – **a-** Isolement de grains circumstellaires par attaques chimiques [39]. **b-** Types de grains circumstellaires identifiés jusqu'à présent dans les météorites [40]. Leurs abondances (fraction en masse), tailles, et sources stellaires sont indiqués. Les grains de graphite et de carbure de silicium contiennent en inclusions des sous-grains de carbures de titane, zirconium, et molybdène [41].

Anomalies nucléosynthétiques du molybdène

La majorité des grains de carbure de silicium et de graphite se sont formés dans les enveloppes d'étoiles TP-AGB, sièges de la nucléosynthèse de type *s*. Ces grains portent des signatures isotopiques héritées de l'environnement nucléosynthétique dans lequel ils se sont formés. Ils sont donc enrichis en nucléides produits par le processus *s*. La composition isotopique du molybdène a été déterminée *in situ* dans des grains de graphite et de SiC grâce à l'instrument CHARISMA mis au point au Argonne National Laboratory [6, 7, 8, 9]. Un faisceau laser focalisé sur la surface de l'échantillon génère un panache contenant des ions, des atomes, et des molécules. Les ions positifs sont supprimés par application d'un champ électrostatique pulsé devant la cible. Les espèces neutres atomiques et moléculaires sont ensuite sélectivemment ionisées par des faisceaux lasers convergents. Les ions ainsi produits sont analysés par un spectromètre de masse à temps de vol. Cet instrument offre une très grande sensibilité et permet, par le jeu de la ionization sélective, de s'affranchir des interférences isobariques possibles du zirconium et du ruthénium sur le molybdène.

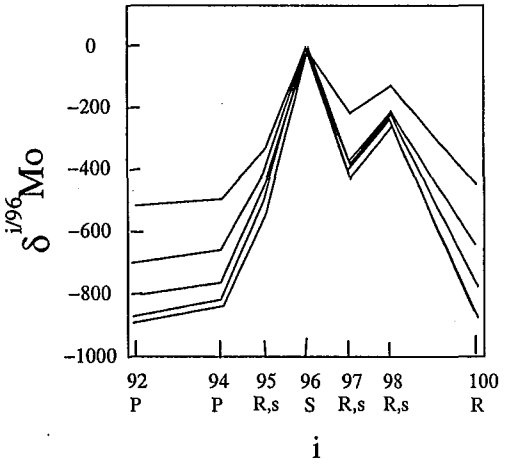

FIG. 11 – Composition isotopique typique du molybdène dans quelques grains circumstellaires de carbure de silicium [6]. Le spectre obtenu correspond à un enrichissement en nucléides produits par le processus *s* de nucléosynthèse [6, 42].

La composition isotopique du molybdène mesurée dans les grains de carbure est très appauvrie en produits des processus *p* et *r* (figure 11). Cette signature est typique de la nucléosynthèse de type *s* et peut être facilement reproduite par un modèle de capture neutronique lente (tableau 2). La composition isotopique a été mesurée également dans des grains de carbure de silicium de type X, vraisemblablement condensés dans les enveloppes de supernovae [8, 9]. Les spectre obtenus sur ces objets sont difficilement interprétables [102].

La concentration en molybdène dans les carbures de silicium isolés varie entre 1 et 50 ppm [41]. L'intervalle interquantile 0.05-0.95 est estimé à 2-28 ppm. Une difficulté se pose quant à l'évaluation de la concentration en molybdène des grains de carbure de silicium. En effet, le traitement chimique qui est imposé aux grains au cours de leur isolement est très corrosif [5, 99], et il est vraisemblable qu'une partie des éléments trace comme le molybdène est lessivée du grain même si celui-ci n'est pas entièrement détruit. La figure 12 illustre l'effet du traitement

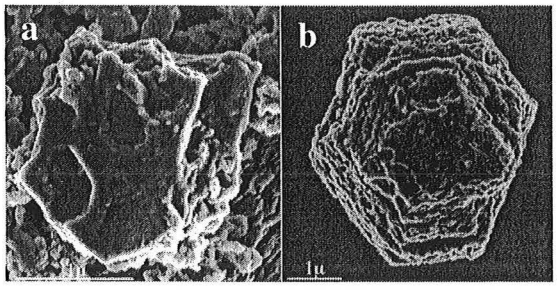

FIG. 12 – Morphologies des grains de carbure de silicium circumstellaires avant (a) et après (b) le traitement chimique utilisé pour les isoler [43]. Une partie du molybdène contenu en inclusions sous forme de carbure de molybdène peut être lessivée du grain lors de ce traitement.

chimique sur l'habitus des grains [43]. L'imagerie isotopique permet d'isoler les grains de SiC sans avoir recours à un traitement chimique corrosif, et il serait certainement instructif de mesurer la concentration en molybdène dans ces grains préservés.

3 Anomalies macroscopiques du molybdène

Comme en témoignent les grains circumstellaires de carbure de silicium et de graphite, la composition isotopique du molybdène est hétérogène à une échelle microscopique. Ceci n'est pas surprenant car à une telle échelle, la plupart des éléments montrent un héritage présolaire. Le mélange des différentes composantes héritées dans la nébuleuse a conduit à une très grande uniformisation de composition aux échelles macroscopiques et mégascopiques. Quelques éléments comme l'oxygène [34] et le chrome [103, 104, 105] montrent des anomalies à une échelle mégascopique. La présence de ces anomalies est discutée ; il pourrait s'agir de nomades ou d'anomalies nucléosynthétiques héritées.

3.1 Hétérogénéité mégascopique de la nébuleuse

Les météorites de fer sont issues de corps différentiés. Les processus de fusion et de mélange associés à la ségrégation métal-silicate garantissent que la composition isotopique des météorites de fer est représentative du corps parent dans son ensemble. Les tailles des corps parents des météorites de fer sont déterminées par des méthodes métallographiques. On estime ainsi que les corps parents devaient avoir une masse de $10^{16} - 10^{19}$ kg environ [14]. La détermination de la composition isotopique dans ces objets différenciés présente deux avantages. Elle permet (*i*) de discuter l'hétérogénéité de la nébuleuse à l'échelle des planétésimaux (rien ne garantit en effet l'homogénéité isotopique du corps parent des météorites primitives) (*ii*) de discuter les relations génétiques possibles entre météorites différenciées. L'oxygène qui est le principal traceur isotopique des filiations est en effet absent d'un très grand nombre de météorites métalliques. Nous avons ainsi mesuré la composition isotopique du molybdène dans des échantillons de météorites de fer, mésosidérites, pallasites, et chondrites et avons mis en évidence la présence d'anomalies non dépendantes de la masse qui présentent un spectre en w correspondant à un déficit en nucléides produits par le processus *s* de nucléosynthèse [19]. Ces anomalies ne résultent pas d'effets nomade car le processus *s* suffit à rendre compte des observations faites. Le molybdène est le troisième élément après l'oxygène [34] et le chrome [105] pour lequel des anomalies sont détectées dans

des météorites différenciées. L'attrait principal de cet élément réside dans le fait qu'il possède de nombreux isotopes et que les sources nucléosynthétiques des différents nucléides sont bien connues. Le molybdène est ainsi le premier élément pour lequel une hétérogénéité *héritée* de la nébuleuse protosolaire est mise en évidence à une échelle planétaire.

3.2 Anomalies et filiations

L'oxygène [34] et le chrome [103, 104, 105], éléments pour lesquels il existe des anomalies isotopiques mégascopiques, ont été utilisés pour discuter les relations génétiques entre les planètes et les planétésimaux. L'intérêt majeur des variations non dépendantes de la masse est qu'elles ne peuvent pas être effacées par les processus de différentiation qui ont pu affecter les corps parents. Les anomalies macroscopiques observées pour le molybdène nous permettent pour la première fois de discuter les filiations qui existent entre les différentes classes de météorites de fer [19]. La taxonomie isotopique que nous dégageons recoupe parfaitement la classification chimique des météorites de fer. Un des grands problèmes qui reste posé en sciences de la terre concerne l'origine de la terre. Notre planète partage de nombreuses propriétés avec les chondrites à enstatite, ce qui a conduit certains à proposer une relation génétique entre ces deux objets [106, 107, 108, 109, 110]. Nous avons mesuré la composition isotopique de chondrites à enstatite et d'un échantillon de basalte de Loihi qui échantillonne certainement une région profonde du manteau [20]. Nous n'avons pas trouvé de différences entre les chondrites à enstatite et la terre, ce qui renforce (sans la démontrer évidemment) l'hypothèse d'une terre formée d'un matériau proche des chondrites à enstatite. La seule observation qui va à l'encontre d'une terre formée de chondrites à enstatite est donné par les isotopes du tungstène [111]. En dépit d'un rapport père-fils Hf/W chondritique, les chondrites à enstatite présentent un déficit en ^{182}W par rapport à la terre et aux chondrites carbonées. Nous proposons que la terre s'est effectivement formée d'un matériau distinct mais proche des chondrites à enstatite et que le noyau terrestre s'est différencié pendant que le ^{182}Hf était encore vivant (50 ± 10 Ma après l'effondrement de la nébuleuse). Ce modèle permet de rendre compte de la différence de composition isotopique observée entre la terre et les chondrites à enstatite [111].

3.3 Distribution des poussières circumstellaires dans la nébuleuse

Les attaques ménagées effectuées sur les météorites primitives ont permis de révéler la présence de composants exotiques dans la nébuleuse [112, 113]. Nous avons ainsi mesuré la composition isotopique dans les fractions lessivées des météorites Orgueil et Allende. Pour des raisons différentes, ces deux météorites représentent le matériau idéal pour identifier et caractériser les éventuelles phases porteuses des anomalies. Des anomalies symétriques ont été mises en évidence dans des fractions lessivées d'Orgueil [21]. A cause de leurs formes, les anomalies caractérisées par un déficit et un excès en produits du processus *s* sont appelées Mo-w et Mo-m, respectivement. La composante Mo-m détectée dans Orgueil est due à un excès en grains circumstellaires de carbure de silicium dans cette fraction. La contribution des grains circumstellaires a donc une influence mesurable sur la composition macroscopique du molybdène. Ainsi, les anomalies Mo-w observées dans Allende et certaines météorites différenciées résultent d'un déficit en grains circumstellaires à une échelle mégascopique dans la région source des corps parents. Nous estimons que la concentration en carbures de silicium normalisée à un élément réfractaire comme le molybdène a dû varier de 30 % dans la nébuleuse protosolaire. Ceci constitue la première preuve d'une distribution hétérogène des grains circumstellaires dans la nébuleuse. Cette hétérogénéité a pu être héritée d'une hétérogénéité présolaire du milieu interstellaire ou peut être due à des

processus de tri dans la nebuleuse.

4 Astrophys. J. 565, 640-644

Molybdenum Evidence for Inherited Planetary Scale Isotope Heterogeneity of the Protosolar Nebula

Dauphas, N., Marty, B., and Reisberg, L.

The Astrophysical Journal (2002) **565**, 640-644

THE ASTROPHYSICAL JOURNAL, 565:640–644, 2002 January 20

MOLYBDENUM EVIDENCE FOR INHERITED PLANETARY SCALE ISOTOPE HETEROGENEITY OF THE PROTOSOLAR NEBULA

N. DAUPHAS, B. MARTY,[1] AND L. REISBERG
Centre de Recherches Pétrographiques et Géochimiques, CNRS UPR 2300, 15 rue Notre-Dame des Pauvres, BP 20, 54501 Vandœuvre-lès-Nancy Cedex, France; dauphas@crpg.cnrs-nancy.fr
Received 2001 September 5; accepted 2001 September 26

ABSTRACT

Isotope anomalies provide important information about early solar system evolution. Here we report molybdenum isotope abundances determined in samples of various meteorite classes. There is no fractionation of molybdenum isotopes in our sample set within 0.1‰ and no contribution from the extinct radionuclide ^{97}Tc at mass 97 (^{97}Tc/^{92}Mo $< 3 \times 10^{-6}$). Instead, we observe clear anomalies in bulk iron meteorites, mesosiderites, pallasites, and chondrites characterized by a coupled excess in *p*- and *r*-process or a mirror deficit in *s*-process nuclides (Mo-w). This large-scale isotope heterogeneity of the solar system observed for molybdenum must have been inherited from the interstellar environment where the Sun was born, illustrating the concept of "cosmic chemical memory." The presence of molybdenum anomalies is used to discuss the filiation between planetesimals.

Subject headings: ISM: abundances — minor planets, asteroids — nuclear reactions, nucleosynthesis, abundances — solar system: formation

1. INTRODUCTION

Variations of isotope abundances within the solar system that depart from mass-dependent fractionation and nuclear effects may occur as a result of inheritance of presolar nucleosynthetic anomalies (Anders & Zinner 1993) and mass-independent isotope effects (Thiemens 1999). Such variations have been detected in bulk meteorite samples for a variety of elements, including oxygen (Clayton 1993), sulfur (Thiemens & Jackson 1995; Farquhar et al. 2000), titanium (Niemeyer 1988), chromium (Shukolyukov & Lugmair 1998; Podosek et al. 1999), zirconium (Yin et al. 2001), molybdenum (Yin, Yamashita, & Jacobsen 2000), and barium (Harper, Weismann, & Nyquist 1992), although some of these observations need confirmation (Thiemens & Jackson 1995; Farquhar et al. 2000; Yin et al. 2001, 2000; Harper et al. 1992). These variations bear information on important subjects such as stellar nucleosynthesis, galactic chemical evolution, heterogeneity of the protosolar nebula, and filiation of planetary objects.

Molybdenum is a promising element to use to address most of these points. Indeed, unprocessed presolar carbide and graphite grains carry extreme molybdenum signatures inherited from the stellar environment where they formed (Nicolussi et al. 1998a, 1998b; Pellin et al. 1999, 2000), and subtle nucleosynthetic anomalies have been detected in macroscopic meteorite samples (Yin et al. 2000). In addition, the *p*-process nuclide ^{97}Tc, which decays by electron capture to ^{97}Mo with a mean life of 3.8 Myr, may have been alive in the early solar system (Yin & Jacobsen 1998), raising the possibility that this element can be used as an extinct chronometer (Podosek & Nichols 1996). Molybdenum is a highly refractory element (Fegley, Lodders, & Palme 1993), so it has largely avoided exchange between gas and dust in the forming solar system. Furthermore, it is a moderately siderophile element (Schmitt, Palme, & Wänke 1989) and therefore is relatively abundant in all meteorite classes, so possible anomalies could be used to trace the filiation between planetesimals.

[1] École Nationale Supérieure de Géologie, Rue du Doyen Marcel Roubault, BP 40, 54501 Vandœuvre-lès-Nancy Cedex, France.

2. Mo-w ISOTOPE ANOMALIES

A protocol based on solvent extraction, ion exchange, and plasma ionization mass spectrometry was developed that permits the precise and accurate determination of molybdenum isotope abundances in natural samples (Dauphas, Reisberg, & Marty 2001). The method takes advantage of the affinity of molybdenum for di (2-ethylhexyl) phosphate and the AG1-X8 strongly basic anion exchanger in order to achieve fine separation of this element from interfering species (Dauphas et al. 2001; Qi-Lu & Masuda 1992a, 1992b, 1994). Isotopic analyses were performed using a Micromass Isoprobe plasma ionization mass spectrometer. Molybdenum isotope abundances were corrected for zirconium (Nomura, Kogure, & Okamoto 1983) and ruthenium (Huang & Masuda 1997) isobaric interferences by monitoring the ion-beam signal at masses 91 and 99. Since we were mostly interested in non–mass-dependent variations, we employed an internal normalization procedure (^{98}Mo/^{96}Mo = 1.4470) in order to correct molybdenum isotope abundances for both natural and instrumental mass fractionation (Dauphas et al. 2001) using the exponential law (Maréchal, Télouk, & Albarède 1999). After internal normalization, no variation is observed among natural terrestrial samples, which demonstrates the reliability of the method (Dauphas et al. 2001). Molybdenum and rhenium concentrations were determined using the standard addition technique. Molybdenum isotopic composition is expressed in ϵ-units, which are relative deviations of the sample relative to terrestrial molybdenum isotopic composition in parts per 10^4,

$$\epsilon^i = \left[\frac{^i\mathrm{Mo}/^{96}\mathrm{Mo}}{(^i\mathrm{Mo}/^{96}\mathrm{Mo})_{\mathrm{std}}} - 1\right] \times 10^4 ,$$

where $i = 92$, 94, 95, 96, 97, 98, or 100. We monitored the raw ratios for mass fractionation by comparison with an external standard but found no variation in our sample set within ~ 0.1‰ amu^{-1} (Table 1).

TABLE 1

MOLYBDENUM ISOTOPE MEASUREMENTS

SAMPLE	CLASS	[Mo] (ppm)	$f_{Re/Mo}$	ϵ^i (per 10^4)							δ (‰ amu^{-1})
				92	94	95	96	97	98	100	
Bitburg	I AB	6.9 ± 0.7	< −0.8	1.20 ± 1.62	0.34 ± 0.81	0.15 ± 0.40	0	0.35 ± 0.26	0	−0.49 ± 0.77	−0.01 ± 0.16
Bitburg	I AB	6.9 ± 0.7	< −0.8	0.15 ± 0.72	0.22 ± 0.42	−0.10 ± 0.32	0	0.14 ± 0.23	0	−0.11 ± 0.22	−0.04 ± 0.21
Canyon Diablo	I AB	5.1 ± 0.8	−0.05 ± 0.04	−0.48 ± 0.90	−0.39 ± 0.49	−0.21 ± 0.54	0	0.07 ± 0.32	0	−0.17 ± 0.28	0.34 ± 0.17
Canyon Diablo	I AB	5.1 ± 0.8	−0.05 ± 0.04	0.59 ± 0.82	0.45 ± 0.58	0.33 ± 0.38	0	0.28 ± 0.21	0	0.21 ± 0.44	0.08 ± 0.16
Canyon Diablo	I AB	5.1 ± 0.8	−0.05 ± 0.04	−0.19 ± 1.35	0.01 ± 0.45	0.00 ± 0.33	0	0.07 ± 0.21	0	−0.28 ± 0.64	0.12 ± 0.27
Braunau	II AB	7.6 ± 0.1	1.05 ± 0.11	2.50 ± 0.93	1.54 ± 0.71	0.28 ± 0.78	0	0.58 ± 0.69	0	0.29 ± 0.83	0.09 ± 0.16
Braunau	II AB	7.6 ± 0.1	1.05 ± 0.11	1.53 ± 0.77	1.90 ± 0.83	0.83 ± 0.40	0	0.30 ± 0.22	0	0.26 ± 0.41	0.04 ± 0.17
Coahuila	II AB	7.5 ± 0.5	2.39 ± 0.18	2.15 ± 0.92	1.11 ± 0.27	0.39 ± 0.33	0	0.49 ± 0.37	0	0.39 ± 0.26	−0.17 ± 0.16
Coahuila	II AB	7.5 ± 0.5	2.39 ± 0.18	1.29 ± 0.75	1.41 ± 0.99	0.71 ± 0.37	0	0.39 ± 0.12	0	0.51 ± 0.16	0.00 ± 0.16
Coahuila	II AB	7.5 ± 0.5	2.39 ± 0.18	0.77 ± 1.79	0.70 ± 1.43	0.74 ± 0.74	0	0.59 ± 0.27	0	0.46 ± 0.55	−0.01 ± 0.16
Guadalupe Y Calvo	II AB	7.0 ± 0.4	6.41 ± 0.37	1.56 ± 0.39	1.48 ± 0.56	0.69 ± 0.28	0	0.51 ± 0.20	0	0.25 ± 0.22	−0.05 ± 0.17
Guadalupe Y Calvo	II AB	7.0 ± 0.4	6.41 ± 0.37	0.03 ± 0.87	0.93 ± 0.88	0.47 ± 0.46	0	0.53 ± 0.49	0	0.08 ± 0.70	−0.23 ± 0.45
Guadalupe Y Calvo	II AB	7.0 ± 0.4	6.41 ± 0.37	1.31 ± 0.60	1.19 ± 0.48	0.66 ± 0.39	0	0.68 ± 0.21	0	0.15 ± 0.26	−0.02 ± 0.18
Scottsville	II AB	6.8 ± 0.8	8.46 ± 0.47	1.57 ± 0.62	1.06 ± 0.57	0.43 ± 0.23	0	0.51 ± 0.21	0	0.06 ± 0.26	0.06 ± 0.19
Scottsville	II AB	6.8 ± 0.8	8.46 ± 0.47	2.07 ± 0.85	1.59 ± 0.50	0.83 ± 0.25	0	0.49 ± 0.13	0	0.23 ± 0.30	0.02 ± 0.16
Sikhote-Alin	II AB	5.9 ± 0.5	< −0.8	1.15 ± 1.10	0.86 ± 0.85	0.30 ± 0.64	0	0.31 ± 0.41	0	0.48 ± 0.44	−0.07 ± 0.20
Sikhote-Alin	II AB	5.9 ± 0.5	< −0.8	1.66 ± 1.23	1.34 ± 0.35	0.82 ± 0.36	0	0.52 ± 0.31	0	0.23 ± 0.66	0.08 ± 0.24
Mont Dieu	II E	6.8 ± 0.4	−0.02 ± 0.05	1.47 ± 0.64	1.18 ± 0.44	0.66 ± 0.29	0	0.19 ± 0.15	0	−0.18 ± 0.41	−0.01 ± 0.16
Mont Dieu	II E	6.8 ± 0.4	−0.02 ± 0.05	1.21 ± 0.89	0.91 ± 0.42	0.97 ± 0.26	0	0.27 ± 0.19	0	−0.84 ± 0.48	−0.28 ± 0.39
Cape York	III AB	6.3 ± 0.1	0.32 ± 0.07	1.34 ± 0.54	1.00 ± 0.54	0.45 ± 0.15	0	0.38 ± 0.27	0	0.16 ± 0.30	0.06 ± 0.17
Cape York	III AB	6.3 ± 0.1	0.32 ± 0.07	2.87 ± 0.76	1.81 ± 0.52	0.88 ± 0.36	0	0.65 ± 0.27	0	−0.26 ± 0.26	−0.05 ± 0.16
Henbury	III AB	8.6 ± 2.4	2.96 ± 0.20	1.70 ± 1.55	0.88 ± 0.59	0.09 ± 0.54	0	0.35 ± 0.30	0	0.02 ± 0.81	0.07 ± 0.17
Henbury	III AB	8.6 ± 2.4	2.96 ± 0.20	0.81 ± 2.11	0.78 ± 0.77	0.22 ± 1.08	0	0.65 ± 0.54	0	1.07 ± 1.17	0.07 ± 0.18
Magnesia	III CD	7.4 ± 0.9	< −0.8	1.88 ± 0.61	1.28 ± 0.48	0.58 ± 0.31	0	0.54 ± 0.24	0	0.01 ± 0.33	0.08 ± 0.15
Magnesia	III CD	7.4 ± 0.9	< −0.8	−0.70 ± 1.92	0.22 ± 0.96	0.18 ± 0.38	0	0.33 ± 0.24	0	−0.06 ± 0.91	−0.25 ± 0.31
Magnesia	III CD	7.4 ± 0.9	< −0.8	1.32 ± 1.41	1.30 ± 0.98	0.74 ± 0.50	0	0.55 ± 0.35	0	0.11 ± 0.56	0.04 ± 0.16
Gibeon	IV A	5.7 ± 0.1	−0.27 ± 0.04	0.84 ± 0.71	0.97 ± 0.77	0.75 ± 0.25	0	0.11 ± 0.30	0	0.21 ± 0.36	0.01 ± 0.17
Gibeon	IV A	5.7 ± 0.1	−0.27 ± 0.04	0.44 ± 1.28	0.50 ± 0.78	0.70 ± 0.32	0	0.16 ± 0.29	0	−0.04 ± 0.26	0.01 ± 0.19
Cape of Good Hope	IV B	25.0 ± 0.2	1.58 ± 0.13	2.05 ± 1.26	1.80 ± 0.60	0.86 ± 0.59	0	0.52 ± 0.41	0	0.38 ± 0.65	0.06 ± 0.17
Cape of Good Hope	IV B	25.0 ± 0.2	1.58 ± 0.13	1.75 ± 0.49	1.21 ± 0.16	0.99 ± 0.24	0	0.43 ± 0.61	0	0.68 ± 1.11	0.06 ± 0.34
Grand Rapids	IRUNG	11.5 ± 0.1	1.07 ± 0.10	1.28 ± 0.62	1.15 ± 0.40	0.89 ± 0.25	0	0.45 ± 0.25	0	0.48 ± 0.36	0.09 ± 0.17
Grand Rapids	IRUNG	11.5 ± 0.1	1.07 ± 0.10	0.40 ± 0.70	0.21 ± 0.68	0.73 ± 0.24	0	0.81 ± 0.16	0	0.60 ± 0.31	−0.04 ± 0.16
Estherville	MES	...	...	1.90 ± 0.62	1.64 ± 0.55	1.00 ± 0.30	0	0.58 ± 0.19	0	0.17 ± 0.50	−0.03 ± 0.25
Estherville	MES	...	...	0.52 ± 1.42	0.98 ± 0.83	0.60 ± 0.56	0	0.40 ± 0.27	0	0.30 ± 0.48	−0.18 ± 0.23
Imilac	MGPAL	...	...	−0.22 ± 1.97	0.09 ± 1.60	0.09 ± 0.74	0	0.53 ± 0.29	0	0.67 ± 0.79	−0.05 ± 0.17
Imilac	MGPAL	...	...	0.08 ± 1.58	0.18 ± 1.26	−0.04 ± 0.73	0	0.46 ± 0.29	0	1.10 ± 0.48	−0.12 ± 0.18
Eagle Sation	ESPAL	...	...	1.57 ± 0.42	1.21 ± 0.53	0.86 ± 0.35	0	0.80 ± 0.31	0	0.84 ± 0.30	−0.03 ± 0.16
Eagle Sation	ESPAL	...	...	0.43 ± 1.55	1.43 ± 1.24	1.35 ± 0.55	0	2.02 ± 0.51	0	1.54 ± 0.68	0.03 ± 0.17
Allende	CV	...	...	2.38 ± 0.57	1.95 ± 0.79	1.98 ± 0.50	0	1.62 ± 0.53	0	1.17 ± 0.50	−0.06 ± 0.38
Allende	CV	...	...	3.54 ± 0.67	2.62 ± 1.26	1.92 ± 0.67	0	0.91 ± 0.41	0	0.56 ± 0.52	0.17 ± 0.23
Allende	CV	...	...	2.57 ± 0.78	1.80 ± 0.46	1.78 ± 0.21	0	1.10 ± 0.53	0	1.67 ± 0.34	0.04 ± 0.16

NOTE.—Molybdenum isotope measurements (Dauphas et al. 2001); $f_{Re/Mo}$ is the Re/Mo fractionation factor; ϵ^i represents the molybdenum isotopic composition after internal normalization; and δ is the composition after external normalization of raw $^{98}Mo/^{96}Mo$ ratios. All uncertainties are 2 σ.

4. Astrophys. J. 565, 640-644

The Allende CV3.2 chondrite is a Rosetta stone for deciphering early solar system evolution. We confirm (Fig. 1*a*) the presence of molybdenum nucleosynthetic anomalies in macroscopic samples of this meteorite (Yin et al. 2000; Yin & Jacobsen 2000). As illustrated in Figure 1*b*, the anomalous isotopic composition observed in Allende may result from either a coupled enrichment in *p*- and *r*- or a mirror deficit in *s*-nuclides (Anders & Grevesse 1989; Burbidge et al. 1957; Cameron 1957). It has been suggested that the molybdenum composition of Allende resulted from incomplete digestion of presolar grains that bear isotopic signatures typical of *s*-nucleosynthesis (Yin et al. 2000). Simple calculation (Becker et al. 1987; Huss & Lewis 1995; Nicolussi et al. 1998a, 1998b; Dauphas et al. 2001) indicates that this cannot be the case because the resulting anomalies would be more than 2 orders of magnitude smaller than those observed (Yin & Jacobsen 2000). This implies that anomalous molybdenum in bulk Allende might be carried by another phase that needs to be identified: possibly metal, sulfide, or oxide presolar grains.

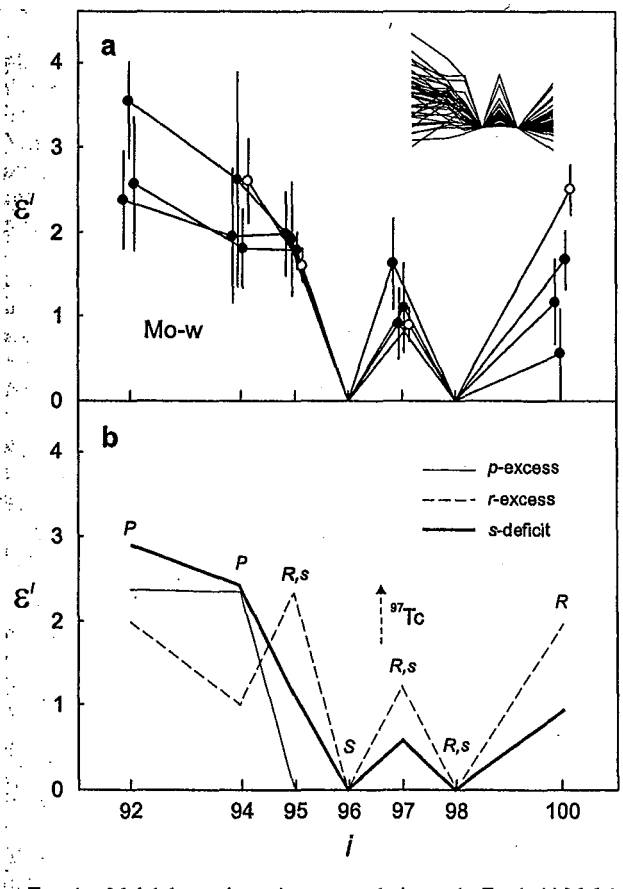

FIG. 1.—Molybdenum isotopic spectra relative to the Earth. (*a*) Molybdenum isotope abundances in Allende (*filled circles*: this study; *open circles*: Yin et al. 2000) depart from usual mass-dependent fractionation. Similar anomalies are observed in iron meteorites, mesosiderites, and pallasites (*top right*), which provides evidence for large-scale isotopic heterogeneity of the protosolar nebula. The top curves of the inset are those of Allende. The isotopic spectrum we observe is denoted Mo-w. Uncertainties are 2 σ. (*b*) Synthetic spectra obtained by adding or subtracting pure *p*-, *r*-, and *s*-nucleosynthetic abundances (Arlandini et al. 1999). Nucleosynthetic sources (Burbidge et al. 1957; Cameron 1957; Anders & Grevesse 1989) of the different nuclides are indicated. There is a possible contribution at mass 97 from the decay of now extinct ^{97}Tc (τ = 3.8 Myr). The spectrum closest to observations is that corresponding to a deficit in *s*- or a mirror excess in *p*- and *r*-nuclides.

Differentiation processes homogenize isotopic compositions originally existing within parent bodies. Thus, differentiated meteorites provide a means of examining isotopic heterogeneity in the protosolar nebula at scales comparable to the regions sampled by the parent bodies, which had masses that were inferred from metallographic cooling rates to be 10^{16}–10^{19} kg (Wood 1964; Goldstein & Ogilvie 1965; Mittlefehldt et al. 1998). For this reason, we measured molybdenum isotope abundances in iron meteorites, mesosiderites, and pallasites (Fig. 1*a*, *top right*). Most meteorite groups exhibit anomalies similar to those observed in Allende but of lesser magnitude. Because we observe no decoupling within uncertainties between the *p*- and *r*-anomalies, we cannot decide whether they result from the presence of *p*- or *r*-, or the absence of *s*-presolar phases. In either case, the observed anomalies provide evidence for large-scale inherited isotope heterogeneity of the protosolar nebula.

The stellar environments where *p*-, *r*-, and *s*-nucleosynthesis develop are not identical (Burbidge et al. 1957; Cameron 1957), and the host phases for these signatures are variable (Anders & Zinner 1993), so that the interstellar medium must be chemically and isotopically heterogeneous. Thus, molybdenum isotope abundances were heterogeneously distributed in the solar system parental molecular cloud, and the large- scale variations we observed were inherited from the interstellar environment where the Sun was born, illustrating the concept of "cosmic chemical memory" (Clayton 1982).

It was suggested that there might be a heterogeneous distribution of short-lived nuclides ^{53}Mn and ^{182}Hf in the early solar system (Lugmair & Shukolyukov 1998; Lee & Halliday 2000). Instead, the discovery of inherited isotope anomalies for molybdenum may support some form of cosmic chemical memory for stable isotopic ratios ^{53}Cr/^{52}Cr and ^{182}W/^{184}W.

3. LIVE ^{97}Tc IN THE EARLY SOLAR SYSTEM?

The positive anomaly at mass ^{97}Mo could potentially represent a radiogenic contribution from the decay of ^{97}Tc (τ = 3.8 Myr) as well as a nucleosynthetic component. The ^{187}Re-^{187}Os system (τ = 62.8 Gyr) offers tempting evidence for diachronism of iron meteorite formation, but the inferred chronologies are contradictory (Shen, Papanastassiou, & Wasserburg 1996; Smoliar, Walker, & Morgan 1996). The timescale inferred from the ^{53}Mn-^{53}Cr system (τ = 5.4 Myr) is equivocal because these nuclides may have been redistributed during the extended cooling history of planetesimals. Yet, some iron meteorites have closure ages within ~7 Myr of Allende refractory inclusions (Hutcheon et al. 1992). The time span between metal condensation in the protosolar nebula and core crystallization in asteroids is best estimated from the ^{107}Pd-^{107}Ag system (τ = 9.4 Myr) to be lower than 10 Myr (Chen & Wasserburg 1996). Thus, iron meteorites crystallized from a metallic magma within ~10 Myr of the solar system birth, when ^{97}Tc might still have been alive. Furthermore, the solid/liquid metal partition coefficient of rhenium (Fleet, Liu, & Crocket 1999) and, by inference, technetium, is higher than that of molybdenum (Liu & Fleet 2001); thus, the Re(Tc)/Mo ratio (Yin & Jacobsen 1998) should have been extensively fractionated during metal crystallization (Table 1). The fractionation

factor notation (Jacobsen & Wasserburg 1984) is employed for the Re(Tc)/Mo ratio,

$$f_{\mathrm{Re/Mo}} = \frac{^{185}\mathrm{Re}/^{96}\mathrm{Mo}}{(^{185}\mathrm{Re}/^{96}\mathrm{Mo})_{\mathrm{std}}} - 1 ,$$

where the standard ratio is that of the chondritic uniform reservoir (CHUR), $^{185}\mathrm{Re}/^{96}\mathrm{Mo} = 0.0454$ (Anders & Grevesse 1989). To test whether a significant radiogenic contribution exists on the ^{97}Mo peak, we use the fact that both ^{97}Mo and ^{100}Mo are *r*-nuclides, so there must be a relationship between the nucleosynthetic component at mass 97 and the anomaly at mass 100. Thus, we have corrected molybdenum isotope measurements for the nucleosynthetic contribution at mass 97 by using the observed anomaly at mass 100,

$$\epsilon^{97*} = \epsilon^{97} - (\rho^{97} - 0.5\rho^{98})/(1 - 2\rho^{98})\epsilon^{100} ,$$

where $\rho^i = (^i\mathrm{Mo}/^{100}\mathrm{Mo})_r/(^i\mathrm{Mo}/^{100}\mathrm{Mo})_\oplus$, and r and $\oplus$ denote the *r*-process and the Earth, respectively. The term ρ^{98} enters into the equation because ^{98}Mo/^{96}Mo is used to correct measurements for mass fractionation (Dauphas et al. 2001). It is estimated that $\rho^{97} = 0.43$ and $\rho^{98} = 0.25$, so $\epsilon^{97*} = \epsilon^{97} - 0.61\epsilon^{100}$ (Arlandini et al. 1999). Rhenium is used as a proxy for technetium, since these elements are likely to have very similar behavior during metal crystallization (Yin & Jacobsen 1998). If there were live ^{97}Tc when the iron meteorites formed, and if all iron meteorites crystallized simultaneously (Chen & Wasserburg 1996), then there should be a linear relationship (Jacobsen & Wasserburg 1984) between the radiogenic contribution at mass 97 (ϵ^{97*}) and the Re(Tc)/Mo fractionation factor ($f_{\mathrm{Re/Mo}}$), the slope of which depends on the ^{97}Tc/^{185}Re ratio at the time of closure,

$$\epsilon^{97*} = Q(^{97}\mathrm{Tc}/^{185}\mathrm{Re})_0 \, f_{\mathrm{Re/Mo}} ,$$

where $Q = 10^4(^{185}\mathrm{Re}/^{97}\mathrm{Mo})_{\mathrm{CHUR}}$, $Q \sim 791$ (Anders & Grevesse 1989). It follows from the definition of ϵ^{97*} that this relationship holds only if the Earth evolved with a chondritic Tc/Mo while ^{97}Tc was still alive. This will be true if the core formed after the extinction of ^{97}Tc, which seems to be the case (Allègre, Manhès, & Göpel 1995; Galer & Goldstein 1996; Lee & Halliday 1995; Halliday et al. 1996).

There is no correlation between $f_{\mathrm{Re/Mo}}$ and ϵ^{97*}, which indicates that ^{97}Tc was extinct when the iron meteorites formed ($^{97}\mathrm{Tc}/^{92}\mathrm{Mo} < 3 \times 10^{-6}$; ^{92}Mo is used for normalization because both are *p*-nuclides and were synthesized in the same stellar environment). This result is consistent with information retrieved from modeling of the chemical evolution of the Galaxy in the solar neighborhood (N. Dauphas et al., in preparation).

4. INFERENCE OF PLANETARY GENETICS

Because there is no radiogenic contribution on ^{97}Mo and because ϵ^{97} is measured much more precisely and accurately than other isotopic ratios, we used ϵ^{97} to trace the filiation between parent bodies (Fig. 2). Terrestrial rocks (stream sediments, porphyry copper millhead, and synthetic glass) are within 0.05 per 10^4 of the terrestrial standard value (Dauphas et al. 2001), which demonstrates that the analytical procedure is accurate. The molybdenum isotopic composition of the silicate Earth is representative of the bulk Earth value because the mantle molybdenum content is largely dominated by the component derived from the proto-Earth rather than from a late-accreting veneer

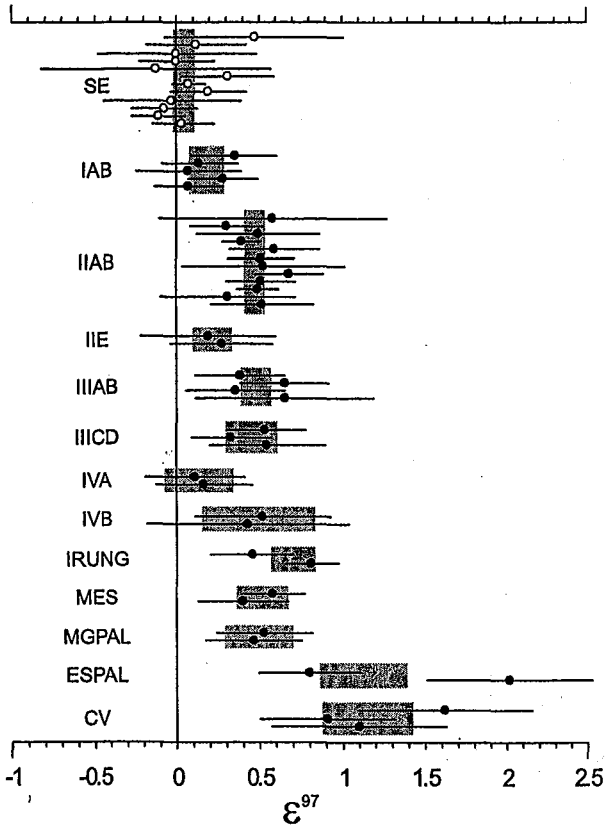

FIG. 2.—Molybdenum isotope taxonomy. SE: silicate Earth (Dauphas et al. 2001); IAB/IRUNG: iron meteorite; MES: mesosiderite; MGPAL/ESPAL: pallasite; CV: carbonaceous chondrite. Shaded rectangles are the mean composition for each group. Uncertainties are 2 σ.

(Righter & Drake 1997). Within each meteorite class, measurements on various specimens are consistent with derivation from a common source, which reinforces the genetic significance of the chemical classification (Scott & Wasson 1975; Sears & Dodd 1988). On the basis of oxygen (Clayton 1993) and chromium (Shukolyukov & Lugmair 1998, 2001; Podosek et al. 1999) isotopic ratios, a genetic relationship between Eagle Station pallasites and some carbonaceous chondrites (ESPAL/CV) has been inferred. This link is corroborated by molybdenum isotope measurements, which demonstrates the virtue of this element for tracing the relationships between planetesimals. The isotopic data support the proposed genetic associations between type IIIAB iron meteorites, mesosiderites, and main group pallasites (IIIAB/MES/MGPAL) but do not substantiate the link between types IAB and IIICD iron meteorites (IAB/IIICD) (Mittlefehldt et al. 1998).

Further analyses must be conducted on both macroscopic samples and separated phases in order to confirm and extend molybdenum isotope taxonomy and search for the possible presolar carriers of Mo-w.

We thank M. Denise and G. Kurat for providing us with the samples, F. Robert for insightful comments on the manuscript, and C. Zimmermann and D. Yeghicheyan for analytical support. This work was funded by grants from the PNP (CNES/INSU) and PRISMS SMT4-CT98-2220 (EC). This is contribution 1557 of the Centre de Recherches Pétrographiques et Géochimiques.

REFERENCES

Allègre, C.-J., Manhès, G., & Göpel, C. 1995, Geochim. Cosmochim. Acta, 59, 1445
Anders, E., & Grevesse, N. 1989, Geochim. Cosmochim. Acta, 53, 197
Anders, E., & Zinner, E. 1993, Meteoritics, 28, 490
Arlandini, C., Käppeler, F., Wisshak, K., Gallino, R., Lugaro, M., Busso, M., & Straniero, O. 1999, ApJ, 525, 886
Becker, R., Koller, P., Morschl, P., Kiesl, & F. Hermann, F. 1987, in The Allende Meteorite Reference Sample, ed. E. Jarosewich, R. S. Clarke, Jr., & J. N. Barrows (Washington: Smithsonian Inst. Press), 16
Burbidge, E. M., Burbidge, G. R., Fowler, W. A., & Hoyle, F. 1957, Rev. Mod. Phys., 29, 547
Cameron, A. G. W. 1957, PASP, 69, 201
Chen, J. H., & Wasserburg, G. J. 1996, in Earth Processes: Reading the Isotopic Code, ed. A. Basu & S. R. Hart (Geophys. Monogr. 95; Washington, DC: AGU), 1
Clayton, D. D. 1982, QJRAS, 23, 174
Clayton, R. N. 1993, Annu. Rev. Earth Planet. Sci., 21, 115
Dauphas, N., Reisberg, L., & Marty, B. 2001, Anal. Chem., 73, 2613
Farquhar, J., Savarino, J., Jackson, T. L., & Thiemens, M. H. 2000, Nature, 404, 50
Fegley, B., Jr., Lodders, K., & Palme, H. 1993, Meteoritics, 28, 346
Fleet, M. E., Liu, M., & Crocket, J. H. 1999, Geochim. Cosmochim. Acta, 63, 2611
Galer, S. J. G., & Goldstein, S. L. 1996, in Earth Processes: Reading the Isotopic Code, ed. A. Basu & S. R. Hart (Geophys. Monogr. 95; Washington, DC: AGU), 75
Goldstein, J. I., & Ogilvie, R. E. 1965, Geochim. Cosmochim. Acta, 29, 893
Halliday, A., Rehkämper, M., Lee, D.-C., & Yi, W. 1996, Earth Planet. Sci. Lett., 142, 75
Harper, C. L., Jr., Weismann, H., & Nyquist, L. E. 1992, Meteoritics, 27, 230
Huang, M., & Masuda, A. 1997, Anal. Chem., 69, 1135
Huss, G. R., & Lewis, R. S. 1995, Geochim. Cosmochim. Acta, 59, 115
Hutcheon, I. D., Olsen, E., Zipfel, J., & Wasserburg, G. J. 1992, Lunar Planet. Sci., 23, 565
Jacobsen, S. B., & Wasserburg, G. J. 1984, Earth Planet. Sci. Lett., 67, 137
Lee, D.-C., & Halliday, A. N. 1995, Nature, 378, 771
———. 2000, Science, 288, 1629
Liu, M., & Fleet, M. E. 2001, Geochim. Cosmochim. Acta, 65, 671
Lugmair, G. W., & Shukolyukov, A. 1998, Geochim. Cosmochim. Acta, 62, 2863
Marêchal, C. N., Télouk, P., & Albarède, F. 1999, Chem. Geol., 156, 251
Mittlefehldt, D. W., McCoy, T. J., Goodrich, C. A., & Kracher, A. 1998, in Planetary Materials, ed. J. J. Papike (Washington: Mineralogical Soc. of Am.), 4-1
Nicolussi, G. K., Pellin, M. J., Lewis, R. S., Davis, A. M., Amari, S., & Clayton, R. N. 1998a, Geochim. Cosmochim. Acta, 62, 1093
Nicolussi, G. K., Pellin, M. J., Lewis, R. S., Davis, A. M., Clayton, R. N., & Amari, S. 1998b, ApJ, 504, 492
Niemeyer, S. 1988, Geochim. Cosmochim. Acta, 52, 2941
Nomura, M., Kogure, K., & Okamoto, M. 1983, Int. J. Mass Spectrom. Ion Phys., 50, 219
Pellin, M. J., Davis, A. M., Calaway, W. F., Lewis, R. S., Clayton, R. N., & Amari, S. 2000, Lunar Planet. Sci., 31, 1934
Pellin, M. J., Davis, A. M., Lewis, R. S., Amari, S., & Clayton, R. N. 1999, Lunar Planet. Sci., 30, 1969
Podosek, F. A., & Nichols, R. H., Jr. 1996, in Astrophysical Implications of the Laboratory Study of Presolar Materials, ed. T. J. Bernatowicz & E. K. Zinner (Woodbury: AIP), 617
Podosek, F. A., Nichols, R. H., Jr., Brannon, J. C., & Dougherty, J. R. 1999, Lunar Planet. Sci., 30, 1307
Qi-Lu, & Masuda, A. 1992a, J. Am. Soc. Mass Spectrom., 3, 10
———. 1992b, Analyst, 117, 869
———. 1994, Int. J. Mass Spectrom. Ion Processes, 130, 65
Righter, K., & Drake, M. J. 1997, Earth Planet. Sci. Lett., 146, 541
Schmitt, W., Palme, H., & Wänke, H. 1989, Geochim. Cosmochim. Acta, 53, 173
Scott, E. R. D., & Wasson, J. T. 1975, Rev. Geophys. Space Phys., 13, 527
Sears, D. W. G., & Dodd, R. T. 1988, in Meteorites and the Early Solar System, ed. J. F. Kerridge, & M. S. Matthews (Tucson: Univ. Arizona Press), 3
Shen, J. J., Papanastassiou, D. A., & Wasserburg, G. J. 1996, Geochim. Cosmochim. Acta, 60, 2887
Shukolyukov, A., & Lugmair, G. W. 1998, Science, 282, 927
———. 2001, Lunar Planet. Sci., 32, 1365
Smoliar, M. I., Walker, R. J., & Morgan, J. W. 1996, Science, 271, 1099
Thiemens, M. H. 1999, Science, 283, 341
Thiemens, M. H., & Jackson, T. 1995, Lunar Planet. Sci., 26, 1405
Wood, J. A. 1964, Icarus, 3, 429
Yin, Q. Z., & Jacobsen, S. B. 1998, Lunar Planet. Sci., 29, 1802
———. 2000, Meteoritics Planet. Sci., 35, A175
Yin, Q. Z., Jacobsen, S. B., Blichert-Toft, J., Télouk, P., & Albarède, F. 2001, Lunar Planet. Sci., 32, 2128
Yin, Q. Z., Yamashita, K., & Jacobsen, S. B. 2000, Lunar Planet. Sci., 31, 1920

5 Geophys. Res. Lett., in press

Inference on Terrestrial Genesis from Molybdenum Isotope Systematics

Dauphas, N., Marty, B., and Reisberg, L.

Geophysical Research Letters, in press

GEOPHYSICAL RESEARCH LETTERS, VOL. 29, NO. 0, 10.1029/2001GL014237, 2002

Inference on terrestrial genesis from molybdenum isotope systematics

Nicolas Dauphas, Bernard Marty,[1] and Laurie Reisberg

Centre de Recherches Pétrographiques et Géochimiques, Vandoeuvre-lès-Nancy, France

Received 25 October 2000; accepted 11 January 2001; published XX Month 2002.

[1] It has been suggested that a genetic relationship exists between the Earth and enstatite chondrites. The discovery of non mass dependent molybdenum isotope anomalies (Mo-w) at a macroscopic scale raises the possibility of using this element as a tracer of genetic relationships. We have determined the molybdenum isotopic compositions of enstatite chondrites (EH and EL) and terrestrial lavas presumably derived from the deep mantle (Loihi seamount, Hawaii). The molybdenum isotopic compositions are identical, suggesting a common source reservoir. The conclusion is that although distinct, the Earth shares similarities with enstatite chondrites from a chemical and isotopic point of view because both formed in the inner regions of the solar system. *INDEX TERMS:* 1040 Geochemistry: Isotopic composition/chemistry; 6240 Planetology: Solar System Objects: Meteorites and tektites; 1060 Geochemistry: Planetary geochemistry (5405, 5410, 5704, 5709, 6005, 6008)

1. Introduction

[2] The Earth is a differentiated body and the composition of rocks found at its surface cannot be readily used to infer the nature of the material from which our planet formed. Isotopic variations that depart from usual mass dependent fractionation and nuclear effects represent faithful witnesses of Earth's accretion because they cannot be erased by subsequent geological processes. Thus, comparison of the isotopic compositions of terrestrial and meteoritic samples provides a means of constraining the nature of terrestrial precursors.

[3] Contrary to other undifferentiated meteorites, enstatite chondrites possess oxygen [*Clayton et al.*, 1984; *Clayton*, 1993] and chromium [*Lugmair and Shukolyukov*, 1998; *Shukolyukov and Lugmair*, 1998] isotopic compositions very close to that of the Earth. Also, in the Urey-Craig diagram, the bulk Earth plots close to enstatite chondrites [*Javoy*, 1999]. Some have argued that these similarities provide evidence for a genetic relationship between enstatite chondites and our planet [*Smith*, 1981; *Javoy et al.*, 1986; *Javoy*, 1995, 1998, 1999]. Yet, inferred elemental ratios of the primitive mantle [*Allègre et al.*, 2001] tend instead to support the view that the Earth was formed from material sharing similarities with carbonaceous chondrites.

[4] Recently, molybdenum nucleosynthetic isotope anomalies have been found in differentiated meteorites [*Dauphas et al.*, 2002a]. After oxygen [*Clayton et al.*, 1973; *Clayton*, 1993] and chromium [*Shukolyukov and Lugmair*, 2001], this is the third piece of evidence for planetary scale isotope heterogeneity of the protosolar nebula. The Mo-w anomalies are characterized by a coupled excess in *p* (92 and 94) and *r* (95, 97, 98, and 100), or a mirror deficit in *s* (95, 96, 97, and 98) nuclides [*Yin et al.*, 2000; *Dauphas et al.*, 2002a, 2002b]. These anomalies were inherited from the interstellar environment where the sun was born, illustrating the concept of "cosmic chemical memory" [*Clayton*, 1982]. The virtue of molybdenum for tracing the relationships between planetesimals has been demonstrated in the case of chondrites, iron meteorites, pallasites, and mesosiderites [*Dauphas et al.*, 2002a]. Accurate and precise determination of the molybdenum isotopic composition of enstatite chondrites and terrestrial samples is thus an important step towards definitive acceptance or rejection of the "enstatite model".

2. Samples and Analyses

[5] Enstatite chondrites are divided into EH and EL subtypes on the basis of their iron content [*Sears and Dodd*, 1988]. Despite the fact that the oxygen isotopic composition of these two groups are identical [*Clayton et al.*, 1984; *Newton et al.*, 2000], they are thought to originate from two distinct parent-bodies [*Keil*, 1989]. We measured enstatite chondrites Indarch (EH4), Saint Sauveur (EH4), and Pillistfer (EL6). Ocean island basalts (OIB) are the surface expression of mantle plumes. Many of these are thought to originate in the deep mantle, below the 660 km discontinuity and possibly at the core-mantle boundary. In this respect, samples from Loihi seamount, Hawaiian plume, are among the best available samples for examining possible isotopic heterogeneities of the silicate Earth. We measured Loihi submarine pillow basalt T4D2 #1 dredged at 4200 m 18°46.0N 155°11.3W by the R/V Thomas Washington [*Valbracht et al.*, 1996].

[6] A protocol based on solvent extraction, ion exchange, and plasma ionization mass spectrometry was developed [*Dauphas et al.*, 2001]. In order to correct for natural and instrumental mass fractionation, molybdenum isotope abundances were normalized to $^{98}Mo/^{96}Mo = 1.4470$ [*Dauphas et al.*, 2001]. Ratios are expressed in ϵ notation,

$$\epsilon^i = \left[\left(^iMo/^{96}Mo\right)\Big/\left(^iMo/^{96}Mo\right)_{std} - 1\right] \times 10^4,$$

where the standard is an Alfa Aesar solution of unknown origin. We measured many sediments for molybdenum isotope abundances [*Dauphas et al.*, 2001] and found no difference except for mass fractionation relative to the standard solution, indicating that this solution must be representative of the molybdenum isotopic composition of the crust. Results are given in Table 1 for both enstatite chondrites and Loihi. All ratios are within error of the terrestrial standard value.

3. Isotope Heterogeneity of the Earth?

[7] There is no "non mass dependent" isotope heterogeneity of the Earth for oxygen [*Robert et al.*, 1992]. Should we expect to observe some isotopic heterogeneity of the silicate Earth for molybdenum? Molybdenum is a moderately siderophile element [*Schmitt et al.*, 1989] that was presumably delivered to the mantle in part by a late veneer after core formation. The molybdenum

[1] Also at École Nationale Supérieure de Géologie, Vandoeuvre-lès-Nancy, France.

0094-8276/02/2001GL014237$05.00

Table 1. Molybdenum Isotope Measurements

		ϵ						
Sample	Type	92	94	95	96	97	98	100
Indarch	EH4	−0.44 ± 1.25	−0.26 ± 0.85	−0.05 ± 0.63	0	−0.21 ± 0.33	0	−0.61 ± 0.38
Indarch	EH4	0.88 ± 0.86	0.58 ± 0.54	0.77 ± 0.47	0	0.49 ± 0.22	0	−0.10 ± 0.33
Saint Sauveur	EH4	0.15 ± 0.62	0.13 ± 0.40	0.48 ± 0.21	0	0.26 ± 0.10	0	0.09 ± 0.28
Saint Sauveur	EH4	0.09 ± 1.86	−0.15 ± 1.19	−0.04 ± 0.92	0	0.19 ± 0.23	0	1.22 ± 0.81
Pillistfer	EL6	−1.03 ± 0.94	−0.74 ± 0.64	−0.27 ± 0.43	0	0.23 ± 0.21	0	0.66 ± 0.32
Pillistfer	EL6	1.04 ± 1.15	0.69 ± 0.81	0.74 ± 0.62	0	0.45 ± 0.20	0	−0.07 ± 0.47
T4D2#1	OIB	−0.08 ± 0.67	0.01 ± 0.57	0.25 ± 0.30	0	0.31 ± 0.26	0	0.23 ± 0.49
T4D2#1	OIB	0.04 ± 1.03	0.05 ± 1.07	0.36 ± 0.37	0	0.30 ± 0.31	0	−0.10 ± 0.49

Molybdenum isotope abundances were normalized to $^{98}Mo/^{96}Mo = 1.4470$ [*Dauphas et al.*, 2001]. The isotopic composition is expressed as $\epsilon^i = [(^iMo/^{96}Mo)/(^iMo/^{96}Mo)_{std} - 1] \times 10^4$. Uncertainties are 2σ. The samples were digested in concentrated HF-HCl-$HClO_4$. The solution was then treated by solvent extraction using HDEHP and ion chromatography using AG1-X8. An Aridus desolvating sample introduction system was used to increase transport efficiency to the torch. The temperatures of the spray chamber and of the desolvator were set at 70 an 160°C, respectively. The sweep gas and nitrogen flows were fixed at 2.1 L/min and 0.16 mL/min, respectively. The acquisition scheme and data reduction technique are the same as those described in *Dauphas et al.* [2001].

concentration of the upper mantle is 5.2×10^{-10} mol.g^{-1} [*McDonough and Sun*, 1995]. Given that osmium was essentially all delivered to the mantle by the late veneer [*Morgan*, 1985] and that the osmium content of the upper mantle is 1.8×10^{-11} mol.g^{-1}, it is straightfoward to compute the fraction of molybdenum from this source using the chondritic ratio Mo/Os = 3.8 [*Anders and Grevesse*, 1989]. It is thus estimated that approximately 87% of the molybdenum inventory of the upper mantle was left by core extraction and that 13% was delivered by the late veneer. Based on the osmium isotopic composition of the mantle, it was recently suggested that the late veneer was not completely homogenized in the whole mantle, its contribution being a factor of 3 ± 2 higher in the upper mantle than in the lower mantle [*Dauphas et al.*, 2002c]. In such a case, the contribution of the residual mantle and the late veneer in the deep mantle would be 95% and 5%, respectively. If there was a contrast of 1 ϵ-unit between the proto-Earth and the late veneer, we should expect to observe a heterogeneity of the Earth of approximately 0.1 ϵ-unit between the deep and the shallow mantle, which is not resolvable at present.

[8] As discussed previously, we measured a lava from Loihi seamount (T4D2 #1) which is thought to have erupted material that was once deep in the Earth [*Valbracht et al.*, 1996]. As illustrated in Figure 1, this sample presents no convincing anomaly relative to the standard or to crustal rocks, indicating that at our level of precision, the Earth is homogeneous for molybdenum isotopic composition after correction for possible mass dependent fractionation.

4. Implications for Planetary Genesis

[9] Determinations of molybdenum isotope abundances in enstatite chondrites allow us to discuss the possible relationships of these two meteorite groups both with each other and with the Earth. *Keil* [1989] presented convincing arguments that the parent-bodies of EH and EL chondrites were distinct. We measured the molybdenum isotopic composition of Indarch (EH4), Saint Sauveur (EH4), and Pillistfer (EL6). As illustrated in Figure 1, these is no obvious difference between EH and EL chondrites. Although EH and EL chondrites originated from two distinct parent-bodies, our results confirm the inference based on oxygen [*Clayton et al.*, 1984; *Newton et al.*, 2000] that they formed from the same isotopic reservoir.

[10] As discussed previously, the contribution of the late veneer to the molybdenum inventory of the silicate Earth was minor and the isotopic composition of the mantle must primarily reflect the composition of terrestrial precursors. There is no obvious anomaly in enstatite chondrites relative to the Earth (Figure 1). This result is consistent with the "enstatite model" of the Earth [*Smith*, 1981; *Javoy et al.*, 1986; *Javoy*, 1995, 1998, 1999].

[11] A complication arises with Hf-W systematics because enstatite chondrites display deficits in ^{182}W relative to the Earth [*Lee and Halliday*, 2000a]. However, this difference can be reconciled with an enstatite model for the Earth [*Javoy*, 2000].

[12] Despite having chondritic Hf/W ratios, enstatite chondrites display deficits in ^{182}W relative to carbonaceous chondrites [*Lee and Halliday*, 2000a]. There are three alternative explanations for this puzzling observation (i) the Hf/W ratio followed a complex evolution while ^{182}Hf was still alive, (ii) the ^{182}Hf extinct radionuclide was heterogeneously distributed in the early solar system, or (iii) as is observed for molybdenum [*Dauphas et al.*, 2002a, 2002b], the non-radiogenic isotopic composition of tungsten was not uniform in the protosolar nebula. We propose that the Earth accreted from material having tungsten isotopic composition similar to enstatite chondrites and that core formation occurred while some ^{182}Hf was still alive. In this case, the difference between the

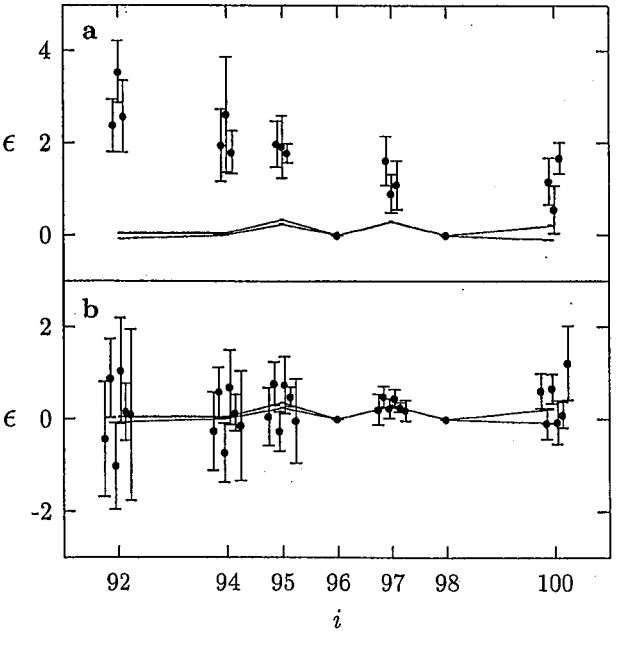

Figure 1. Molybdenum isotope spectra relative to the Earth's surface. The isotopic composition of the deep mantle (Loihi OIB) is given for comparison (broken line). (a) Mo-w isotope anomalies in the Allende CV3.2 carbonaceous chondrite [*Dauphas et al.*, 2002a]. (b) Isotopic compositions of EH and EL enstatite chondrites.

tungsten isotopic composition of the Earth and enstatite chondrites might simply result from the decay of ^{182}Hf in the terrestrial mantle. The $^{182}W/^{184}W$ ratios of the Earth and enstatite chondrites are taken to be 0.865000 and 0.864816 ± 0.000046 [*Lee and Halliday*, 2000a], respectively. The $^{180}Hf/^{184}W$ ratios of the silicate Earth and enstatite chondrites are estimated to be 13–53 [*Newsom et al.*, 1996] and 1.1 ± 0.5 [*Lee and Halliday*, 2000a], respectively. In the case of a two stage segregation model [*Lee and Halliday*, 1995], the $^{182}Hf/^{180}Hf$ at the time of core formation would have been $0.3–1.3 \times 10^{-5}$. The initial $^{182}Hf/^{180}Hf$ of the solar system is $2.75 \pm 0.24 \times 10^{-4}$ [*Lee and Halliday*, 2000b]. Thus, the terrestrial core would have differentiated 50 ± 10 Ma after collapse of the protosolar nebula. This estimate is consistent with the timing of core formation inferred from lead isotope systematics to be 80 ± 40 Ma [*Galer and Goldstein*, 1996].

[13] Current modelling of planetary formation predicts that terrestrial precursors originated from a variety of heliocentric distances and that the Earth was built from the accretion of this odd assortment [*Morbidelli et al.*, 2000]. Our opinion is that the Earth lacks a strict equivalentamong available meteorites but that the enstatite model is still viable in a relaxed formulation: although distinct, the Earth shares similarities with enstatite chondrites from a chemical and isotopic point of view because both formed in the inner regions of the solar system.

[14] **Acknowledgments.** This work benefited from fruitful discussions with M. Javoy and U. Ott. We are grateful to M. Denise, G. Kurat, and H. Staudigel for generously donating the samples. We thank C. Zimmermann for analytical support. This work was funded by grants from the PNP (CNES/INSU) and PRISMS SMT4-CT98-2220 (EC). This is contribution 1561 of the Centre de Recherches Pétrographiques et Géochimiques.

References

Allègre, C., G. Manhès, and E. Lewin, Chemical composition of the Earth and the volatility control on planetary genetics, *Earth Planet. Sci. Lett.*, *185*, 49–69, 2001.

Anders, E., and N. Grevesse, Abundances of the elements: Meteoritic and solar, *Geochim. Cosmochim. Acta*, *53*, 197–214, 1989.

Clayton, R. N., L. Grossman, and T. K. Mayeda, A component of primitive nuclear composition in carbonaceous meteorites, *Science*, *182*, 485–488, 1973.

Clayton, D. D., Cosmic chemical memory: a new astronomy, *Quart. J. Roy. Astron. Soc.*, *23*, 174–212, 1982.

Clayton, R. N., T. K. Mayeda, and A. E. Rubin, Oxygen isotopic compositions of enstatite chondrites and aubrites, *J. Geophys. Res.*, *89*, C245–C249, 1984.

Clayton, R. N., Oxygen isotopes in meteorites, *Ann. Rev. Earth Planet. Sci.*, *21*, 115–149, 1993.

Dauphas, N., L. Reisberg, and B. Marty, Solvent extraction, ion chromatography, and mass spectrometry of molybdenum isotopes, *Anal. Chem.*, *73*, 2613–2616, 2001.

Dauphas, N., B. Marty, and L. Reisberg, Molybdenum evidence for inherited planetary scale isotope heterogeneity of the protosolar nebula, *Astrophys. J.*, *565*, 640–644, 2002a.

Dauphas, N., B. Marty, and L. Reisberg, Molybdenum nucleosynthetic polarization revealed in primitive meteorites, *Astrophys. J.*, submitted 2002b.

Dauphas, N., L. Reisberg, and B. Marty, An alternative explanation for the distribution of highly siderophile elements in Earth, *Geochem. J.*, in press 2002c.

Galer, S. J. G., and S. L. Goldstein, Influence of accretion on lead in the Earth, in *Earth Processes: Reading the Isotopic Code*, edited by A. Basu, and S. Hart, pp. 75–98, American Geophysical Union, Washington, 1996.

Javoy, M., The integral enstatite chondrite model of the earth, *Geophys. Res. Lett.*, *22*, 2219–2222, 1995.

Javoy, M., The birth of the Earth's atmosphere: the behaviour and fate of its major elements, *Chem. Geol.*, *147*, 11–25, 1998.

Javoy, M., Chemical Earth models, *C. R. Acad. Sci. Paris, Sciences de la terre et des planètes*, *329*, 537–555, 1999.

Javoy, M., The EH Earth and the chronology of its formation, *J. Conf Abs.*, *5*, 554, 2000.

Javoy, M., F. Pineau, and H. Delorme, Carbon and nitrogen isotopes in the mantle, *Chem. Geol.*, *57*, 41–62, 1986.

Keil, K., Enstatite meteorites and their parent bodies, *Meteoritics*, *24*, 195–208, 1989.

Lee, D.-C., and A. N. Halliday, Hafnium-tungsten chronometry and the timing of terrestrial core formation, *Nature*, *378*, 771–774, 1995.

Lee, D.-C., and A. N. Halliday, Accretion of primitive planetesimals: Hf-W isotopic evidence from enstatite chondrites, *Science*, *288*, 1629–1631, 2000a.

Lee, D.-C., and A. N. Halliday, Hf-W internal isochrons for ordinary chondrites and the initial $^{182}Hf/^{180}Hf$ of the solar system, *Chem. Geol.*, *169*, 35–43, 2000b.

Lugmair, G. W., and A. Shukolyukov, Early solar system timescales according to $^{53}Mn–^{53}Cr$ systematics, *Geochim. Cosmochim. Acta*, *62*, 2863–2886, 1998.

McDonough, W. F., and S.-S. Sun, The composition of the Earth, *Chem. Geol.*, *120*, 223–253, 1995.

Morbidelli, A., J. Chambers, J. I. Lunine, J. M. Petit, F. Robert, G. B. Valsecchi, and K. E. Cyr, Source regions and timescales for the delivery of water to the Earth, *Meteoritics Planet. Sci.*, *35*, 1309–1320, 2000.

Morgan, J. W., Osmium isotope constraints on Earth's late accretionary history, *Nature*, *317*, 703–705, 1985.

Newsom, H. E., K. W. W. Sims, P. D. Noll Jr., W. L. Jaeger, S. A. Maehr, and T. B. Bessera, The depletion of tungsten in the bulk silicate earth: Constraints on core formation, *Geochim. Cosmochim. Acta*, *60*, 1155–1169, 1996.

Newton, J., I. A. Franchi, and C. T. Pillinger, The oxygen-isotopic record in enstatite meteorites, *Meteoritics Planet. Sci.*, *35*, 689–698, 2000.

Robert, F., A. Rejou-Michel, and M. Javoy, Oxygen isotopic homogeneity of the Earth: new evidence, *Earth Planet. Sci. Lett.*, *108*, 1–9, 1992.

Schmitt, W., H. Palme, and H. Wänke, Experimental determination of metal/silicate partition coefficients for P, Co, Ni, Cu, Ga, Ge, Mo, and W and some implications for the early evolution of the Earth, *Geochim. Cosmochim. Acta*, *53*, 173–185, 1989.

Sears, D. W. G., and R. T. Dodd, Overview and classification of meteorites, in *Meteorites and the Early Solar System*, edited by J. F. Kerridge, and M. S. Matthews, pp. 3–31, The University of Arizona Press, Tucson, 1988.

Shukolyukov, A., and G. W. Lugmair, The $^{53}Mn–^{53}Cr$ isotope system in the Indarch EH4 chondrite: a further argument for ^{53}Mn heterogeneity in the early solar system, *Lunar Planet. Sci.*, *XXIX*, #1208, 1998.

Shukolyukov, A., and G. W. Lugmair, Cr isotope systematics in the pallasite Eagle Station: chronology and evidence for a genetic link to carbonaceous chondrites, *Lunar Planet. Sci.*, *XXXII*, #1365, 2001.

Smith, J. V., Should enstatite chondrites be considered when modeling the chemical composition of the Earth?, *Lunar Planet. Sci.*, *12*, 1002–1004, 1981.

Valbracht, P. J., H. Staudigel, M. Honda, I. McDougall, and G. R. Davies, Isotopic tracing of volcanic source regions from Hawaii: decoupling of gaseous from lithophile magma components, *Earth Planet. Sci. Lett.*, *144*, 185–198, 1996.

Yin, Q. Z., K. Yamashita, and S. B. Jacobsen, Mo and Zr isotopic signatures in the "haystack": evidence for presolar silicates of supernova origin?, *Lunar Planet. Sci.*, *XXXI*, #1920, 2000.

N. Dauphas, B. Marty, and L. Reisberg, Centre de Recherches Pétrographiques et Géochimiques, CNRS UPR 2300, 15 rue Notre-Dame des Pauvres, BP 20, 54501 Vandoeuvre-lès-Nancy Cedex, France. (dauphas@crpg.cnrs-nancy.fr; bmarty@crpg.cnrs-nancy.fr; reisberg@crpg.cnrs-nancy.fr)

6 Astrophys. J. Lett., in press

Molybdenum Nucleosynthetic Dichotomy Revealed in Primitive Meteorites

Dauphas, N., Marty, B., and Reisberg, L.

Astrophys. J. Lett., in press

THE ASTROPHYSICAL JOURNAL, 569:L000–L000, 2002 April 10

MS# 16081 APJL 110(3), pt. 2 Copyeditor: rld
Tuesday Mar 12 2002 01:01 PM

MOLYBDENUM NUCLEOSYNTHETIC DICHOTOMY REVEALED IN PRIMITIVE METEORITES

N. DAUPHAS, B. MARTY,[1] AND L. REISBERG
Centre de Recherches Pétrographiques et Géochimiques, CNRS UPR 2300, 15 rue Notre Dame des Pauvres, BP 20, 54501 Vandoeuvre lès Nancy Cedex, France; dauphas@crpg.cnrs-nancy.fr

Received 2002 January 30; accepted 2002 March 8; published 2002 March 00

ABSTRACT

The collapse of the presolar cloud gave rise to a global homogenization of material available to form the Sun and planets. In the resulting, presumably homogeneous solar system, the nuclides are present in proportions referred to as their cosmic abundances. Here we report molybdenum isotopic compositions of bulk samples and leachate fractions of the primitive meteorites Orgueil and Allende. Two complementary nucleosynthetic components are revealed in Orgueil. One (Mo-m) is enriched in *s*-process nuclides and may be hosted in presolar grains while the other (Mo-w) is probably distributed in various phases and is depleted in *s*-process nuclides. The most likely carrier of Mo-m is silicon carbide, although we cannot exclude graphite or an unidentified presolar phase. Excesses in Mo-w are also detected in the bulk sample and all leachate fractions of Allende. These results illustrate that the apparent cosmic abundance pattern of the nuclides, in fact, reflects a mixture of various nucleosynthetic components that survived planetary-scale homogenization in the protosolar nebula.

Subject headings: minor planets, asteroids — nuclear reactions, nucleosynthesis, abundances — solar system: formation — Sun: abundances

1. INTRODUCTION

Heavy elements such as molybdenum were synthetized in stars by various nucleosynthetic processes, each taking place in a specific stellar environment (Burbidge et al. 1957; Cameron 1957). The composition of the interstellar medium at the time of solar system birth resulted from the integration over Galactic time of many individual stellar sources (Pagel 1997). Around these stars, circumstellar grains condensed. When the solar system formed, some of these grains escaped homogenization (Anders & Zinner 1993) and now provide evidence for isotopic heterogeneity of the presolar molecular cloud. However, the distribution of these refractory grains in the protosolar nebula remains largely unknown. While noble gases permit the determination of presolar grain abundances currently present in meteorites (Huss & Lewis 1995), these tracers are erased by metamorphism and differentiation. They therefore provide no direct information on the distribution of circumstellar dust in the parent material.

Molybdenum has appealing features for examining this issue. Indeed, unprocessed presolar carbide and graphite grains host extreme molybdenum isotopic signatures (Nicolussi et al. 1998a, 1998b) inherited from the stellar environment in which they condensed (Gallino, Busso, & Lugaro 1997). In addition, subtle molybdenum isotope anomalies have been observed in both primitive (Yin, Yamashita, & Jacobsen 2000; Dauphas, Marty, & Reisberg 2002a) and differentiated (Dauphas et al. 2002a) meteorites, providing evidence for isotope heterogeneity of the protosolar nebula at spatial dimensions comparable to the source regions of the parent bodies (Dauphas et al. 2002a). In the current contribution, we demonstrate the existence of extreme molybdenum isotopic heterogeneity in a primitive meteorite, Orgueil. This suggests the presence of different molybdenum components with *s*- and *p*, *r*-process signatures, hosted by presolar grains and a homogeneous solar component, respectively.

Sequential digestion of primitive meteorites has proved very useful in the past for characterizing the fine-scale isotope heterogeneity of the solar system and revealing the presolar carrier phases of isotope anomalies (Rotaru, Birck, & Allègre 1992; Amari, Lewis, & Anders 1994; Huss & Lewis 1995; Podosek et al. 1997, 2000). We have thus determined molybdenum isotope abundances in bulk samples and leachate fractions of carbonaceous chondrites Orgueil (CI1) and Allende (CV3.2).

2. ISOTOPE MEASUREMENTS

Powdered samples of Orgueil and Allende were sequentially digested with reagents of increasing strength (Rotaru et al. 1992; Podosek et al. 1997, 2000). The molybdenum isotope abundances of each leachate fraction were determined (Table 1) using a protocol based on solvent extraction, ion chromatography, and plasma ionization mass spectrometry (Dauphas, Reisberg, & Marty 2001; Dauphas et al. 2002a, 2002b). The blank of the separation procedure is estimated to be 6 ± 3 ng. Molybdenum isotopic ratios were corrected for mass fractionation by internal normalization ($^{98}Mo/^{96}Mo = 1.4470$; Dauphas et al. 2001) and are expressed in epsilon notation (relative deviation in parts per 10^4 from a terrestrial standard; Table 1). The ratios corrected for mass fractionation using external normalization are displayed in Dauphas, Marty, & Reisberg (2002c).

As illustrated in Figure 1, the molybdenum isotopic composition of bulk Orgueil (step 0) is identical within uncertainties to the terrestrial value. However, acid digestion steps (1–4) reveal that the isotopic composition of Orgueil is in fact a mixture between two distinct components having extreme and complementary isotopic compositions (steps 2 and 3). The summation of individual digestion steps (1–4) is consistent with the observed bulk composition (step 0). The positive pattern revealed in step 2 is denoted Mo-w in reference to its shape (Dauphas et al. 2002a). It is identical to, although more extreme than, that observed in macroscopic samples of many primitive and differentiated meteorites and corresponds to a deficit in *s*-nuclides (Dauphas et al. 2002a). The negative pattern observed in step 3 mirrors that revealed in step 2 and is thus denoted Mo-m. This pattern is similar to that measured in circumstellar carbide and graphite grains (Nicolussi et al. 1998a, 1998b) and

[1] École Nationale Supérieure de Géologie, rue du doyen Marcel Roubault, BP 40, 54501 Vandoeuvre lès Nancy Cedex, France.

TABLE 1

MOLYBDENUM ISOTOPE MEASUREMENTS

SAMPLE	STEP	DIGESTION	FRACTION	BLANK	ϵ^i (per 10^4)							
					92	94	95	96	97	98	100	97*
Allende CV3.2	0	Bulk	...	...	2.38 ± 0.57	1.95 ± 0.79	1.98 ± 0.50	0	1.62 ± 0.53	0	1.17 ± 0.50	0.70 ± 0.66
	0	Bulk	...	...	3.54 ± 0.67	2.62 ± 1.26	1.92 ± 0.67	0	0.91 ± 0.41	0	0.56 ± 0.52	0.47 ± 0.58
	0	Bulk	...	...	2.57 ± 0.78	1.80 ± 0.46	1.78 ± 0.21	0	1.10 ± 0.53	0	1.67 ± 0.34	−0.22 ± 0.60
	0	Bulk	...	...	1.23 ± 0.39	1.04 ± 0.31	0.98 ± 0.20	0	0.74 ± 0.19	0	0.43 ± 0.21	0.40 ± 0.25
	1	CH_3COOH 8.5 M, 20°C, 1 d	0.05 ± 0.01	0.080 ± 0.042	3.16 ± 1.73	1.76 ± 2.44	1.94 ± 0.52	0	1.80 ± 1.08	0	0.69 ± 0.97	1.25 ± 1.32
	2	HNO_3 4 M, 20°C, 5 d	0.44 ± 0.13	0.009 ± 0.005	2.37 ± 0.64	1.67 ± 0.43	1.58 ± 0.27	0	0.84 ± 0.40	0	0.20 ± 0.51	0.68 ± 0.57
	3	HCl 3 M–HF 13.5 M, 100°C, 4 d	0.46 ± 0.14	0.012 ± 0.006	3.19 ± 0.53	2.06 ± 0.52	1.87 ± 0.29	0	1.30 ± 0.21	0	0.89 ± 0.32	0.60 ± 0.33
	4	HNO_3 8 M–HF 13.5 M–$HClO_4$ 0.5 M, 160°C, 14 d	0.05 ± 0.02	0.121 ± 0.066	3.82 ± 2.60	2.60 ± 3.73	1.81 ± 1.78	0	1.37 ± 0.95	0	0.75 ± 1.99	0.78 ± 1.84
Orgueil CI1	0	Bulk	...	...	0.53 ± 0.57	0.13 ± 0.49	0.72 ± 0.25	0	0.39 ± 0.30	0	−0.47 ± 0.35	0.76 ± 0.41
	1	CH_3COOH 8.5 M, 20°C, 1 d	0.08 ± 0.02	0.158 ± 0.087	0.15 ± 4.19	−0.22 ± 1.67	0.84 ± 2.08	0	0.97 ± 0.23	0	1.38 ± 4.39	−0.12 ± 3.48
	2	HNO_3 4 M, 20°C, 5 d	0.67 ± 0.20	0.019 ± 0.011	9.90 ± 0.52	7.93 ± 0.50	5.25 ± 0.32	0	2.97 ± 0.52	0	3.34 ± 0.39	0.33 ± 0.64
	3	HCl 3 M–HF 13.5 M, 100°C, 4 d	0.16 ± 0.05	0.105 ± 0.052	−40.21 ± 1.65	−31.76 ± 0.89	−19.32 ± 0.97	0	−9.96 ± 0.99	0	−11.31 ± 1.83	−1.03 ± 1.88
	4	HNO_3 8 M–HF 13.5 M–$HClO_4$ 0.5 M, 160°C, 14 d	0.09 ± 0.03	0.212 ± 0.105	0.16 ± 3.27	0.55 ± 0.96	0.91 ± 1.38	0	0.47 ± 1.26	0	0.08 ± 2.92	0.41 ± 2.63

NOTE.—"Fraction" represents the proportion of molybdenum leached in each dissolution step (1–4). "Blank" is the contribution of the digestion and separation blank to the measurement. Molybdenum isotope abundances were normalized to $^{98}Mo/^{96}Mo = 1.4470$ (Dauphas et al. 2001). The isotopic composition is expressed as $\epsilon^i = [(^iMo/^{96}Mo)/(^iMo/^{96}Mo) - 1] \times 10^4$. Uncertainties are 2 σ. The acquisition scheme and data reduction technique are described in Dauphas et al. (2001). The anomaly at mass 97 has been corrected for the presence of the nucleosynthetic component using the observed anomaly at mass 100, $\epsilon^{97*} = \epsilon^{97} - 0.79 \pm 0.06\epsilon^{100}$ (Dauphas et al. 2002a, 2002d). The first three bulk Allende measurements are from Dauphas et al. (2002a).

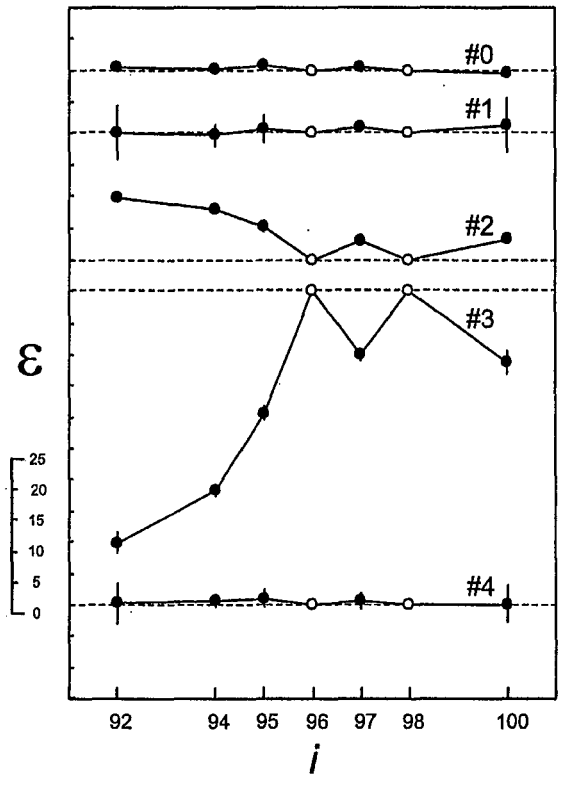

FIG. 1.—Molybdenum isotopic composition of bulk sample 0 and leachate fractions 1–4 of Orgueil CI1 (see Table 1).

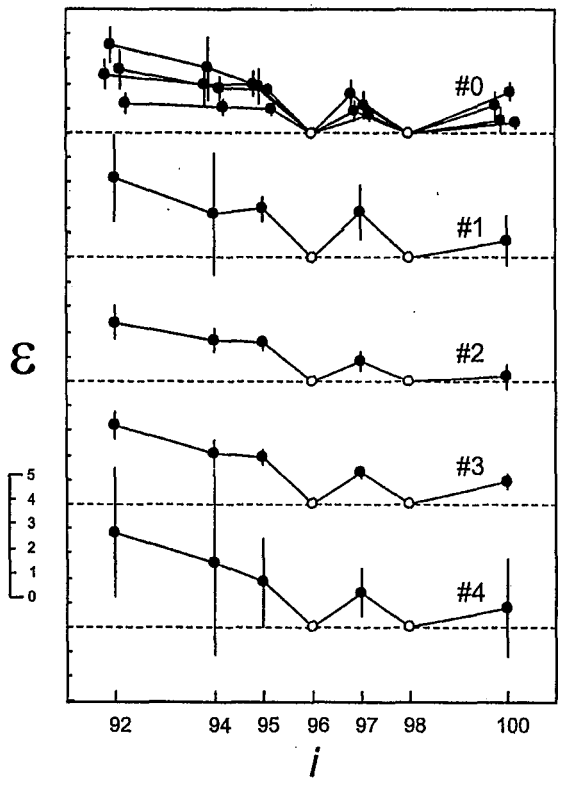

FIG. 2.—Same as Fig. 1, but of Allende CV3.2 (see Table 1)

corresponds to an excess in *s*-nuclides (Nicolussi et al. 1998a, 1998b; Gallino et al. 1997).

In Figure 2, molybdenum isotope abundances of bulk samples and leachate fractions of Allende are displayed. Replicate measurements of bulk Allende (step 0) show clear anomalies relative to the terrestrial standard. Contrary to Orgueil, acid digestion steps (1–4) reveal no internal heterogeneity in Allende. The summation of individual digestion steps (1–4) is again consistent with the bulk composition (step 0). The isotopic spectra observed in bulk (step 0) and individual digestion steps (1–4) of Allende are nearly identical in form to the Mo-w pattern identified in the dissolution sequence of Orgueil (step 2).

Note that after correction for the presence of nucleosynthetic anomalies (Dauphas et al. 2002a, 2002d), there is no evidence for a radiogenic component at mass 97 owing to the decay of now extinct ^{97}Tc ($\epsilon^{97*} = 0$; Table 1).

3. POSSIBLE CARRIERS OF Mo-w AND Mo-m

There is no reason to expect to find specific presolar host phases with the Mo-w spectrum, because the *p*- and *r*-process enrichments that contribute to this pattern have no reason to be coupled. Stated otherwise, a stellar environment where *p*- and *r*-nuclides are produced in strictly solar proportions, as is observed, is unlikely to exist. Thus, Mo-w must represent the homogenized portion of the presolar cloud.

The possible carriers of Mo-m are silicon carbide, graphite, or some unidentified presolar phase. Previous studies have shown that the molybdenum isotope anomalies contained in presolar graphite are quite small (Nicolussi et al. 1998b). Graphite is thus unlikely to be the phase that hosts the *s*-process molybdenum released during leaching step 3 of Orgueil. The simplest explanation is that this step has removed molybdenum hosted by silicon carbides. Using the molybdenum isotopic composition of silicon carbide (Nicolussi et al. 1998a) and the Earth (Dauphas et al. 2001), the silicon carbide concentration of Orgueil (Huss & Lewis 1995), and the molybdenum concentration of Orgueil (Wieser & De Laeter 2000), we estimate by mass balance a molybdenum concentration of 33 ± 15 parts per million (ppm) in silicon carbide in order to explain the presence of the anomalous spectrum detected in leachate 3 of Orgueil. Molybdenum concentrations in separated SiC grains determined by synchrotron X-ray fluorescence range from 1 to 50 ppm (Kashiv et al. 2001). Nevertheless, the average concentration is 9 ± 6 ppm (Kashiv et al. 2001), lower than the value we infer. This difference might reflect molybdenum loss during the acid leaching steps (Amari, Lewis, & Anders 1994; Huss & Lewis 1995) used for silicon carbide grain extraction. Separation of silicon carbide involves lengthy treatment with HF-HCl aimed at destroying the surrounding matrix (Amari, Lewis, & Anders 1994; Huss & Lewis 1995). Although intriguing, leaching of molybdenum from presolar silicon carbide in step 3 (HF-HCl) is not impossible. Indeed, (1) the behavior of molybdenum carbide inclusions is likely to be different from that of silicon carbide, and it is possible to leach molybdenum without destroying the host grain; (2) the treatment used for silicon carbide extraction (Amari, Lewis, & Anders 1994; Huss & Lewis 1995) does not destroy the grain but alters its surface morphology (Bernatowicz et al. 2000), indicating that such treatment is not innocuous; and (3) the treatment used in the present study (HCl 3 M–HF 13.5 M, 100°C, 4 d) is probably harsher than that used for silicon carbide grain extraction (Amari, Lewis, & Anders 1994; Huss & Lewis 1995). Thus,

it seems most likely that Mo-m is hosted in presolar silicon carbide, although we cannot dismiss the possibility that it is hosted in a presolar phase that is currently unidentified.

4. SPATIAL DISTRIBUTION OF CIRCUMSTELLAR DUST

Solar system molybdenum is thus a mixture between two components. As shown by the leaching study of Orgueil, one is hosted in a presolar phase, possibly silicon carbide (Nicolussi et al. 1998a), and is leached in step 3 (Mo-m), while the other is distributed in other phases and is leached in step 2 (Mo-w). If there are indeed two nucleosynthetic components coexisting in the protosolar nebula, then subtle decoupling between these two would have resulted in macroscopic molybdenum isotope variations. Thus, the determination of molybdenum isotope abundances in bulk samples provides a means of addressing the planetary-scale distribution of circumstellar dust in the protosolar nebula.

The lack of molybdenum isotopic heterogeneity in Allende probably results from thermal processing either before or after accretion. This process may explain the very low silicon carbide content, 10^3 times lower than that of Orgueil, currently observed in this meteorite (Huss & Lewis 1995). As discussed in the case of Orgueil, the extent of the original silicon carbide contribution might control the isotopic composition of molybdenum in leachate fractions. Thus, the anomalous pattern detected in bulk Allende may be explained by a macroscopic deficiency in silicon carbide existing prior to thermal processing. Assuming that the two mixing end members are identical for Allende and Orgueil (Mo-m hosted in SiC and Mo-w leached in Orgueil step 2), then the contribution of silicon carbide to the bulk molybdenum inventory of Allende must have been 30% lower than that of Orgueil. Hence, the abundance of silicon carbide grains normalized to the abundance of a refractory element like molybdenum must have varied by at least 30% in the protosolar nebula. The Mo-w pattern was also detected in differentiated objects such as iron meteorites, mesosiderites, and pallasites (Dauphas et al. 2002a), indicating that the heterogeneous distribution of silicon carbide grains was a planetary-scale feature. There are two alternative explanations for this puzzling observation that are variants of the same idea. (1) Circumstellar dust was heterogeneously distributed in the presolar molecular cloud, and this distribution was preserved in the nascent solar system. (2) At some stage, the protosolar nebula was homogenized on a large scale, but cosmic chemical memory was recovered owing to nebular processes such as granular sorting or decoupling between the gas and the dust. In either case, these results provide the first evidence for decoupling between refractory silicon carbide and other carriers of refractory elements in the protosolar nebula. If the silicon carbide contribution to the bulk inventory is significant for additional elements such as Ti, Sr, Zr, Ru, Ba, Ce, Nd, and W (Amari et al. 1995; Kashiv et al. 2001), then there might be macroscopic isotopic variations for these elements as well, raising the possibility that they may be used as tracers of genetic relationships between planets and planetesimals (Dauphas et al. 2002a, 2002b). Thus, the barium isotope anomalies observed in bulk meteorite samples (Harper, Weismann, & Nyquist 1992) may perhaps be explained by such a deficit in presolar grains carrying anomalous isotopic compositions (Prombo et al. 1993; Pellin et al. 2001) typical of nucleosynthesis in asymptotic giant branch stars.

This work benefited from insightful comments by an anonymous reviewer as well as discussions with U. Ott. We are grateful to M. Denise for generously donating the samples. We thank C. Zimmermann and D. Yeghicheyan for analytical support. This work was funded by grants from the PNP (CNES/INSU) and PRISMS SMT4-CT98-2220 (EU). This is contribution 1567 of the CRPG.

REFERENCES

Amari, S., Hoppe, P., Zinner, E., & Lewis, R. S. 1995, Meteoritics, 30, 679
Amari, S., Lewis, R. S., & Anders, E. 1994, Geochim. Cosmochim. Acta, 58, 459
Anders, E., & Zinner, E. 1993, Meteoritics, 28, 490
Bernatowicz, T., Swan, P., Messenger, S., Walker, R., & Amari, S. 2000, Lunar Planet. Sci. Conf., 31, 1238
Burbidge, E. M., Burbidge, G. R., Fowler, W. A., & Hoyle, F. 1957, Rev. Mod. Phys., 29, 547
Cameron, A. G. W. 1957, PASP, 69, 201
Dauphas, N., Marty, B., & Reisberg, L. 2002a, ApJ, 565, 640
———. 2002b, Geophys. Res. Lett., in press
———. 2002c, Lunar Planet. Sci. Conf., 33, 1198
Dauphas, N., Rauscher, T., Schatz, H., Marty, B., & Reisberg, L. 2002d, ApJ, submitted
Dauphas, N., Reisberg, L., & Marty, B. 2001, Anal. Chem., 73, 2613
Gallino, R., Busso, M., & Lugaro, M. 1997, in AIP Conf. Proc. 402, Astrophysical Implications of the Laboratory Study of Presolar Materials, ed. T. J. Bernatowicz & E. K. Zinner (Woodbury: AIP), 115
Harper, C. L., Jr., Weismann, H., & Nyquist, L. E. 1992, Meteoritics, 27, 230
Huss, G. R., & Lewis, R. S. 1995, Geochim. Cosmochim. Acta, 59, 115
Kashiv, Y., Cai, Z., Lai, N., Sutton, S. R., Lewis, R. S., Davis, A. M., Clayton, R. N., & Pellin, M. J. 2001, Lunar Planet. Sci. Conf., 32, 2192
Nicolussi, G. K., Pellin, M. J., Lewis, R. S., Davis, A. M., Amari, S., & Clayton, R. N. 1998a, Geochim. Cosmochim. Acta, 62, 1093
Nicolussi, G. K., Pellin, M. J., Lewis, R. S., Davis, A. M., Clayton, R. N., & Amari, S. 1998b, ApJ, 504, 492
Pagel, B. E. J. 1997, Nucleosynthesis and Chemical Evolution of Galaxies (Cambridge: Cambridge Univ. Press)
Pellin, M. J., Davis, A. M., Savina, M. R., Kashiv, Y., Clayton, R. N., Lewis, R. S., & Amari, S. 2001, Lunar Planet. Sci. Conf., 32, 2125
Podosek, F. A., Nichols, R. H., Brannon, J. C., Meyer, B. S., Ott, U., Jennings, C. L., & Luo, N. 2000, Geochim. Cosmochim. Acta, 64, 2351
Podosek, F. A., Ott, U., Brannon, J. C., Neal, C. R., Bernatowicz, T. J., Swan, P., & Mahan, S. E. 1997, Meteoritics Planet. Sci., 32, 617
Prombo, C. A., Podosek, F. A., Amari, S., & Lewis, R. S. 1993, ApJ, 410, 393
Rotaru, M., Birck, J.-L., & Allègre, C. J. 1992, Nature, 358, 465
Wieser, M. E., & De Laeter, J. R. 2000, Fresenius J. Anal. Chem., 368, 303
Yin, Q. Z., Yamashita, K., & Jacobsen, S. B. 2000, Lunar Planet. Sci. Conf., 31, 1920

Évolution Chimique de la Galaxie

Riche de la sève du Monde, je monte vers l'Esprit qui me sourit au-delà de toute conquête, drapé dans la splendeur concrète de l'Univers.

Pierre Teilhard de Chardin

Beaucoup des questions fondamentales posées par l'humanité ont trait à la mesure du temps. Depuis combien de temps l'univers, la Galaxie, le soleil, la vie, ou l'homme existent-ils ? Les réponses à ces questions sont longtemps restées théologiques. Depuis un siècle environ, les scientifiques ont mis au point des outils pour dater précisemment les objets naturels qui composent notre environnement. La plupart des méthodes de datation reposent sur le principe de la décroissance radioactive. Certains nucléides sont instables et décroissent naturellement vers un nucléide fils stable. En mesurant l'abondance du nucléide fils, il est ainsi possible de déterminer l'âge de l'objet étudié.

L'expression *radioactivité éteinte* recouvre tous les radionucléides qui ont une demi-vie trop courte pour être détectés à l'heure actuelle mais qui étaient présents lorsque le système solaire s'est formé [11, 12]. La présence antérieure des radionucléides éteints peut-être déduite des traces de fission ou de la composition isotopique de l'élément porteur du nucléide fils. Une des plus remarquables radioactivités éteintes est représentée par le couple ^{26}Al-^{26}Mg [44]. L'aluminium-26 décroît par capture électronique en ^{26}Mg avec une demi-vie de 0.74 Ma. On montre simplement que si ce radionucléide était présent quand le système solaire s'est formé, alors il devrait y avoir une relation linéaire entre la composition isotopique du magnésium et le rapport aluminium sur magnésium (figure 1),

$$\left(\frac{^{26}\mathrm{Mg}}{^{24}\mathrm{Mg}}\right) = \left(\frac{^{26}\mathrm{Mg}}{^{24}\mathrm{Mg}}\right)_0 + \left(\frac{^{26}\mathrm{Al}}{^{27}\mathrm{Al}}\right)_0 \left(\frac{^{27}\mathrm{Al}}{^{24}\mathrm{Mg}}\right), \tag{1}$$

la pente de cette droite représente le rapport ^{26}Al/^{27}Al initial. Les mesures effectuées dans des inclusions réfractaires d'Allende [44, 45] indiquent un rapport initial canonique de 5×10^{-5} (figure 2). L'attrait particulier de ce radionucléide éteint réside dans le fait qu'il a pu constituer une source de chaleur significative, susceptible de provoquer la fusion des planétésimaux.

Deux corps s'étant formés à des temps distincts ont incorporé lors de leurs formations de l'aluminium avec des rapports ^{26}Al/^{27}Al distincts car, pendant le laps de temps qui les sépare, l'aluminium-26 a décru. Ce radionucléide constitue donc un chronomètre qui permet de discuter la chronologie des événements qui ont participé à la formation du système solaire.

D'autres radioactivités éteintes ont été découvertes qui permettent de discuter la chronologie du système solaire [11, 12]. Trois modèles coexistent à l'heure actuelle pour expliquer l'origine des

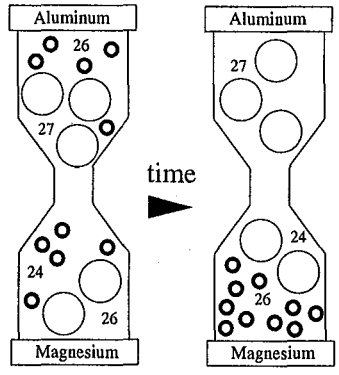

FIG. 1 – Dessin illustrant le principe de datation basé sur les radioactivités éteintes, en l'occurence l'aluminium-26. Plus le rapport $^{26}Al/^{24}Mg$ (et donc le rapport $^{27}Al/^{24}Mg$ pour un rapport $^{26}Al/^{27}Al$ donné) est important à l'origine, plus l'effet isotopique sur le rapport $^{26}Mg/^{24}Mg$ actuel est important.

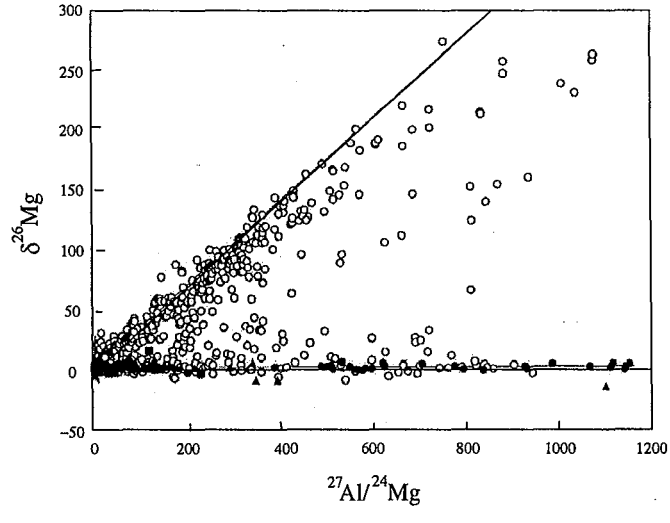

FIG. 2 – Corrélation entre la composition isotopique du fils et le rapport père-fils illustrant l'effet de la décroissance de ^{26}Al. Dans la plupart des inclusions réfractaires, le rapport initial $^{26}Al/^{27}Al$ est estimé à 5×10^{-5} (rapport canonique) [44, 45].

radioactivités éteintes. Elles pourraient être (*i*) le résultat de l'évolution chimique de la Galaxie et représenter le bruit de fond nucléosynthétique du milieu interstellaire [81, 82, 22], (*ii*) le produit de l'injection dans le nuage présolaire d'une étoile massive proche dont l'onde de choc associée à l'explosion aurait pu provoquer l'effondrement du nuage présolaire [114, 115, 116, 117], ou (*iii*) des produits d'irradiation dans le nuage protosolaire [118, 119]. Dans le cas (*i*) où les radionucléides sont le résultat de l'évolution chimique de la Galaxie dans le voisinage solaire, les radioactivités éteintes permettent de discuter le temps qui a séparé l'isolement nucléosynthétique du nuage moléculaire présolaire de l'effondrement de la nébuleuse protosolaire (*intervalle de décroissance libre*). Les radionucléides éteints produits par le processus *p* de nucléosynthèse n'ont pas pu être synthétisés dans le système solaire naissant mais ont pu être injectés dans la nébuleuse protosolaire par l'explosion d'une supernova proche ou être hérités de l'évolution chimique de la Galaxie dans le voisinage solaire. Ils permettent donc de discuter ces deux scenarii et le cas échéant de quantifier l'intervalle de décroissance libre.

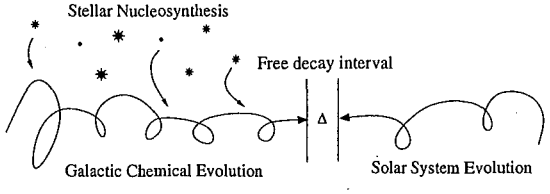

FIG. 3 – Les abondances des radionucléides héritées du milieu interstellaire peuvent être estimées de deux manières. Connaissant les rapports de production dans les sources nucléosynthétiques, il est possible d'estimer dans le cadre d'un modèle d'évolution chimique de la Galaxie, les abondances au moment de l'isolement du nuage moléculaire présolaire. En analysant les météorites, il est également possible d'estimer les abondances dans la nébuleuse protosolaire. Un intervalle de décroissance libre a pu séparer ces deux événements (isolement du nuage moléculaire présolaire et effondrement de la nébuleuse protosolaire).

Afin de discuter le modèle d'héritage du bruit de fond interstellaire, il est nécessaire de construire un modèle d'évolution chimique de la Galaxie qui rende compte des principales caractéristiques de la Galaxie dans le voisinage solaire (figure 4).

1 Modèle fermé

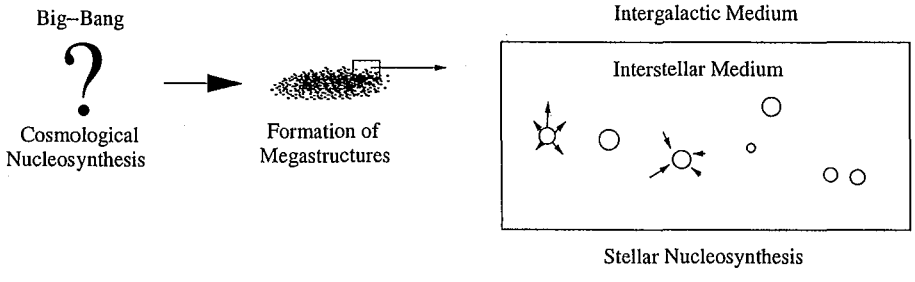

FIG. 4 – Schéma illustrant les fondements du modèle fermé (closed-box).

C'est le plus élémentaire des modèles d'évolution chimique de la Galaxie. On considère que la formation de la Galaxie a été instantanée et que ce réservoir de gaz a ensuite évolué par le jeu de la nucléosynthèse stellaire (figure 4). On convient de noter Σ_g la densité surfacique du gaz, et Ψ et E les taux respectifs de formation et d'éjection de matière stellaire [120, 81, 82, 22, 80]. On a alors simplement,

$$\frac{\mathrm{d}\Sigma_g}{\mathrm{d}t} = -\Psi + \mathrm{E}. \tag{2}$$

L'abondance d'un nucléide quelconque dans le milieu interstellaire est $Z\Sigma_g$ et son taux de variation s'écrit dans le cas de l'approximation du recyclage instantané,

$$\frac{\mathrm{d}Z\Sigma_g}{\mathrm{d}t} = -\Psi Z + \mathrm{E}Z_\mathrm{E} - \lambda Z\Sigma_g. \tag{3}$$

On suppose que le taux de formation des étoiles est proportionnel à la densité du gaz et l'on définit la constante d'épuisement du gaz $\omega = (\Psi - \mathrm{E})/\Sigma_g$. On introduit également y, le rendement (*yield*) qui est la quantité du nucléide Z créée par unité de matière prisonnière des résidus stellaires, $y = \mathrm{E}(Z_\mathrm{E} - Z)/(\Psi - \mathrm{E})$. Il vient alors,

$$\frac{\mathrm{d}\Sigma_g}{\mathrm{d}t} = -\omega\Sigma_g, \tag{4}$$

et,

$$\frac{\mathrm{d}Z}{\mathrm{d}t} = y\omega - \lambda Z. \tag{5}$$

L'intégration de cette équation par la méthode de la variation de constante ne présente aucune difficulté,

$$Z = \frac{y\omega}{\lambda}(1 - e^{-\lambda t}). \tag{6}$$

On définit le *rapport restant* (*remainder ratio*) $\Re$ comme l'abondance d'un nucléide radioactif divisée par l'abondance qu'il aurait s'il avait été stable,

$$\Re = \frac{Z(\lambda)}{Z(\lambda = 0)}. \tag{7}$$

Dans le cas d'un radionucléide à courte demi-vie, $e^{-\lambda \mathrm{T}}$ est très petit devant 1 (où T est l'âge présolaire de la Galaxie) et il vient,

$$\Re = \frac{1}{\lambda \mathrm{T}}. \tag{8}$$

Le modèle fermé permet d'estimer simplement le rapport restant dans le milieu interstellaire au moment de la formation du système solaire. Ce modèle ne permet cependant pas de rendre compte de toutes les observations faites et d'autres descriptions plus complètes sont utilisées. Il garde néanmoins un intérêt heuristique.

2 Modèle ouvert

Le modèle fermé ne permet pas de rendre compte d'observations importantes comme la distribution en métallicité des étoiles naines de type G [121, 122, 80, 123]. Pour expliquer cette lacune, il est communément admis que la Galaxie ne s'est pas comportée en système fermé mais qu'elle a été continuellement enrichie en gaz à faible métallicité (modèle ouvert d'accrétion ou *infall model*) [81, 82]. Des preuves observationnelles sont venues récemment soutenir cette idée

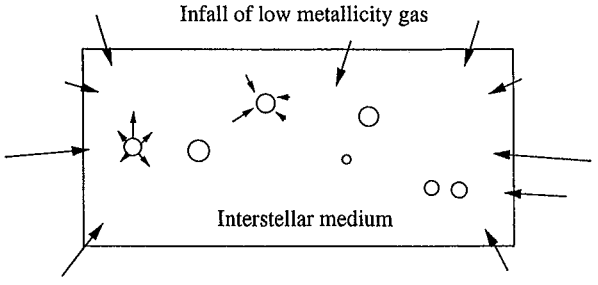

FIG. 5 – Schéma illustrant les fondements du modèle ouvert d'accrétion (*infall*).

[124]. Ce modèle est en tous points identique au modèle fermé excepté que l'on considère que le disque galactique a continuellement été enrichi en gaz à faible métallicité par accrétion (figure 5).

On introduit f le taux d'accrétion de gaz par le disque galactique au voisinage solaire. Les équations qui gouvernent le taux de variation de la densité surfacique de gaz et de l'abondance d'un radionucléide sont respectivement,

$$\frac{\mathrm{d}\Sigma_g}{\mathrm{d}t} = -\Psi + \mathrm{E} + f, \tag{9}$$

et,

$$\frac{\mathrm{d}Z\Sigma_g}{\mathrm{d}t} = -\Psi Z + \mathrm{E}Z_{\mathrm{E}} + fZ_f - \lambda Z\Sigma_g, \tag{10}$$

où Z_f est la concentration dans le gaz accrété (proche de zéro). En procédant de la même manière que dans la cas du modèle fermé on montre,

$$\frac{\mathrm{d}Z}{\mathrm{d}t} = y\omega - \frac{f}{\Sigma_g}(Z - Z_f) - \lambda Z. \tag{11}$$

On introduit le *nombre de cycles*,

$$\frac{\mathrm{d}\theta}{\mathrm{d}t} = \frac{f}{\Sigma_g}. \tag{12}$$

Il vient alors,

$$\frac{\mathrm{d}Z}{\mathrm{d}t} = y\omega - (Z - Z_f)\frac{\mathrm{d}\theta}{\mathrm{d}t} - \lambda Z. \tag{13}$$

Posons $A(t)$ tel que,

$$Z(t) = A(t)e^{-\lambda t - \theta(t)}. \tag{14}$$

On montre que l'équation différentielle qui gouverne le taux de variation de $A(t)$ est,

$$\frac{\mathrm{d}A(t)}{\mathrm{d}t} = \left(y\omega + Z_f\frac{\mathrm{d}\theta}{\mathrm{d}t}\right)e^{\lambda t + \theta(t)}. \tag{15}$$

Cette équation s'écrit également,

$$\frac{\mathrm{d}A(t)}{\mathrm{d}t} = (y\omega - \lambda Z_f)e^{\lambda t + \theta(t)} + Z_f\frac{\mathrm{d}\left[e^{\lambda t + \theta(t)}\right]}{\mathrm{d}t}. \tag{16}$$

A ce stade, l'intégration ne présente aucune difficulté et l'on montre,

$$Z(\mathrm{T}) - Z_f = e^{-\lambda \mathrm{T} - \theta(\mathrm{T})} \left[(y\omega - \lambda Z_f) \int_0^{\mathrm{T}} e^{\lambda t + \theta(t)} \mathrm{d}t + Z(0) - Z_f \right]. \tag{17}$$

On considère que le gaz initial et le gaz accrété sont dépourvus du nucléide qui nous intéresse; $Z(0) = Z_f = 0$. Le rapport restant dans le milieu interstellaire au moment de l'isolement du nuage moléculaire présolaire s'exprime alors,

$$\Re = \int_{\mathrm{T}} e^{\lambda t + \theta(t)} \mathrm{d}t \, / \int_{\mathrm{T}} e^{\lambda \mathrm{T} + \theta(t)} \mathrm{d}t. \tag{18}$$

Clayton [81, 82] a étudié l'évolution chimique de la Galaxie dans le cas où le nombre de cycles est paramétré selon,

$$\frac{\mathrm{d}\theta}{\mathrm{d}t} = \frac{k}{t + \Delta}, \tag{19}$$

où k et Δ sont des paramètres libres du modèle. Le nombre de cycles prend dans ce cas la forme $\theta(t) = \ln(t/\Delta + 1)^k$. On introduit $\mathrm{x} = (t + \Delta)/\Delta$ et $X = (\mathrm{T} + \Delta)/\Delta$. Le rapport restant peut s'écrire,

$$\Re = \frac{(k+1)e^{-\lambda \mathrm{T}}}{\Delta(X^{k+1} - 1)} \int_0^{\mathrm{T}} e^{\lambda t} x^k \mathrm{d}t. \tag{20}$$

Soit,

$$I_k = \int_0^{\mathrm{T}} x^k e^{\lambda t} \mathrm{d}t. \tag{21}$$

On montre par récursivité que,

$$\lambda I_k = X^k e^{\lambda \mathrm{T}} - 1 - (k/\Delta) I_{k-1}, \tag{22}$$

avec $\lambda I_0 = e^{\lambda \mathrm{T}} - 1$. Dans le cas d'un radionucléide à courte demi-vie, on a

$$I_k \simeq \frac{X^k e^{\lambda \mathrm{T}}}{\lambda}. \tag{23}$$

Pour Δ suffisamment petit devant T, il vient,

$$\Re \simeq \frac{k+1}{\lambda \mathrm{T}}, \tag{24}$$

avec k compris entre 1 et 3 [81, 82]. Le cas $k = 0$ revient au modèle fermé où l'on avait $\Re = 1/(\lambda \mathrm{T})$.

Une des hypothèses fondamentales dans ce modèle est que le taux de formation des étoiles est une fonction linéaire de la densité de gaz [125]. En fait, Ψ semble suivre une loi puissance de Σ_g avec un exposant différent de l'unité [126, 127].

3 Modèle ouvert non-linéaire

On considère maintenant que le taux de formation des étoiles est une fonction puissance n de la densité surfacique de gaz [22]. On redéfinit ω la constante d'épuisement du gaz $\omega = (\Psi - \mathrm{E})/\Sigma_g^n$. Le taux de variation de Σ_g s'écrit,

$$\frac{\mathrm{d}\Sigma_g}{\mathrm{d}t} = -\omega \Sigma_g^n + f. \tag{25}$$

En conservant la même définition pour le rendement y que précedemment il vient,

$$\frac{\mathrm{d}Z}{\mathrm{d}t} = y\omega\Sigma_g^{n-1} - \frac{f}{\Sigma_g}Z - \lambda Z. \tag{26}$$

Par la méthode de la variation de constante, on montre simplement que,

$$\Re = \int_0^{\mathrm{T}} \Sigma_g^{n-1} e^{\lambda t+\theta(t)}\mathrm{d}t \Big/ \int_0^{\mathrm{T}} \Sigma_g^{n-1} e^{\lambda \mathrm{T}+\theta(t)}\mathrm{d}t. \tag{27}$$

Comme dans le cas du modèle ouvert linéaire, le rapport restant peut se mettre sous la forme,

$$\Re = \frac{\kappa}{\lambda T}. \tag{28}$$

L'évaluation de κ n'est pas triviale car du fait de la non-linéarité des équations, celles-ci doivent être résolues numériquement pour rendre compte de la densité surfacique de la Galaxie dans le voisinage solaire, du rapport de densité gaz/étoiles, de la métallicité du système solaire, et de la distribution en métallicité des étoiles naines de type G. La valeur de κ qui intégre toutes ces contraintes est estimée à 2.9 ± 0.4 [22].

4 Technétium-97 et p-radionucléides

Le modèle ouvert non linéaire [22] a été construit dans le dessein de discuter les abondances des radionucléides p éteints dans le système solaire. Cette étude a été effectuée en collaboration avec Thomas Rauscher de l'Université de Bâle en Suisse.

Des contraintes ont été posées sur les abondances de quatre p-radionucléides éteints dans le système solaire ; le ^{97}Tc qui décroît en ^{97}Mo ($\lambda^{-1} = 3.8$ Ma) [19, 22], le ^{98}Tc qui décroît en ^{98}Ru ($\lambda^{-1} = 6.1$ Ma) [128], le ^{92}Nb qui décroît en ^{92}Zr ($\lambda^{-1} = 50.1$ Ma) [129, 130, 131, 132, 133, 134], et le ^{146}Sm qui décroît en ^{142}Nd ($\lambda^{-1} = 149$ Ma) [135, 136, 137, 138, 139, 140, 141]. Les rapports de production de ces nucléides dans les SNII ont été calculés par Thomas Rauscher [38, 22]. En utilisant le modèle ouvert non linéaire décrit précedemment [22], il est possible d'estimer le rapport restant dans le milieu interstellaire au moment de l'isolement du nuage moléculaire présolaire,

$$\Re_{\mathrm{ISM}} = \frac{\kappa}{\lambda \mathrm{T}} \tag{29}$$

Soit R le rapport d'abondance d'un radionucléide normalisé à un nucléide stable produit par le même processus, et P le rapport de production. Si le radionucléide était stable, son abondance dans le système solaire serait égale à l'abondance du nucléide stable S multipliée par le rapport de production P. L'abondance à la naissance du système solaire est en fait l'abondance S multipliée par le rapport initial R. Le rapport restant dans le système solaire au moment de sa formation peut donc être calculé en formant le rapport,

$$\Re_{\mathrm{ESS}} = \frac{\mathrm{R}}{\mathrm{P}}. \tag{30}$$

Un intervalle de décroissance libre a pu séparer l'isolement du nuage moléculaire présolaire de l'effondrement de la nébuleuse protosolaire,

$$\Re_{\mathrm{ESS}} = \Re_{\mathrm{ISM}}\, e^{-\lambda\Delta}. \tag{31}$$

Dans l'article qui suit [22], nous avons montré que les abondances des p-radionucléides ^{97}Tc, ^{98}Tc, ^{92}Nb, et ^{146}Sm sont toutes cohérentes avec un héritage du milieu interstellaire pour un intervalle de décroissance libre inférieur à 10 Ma environ. La présence des radioactivités éteintes dans le système est vraisemblablement la combinaison (i) d'un héritage du milieu interstellaire et (ii) d'une production par irradiation dans le système solaire.

5 Astrophys. J., submitted

Short-Lived p-Nuclides in the Early Solar System, Bridging the Gap Between Galactic Chemical Evolution and Solar System Formation

Dauphas, N., Rauscher, T., Schatz, H., Marty, B., and Reisberg, L.

The Astrophysical Journal, submitted

SHORT-LIVED *P*-NUCLIDES IN THE EARLY SOLAR SYSTEM, BRIDGING THE GAP BETWEEN GALACTIC CHEMICAL EVOLUTION AND SOLAR SYSTEM FORMATION

N. DAUPHAS
Centre de Recherches Pétrographiques et Géochimiques, CNRS UPR 2300, 15 rue Notre-Dame des Pauvres, BP 20, 54501 Vandœuvre-lès-Nancy Cedex, France
dauphas@crpg.cnrs-nancy.fr

T. RAUSCHER
Departement für Physik und Astronomie, Universität Basel, Klingelbergstrasse 82, CH-4056 Basel, Schweiz

H. SCHATZ
Department of Physics and Astronomy and National Cyclotron Laboratory, Michigan State University, East Lansing, MI 48824, USA
AND

B. MARTY[1] AND L. REISBERG
Centre de Recherches Pétrographiques et Géochimiques, CNRS UPR 2300, 15 rue Notre-Dame des Pauvres, BP 20, 54501 Vandœuvre-lès-Nancy Cedex, France
Submitted to ApJ

ABSTRACT

The origin of extinct radionuclides is uncertain. Their presence in the early solar system might result either from (*i*) inheritence from the chemical evolution of the Galaxy, (*ii*) injection from a nearby giant star, or (*iii*) local irradiation within the early solar system. In the present contribution, we first evaluate the abundances of the short-lived *p*-nuclides that might have been present in the nascent solar system (^{97}Tc, ^{98}Tc, ^{92}Nb, and ^{146}Sm). Then we present a model of the chemical evolution of the Galaxy incorporating infall of low metallicity gas. This allows to compare the remainder ratio of SNIa, SNII, and X-ray burst ejecta in the interstellar medium at the time of solar system birth to the remainder ratio within the early solar system. It is concluded that the abundances of short-lived *p*-nuclides ^{97}Tc, ^{98}Tc, ^{92}Nb, and ^{146}Sm are consistent with derivation from continuous chemical evolution of the Galaxy employing a comparatively short free-decay interval ($\Delta < 100$ Ma) and assuming that the main sources are SNIa and SNII. Furthermore, we derive a strong constraint on the possible contribution of X-ray bursts. Finally, we propose a model for the origin of extinct radionuclides in the nascent solar system combining chemical evolution of the Galaxy and local irradiation within the early solar system.

Subject headings: solar system: formation—Galaxy: evolution—nuclear reactions, nucleosynthesis, abundances—supernovae: general

1. INTRODUCTION

Extinct nuclides are those radioactive nuclides which were present in the early solar system but have now decayed to extinction. Although they have now decayed below detection levels, their prior presence can be inferred from abundance variations of their daughter nuclides in solar system formation remnants (Podosek & Nichols 1996). The origin of short-lived nuclides in the early solar system is the subject of much debate. They may have resulted from (*i*) inheritence from the chemical evolution of the Galaxy (Schramm & Wasserburg 1970; Clayton 1985), (*ii*) injection from a nearby giant star that might have triggered the protosolar nebula into collapse (Cameron et al. 1996), and (*iii*) irradiation within the solar system by intense stellar flares (Lee 1978; Clayton & Jin 1995; Lee et al. 1998; McKeegan et al. 2000; Gounelle et al. 2001; Chaussidon et al. 2002; Leya et al. 2002). Thus, short-lived nuclides bear important information on star formation.

Howard (1993) suggested that the *p*-process radionuclides ^{97}Tc, ^{98}Tc, ^{92}Nb, and ^{146}Sm might have been present in the early solar system when the first solids condensed. In order to investigate the formation of the solar system, one can proceed either forward or backward in time. The abundances of short-lived *p*-nuclides in the interstellar medium at solar system birth can be derived from modelling of galactic chemical evolution (Schramm & Wasserburg 1970; Clayton 1985) and stellar nucleosynthesis (Howard et al. 1991; Rayet et al. 1995). The abundances of short-lived *p*-nuclides in the early solar system can also be derived from laboratory measurements of solar system formation remnants (Podosek & Nichols 1996). Comparison between the predicted and the observed abundances provides unequalled information on the origin of extinct radionuclides and solar system birth.

The wealth of new data on abundances in the early solar system drawn from the investigation of meteorites make a reinvestigation worthwhile. In Sec. 2 we provide an overview over the most recently available data and in Sec. 3 the production of *p*-nuclides in SNIa, SNII, and X-ray bursts is discussed. The initial abundances and the predicted stellar production ratios are then used in a model of galactic chemical evolution which is presented in Sec.

[1] École Nationale Supérieure de Géologie, rue du doyen Marcel Roubault, BP 40, 54501 Vandœuvre-lès-Nancy Cedex, France

4. The simple model has been specifically chosen to minimize the number of parameters and to keep arbitrary formalism to a minimum. Finally, from the remainder ratio introduced in Sec. 5 we draw conclusions concerning the free-decay interval and compare it to previous results in Sec. 6.

2. ABUNDANCES IN THE EARLY SOLAR SYSTEM

In this section, all short-lived nuclides were normalized to stable neighbor nuclides synthesized according to the same nucleosynthetic process (Anders & Grevesse 1989). Thus, the ratios that are discussed in the text are not necessarily those discussed in the original papers. The initial ratios in the solar system are compiled in Table 1.

2.1. *Technetium-97*

The even-odd p-nuclide ^{97}Tc EC-decays to ^{97}Mo with a mean life of 3.8 Ma. It is bypassed by the s-process and shielded against an r-process contribution so that it is only synthesized by the p-process (Lambert 1992). It has been suggested that ^{97}Tc was alive when the terrestrial core segregated (Yin & Jacobsen 1998; Yin et al. 1999) but this result is at odds with the timing of core formation inferred from the ^{182}Hf–^{182}W and Pb chronometers (Lee & Halliday 1995; Halliday et al. 1996; Dauphas et al. 2002b; Allègre et al. 1995; Galer & Goldstein 1996). Determining whether ^{97}Tc was alive in the protosolar nebula or not has profound implications on both early solar system chronology and p-nucleosynthesis.

The behavior of technetium in the chain of events that led to the formation of meteorites is poorly known (Fegley et al. 1993). Because of the similarity in chemical properties between Re and Tc, the Re/Mo ratio can be taken as a proxy for the Tc/Mo ratio (Yin & Jacobsen 1998). Refractory inclusions are promising hosts for now extinct ^{97}Tc because they were among the first solids to form in the solar system 4.56 Ga ago (Allègre et al. 1995). In addition, most inclusions exhibit high parent to daughter Re(Tc)/Mo ratios (Fegley & Palme 1984; Fegley et al. 1993). Iron meteorites formed soon after refractory inclusions (Hutcheon et al. 1992; Chen & Wasserburg 1996; Shen et al. 1996; Smoliar et al. 1996; Birck & Allègre 1998; Horan et al. 1998; Carlson & Hauri 2001). These objects contain appreciable amounts of molybdenum (Smales et al. 1967). In addition, the Re(Tc)/Mo ratio was extensively fractionated in iron meteorite parent-bodies due to the difference between liquid/solid metal partition coefficients of Mo and Re (Fleet et al. 1999; Liu & Fleet 2001). Thus, iron meteorites appear to be ideal candidates to search for the presence of live ^{97}Tc in the early solar system.

Iron meteorite samples weighing 0.2 to 0.8 g were digested in 10 ml of HCl 11 mol.l^{-1} – HF 3 mol.l^{-1}. Sample aliquots were used for Mo and Re abundance determinations by the standard addition technique. The fractionation factor $f_{\rm Re/Mo}$ is defined as,

$$f_{\rm Re/Mo} = (^{185}{\rm Re}/^{96}{\rm Mo})/(^{185}{\rm Re}/^{96}{\rm Mo})_{\rm chur} - 1, \quad (1)$$

where *chur* denotes the chondritic uniform reservoir. Molybdenum isotope abundances were determined with a multiple collection inductively coupled plasma hexapole mass spectrometer after solvent extraction with di(2-ethylhexyl) phosphate and ion chromatography using AG1-X8 strongly basic anion exchanger (Dauphas et al. 2001). Molybdenum isotopic composition was corrected for exponential mass fractionation (Maréchal et al. 1999) by normalization to ^{98}Mo/^{96}Mo=1.4470 (Dauphas et al. 2001). Molybdenum isotope abundances are expressed in ε-notation,

$$\varepsilon^i = [(^i{\rm Mo}/^{96}{\rm Mo})/(^i{\rm Mo}/^{96}{\rm Mo})_\oplus - 1] \times 10^4. \quad (2)$$

Molybdenum nucleosynthetic anomalies were observed in macroscopic samples and leachate fractions of primitive meteorites (Dauphas et al. 2002a,c). These are characterized by a deficit (Mo-w) or an excess (Mo-m) in s-nuclides (Dauphas et al. 2002a,c). Thus, an anomaly at mass 97 could potentially represent a nucleosynthetic component as well as a radiogenic contribution from the decay of ^{97}Tc. Molybdenum-100 is an r-only nuclide, raising the possibility that the observed anomaly at mass 100 can be used to correct that at mass 97 for the nucleosynthetic contribution through,

$$\varepsilon^{97*} = \varepsilon^{97} - (\varrho^{97} - 0.5\varrho^{98})/(1 - 2\varrho^{98}) \times \varepsilon^{100}, \quad (3)$$

where $\varrho^i = (^i{\rm Mo}/^{100}{\rm Mo})_r/(^i{\rm Mo}/^{100}{\rm Mo})_\oplus$, r denotes the r-process. ϱ^{98} enters into the equation because the ^{98}Mo/^{96}Mo ratio is used to correct molybdenum isotope measurements for mass fractionation. The r-process normalized isotopic ratios can be estimated using the signatures measured in presolar carbide and graphite grains (Nicolussi et al. 1998a,b). In a $\mathrm{R}^{96} - \mathrm{R}^{97,98}$ plot, where $\mathrm{R}^i = (^i{\rm Mo}/^{100}{\rm Mo})/(^i{\rm Mo}/^{100}{\rm Mo})_\oplus$, the Earth and presolar grains align along straight mixing lines (Fig. 1). Because ^{96}Mo is an s-only nuclide, the intersection between these mixing lines and the y-axis corresponds to the r-process normalized isotopic ratios. Thus, ϱ^{97} and ϱ^{98} are estimated to be 0.48 ± 0.02 and 0.27 ± 0.01, resulting in $\varepsilon^{97*} = \varepsilon^{97} - 0.79 \pm 0.06 \times \varepsilon^{100}$. Note that these estimates are in good agreement with those inferred from residuals obtained by detailed modelling of s-nucleosynthesis in AGB stars (Arlandini et al. 1999), $\varrho^{97} = 0.43$ and $\varrho^{98} = 0.25$, leading to $\varepsilon^{97*} = \varepsilon^{97} - 0.61 \times \varepsilon^{100}$ (Dauphas et al. 2002a).

The ^{187}Re – ^{187}Os system (mean life 62.8 Ga) allows precise dating of metal crystallization in asteroids. Shen et al. (1996) and Smoliar et al. (1996) reported intriguing evidence for diachronism of iron meteorite formation but the chronologies they inferred contradict each other. Metal differentiation in planetesimals occured in all probability within $\sim$ 50 Ma of solar system formation (Shen et al. 1996; Smoliar et al. 1996; Birck & Allègre 1998; Horan et al. 1998). Tighter constraints can be set on the timing of iron meteorite formation from the ^{107}Pd – ^{107}Ag extinct chronometer (mean life 9.4 Ma). In order to produce the observed variations in ^{107}Ag isotopic abundance, the time span between metal condensation in the protosolar nebula and crystallization in asteroids must have been lower than $\sim$ 10 Ma (Chen & Wasserburg 1996; Carlson & Hauri 2001). The timescale inferred from the ^{53}Mn – ^{53}Cr system (mean life 5.4 Ma) is more equivocal because these nuclides might have been redistributed during the extended cooling history of planetesimals (Chen & Wasserburg 1996). Yet, some iron meteorites have closure ages within $\sim$ 7 Ma that of the Allende refractory inclusions (Hutcheon et al. 1992). On the whole, it seems that most iron meteorites crystallized from a metallic magma within $\sim$10 Ma of the solar system birth. In case iron meteorites isolated

simultaneously from the chondritic uniform reservoir, the radiogenic molybdenum isotopic composition ε^{97*} is a linear function of the fractionation factor $f_{\mathrm{Re/Mo}}$ (Jacobsen & Wasserburg 1984),

$$\varepsilon^{97*} = Q \frac{^{97}\mathrm{Tc}}{^{185}\mathrm{Re}} f_{\mathrm{Re/Mo}}, \quad (4)$$

where $Q = 10^4 \times (^{185}\mathrm{Re}/^{97}\mathrm{Mo})_{\mathrm{chur}}$, $Q \sim 791$ (Anders & Grevesse 1989), and $^{97}\mathrm{Tc}/^{185}\mathrm{Re}$ is the initial ratio. Note that this relationship implicitly assumes that ^{97}Tc was extinct when the terrestrial core formed (Lee & Halliday 1995; Halliday et al. 1996; Dauphas et al. 2002b; Allègre et al. 1995; Galer & Goldstein 1996).

In Fig. 2, the molybdenum isotopic composition $\varepsilon^{97,97*}$ is reported as a function of the Re(Tc)/Mo fractionation factor $f_{\mathrm{Re/Mo}}$. The slope of this relationship depends on the $^{97}\mathrm{Tc}/^{185}\mathrm{Re}$ ratio at the time of closure. There is no correlation between ε^{97*} and $f_{\mathrm{Re/Mo}}$, implying that there was no live ^{97}Tc when the metal crystallized in iron meteorite parent-bodies ($^{97}\mathrm{Tc}/^{98}\mathrm{Ru} < 3 \times 10^{-5}$, ^{98}Ru is used for normalization instead of ^{185}Re because both ^{97}Tc and ^{98}Ru are p-nuclides). Because there might have been a 10 Ma time gap between condensation of the first solids in the solar system and crystallization of metal, the upper-limit must be corrected for this delay, thus $^{97}\mathrm{Tc}/^{98}\mathrm{Ru} < 4 \times 10^{-4}$.

2.2. *Technetium-98*

The odd-odd p-nuclide ^{98}Tc β-decays to ^{98}Ru with a mean life of 6.1 Ma. The isotopes ^{98}Ru and ^{99}Ru might have received contributions from the now extinct radionuclides ^{98}Tc and ^{99}Tc, raising the possibility that the chronology of the early solar system may be inferred from technetium daughter nuclides alone. Tentative evidence was found for the presence of live ^{98}Tc in iron meteorites (Smoliar 1998; Becker & Walker 2000) but these results were not confirmed by subsequent measurements (Becker & Walker 2001). The equation derived in the case of ^{97}Tc $-^{97}$ Mo (Eq. 4) can be applied to ^{98}Tc $-^{98}$ Ru as well. The ruthenium isotopic composition was measured precisely in some iron meteorites by negative thermal ionization mass spectrometry (Becker & Walker 2001). Some of these meteorites were measured for Re(Tc)/Ru ratios as well (Pernicka & Wasson 1987). Combining these observations, we estimate that the $^{98}\mathrm{Tc}/^{185}\mathrm{Re}$ at the time of metal crystallization must have been lower than 3×10^{-5}. If one corrects for the possible delay between formation of the solar system and metal crystallization in iron meteorite parent-bodies, then $^{98}\mathrm{Tc}/^{98}\mathrm{Ru} < 8 \times 10^{-5}$.

2.3. *Niobium-92*

The odd-odd p-nuclide ^{92}Nb EC-decays to ^{92}Zr with a mean life of 50.1 Ma. The initial $^{92}\mathrm{Nb}/^{92}\mathrm{Mo}$ ratio of the solar system is a matter of controversy, oscillating between 10^{-5} and 10^{-3} in the last decade. Three studies (Yin et al. 2000b; Münker et al. 2000; Sanloup et al. 2000) concluded that the initial $^{92}\mathrm{Nb}/^{92}\mathrm{Mo}$ ratio was $\sim 10^{-3}$. Harper (1996) provided convincing evidence for the presence of live ^{92}Nb in rutiles (TiO_2) from the Toluca iron meteorite (IAB). He assumed that the formation of these rutiles occurred simultaneously with the formation of the solar system and estimated that the initial $^{92}\mathrm{Nb}/^{92}\mathrm{Mo}$ must have been $3.0 \pm 0.6 \times 10^{-5}$. Furthermore, Hirata (2001) found no excess of ^{92}Zr in extraterrestrial zircons, which is consistent with the $^{92}\mathrm{Nb}/^{92}\mathrm{Mo}$ being lower than 10^{-4}. Finally, Schönbächler et al. (2001) measured the $^{92}\mathrm{Zr}/^{90}\mathrm{Zr}$ and Nb/Zr ratios in bulk samples and mineral separates of Estacado (H6) and Vaca Muerta (MES). The slopes of the isochrons they derived are consistent with the ratio inferred by Harper (1996) and the upper-limit derived by Hirata (2001). Thus, it seems that $^{92}\mathrm{Nb}/^{92}\mathrm{Mo} = 5.2 \pm 1.5 \times 10^{-5}$.

2.4. *Samarium-146*

The even-even p-nuclide ^{146}Sm α-decays to ^{142}Nd with a mean life of 149 Ma. The search for ^{146}Sm in the early solar system was triggered by a suggestion made by Audouze & Schramm (1972) that there should be measurable anomalies in neodymium isotope abundances. This inference was based on an empirical determination of the $^{146}\mathrm{Sm}/^{144}\mathrm{Sm}$ production ratio derived from the observed correlation between abundance and atomic mass (Fig. 3). A few years later, the first hint of the presence of live ^{146}Sm was indeed found (Lugmair & Marti 1977). This hint was confirmed by subsequent measurements (Lugmair & Shimamura 1983; Jacobsen & Wasserburg 1984; Lugmair & Galer 1992; Prinzhofer et al. 1992; Nyquist et al. 1994). All recent studies (Lugmair & Galer 1992; Prinzhofer et al. 1992; Nyquist et al. 1994) converge to an initial ratio $^{146}\mathrm{Sm}/^{144}\mathrm{Sm} = 7.6 \pm 1.3 \times 10^{-3}$.

3. STELLAR PRODUCTION RATIOS

3.1. *Type II supernovae*

Core-collapse supernovae of type II (SNII) have been suggested to be the site for the so-called p- or γ-process synthesizing the proton-rich p-nuclides by photodisintegration of s-process material present since the formation of the progenitor star and produced in earlier burning stages. The necessary temperatures of about $2 \leq T_9 \leq 3$ (with T_9 being the temperature in 10^9 K) can be reached in their oxygen- and neon-rich layers. The process is discussed in detail in Woosley & Howard (1978); Prantzos et al. (1990); Rayet et al. (1990); Lambert (1992); Rayet et al. (1995); Wallerstein et al. (1997); Arnould & Takahashi (1999); Langanke (1999).

For the initial production ratios ejected from the site of the p-process and used in our chemical evolution model described in Sec. 4, we have taken ratios from a recent study of nucleosynthesis in SNII (Rauscher et al. 2002). The advantage of that investigation is that for the first time, the yields of all nuclides (including p-nuclides) have been self-consistently calculated in an extended reaction network (Heger et al. 2000; Rauscher et al. 2001a; Heger et al. 2001). Moreover, the nuclear physics input was updated which should lead to more reliable results in the yield ratios (Rauscher et al. 2001b,c). This is especially important for the production of ^{146}Sm. The ^{146}Sm yield is dependent on the $(\gamma,\alpha)/(\gamma,n)$ reaction branching at ^{148}Gd which, in turn, is very sensitive to the used α+^{144}Sm potential (Woosley & Howard 1990; Rauscher et al. 1995). Recently, the reaction $^{144}\mathrm{Sm}(\alpha,\gamma)^{148}\mathrm{Gd}$ was studied experimentally down to energies close to the relevant Gamow window for the p-process (Somorjai et al. 1998). With these data it

became possible to more reliably establish the α+^{144}Sm optical potential and determine the rate at the relevant energy around 9 MeV. This rate and other rates derived from such experimental information have been used in the SNII nucleosynthesis study. The remaining error in the ^{146}Sm production is estimated to be about 30% (Rauscher et al. 1995).

While p-nuclides with $A > 100 - 110$ are produced in amounts in agreement with solar abundances, for the Mo-Ru region the new model exhibits underproduction features similar to those found in previous studies (Woosley & Howard 1978; Rayet et al. 1995). For instance, ^{92}Mo is underproduced by about a factor of 10. The reasons for this remain unclear. The majority of the photodisintegration rates acting in this region are derived from theory which might leave room for a possible alleviation of this problem by removing the nuclear physics uncertainties, provided that sufficient (s-process) seed nuclei are available. However, the experimental neutron capture data (Bao et al. 2000) as well as the rare data on proton capture in this region (Harissopulos et al. 2001) agree well with the predictions (Rauscher & Thielemann 2000, 2001). Nevertheless, further experiments are necessary. Costa et al. (2000) have suggested that an increased ^{22}Ne(α,n)^{25}Mg rate could cure the underproduction in the Mo-Ru region by enhancing the s-process seeds. This effect could not be confirmed when varying this neutron producing rate in the model using the extended reaction network (Rauscher et al. 2001b; Heger et al. 2001, 2002). At the same time the Mo-Ru region is enhanced also other isotopic yields experience enhancement leading to disagreement with observation. Furthermore, more stringent upper limits on the ^{22}Ne(α,n)^{25}Mg reaction rate from recent laboratory measurements (Jaeger et al. 2001) exclude the increased rate assumed by Costa et al. (2000). For the scope of this paper, however, this issue is of minor importance because we only compare nuclides within the same (underproduced) mass region. Using abundance ratios, the absolute production factors cancel out. Obviously, we have to assume that SNII (or SNIa, see below) produce them at all. The error in the ratios is also estimated to be about 30%, stemming from remaining nuclear physics uncertainties.

The SNII yields were computed for three progenitor masses, 15, 21, and 25 $M_\odot$. These yields must be integrated over the initial mass function (Salpeter 1955) describing the birth rate ϕ of stars with different initial mass m ($\phi \propto dN/dm$). For stars with initial mass higher than $M_\odot$, the initial mass function follows a power law of the mass $\phi \propto m^{-\alpha}$, where $\alpha = 2.3 \pm 0.7$ (Kroupa 2001). In order to calculate the IMF-averaged yields, we proceeded like Rayet et al. (1995). The mass interval 12.5-27.5 was further divided into three intervals 12.5-17.5, 17.5-22.5, and 22.5-27.5. The yields of the 15, 21, and 25 $M_\odot$ mass stars were then weighted by the IMF integrated over the three mass intervals. The uncertainty on the IMF was propagated in the calculation. This source of error does not contribute significantly to the global uncertainty. The IMF-integrated SNII production ratios are compiled in Table 1.

3.2. *Type Ia supernovae*

Additional sites for the p-process have mainly drawn interest because of the problem with producing the Mo-Ru region. It has been proposed that the temperatures required for the photodisintegrations of the p-process could be reached in the C-rich zone of type Ia supernovae (SNIa) (Howard et al. 1991). Early claims that the problem in the Mo-Ru region could also be alleviated have not been substantiated by making use of more realistic astrophysical models (Howard & Meyer 1993), as is also stated in Rayet et al. (1995). In general, the main problems in SNIa models are the question of pre-explosive flashes and the propagation of the explosive burning front (Nomoto et al. 1984; Iwamoto et al. 2000; Thielemann et al. 2001). Nucleosynthesis is influenced by the unknown propagation mode of the burning front (Niemeyer et al. 1999) as well as by the composition of the ignited material and nuclear properties such as electron capture rates (Langanke & Martinez-Pinedo 2000). It seems evident that Fe-group nuclei could be produced in an explosion with a different signature than in SNII. Few investigations have studied the production of p-process nuclei in SNIa. Howard & Meyer (1993) used the delayed detonation models of Khokhlov (1991) to follow a parameterized p-process. They find that they cannot produce p-nuclei in sufficient quantities to become a significant Galactic contribution unless the s-process seeds are enhanced by several orders of magnitude. Furthermore, they observe that the production trends with respect to mass number are similar to those observed in SNII models. This can be understood by the fact that the burning during accretion on the C/O core proceeds in a similar manner as the late burning stages of SNII progenitors. The actual photodisintegration process (γ-process) is the same.

The above results seem to support the view that either SNIa do not contribute to the p-ratios or, if they do, the ratios are not significantly changed from those obtained with SNII models. One also has to keep in mind that in the solar neighborhood, SNIa are far less frequent than SNII.

3.3. *The rp-process*

Another process producing proton-rich nuclei is the manifestation of the rp-process which was suggested to explain certain types of X-ray bursts (for more rp-process scenarios, see Schatz et al. 1998). In this rp-process scenario a thermonuclear runaway is ignited in the proton-rich layer accreted on the surface of a neutron star by mass flow from a companion star (Wallace & Woosley 1981; Taam et al. 1993). It has been shown that proton-rich nuclei can be synthesized in the subsequent explosive H and He burning. The rp-process path closely follows the proton drip-line. In the final freeze-out phase, the nuclides in the rp-path decay towards stability and form p-nuclides (Schatz et al. 1998). Recently, a definite endpoint of the rp-process was identified which confines the possible production of p-nuclides to the mass region of about $A < 110$ (Schatz et al. 2001). Thus, this scenario would not interfere with the production in SNII but rather might account for the missing abundances in the Mo-Ru region.

In the current rp-calculations (Schatz et al. 1998, 2001) overproduction factors of p-nuclides of 10^8 with respect to solar are found. Therefore, the solar contributions could

be explained by only a small mass loss during each burst. At this time, however, it is not known whether any material is ejected at all during such an X-ray burst and the production of p-nuclei remains therefore speculative.

In the following, we present two scenarios, one of them assuming that X-ray bursters have contributed to the solar p-nuclei via a yet unknown ejection mechanism. Among the isotopes considered here, the rp-process can produce ^{92}Mo, ^{97}Tc, and ^{98}Ru. The nuclides ^{92}Nb and ^{98}Tc cannot be synthesized because they are shielded by stable nuclides from the decay chains coming from the proton-rich progenitors created in the rp-process path. This is similar to the case of s-only isotopes which are shielded from r-process contributions.

Test calculations with varying ignition conditions have shown that the produced isotopic ratios are remarkably robust (5% variation) for bursts that synthesize nuclei in the Mo-Ru region.

3.4. *Production ratios*

The production ratios in SNIa, SNII, and X-ray bursts are compiled in Table 1. As discussed previously, the stellar environment where p-process nuclides were synthesized is still uncertain. One can consider two extreme scenarios, (*i*) supernovae produced all p-nuclides, including those in the Mo-Ru region with the given production ratios, and (*ii*) X-ray bursts produced 90% of the p-nuclides in the Mo-Ru region and supernovae synthesized the rest. The *production ratio* can be expressed as,

$$\mathrm{P} = \alpha \mathrm{P_{SN}} + (1-\alpha)\mathrm{P_X}, \qquad (5)$$

where $\mathrm{P_{SN}}$ and $\mathrm{P_X}$ are the production ratios of supernovae and X-ray bursts compiled in Table 1, and α is the fraction from supernovae to the cosmic abundance of the normalization nuclide. Case (*i*) corresponds to $\alpha = 1$. Case (*ii*) corresponds to $\alpha = 0.10 \pm 0.03$ for ^{92}Mo and ^{98}Ru, and $\alpha = 1$ for ^{144}Sm. The *production ratios* calculated according to the two scenarios labelled SN and SN+X are compiled in Table 2.

4. OPEN NON-LINEAR GCE

The chemical evolution of the Galaxy in the solar neighborhood is governed by several mechanisms such as stellar formation, evolution, and disruption, accretion by the disk of low-metallicity gas, and radial and tangential transports (Pagel 1997). We shall adopt the instantaneous recycling approximation which relies on the assumption that the evolutionary time-scale of p-progenitors is much lower than that of the Galaxy.

The surface density of the disk in the solar neighborhood Σ grew with time from zero to its present-day value as a result of the accretion of low-metallicity gas. The infall rate is modelled as a normal density law $\mathcal{G}$ with standard deviation equal to the mean τ, where τ is the infall time-scale (Chang et al. 1999). The rationale behind this choice is that at the beginning, the infall rate increases with time together with the disk gravitational potential. After a while, the gas reservoir becomes depleted and the accretion rate decreases. This parametrization has the virtue of keeping arbitrary formalism to a minimum,

$$\frac{\mathrm{d}\Sigma}{\mathrm{d}t} = \xi\, \mathcal{G}(\tau). \qquad (6)$$

The net evolution of the gas surface density Σ_g is a balance between star formation and disruption on the one hand, and infall of low metallicity gas on the other hand. The rate of star formation depends on the gas density in a non-linear manner according to Schmidt's law (Schmidt 1959),

$$\frac{\mathrm{d}\Sigma_\mathrm{g}}{\mathrm{d}t} = -\omega\, \Sigma_\mathrm{g}^\mathrm{n} + \xi\, \mathcal{G}(\tau). \qquad (7)$$

For a nuclide for which the instantaneous recycling approximation is valid, its concentration in the interstellar medium Z evolves through time as a result of stellar nucleosynthesis (y is the yield defined as the ratio of newly created matter of that nucleus to newly created mass of permanent stellar remnants), dilution by infall of low-metallicity gas, and radioactive decay,

$$\frac{\mathrm{dZ}}{\mathrm{d}t} = \mathrm{y}\omega\, \Sigma_\mathrm{g}^{\mathrm{n}-1} - \frac{\xi\, \mathcal{G}(\tau)}{\Sigma_\mathrm{g}} (\mathrm{Z} - \mathrm{Z}_\xi) - \lambda \mathrm{Z} \quad . \qquad (8)$$

Three parameters (ξ, τ, and ω) are enough to describe the chemical evolution of the Galaxy in the solar neighborhood and to characterize its most important features. In order to constrain these parameters, we proceeded like Sommer-Larsen (1991). The present disk surface density, gas mass fraction, and metallicity in the solar neighborhood are known. Knowledge of these boundary conditions allows a straightforward derivation of the dependence of ξ, ω, and $\mathrm{y_o}$ upon τ. An independent observation is required in order to constrain τ. The G-dwarf metallicity distribution in the solar neighborhood is known to be very sensitive to the shape of the infall rate. This observation is thus used in order to estimate τ (and all other parameters which depend on it) using a χ^2 minimization algorithm (Ihaka & Gentleman 1996).

The exponent of the Schmidt power law is estimated to be 1.4 ± 0.15 (Gerritsen & Icke 1997; Kennicutt 1998). The initial disk density is taken to be zero and its present-day value $45 \pm 5\ \mathrm{M_\odot\ pc^{-2}}$ (Holmberg & Flynn 2000; Crézé et al. 1998). The gas density is estimated to be $13 \pm 4\ \mathrm{M_\odot\ pc^{-2}}$ (Holmberg & Flynn 2000). The metallicity at solar system birth is $[\mathrm{O/H}] = 0$. The metallicity of the infalling gas is assumed to have been constant through time, $[\mathrm{O/H}] \sim -1$ (Sommer-Larsen 1991; Wakker et al. 1999). The age of the Galaxy is estimated to be $> 13.2 \pm 1.5$ Ga (Chaboyer 2001). The G-dwarf metallicity distribution in the solar neighborhood is taken from Haywood (2001). The model that best fits the G-dwarf metallicity distribution (Fig. 4) corresponds to $(\xi, \tau, \omega) = (56, 4.8, 0.065)$.

Quantifying confidence limits on fitted parameters is a bit involved because the relationships that relate observations to parameters are complicated. Monte-Carlo simulations provide a reliable means of estimating these uncertainties (Press et al. 1992). A set of possible observations is first simulated. Then, each simulated set is used to compute a set of possible model parameters. Finally, this set of possible model parameters is examined for its distribution. The exponent of the Schmidt power law, the present surface density of the Galaxy in the solar neighborhood, and the gas density were simulated as normal density laws. Residuals between the best fit G-dwarf metallicity distribution and the observed distribution were calculated. These residuals were then resampled with repetition and added to the best fit distribution. This procedure permitted the simulation of a set of possible G-dwarf

metallicity distributions. Thus, the estimated uncertainties on model parameters for a galactic age of 13.2 Ga are $(\xi, \tau, \omega) = (46-68, 3.6-6.3, 0.02-0.14)$. Model parameters are correlated with each other and one should speak instead of uncertainty ellipsoids. Using these parameters, it is then possible to calculate the theoretical abundance of a p-nuclide in the interstellar medium at solar system birth.

5. THE REMAINDER RATIO

The remainder ratio ($\Re$) is defined as the ratio of the abundance of a radioactive nuclide to the abundance it would have if it were stable (Clayton 1988).

The remainder ratio in the interstellar medium at the time of isolation of the presolar molecular cloud $\Re_{\rm ISM}$ can be evaluated within the framework of the galactic chemical evolution model that we have presented,

$$\Re_{\rm ISM} = \int_{T_\odot} \Sigma_{\rm g}^{n-1}\, e^{\theta+\lambda t}\, dt \;/\; \int_{T_\odot} \Sigma_{\rm g}^{n-1}\, e^{\theta+\lambda T_\odot}\, dt, \qquad (9)$$

where θ is the cycle number defined as $d\theta/dt = \xi\mathcal{G}(\tau)/\Sigma_{\rm g}$ (Clayton 1988). Using the parameters calculated in the previous section, it can be shown that for short lived nuclides, the remainder ratio takes the form,

$$\Re_{\rm ISM} = \kappa/(\lambda T_\odot), \qquad (10)$$

with $\kappa = 2.7 \pm 0.4$, where the confidence interval accounts for model uncertainties and $T_\odot$ is the presolar age of the Galaxy 8.7 ± 1.5 Ga (κ=1 corresponds to the closed-box model). Clayton (1985) developed a model of the chemical evolution of the Galaxy that he applied to radioactive nuclides. Despite great difference between his model and ours, he estimated that κ must be within 2 and 4.

The remainder ratio within the solar system at solar system birth $\Re_{\rm ESS}$ can be estimated using stellar production ratios and observed abundances in meteorites,

$$\Re_{\rm ESS} = R/P, \qquad (11)$$

where R is the early solar system ratio of a radioactive nuclide to a stable nuclide produced by the same process and P is the production ratio.

There might have been a delay between isolation of the presolar molecular cloud from fresh nucleosynthetic inputs and solar system formation. This possibility is accounted for by multiplying $\Re_{\rm ISM}$ by a decay term,

$$\Re_{\rm ESS} = \Re_{\rm ISM}\, e^{-\lambda\Delta}, \qquad (12)$$

where λ is the decay constant and Δ is the free decay interval. If all short-lived p-nuclides were derived from the deterministic chemical evolution of the Galaxy, they should define a unique free decay interval. It is worthwhile to note that the continuous chemical evolution model of the Galaxy probably breaks down for very short-lived nuclides with mean lives below ~10 Ma because granularity might play a role, which would require a stochastic treatment (Meyer & Luo 1997). Also, the instantaneous recycling approximation might not be applicable for X-ray bursts that typically occur in low mass X-ray binaries (Iben et al. 1995). This introduces an additional systematic uncertainty in R and $\Re_{\rm ESS}$ for ^{97}Tc in the case of a contribution from X-ray bursts (case (*ii*) in Sec. 3.4). The remainder ratios of ^{97}Tc, ^{98}Tc, ^{92}Nb, and ^{146}Sm are compiled in Table 2.

6. PERSPECTIVES

6.1. *Supernovae, X-ray bursts, and niobium-92*

Niobium-92 is the only p-nuclide in the Mo-Ru region that cannot be synthesized in X-ray bursts but was alive in the early solar system. Thus, the abundance of this nuclide in the solar system may be used to test whether X-ray bursts significantly contributed to the synthesis of proton-rich nuclides. In Fig. 5, the remainder ratio in the early solar system is reported as a function of the remainder ratio in the interstellar medium at solar system birth for a variety of free decay intervals. As illustrated in this diagram, ^{92}Nb is overabundant in the early solar system relative to what would be expected if X-ray bursts synthesized p-nuclides that are underproduced by supernovae (case (*ii*) in Sec. 3.4). If one assumes that the isotopic ratios in the Mo-Ru region coming from SN are understood, then this is a strong argument against a significant contribution of X-ray bursts to the synthesis of p-nuclides in the Mo-Ru region.

Turning the argument around and assuming that we know the isotopic ratios from X-ray bursts better, the SN ratios necessary to bring the result into accordance with case (*i*) can be derived. We obtain $(^{92}\mathrm{Nb}/^{92}\mathrm{Mo})_{\rm SN} = 2.9 \pm 1.6 \times 10^{-2}$, more than a factor of 10 higher than the value coming from SNII. In other words, the production of ^{92}Nb would have to be enhanced by the given factor while still keeping the underproduction of ^{92}Mo at the same level of 10% as before. It appears unlikely that this is feasible in a SN scenario.

To summarize, either scenario is in conflict with current supernova p process model predictions: If X-ray bursts are the major source of the Mo and Ru p nuclides then there is a conflict with predicted ^{92}Nb/^{92}Mo ratios, if not then there is a conflict with the predicted absolute production level. The problem of the origin of the Mo and Ru p nuclei therefore remains unsolved and clearly warrants further research.

6.2. *Bridging the gap between ISM and ESS*

As can be seen in Fig. 5, all short-lived p-nuclides ^{97}Tc, ^{98}Tc, ^{92}Nb, and ^{146}Sm are consistent with synthesis in supernovae and derivation from the ISM with a comparatively short free-decay interval ($\Delta < 100$ Ma). Assuming that there was no free decay interval between chemical evolution of the Galaxy and condensation of the first solids in the solar system and that short-lived p-nuclides were produced in supernovae, then we estimate that the initial ^{97}Tc/^{98}Ru and ^{98}Tc/^{98}Ru ratios at solar system birth would be $5.3 \pm 2.0 \times 10^{-5}$ and $1.4 \pm 0.6 \times 10^{-5}$, respectively. How does the upper-limit derived for Δ compare with that derived from other short-lived nuclides? Wasserburg et al. (1996) discussed the presence of short-lived r-nuclides in the early solar system. They concluded that the abundances of ^{182}Hf and ^{244}Pu were consistent with synthesis in supernova actinide sources and derivation from the interstellar medium with a short free decay interval ($\Delta < 10$ Ma). This result is consistent with the value we infer. They also discussed the case of ^{107}Pd and ^{129}I and suggested that these r-nuclides were inherited from the continuous chemical evolution of the Galaxy but that the stellar environment where they formed was distinct from

that which produced ^{182}Hf and ^{244}Pu. Later, Qian et al. (1998) identified these two r-progenitors with low and high frequency events (for the latter type II supernovae were suggested, the identification of the additional site remains controversial). Thus, it seems that most short-lived nuclides were inherited from the chemical evolution of the Galaxy and that the solar system placental molecular cloud was not isolated from fresh nucleosynthetic inputs for more than a few tens of million years. All extinct radioactivities were probably not synthesized by a single event in the molecular cloud where the sun was born as was advocated by Cameron (Cameron et al. 1996; Cameron 2001).

6.3. *Origin of extinct radioactivities*

There are a few very short-lived nuclides that cannot easily be explained by long-term chemical evolution of the Galaxy. These short-lived nuclides are ^{7}Be, ^{10}Be, ^{26}Al, ^{53}Mn, and ^{41}Ca. They may have been injected in the nascent solar system by a nearby giant star that might have triggered the protosolar cloud into collapse (Cameron et al. 1996). They may also have been synthesized within the solar system by local irradiation (Lee 1978; Clayton & Jin 1995; Lee et al. 1998; McKeegan et al. 2000; Gounelle et al. 2001; Chaussidon et al. 2002; Leya et al. 2002). Both models face difficulties but the recent discovery of ^{10}Be (McKeegan et al. 2000; Sugiura et al. 2000; MacPherson & Huss 2001) and possibly ^{7}Be (Chaussidon et al. 2002) in refractory inclusions favors the local irradiation model (Lee et al. 1998; McKeegan et al. 2000; Gounelle et al. 2001; Chaussidon et al. 2002; Leya et al. 2002) although further work on the injection model is required (Cameron 2001). Thus, the presence of short-lived nuclides in the nascent solar system is probably a combination of chemical evolution of the Galaxy and local irradiation within the solar system (Fig. 6). Because technetium isotopes 97 and 98 have very short mean-lives, evidence for their presence in the early solar system will allow to test whether stochasticity played a role or not.

We thank F.-K. Thielemann and G.W. Lugmair for extended discussions. This work is supported in part by the French CNES/INSU (PNP), the Swiss NSF (grant 2000-061822.00), and the European Union (SMT4-CT98-2220). T. R. acknowledges support by a PROFIL professorship (Swiss NSF grant 2124-055832.98). H. S. acknowledges support through NSF Grant No. PHY 95-28844 and the Alfred P. Sloan Foundation.

REFERENCES

Allègre, C.-J., Manhès, G., & Göpel, C. 1995, Geochim. Cosmochim. Acta, 59, 1445
Anders, E., & Grevesse, N. 1989, Geochim. Cosmochim. Acta, 53, 197
Arlandini, C., Käppeler, F., Wisshak, K., Gallino, R., Lugaro, M., Busso, M., & Straniero, O. 1999, ApJ, 525, 886
Arnould, M. & Takahashi, K. 1999, Rep. Prog. Phys. , 62, 395
Audouze, J., & Schramm, D.N. 1972, Nature, 237, 447
Bao, Z. Y., Beer, H., Käppeler, F., Voss, F., Wisshak, K., & Rauscher, T. 2000, At. Data Nucl. Data Tables, 76, 70
Becker, H., & Walker, R.J. 2000, Lunar Planet. Sci., XXXI, # 1484
Becker, H., & Walker, R.J. 2001, Eleventh Annual V.M. Goldschmidt Conference, # 3047
Birck, J.-L., & Allègre, C.-J. 1998, Meteoritics Planet. Sci., 3, 647
Cameron, A.G.W. 2001, Lunar Planet. Sci. XXXII, # 1035
Cameron, A.G.W., Vanhala, H., & Höflich, P. 1996, in Astrophysical Implications of the Laboratory Study of Presolar Materials, ed. T.J. Bernatowicz, & E. Zinner (Woodbury: American Institute of Physics), 665
Carlson, R.W., & Hauri, E.H. 2001, Geochim. Cosmochim. Acta, 65, 1839
Chaboyer, B. 2001, in Astrophysical Ages and Time Scales, ASP Conference Series 245, ed. T.V. Hippel, C. Simpson, & N. Manset (San Francisco: Astronomical Society of the Pacific), 162
Chang, R.X., Hou, J.L., Shu, C.G., & Fu, C.Q. 1999, A&A, 350, 38
Chaussidon, M., Robert, F., & McKeegan, K.D. 2002, Lunar Planet. Sci., XXXIII, #1563
Chen, Y.Q., Nissen, P.E., Zhao, G., Zhang, H.W., & Benoni, T. 2000, A&AS, 141, 491
Chen, J.H., & Wasserburg, G.J. 1996, in Earth Processes: Reading the Isotopic Code, Geophysical Monograph 95, ed. A. Basu, & S. Hart (Washington: American Geophysical Union), 1
Clayton, D.D. 1985, in Nucleosynthesis: Challenges & New Developments, ed. W.D. Arnett, & J.W. Truran (Chicago: University of Chicago Press), 65
Clayton, D.D. 1988, MNRAS, 234, 1
Clayton, D.D., & Jin, L. 1995, ApJ, 451, L87
Costa, V., Rayet, M., Zappalà, R.A., & Arnould, M. 2000, A&A, 358, L67
Crézé, M., Chereul, E., Bienaymé, O., & Pichon, C. 1998, A&A, 329, 920
Dauphas, N., Marty, B., & Reisberg, L. 2002a, ApJ, 565, 640
Dauphas, N., Marty, B., & Reisberg, L. 2002b, Geophys. Res. Lett., in press
Dauphas, N., Marty, B., & Reisberg, L. 2002c, ApJ, submitted
Dauphas, N., Reisberg, L., & Marty, B. 2001, Anal. Chem., 73, 2613
Fegley, B., Jr., Lodders, K., & Palme, H. 1993, Meteoritics, 28, 346
Fegley, B., Jr., & Palme, H. 1984, Earth Planet. Sci. Lett., 72, 311
Fleet, M.E., Liu, M., & Crocket, J.H. 1999, Geochim. Cosmochim. Acta, 63, 2611
Galer, S.J.G., & Goldstein, S.L. 1996, in Earth Processes: Reading the Isotopic Code, Geophysical Monograph 95, ed. A. Basu, & S. Hart (Washington: American Geophysical Union), 75
Gerritsen, J.P.E. & Icke, V. 1997, A&A, 325, 972
Goriely, S., Arnould, M., Borzov, I., & Rayet, M. 2001, A&A, 375, L35
Gounelle, M., Shu, F.H., Shang, H., Glassgold, A.E., Rehm, K.E., & Lee, T. 2001, ApJ, 548, 1051
Halliday, A., Rehkämper, M., Lee, D.-C., & Yi, W. 1996, Earth Planet. Sci. Lett., 142, 75
Harissopulos, S., et al. 2001, Phys. Rev. C, 64, 055804
Harper, C.L. Jr. 1996, ApJ, 466, 437
Haywood, M. 2001, MNRAS, 325, 1365
Heger, A., Hoffman, R. D., Rauscher, T., & Woosley, S. E. 2000, in Proc. X Workshop on Nuclear Astrophysics, eds. W. Hillebrandt, E. Müller, MPA/P12 (MPA, Garching), 105 (astro-ph/0006350)
Heger, A., Woosley, S. E., Rauscher, T., Hoffman, R. D., & Boyes, M. M. 2001, New Astronomy Reviews, in press
Heger, A. et al. 2002, ApJ, in preparation
Hirata, T. 2001, Chem. Geol., 176, 323
Holmberg, J., & Flynn, C. 2000, MNRAS, 313, 209
Horan, M.F., Smoliar, M.I., & Walker, R.J. 1998, Geochim. Cosmochim. Acta, 62, 545
Howard, W.M. 1993, Meteoritics, 28, 365
Howard, W.M., Meyer, B.S., & Woosley, S.E. 1991, ApJ, 373, L5
Howard, W.M. & Meyer, B.S. 1993, in Nuclei in the Cosmos, eds. F. Käppeler, & K. Wisshak (IOP Publishing, Bristol), 575
Hutcheon, I.D., Olsen, E., Zipfel, J., & Wasserburg, G.J. 1992, Lunar Planet. Sci. , XXIII, 565
Iben, I. Jr., Tutukov, A.V., & Yungelson, L.R. 1995, ApJS, 100, 233
Ihaka, R., & Gentleman, R. 1996, J. Comput. Graph. Stat., 5, 299
Iwamoto, K. et al. 2000, ApJS, 125, 439
Jacobsen, S.B., & Wasserburg, G.J. 1984, Earth Planet. Sci. Lett., 67, 137
Jaeger, M., Kunz, R., Mayer, A., Hammer, J.W., Staudt, G., Kratz, K.L., & Pfeiffer, B. 2001, Phys. Rev. Lett., 87, 202501
Kennicutt, R.C., Jr. 1998, ApJ, 498, 541
Khokhlov, A.M. 1991, A&A, 245, 114
Kroupa, P. 2001, MNRAS, 322, 231
Lambert, D.L. 1992, A&A Rev., 3, 201
Langanke, K.-H. 1999, Nucl. Phys. A, 564, 330c
Langanke, K.-H. & Martinez-Pinedo, G. 2000, Nucl. Phys. A, 673, 481
Lee, D.-C., & Halliday, A.N. 1995, Nature, 378, 771
Lee, T. 1978, ApJ, 224, 217

Lee, T., Shu, F.H., Shang, H., Glassgold, A.E., & Rehm, K.E. 1998, ApJ, 506, 898
Leya, I., Wieler, R., & Halliday, A.N. 2002, Lunar Planet. Sci., XXXIII, #1268
Liu, M., & Fleet, M.E. 2001, Geochim. Cosmochim. Acta, 65, 671
Lugmair, G.W., & Marti, K. 1977, Earth Planet. Sci. Lett., 35, 273
Lugmair, G.W., Shimamura, T., Lewis, R.S., & Anders, E. 1983, Science, 222, 1015
Lugmair, G.W., & Galer, S.J.G. 1992, Geochim. Cosmochim. Acta, 56, 1673
MacPherson, G.J., & Huss, G.R. 2001, Lunar Planet. Sci., XXXII, # 1882
Maréchal, C.N., Télouk, P., & Albarède, F. 1999, Chem. Geol., 156, 251
McKeegan, K.D., Chaussidon, M., & Robert, F. 2000, Science, 289, 1334
Meyer, B.S., & Luo, N. 1997, Lunar Planet. Sci., XXVIII, # 1841
Münker, C., Weyer, S., Mezger, K., Rehkämper, M., Wombacher, F., & Bischoff, A. 2000, Science, 289, 1538
Nicolussi, G.K., Pellin, M.J., Lewis, R.S., Davis, A.M., Amari, S., & Clayton, R.N. 1998a, Geochim. Cosmochim. Acta, 62, 1093
Nicolussi, G.K., Pellin, M.J., Lewis, R.S., Davis, A.M., Clayton, R.N., & Amari, S. 1998b, ApJ, 504, 492
Niemeyer, J. C., Bushe, W. K., & Ruetsch, G. R. 1999, ApJ, 524, 290
Nomoto, K., Thielemann, F.-K., & Yokoi, K. 1984, ApJ, 286, 644
Nyquist, L.E., Bansal, B., Wiesmann, H., & Shih, C.-Y. 1994, Meteoritics, 29, 872
Pagel, B.E.J. 1997, Nucleosynthesis & Chemical Evolution of Galaxies (Cambridge: Cambridge University Press)
Pernicka, E., & Wasson, J.T. 1987, Geochim. Cosmochim. Acta, 51, 1717
Podosek, F.A., & Nichols, R.H. 1996, in Astrophysical Implications of the Laboratory Study of Presolar Materials, ed. T.J. Bernatowicz, & E. Zinner (Woodbury: American Institute of Physics), 617
Prantzos, N., Hashimoto, M., Rayet, M., & Arnould, M. 1990, A&A, 238, 455
Press, W.H., Teukolsky, S.A., Vetterling, W.T., & Flannery, B.P. 1992, Numerical Recipes in C (Cambridge: Cambridge University Press)
Prinzhofer, A., Papanastassiou, D.A., & Wasserburg, G.J. 1992, Geochim. Cosmochim. Acta, 56, 797
Qian, Y.-Z., Vogel, P., & Wasserburg, G.J. 998, ApJ, 494, 285
Rauscher, T., Heger, A., Hoffman, R. D., & Woosley, S. E. 2001a, Nucl. Phys. A, 688, 193
Rauscher, T., Heger, A., Hoffman, R. D., & Woosley, S. E. 2002, ApJ, submitted (astro-ph/0112478)
Rauscher, T., Heger, A., Woosley, S. E., & Hoffman, R. D. 2001b, in Proc. 9th Int. Sem. Interactions of Neutrons With Nuclei (ISINN-9), Dubna, in press (astro-ph/0106289)
Rauscher, T., Hoffman, R. D., Heger, A., & Woosley, S. E. 2001c, in Proc. Int. Conf. Structure of the Nucleus at the Dawn of the Century, Bologna, in press (nucl-th/0008065)
Rauscher, T. & Thielemann, F.-K. 2000, At. Data Nucl. Data Tables, 75, 1
Rauscher, T. & Thielemann, F.-K. 2001, At. Data Nucl. Data Tables, 79, 47
Rauscher, T., Thielemann, F.-K., & Oberhummer, H. 1995, ApJ, 451, L37
Rayet, M., Prantzos, N., & Arnould, M. 1990, A&A, 227, 271
Rayet, M., Arnould, M., Hashimoto, M., Prantzos, N., & Nomoto, K. 1995, A&A, 298, 517
Salpeter, E.E. 1955, ApJ, 121, 161
Sanloup, C., Blichert-Toft, J., Télouk, P., Gillet, P., & Albarède, F. 2000, Earth Planet. Sci. Lett., 184, 75
Schatz, H., et al. 1998, Phys. Rep., 294, 167
Schatz, H., et al. 2001, Phys. Rev. Lett., 86, 3471
Schönbächler, M., Rehkämper, M., Halliday, A.N., Lee, D.-C., Zanda, B., Bourot-Denise, M., Hattendorf, B., & Günther, D. 2001, Meteoritics Planet. Sci., 36, A184
Schmidt, M. 1959, ApJ, 129, 243
Schramm, D.N., & Wasserburg, G.J. 1970, ApJ, 162, 57
Shen, J.J., Papanastassiou, D.A., & Wasserburg, G.J. 1996, Geochim. Cosmochim. Acta, 60, 2887
Smales, A.A., Mapper, D., & Fouch, K.F. 1967, Geochim. Cosmochim. Acta, 31, 673
Smoliar, M.I. 1998, Lunar Planet. Sci., XXIX, # 1202
Smoliar, M.I., Walker, R.J., & Morgan, J.W. 1996, Science, 271, 1099
Sommer-Larsen, J. 1991, MNRAS, 249, 368
Somorjai, E., et al. 1998, A&A, 333, 1112
Sugiura, N., Shuzou, Y., & Ulyanov, A.A. 2000, Meteoritics Planet. Sci., 35, 154
Taam, R. E., Woosley, S. E., Weaver, T. A., & Lamb, D. Q. 1993, ApJ, 413, 324
Thielemann, F.-K., et al. 2001, Prog. Part. Nucl. Phys., 46, 5
Wakker, B.P., et al. 1999, Nature, 402, 388
Wallace, R. K., & Woosley, S. E. 1981, ApJS, 45, 389
Wallerstein, G., et al. 1997, Rev. Mod. Phys., 69, 995
Ward, R.A., & Beer, H. 1981, A&A, 103, 189
Wasserburg, G.J., Busso, M., & Gallino, R. 1996, ApJ, 466, L109
Woosley, S.E., Hartmann, D.H., Hoffman, R.D., & Haxton, W.C. 1990, ApJ, 356, 272
Woosley, S.E., & Howard, W. M. 1978, ApJS, 36, 285
Woosley, S.E., & Howard, W. M. 1990, ApJ, 354, L21
Yin, Q.Z., & Jacobsen, S.B. 1998, Lunar Planet. Sci., XXIX, # 1802
Yin, Q.Z., Yamashita, K., & Jacobsen, S.B. 1999, Ninth Annual V.M. Goldschmidt Conference, # 7637
Yin, Q.Z., Yamashita, K., & Jacobsen, S.B. 2000a, Lunar Planet. Sci., XXXI, # 1920
Yin, Q.Z., Jacobsen, S.B., McDonough, W.F., Horn, I., Petaev, M.I., & Zipfel, J. 2000b, ApJ, 536, L49

TABLE 1

PRODUCTION RATIOS IN SNIa, SNII, AND X-RAY BURSTS

Nuclide	Ratio	$P_{SNIa,SNII}$	P_{X-ray}
Technetium-97	$^{97}Tc/^{98}Ru$	$4.4 \pm 1.3 \times 10^{-2}$	$2.0 \pm 0.1 \times 10^{-1}$
Technetium-98	$^{98}Tc/^{98}Ru$	$7.3 \pm 2.5 \times 10^{-3}$	0
Niobium-92	$^{92}Nb/^{92}Mo$	$1.5 \pm 0.6 \times 10^{-3}$	0
Samarium-146	$^{146}Sm/^{144}Sm$	$1.8 \pm 0.6 \times 10^{-1}$	0

Note. — See section 3 for details and references.

TABLE 2

ABUNDANCES OF SHORT-LIVED p-NUCLIDES

Nuclide	$1/\lambda$ (Ma)		R	P		$\Re_{ESS}$		$\Re_{ISM}$
				SN	SN+X	SN	SN+X	
Technetium-97	3.8	$^{97}Tc/^{98}Ru$	$< 4 \times 10^{-4}$	$4.4 \pm 1.3 \times 10^{-2}$	$1.8 \pm 0.1 \times 10^{-1}$	$< 1.3 \times 10^{-2}$	$< 2.3 \times 10^{-3}$	$1.2 \pm 0.3 \times 10^{-3}$
Technetium-98	6.1	$^{98}Tc/^{98}Ru$	$< 8 \times 10^{-5}$	$7.3 \pm 2.5 \times 10^{-3}$	$7.3 \pm 4.7 \times 10^{-4}$	$< 1.7 \times 10^{-2}$	$< 3.1 \times 10^{-1}$	$1.9 \pm 0.5 \times 10^{-3}$
Niobium-92	50.1	$^{92}Nb/^{92}Mo$	$5.2 \pm 1.5 \times 10^{-5}$	$1.5 \pm 0.6 \times 10^{-3}$	$1.5 \pm 1.0 \times 10^{-4}$	$3.5 \pm 1.7 \times 10^{-2}$	$3.5 \pm 2.5 \times 10^{-1}$	$1.6 \pm 0.4 \times 10^{-2}$
Samarium-146	149	$^{146}Sm/^{144}Sm$	$7.6 \pm 1.3 \times 10^{-3}$	$1.8 \pm 0.6 \times 10^{-1}$	$1.8 \pm 0.6 \times 10^{-1}$	$4.2 \pm 1.6 \times 10^{-2}$	$4.2 \pm 1.6 \times 10^{-2}$	$4.6 \pm 1.1 \times 10^{-2}$

Note. — R is the initial ratio in the solar system derived from meteorite measurements, P is the production ratio, $\Re_{ESS}$ is the remainder ratio in the early solar system calculated as R/P, and $\Re_{ISM}$ is the remainder ratio in the interstellar medium derived from GCE modelling (see text).

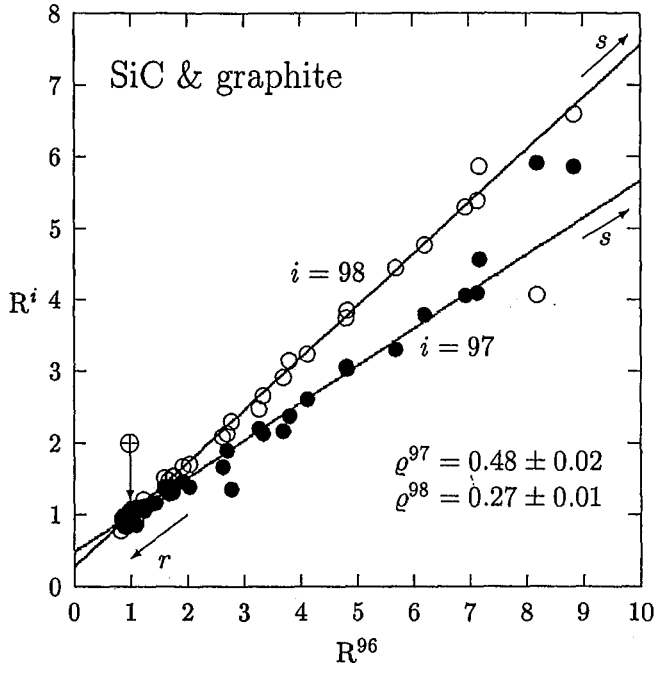

FIG. 1.— Molybdenum normalized isotopic ratios in presolar SiC and graphite grains (Nicolussi et al. 1998a,b). R^i is defined as $(^iMo/^{100}Mo)/(^iMo/^{100}Mo)_\oplus$. The data points align along straight mixing lines extending between r- (lower left corner) and s-process (upper right corner). The lines are constrained (1,1) least square regressions through the data (Ihaka & Gentleman 1996). The intersections between these lines and the y-axis correspond to pure r-process normalized isotopic ratios (ϱ^i).

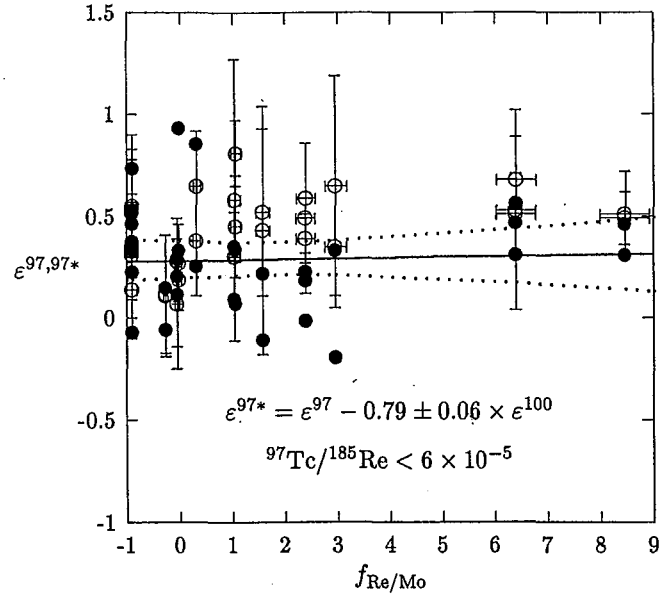

FIG. 2.— Extinct radionuclide isochron. The molybdenum isotopic composition (ε^{97} raw ratios white dots and ε^{97*} corrected ratios black dots) is reported as a function of the Re/Mo fractionation factor ($f_{Re/Mo}$) (Dauphas et al. 2002a). The slope of this correlation depends on the $^{97}Tc/^{185}Re$ ratio at the time of formation (4.5 Ga ago). The heavy line is the best fit regression line. The dotted curves are 95 % confidence intervals (Ihaka & Gentleman 1996).

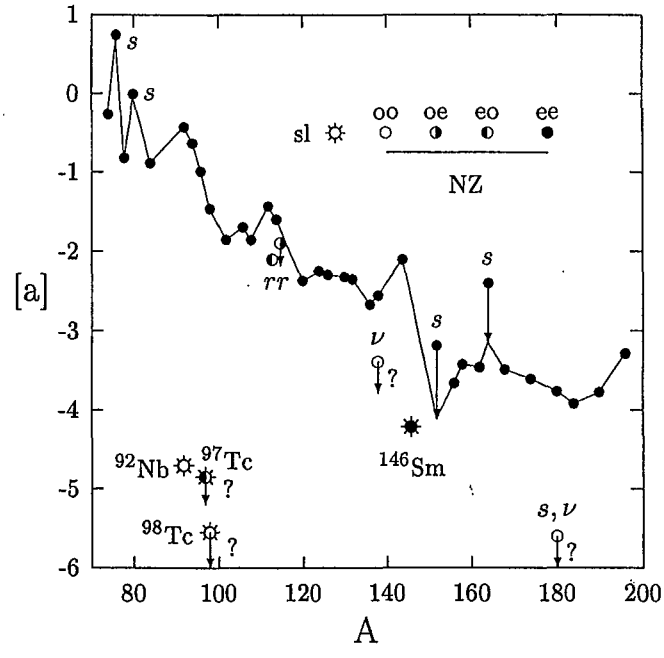

FIG. 3.— p-nuclide abundances (log atoms/10^6Si) in the early solar system (Anders & Grevesse 1989). Some of these nuclides have significant contributions from the s- (^{76}Se, ^{80}Kr, ^{152}Gd, ^{164}Er, and ^{180}Ta) (Arlandini et al. 1999), the r- (^{113}In and ^{115}Sn) (Ward & Beer 1981), and the ν-process (^{138}La and ^{180}Ta) (Woosley et al. 1990; Goriely et al. 2001). When possible, these contributions have been corrected for (arrows). o, e, and sl denote odd, even, and short-lived, respectively. Arrows associated with question marks correspond to upper limits.

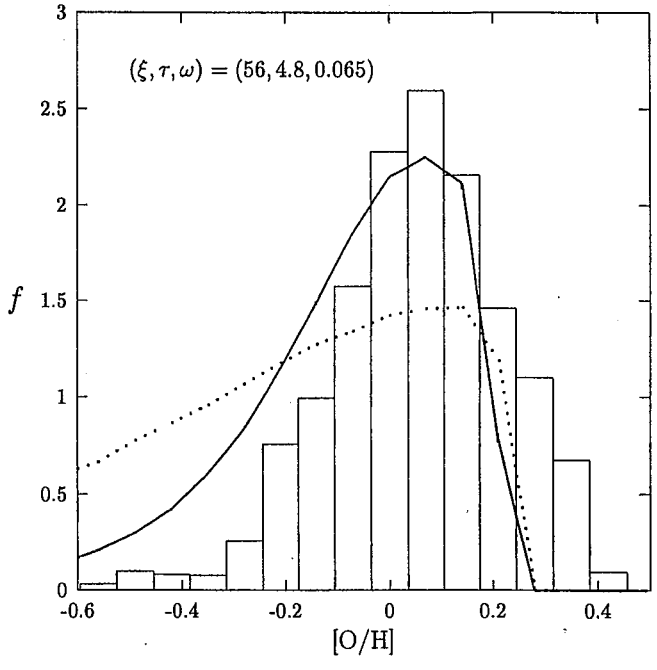

FIG. 4.— G-dwarf metallicity distribution (density) in the solar neighborhood (Haywood 2001). The [Fe/H] was converted to [O/H] using $[O/H] = 0.70 \pm 0.04[Fe/H] + 0.07 \pm 0.02$ (Chen et al. 2000). Histogram: observations (Haywood 2001), dotted line: closed-box model, solid line: best infall model, χ^2 minimization (Ihaka & Gentleman 1996). The parameters describing the best infall model are indicated at the top left corner.

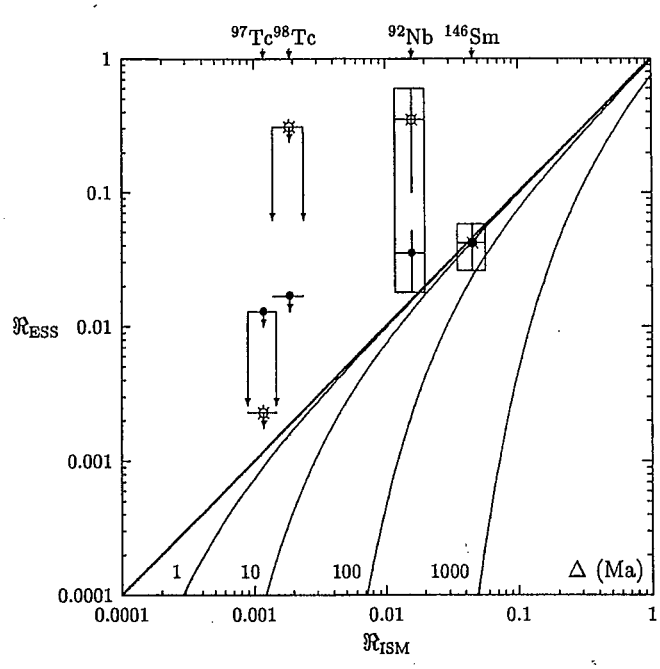

FIG. 5.— The remainder ratio in the early solar system $\Re_{ESS}$ is reported as a function of the remainder ratio in the interstellar medium at solar system birth $\Re_{ISM}$ for a variety of free decay intervals Δ. The points represent the positions of short-lived p-nuclides in this diagram (Table 2, see text for details). Two scenarios are envisioned. One (black dots, SN in Table 2, case (*i*) in text) assumes that supernovae synthesized all p-nuclides, including those in the Mo-Ru region. The other (white dots, SN+X in Table 2, case (*ii*) in text) assumes that X-ray bursts produced 90% of the proton-rich nuclides in the Mo-Ru region and supernovae synthesized the rest.

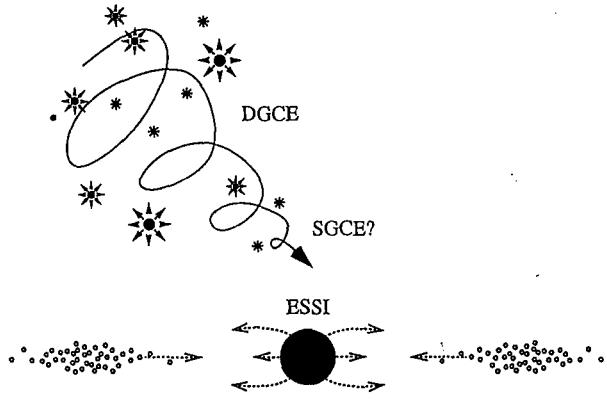

FIG. 6.— Cartoon illustrating the origin of short-lived nuclides. Their presence in the nascent solar system is probably a combination of deterministic chemical evolution of the Galaxy (DGCE) with some possible stochasticity (SGCE?) and local irradiation within the early solar system (ESSI). See text for details.

Perspectives

Nous deviendrons tous des hommes aériens, nous connaîtrons la force de l'attraction vers le haut, vers l'espace, vers le vide et en même temps le tout; lorsque les forces de l'attraction terrestre auront été ainsi dominées, nous léviterons littéralement vers la liberté physique et spirituelle.

Yves Klein

L'avènement récent de spectromètres de masse à sources plasma équipés de systèmes multi-collection permet d'aborder des champs inexplorés de la connaissance. La détermination de la composition isotopique du molybdène [4] répond à de nombreuses problématiques :

(*i*) Les processus d'évaporation-condensation dans la nébuleuse et le partage métal solide-métal liquide dans les noyaux des planétésimaux ont pu provoquer un fractionnement des isotopes du molybdène dépendant de la masse. Couplé à un travail experimental, la détermination du fractionnement de masse dans des météorites de fer évoluées et des inclusions réfractaires appauvries en molybdène permettrait de mieux contraindre les processus qui ont gouverné les variations d'abondance du molybdène.

(*ii*) Le technétium-97 est un p-nucléide pair-impair qui décroît par capture électronique en molybdène-97 avec une vie moyenne de 3.8 Ma. A l'instar d'autres radionucléides à courtes demi-vies produits par le processus p de nucléosynthèse (^{92}Nb et ^{146}Sm), ce nucléide a pu être présent quand le système solaire s'est formé et représenter ainsi une radioactivité éteinte. La découverte de ^{97}Mo radiogénique aurait des répercussions importantes sur la chronologie du système solaire, l'origine des radioactivités éteintes, et les modèles d'évolution chimique de la Galaxie.

(*iii*) Les trois processus p, s, et r ont contribué à la nucléosynthèse stellaire du molybdène. Le système solaire est le résultat d'une maturation lente et complexe de la matière. De nombreuses observations indiquent que la nébuleuse protosolaire devait être isotopiquement hétérogène à toutes les échelles. La cause de cette hétérogénéité est encore incertaine (héritage présolaire ou nomades). La découverte d'anomalies héritées permettrait de discuter plus avant la source des hétérogénéités isotopiques de la nébuleuse et, le cas échéant, de discuter les filiations entre corps primitifs et différenciés.

La mesure de la composition isotopique du molybdène dans des objets naturels répond effectivement à plusieurs des problématiques envisagées :

(*i*) Les météorites de fer et les chondrites primitives ne montrent pas de fractionnement de masse supérieur à 0.1 $\permil$.amu^{-1} [19]. Il semble donc que les partages métal-silicate ou métal liquide-métal solide n'aient pas induit de fractionnement de masse pour les isotopes du molybène.

Un des aspects qui reste inexploré est l'analyse du fractionnement de masse dans les inclusions

réfractaires appauvries en molybdène. Cette détermination est difficile (faible abondance du molybdène et difficulté de trouver les échantillons adéquats) et ne présente d'intérêt que si elle est couplée à un travail experimental. Cet aspect n'a pas été développé dans cette étude.

(*ii*) Pour observer des effets significatifs dus à la décroissance du ^{97}Tc, il est nécessaire de sélectionner des objets naturels dont le rapport père/fils Tc/Mo a pu être fractionné. Le rhénium est un analogue du technétium ; il peut donc servir de guide pour apprécier les fractionnements père/fils. Deux catégories d'objets ont été sélectionnées. Les météorites de fer constituent des candidats sérieux pour rechercher le ^{97}Tc car la cristallisation fractionnée des noyaux des planétésimaux a induit un fort fractionnement Re/Mo (Tc/Mo). Après correction de la composante nucléosynthétique, aucune preuve de la présence du ^{97}Tc n'a été trouvée dans les météorites de fer. Nous estimons que le rapport ^{97}Tc/^{98}Ru a dû être inférieur à 4×10^{-4} au moment de la formation du système solaire [19, 22].

Les inclusions réfractaires sont des objets dans lesquels la présence de ^{97}Tc peut se manifester car ces inclusions se sont formées très tôt dans l'histoire du système solaire et car dans certaines, le molybdène est très appauvri par rapport au rhénium et au technétium. Les mesures sur ces objets n'ont pas été faites car le système de désolvatation Aridus est arrivé trop tard dans le développement de la thèse. La page sur la présence ou l'absence de ^{97}Tc dans la nébuleuse protosolaire n'est donc pas définitivement écrite car il reste encore à mesurer la composition isotopique du molybdène dans les inclusions réfractaires.

La limite supérieure imposée sur l'abondance du ^{97}Tc permet d'ores et déjà de discuter l'origine des radioactivités éteintes produites par le processus p de nucléosynthése (^{97}Tc, ^{98}Tc, ^{92}Nb, et ^{146}Sm). Toutes ces radioactivités s'inscrivent dans un modèle d'évolution chimique de la Galaxie ouvert non linéaire avec une production dans les supernovae de type II et un intervalle de décroissance libre inférieur à 10 Ma [22]. La présence des radionucléides éteints dans le système solaire est vraisemblablement la combinaison d'un héritage du milieu interstellaire et d'une production locale par irradiation.

(*iii*) De nombreuses anomalies ont été détectées dans des objets microscopiques ou des météorites indifférenciées qui échantillonnent des réservoirs de faibles masses (au plus 10^3 kg). Des anomalies ont été détectées dans des météorites différenciées pour le chrome et l'oxygène. Nous avons mis en évidence la présence d'anomalies isotopiques pour le molybdène dont le spectre est appelé Mo-w en référence à sa forme et qui résultent d'un déficit macroscopique en nucléides produits par le processus s de nucléosynthèse [19]. La présence de ces anomalies à une échelle mégascopique permet de discuter la filiation entre les météorites différenciées qui ne portent pas d'oxygène.

Ces anomalies fournissent un argument supplémentaire en faveur du modèle enstatite de la terre [20]. En effet, la composition isotopique des chondrites à enstatite est identique à la composition de la terre (homogène entre le manteau profond et la surface). Nous ne possédons certainement pas dans les collections de météorites des échantillons représentatifs de la terre indifférenciée mais il semble que les chondrites à enstatite se soient formées dans un réservoir isotopique et chimique proche de la terre. Pour réconcilier les différences de compositions isotopiques du tungstène entre la terre et les chondrites à enstatite, un modèle est envisagé qui considère que le noyau terrestre s'est différencié alors que le ^{182}Hf était encore vivant (50 ± 10 Ma après la condensation des premiers solides).

La digestion sélective des météorites primitives s'est montrée très utile dans le passé pour caractériser les phases porteuses des anomalies isotopiques. L'attaque sélective d'Orgueil met en évidence deux spectres opposés portés par les grains de carbure de silicium présolaire (Mo-m) et la fraction homogène de la nébuleuse (Mo-w) [21]. Les anomalies mégascopiques observées résultent d'un déficit à grande échelle des carbures de silicium. L'abondance des grains circumstellaires

normalisée à l'abondance d'un élément réfractaire comme le molybdène a pu varier de 30 %. Ce résultat inattendu peut être le résultat de l'héritage d'une hétérogénéité du milieu interstellaire ou peut être le produit de processus nébulaires internes au système solaire.

J'envisage dans un futur proche de documenter la composition isotopique de nombreux éléments dans les attaques sélectives de météorites primitives. Les principales cibles de ces études seront dans l'ordre décroissant d'intérêt le ruthénium, le tungstène, le tellure, l'étain, le zirconium, le titane, le calcium,, le magnésium, le sélénium, et le fer. Des résultats ont été obtenus en collaboration avec Olivier Rouxel pour le fer et le sélénium qui montrent qu'il n'existe pas d'hétérogénéité isotopique de la nébuleuse pour ces deux éléments (figure 6).

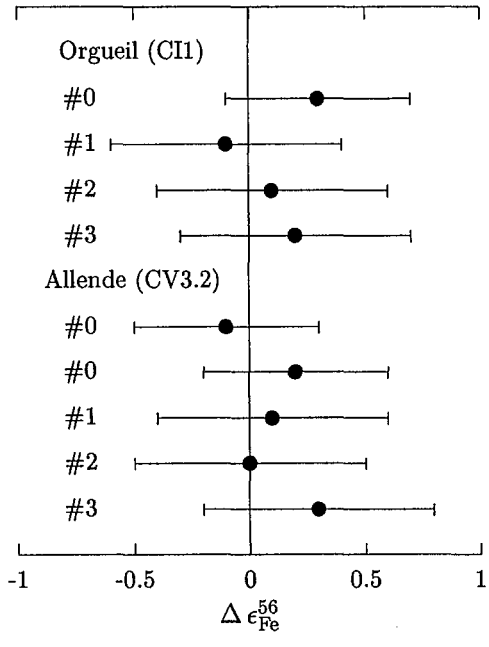

FIG. 6 – Composition isotopique du fer dans les fractions lessivées d'Allende et d'Orgueil, $\Delta\,\epsilon^{56}_{Fe} = \epsilon^{56} - 2/3\epsilon^{57}$.

Annexes

Quand un savant distingué mais vieillissant déclare que quelque chose est possible, il a presque certainement raison. Quand il déclare que quelque chose est impossible, il a très probablement tort. (...) Trop d'imagination est plus rare que trop peu ; quand le cas se produit, le malheureux qui en est affligé n'en retire qu'échecs et frustration, à moins qu'il ne soit assez sensé pour tirer un parti littéraire de ses idées, sans attendre leur réalisation.

Arthur C. Clarke

1 Science 286, 2488-2490

Heavy Nitrogen in Carbonatites of the Kola Peninsula : A Possible Signature of the Deep Mantle

Dauphas, N., and Marty, B.

Science (1999) **286**, 2488-2490

Science
www.sciencemag.org

Heavy Nitrogen in Carbonatites of the Kola Peninsula: A Possible Signature of the Deep Mantle

Nicolas Dauphas[1]* and Bernard Marty[1,2]

Nitrogen and argon isotopes were measured in carbonatites and associated rocks from the Kola Peninsula in Russia. The Kola mantle source, which is thought to be located in the deep mantle, is enriched in heavy nitrogen (+3 per mil relative to air) as compared to Earth's surface (atmosphere and crust, +2 per mil) and the shallow mantle (−4 per mil). Recycling of oceanic crust (+6 per mil) or metal-silicate partitioning may account for the nitrogen isotopic composition of the deep mantle.

Determining the structure and composition of the mantle is necessary in order to understand current and past mantle dynamics and mantle-to-crust interactions. For example, some have argued that part of the mantle has been isolated from mantle convection for most of Earth's history, allowing the preservation of a primitive component that is only sampled by plumes. Evidence in support of this view arises mainly from noble gases, because plume-derived magmas often show lower radiogenic/primordial isotope ratios than do mid-ocean ridge basalts (MORBs) (*1*). At variance with these models are geophysical (*2*), experimental (*3*), and geochemical (*4*) lines of evidence that suggest that some of the subducting slabs sink through the 670-km-deep seismic discontinuity, implying global stirring of the mantle.

The nitrogen isotopic composition of the shallow mantle that feeds MORs, which is expressed as per mil (‰) deviation relative to the composition of air [in $\delta^{15}N$ notation (*5*)], is estimated to be ~−4‰ (*6*–*13*). This signature may be a remnant of the nitrogen isotopic composition of Earth-forming planetesimals, which later evolved as a result of (i) addition of meteoritic (*14*, *15*) and cometary (*15*) volatiles, or (ii) fractional loss of atmospheric volatiles (*16*), or both. Biologic activity leads to a fractionation of nitrogen isotopes and gives sedimentary rocks a specific composition [$\delta^{15}N \sim +6$‰ (*17*)]. Nitrate is used by denitrifying bacteria as the terminal electron acceptor in energy generation when oxygen is unavailable. Associated with denitrification is a kinetic isotope effect that enriches the residual nitrate in ^{15}N (*18*). Because NO_3^- is the main nitrogen-bearing nutrient, marine organisms and sediments are enriched in ^{15}N relative to the atmosphere (*17*). The oceanic crust thus enriched in ^{15}N is subducted back into Earth at convergent plate margins, which makes nitrogen a potentially powerful tracer of volatile recycling in the mantle.

Mantle plumes, which are assumed to be fixed relative to plate motion, sample a deeper region than that feeding MORs (*19*). The isotopic composition of nitrogen in plumes has not been documented (*20*). Low $^4He/^3He$ ratios and a steep $^{20}Ne/^{22}Ne$-$^{21}Ne/^{22}Ne$ correlation (*21*) indicate that a mantle plume contributed to the 370-million-year-old (*22*) ultrabasic-alkaline-carbonatite magmatism in the Kola Peninsula in Russia (the eastern segment of the Baltic Shield). The Kola rocks crystallized at depth (*23*), which prevented them from being extensively outgassed, minimizing any subsequent

[1]Centre de Recherches Pétrographiques et Géochimiques, CNRS UPR 9046, 15 rue Notre-Dame des Pauvres, Boîte Postale 20, 54501 Vandoeuvre-lès-Nancy Cedex, France. [2]Ecole Nationale Supérieure de Géologie, rue du doyen Marcel Roubault, Boîte Postale 40, 54501 Vandoeuvre-lès-Nancy Cedex, France.

*To whom correspondence should be addressed. E-mail: dauphas@crpg.cnrs-nancy.fr

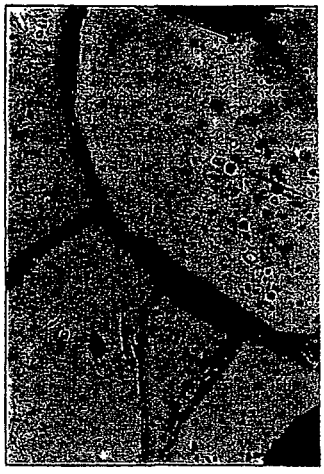

2488
A gassed mantle

REPORTS

contamination by atmospheric volatiles. To document the nitrogen isotopic composition of the deep, plume-type mantle, we have measured nitrogen and argon isotopes in carbonatites and associated rocks from the Kola Peninsula [referred to as Kola rocks hereafter (Table 1)]. Volatiles trapped in fluid inclusions were released by stepwise crushing, followed by online nitrogen-argon purification and high-resolution static-vacuum mass spectrometry (*10*, *24*).

The Ne isotopic composition of the mantle is different from that of the atmosphere (*25*), making this element a Rosetta stone when deciphering the isotopic message of terrestrial volatiles. Neon and Ar isotopic ratios correlate in Kola rocks and MORBs, which allows us to estimate the deep and shallow mantle $^{40}Ar/^{36}Ar$ ratios at 4000 to 6000 (*21*) and at 25,000 to 44,000 (*26*), respectively (^{40}Ar is a decay product of ^{40}K, whereas ^{36}Ar is primordial in origin). These ratios are used hereafter to determine the isotopic and elemental characteristics of the mantle.

In Kola rocks [and MORBs (*10*, *13*, *27*)], the $N_2/^{36}Ar$ ratio correlates with the $^{40}Ar/^{36}Ar$ ratio (Fig. 1). The $^{40}Ar/^{36}Ar$ ratio is a reliable indicator of shallow contamination by sediments, air, or air-saturated water. A comparatively K-rich (3.59×10^{-4} mol g^{-1}) ijolite exhibits systematically high $^{40}Ar/^{36}Ar$ ratios at low $N_2/^{36}Ar$ ratios, which may reflect a late (postcrystallization) ^{40}Ar radiogenic ingrowth. A sedimentary contribution is suggested by the high $N_2/^{40}Ar$ ratios (up to 114) of some carbonatites. During partial melting, vesiculation, and formation of fluid inclusions, one might expect a complete extraction of N and Ar and an inheritance of the isotopic and elemental compositions of the source (*28*). When extrapolating the mixing relationships to the source end-member $^{40}Ar/^{36}Ar$ ratios, one can estimate the $N_2/^{36}Ar$ ratios of the deep mantle (from the Kola rocks) and shallow mantle (from the MORBs) at approximately 3×10^5 and 5×10^6, respectively. The $N_2/^{40}Ar$ ratio of the deep mantle (60 ± 5) is lower than that of the shallow mantle [124 ± 20 (*13*)], which leads to a new estimate of the bulk N_2 content of the mantle ($3.6 \pm 1.4 \times 10^{-8}$ mol g^{-1}), as derived from a global K-Ar-N mass balance of the silicate Earth (*27*).

As in the case of MORBs (*10*, *13*), Kola rocks form a triangular array in a N-Ar isotope plot (Fig. 2). This feature is consistent with mixing between air (or air-saturated water), sediments, and mantle gases. The fluid inclusions that host the heavy nitrogen show plume-type $^4He/^3He$ and $^{21}Ne/^{22}Ne$ ratios and comparative-

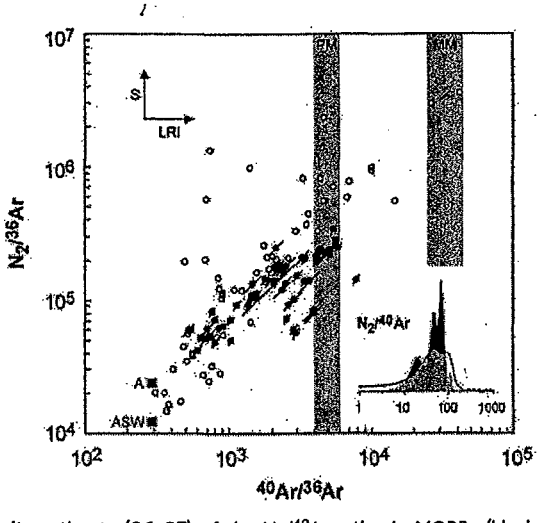

Fig. 1. $N_2/^{36}Ar$-$^{40}Ar/^{36}Ar$ correlations in MORBs [white dots (*10*, *13*, *27*)] and Kola rocks [black dots (Table 1)]. Data points fall on mixing lines between the mantle (PM, plume-type deep mantle; MM, MOR-type shallow mantle) and Earth's surface (A, air; ASW, air-saturated water; S, sediments). This correlation was lately disturbed by ^{40}Ar radiogenic ingrowth (LRI). The uncertainties (depicted as the main axis of standard ellipses) are correlated because they mainly result from the ^{36}Ar blank correction. For the purpose of clarity, uncertainties for MORBs are omitted. The source end-member $^{40}Ar/^{36}Ar$ ratios (shaded regions) are derived from Ar-Ne isotope correlations (*21*, *26*). (Bottom right) Kernel density estimate (*36*, *37*) of the $N_2/^{40}Ar$ ratios in MORBs (black area) and Kola rocks (white area).

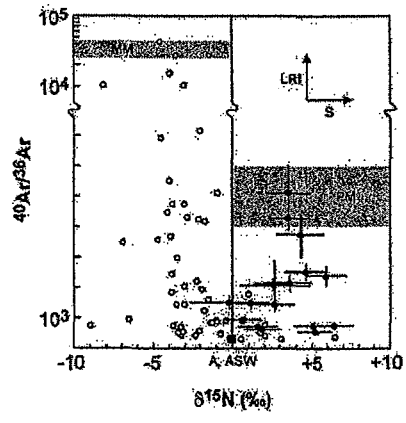

Fig. 2. Nitrogen-argon isotope correlations. Note the change in scale at $^{40}Ar/^{36}Ar = 10^4$. Symbols and abbreviations are as in Fig. 1. MORBs (*10*, *13*) and Kola rocks (Table 1) form triangular mixing arrays between the mantle, air (or air-saturated water), and sediments.

Table 1. N-Ar-K data in carbonatites and associated paragenesis from the Kola Peninsula (additional data are available at www.sciencemag.org/feature/data/1044003.shl). Uncertainties are one sigma.

Complex	Rock (mineral)	N_2 (10^{-9} mol g^{-1})	$\delta^{15}N$ (‰)	^{40}Ar (10^{-11} mol g^{-1})	$^{40}Ar/^{36}Ar$	K (10^{-5} mol g^{-1})
Lesnaya Varaka	Dunite with perovskite and titanomagnetite	3.96 ± 0.10	1.9 ± 1.1	5.68 ± 0.14	612 ± 55	<0.2
	Dunite (magnetite)	1.74 ± 0.05	3.5 ± 1.4	3.89 ± 0.13	5103 ± 899	<0.2
Kovdor	Turjaite	6.06 ± 0.15	3.5 ± 1.1	13.02 ± 0.33	4281 ± 394	3.2 ± 0.3
	Dunite	1.42 ± 0.04	4.6 ± 1.3	2.63 ± 0.07	2497 ± 266	5.1 ± 0.5
	Phoscorite (magnetite)	1.30 ± 0.03	6.0 ± 1.3	2.57 ± 0.06	2376 ± 308	<0.2
	Pyroxenite (diopside)	0.27 ± 0.01	2.7 ± 2.2	0.42 ± 0.01	2062 ± 820	6.2 ± 0.6
Seblyavr	Pyroxenite	3.40 ± 0.09	2.6 ± 1.2	3.93 ± 0.10	2102 ± 209	15.3 ± 0.3
	Pyroxenite (pyroxene)	0.57 ± 0.01	−0.2 ± 2.5	0.63 ± 0.02	1485 ± 201	12.1 ± 0.2
	Calcite carbonatite	7.96 ± 0.20	5.3 ± 1.1	7.00 ± 0.19	532 ± 51	17.6 ± 0.4
	Calcite carbonatite	20.20 ± 0.51	1.7 ± 1.2	27.23 ± 0.69	691 ± 61	0.42 ± 0.04
	Dunite	6.08 ± 0.15	3.6 ± 1.4	5.27 ± 0.14	2144 ± 251	13.4 ± 0.3
	Dolomite carbonatite	2.50 ± 0.06	6.5 ± 1.2	3.38 ± 0.09	745 ± 89	1.5 ± 0.1
	Ijolite	1.75 ± 0.04	4.3 ± 1.5	4.68 ± 0.12	3720 ± 667	35.9 ± 0.7
	Apatite-phlogopite-diopside ore	1.49 ± 0.04	2.6 ± 1.2	2.10 ± 0.05	1415 ± 166	10.2 ± 1.0
	Apatite-diopside-phlogopite ore	6.91 ± 0.17	1.1 ± 1.2	9.23 ± 0.23	1456 ± 132	26.3 ± 0.5
	Clinopyroxenite with perovskite and titanomagnetite	3.52 ± 0.09	0.7 ± 1.1	5.10 ± 0.13	926 ± 86	2.8 ± 0.3
	Dolomite carbonatite	2.83 ± 0.07	5.1 ± 1.2	3.33 ± 0.08	716 ± 68	0.21 ± 0.02

ly high $^{40}Ar/^{36}Ar$ ratios, which all together indicate a mantle source region (*21*). The coupled Sr and Nd isotope systematics in the Kola Peninsula provide no evidence for crustal contamination (*29*). Independently, preliminary measurements in our laboratory on basalt glasses from the Society Island hot spot yield positive $\delta^{15}N$ values, suggesting that heavy nitrogen is a common feature of plume-derived magmas. In contrast to the characteristics of the shallow mantle, which is depleted in heavy nitrogen by ~−4‰ relative to the atmosphere (*6–13*), the deep mantle appears to be enriched by ~+3‰. The $\delta^{15}N$ value of the deep mantle outside the range defined by the shallow mantle (*6–13*) and Earth's surface [crust and atmosphere, ~+2‰ (*10*)] suggests that the heavy nitrogen is not primordial in origin. It is noteworthy that the late accretion of extraterrestrial matter depleted in ^{15}N relative to the deep mantle would fail to account for the ^{15}N depletion of the shallow mantle relative to the atmosphere.

Long-term isotopic fractionation of N during magma genesis and subsequent degassing, if any (*28*), are unable to account for the isotopic heterogeneity of present-day Earth. Models of N isotope fractionation between silicate melt and vapor predict that the residual N in the silicates after magma degassing should be enriched in ^{15}N (*7*, *30*). Because noble gas isotopic ratios suggest that the deep mantle is less degassed than the shallow mantle (*1*), one should expect the shallow mantle to be enriched in ^{15}N relative to the deep mantle, which is contrary to the observation.

Nitrogen is a siderophile element (*31*), whereas Ar is not (*32*). Hence, uptake of N by the core would lower the $N_2/^{36}Ar$ ratio of the mantle. The solubility of N_2 in Fe-Ni alloys follows Sieverts' law (N_2 gas $\rightleftharpoons$ 2N dissolved). Because the ^{14}N-^{14}N bond is weaker than the ^{15}N-^{14}N or ^{15}N-^{15}N bonds, the residual N in the mantle is presumably enriched in ^{15}N relative to its metal counterpart. Such a possibility would require appreciable fractionation of nitrogen isotopes to account for the isotopic stratification of present-day Earth, which calls for experimental as well as theoretical confirmation.

Phanerozoic marine sediments and the deep mantle both exhibit high $N_2/^{36}Ar$ ratios and high $\delta^{15}N$ values relative to the atmosphere. An appealing possibility is that the nitrogen carried from the deep mantle to the surface of Earth by plumes is of recycled origin. This interpretation is consistent with the recycling of Ar in Earth's interior (*21*, *33*) but creates a paradox. If the ^{15}N depletion of the shallow mantle was primordial in origin, as is generally thought (*6–16*), preferential recycling of sediments in the deep mantle would at the same time increase the $N_2/^{36}Ar$ ratio and the $\delta^{15}N$ value of the deep mantle relative to the shallow mantle, which is apparently not the case. A way to get around this difficulty is to consider that the nitrogen isotopic composition of the shallow mantle is not primordial in origin but rather results from the recycling of Archean, ^{15}N-depleted, sedimentary organic matter (*34*). An alternative explanation is that the $N_2/^{36}Ar$ ratio of the primitive mantle was lower than the inferred present-day ratio of the deep mantle ($\sim 3 \times 10^5$). Early degassing of the shallow mantle would have increased the $N_2/^{36}Ar$ ratio to $\sim 5 \times 10^6$ as a result of preferential retention of nitrogen in silicates under the reducing conditions prevailing at that time (*35*). Later on, the $N_2/^{36}Ar$ ratio of the deep mantle would have increased to its present-day value through recycling of surface nitrogen. Further investigation of the nitrogen isotopic composition of ocean islands such as Hawaii or Iceland will allow this unique stable isotope heterogeneity of Earth to be documented.

References and Notes

1. In the mantle, ^3He and ^{22}Ne are mainly primordial in origin (they were trapped in our planet at the time of its accretion), whereas ^4He and ^{21}Ne have been produced throughout Earth's history. Less degassed reservoirs exhibit low time-integrated $(U+Th)/^3He$ and $(U+Th)/^{22}Ne$ ratios, and consequently low $^4He/^3He$ ratios [M. D. Kurz, W. J. Jenkins, S. R. Hart, *Nature* **297**, 43 (1982)] and $^{21}Ne/^{22}Ne$ ratios [M. Honda, I. McDougall, D. B. Patterson, A. Doulgeris, D. A. Clague, *Nature* **349**, 149 (1991)].
2. R. D. van der Hilst, S. Widiyantoro, E. R. Engdahl, *Nature* **386**, 578 (1997).
3. K. Hirose, Y. Fei, Y. Ma, H.-K. Mao, *Nature* **397**, 53 (1999).
4. A. W. Hofmann, *Nature* **385**, 219 (1997).
5. $\delta^{15}N = [(^{15}N/^{14}N)_{sample}/(^{15}N/^{14}N)_{air} - 1] \times 1000$.
6. M. Javoy, F. Pineau, D. Demaiffe, *Earth Planet. Sci. Lett.* **68**, 399 (1984).
7. M. Javoy, F. Pineau, H. Delorme, *Chem. Geol.* **57**, 41 (1986).
8. S. R. Boyd and C. T. Pillinger, *Chem. Geol.* **116**, 43 (1994).
9. P. Cartigny, S. R. Boyd, J. W. Harris, M. Javoy, *Terra Nova* **9**, 175 (1997).
10. B. Marty and F. Humbert, *Earth Planet. Sci. Lett.* **152**, 101 (1997).
11. P. Cartigny, J. W. Harris, M. Javoy, *Science* **280**, 1421 (1998).
12. P. Cartigny, J. W. Harris, D. Phillips, M. Girard, M. Javoy, *Chem. Geol.* **147**, 147 (1998).
13. B. Marty and L. Zimmermann, *Geochim. Cosmochim. Acta* **63**, 3619 (1999).
14. M. Javoy, *Geophys. Res. Lett.* **24**, 177 (1997); *Chem. Geol.* **147**, 11 (1998).
15. N. Dauphas, F. Robert, B. Marty, *Meteorit. Planet. Sci.* **33**, A38 (1998).
16. I. N. Tolstikhin and B. Marty, *Chem. Geol.* **147**, 27 (1998).
17. K. E. Peters, R. E. Sweeney, I. R. Kaplan, *Limnol. Oceanogr.* **23**, 598 (1978).
18. E. Wada, T. Kadonaga, S. Matsuo, *Geochem. J.* **9**, 139 (1975).
19. Geophysical investigations [L. Bréger and B. Romanowicz, *Science* **282**, 718 (1998); D. V. Helmberger, L. Wen, X. Ding, *Nature* **396**, 251 (1998); S. A. Russell, T. Lay, E. J. Garnero, *Nature* **396**, 255 (1998); H. Bijwaard and W. Spakman, *Earth Planet. Sci. Lett.* **166**, 121 (1999)] together with geochemical investigations [R. J. Walker, J. W. Morgan, M. F. Horan, *Science* **269**, 819 (1995); E. Widom and S. B. Shirey, *Earth Planet. Sci. Lett.* **142**, 451 (1996); R. J. Walker *et al.*, *Geochim. Cosmochim. Acta* **61**, 4799 (1997); A. D. Brandon, R. J. Walker, J. W. Morgan, M. D. Norman, H. M. Prichard, *Science* **280**, 1570 (1998); J. E. Snow and G. Schmidt, *Nature* **391**, 166 (1998); J. M. Bird, A. Meibom, R. Frei, T. F. Nägler, *Earth Planet. Sci. Lett.* **170**, 83 (1999)] suggest that plumes emerge from the core-mantle boundary.
20. R. A. Exley, S. R. Boyd, D. P. Mattey, and C. T. Pillinger [*Earth Planet. Sci. Lett.* **81**, 163 (1986/87)] measured positive $\delta^{15}N$ values in basalt glasses from Loihi seamount, but also positive and negative values for MORBs. These results are inconclusive because there was no simultaneous control of shallow contamination by argon isotopes (*10*, *13*).
21. B. Marty *et al.*, *Earth Planet. Sci. Lett.* **164**, 179 (1998).
22. U. Kramm, L. N. Kogarko, V. A. Kononova, H. Vartiainen, *Lithos* **30**, 33 (1993).
23. A. A. Kukharenko *et al.*, *The Caledonian Complex of Ultrabasic Alkaline Rocks and Carbonatites of the Kola Peninsula and Northern Karelia* (Nedra, Moscow, 1965).
24. Samples weighing 0.1 to 0.4 g were crushed under ultrahigh vacuum ($\sim 2 \times 10^{-9}$ torr) with a soft iron piston cylinder activated by an external solenoid. Gases were then purified in a glass line where H, C, and S compounds were oxidized (in the presence of Pt foils held at 723 K) with O_2 produced by heating a CuO furnace at 1023 K ($4CuO \rightleftharpoons 2Cu_2O + O_2$). Condensible gases (for example, H_2O, CO_2, and SO_2) were trapped in a cold finger held at 90 K. Excess oxygen was resorbed onto the CuO at 723 K. Nitrogen was then admitted into a Micromass VG5400 static-vacuum mass spectrometer. The trap current of the Nier type source was 20 μA, resulting in a N_2 sensitivity of 2.8×10^{-5} A $torr^{-1}$. The nitrogen isotopic composition was determined as the 29/28 ion beam ratio on a Faraday collector. Possible isobaric interferences with N_2 of CO, N_2H, and C_2H_x at masses 28 and 29 were monitored at mass 30 and were always negligibly small. Gases left in the purification line were further purified over hot Ti sponge getters. Argon was then admitted to the mass spectrometer, where ^{40}Ar was analyzed with a Faraday collector (with a sensitivity of 5.0×10^{-5} A $torr^{-1}$) and ^{36}Ar was measured by ion counting after amplification by an electron multiplier.
25. The highest $^{20}Ne/^{22}Ne$ ratio measured so far in mantle rocks [M. Ozima and S. Zashu, *Geochim. Cosmochim. Acta* **52**, 19 (1988)] is close to the solar ratio [J.-P. Benkert, H. Baur, P. Signer, R. Wieler, *J. Geophys. Res.* **98**, 13147 (1993)] and is much higher than any other known component such as Ne-E [M. H. A. Jungck and P. Eberhardt, *Meteoritics* **14**, 439 (1979)], cosmogenic Ne [E. Mazor, D. Heymann, E. Anders, *Geochim. Cosmochim. Acta* **34**, 781 (1970)], Ne-A [M. Tang and E. Anders, *Geochim. Cosmochim. Acta* **52**, 1245 (1988)], or Ne-Q [R. Wieler, E. Anders, H. Baur, R. S. Lewis, P. Signer, *Geochim. Cosmochim. Acta* **56**, 2907 (1992)].
26. M. Moreira, J. Kunz, C.-J. Allègre, *Science* **279**, 1178 (1998).
27. B. Marty, *Nature* **377**, 326 (1995).
28. The N_2/Ar ratios in mantle vesicles do not correlate with any index of partial melting or degassing, which suggests a comparable behavior of Ar and N. Because Ar is incompatible, this element and by inference N are thoroughly extracted from the mantle during magma genesis and subsequent degassing (*10*, *13*, *27*).
29. U. Kramm, *Eur. J. Mineral.* **5**, 985 (1993).
30. P. Richet, Y. Bottinga, M. Javoy, *Annu. Rev. Earth Planet. Sci.* **5**, 65 (1977).
31. K. Hashizume, T. Kase, J. Matsuda, H. Sato, *Kazan* **42**, S293 (1997).
32. J. Matsuda *et al.*, *Science* **259**, 788 (1993).
33. P. Sarda, M. Moreira, T. Staudacher, *Science* **283**, 666 (1999).
34. V. Beaumont and F. Robert, *Precambrian Res.* **96**, 63 (1999).
35. F. Humbert, B. Marty, G. Libourel, *Lunar Planet. Sci.* XXX, 1955 (1999).
36. S. J. Sheather and M.C. Jones, *J. R. Stat. Soc. B* **53**, 683 (1991).
37. A. W. Bowman and A. Azzalini, *Applied Smoothing Techniques for Data Analysis: the Kernel Approach With S-Plus Illustrations* (Oxford Univ. Press, Oxford, 1997).

38. We thank I. N. Tolstikhin for providing us with these unique samples; K. Hashizume and S. R. Boyd for insightful discussions; and L. Zimmermann, P. Robert, and G. Sauder for help in keeping the mass spectrometer in fine shape. This is contribution 1434 of the Centre de Recherches Pétrographiques et Géochimiques.

28 July 1999; accepted 2 November 1999

2 Icarus 148, 508-512

The Late Asteroidal and Cometary Bombardment of Earth as Recorded in Water Deuterium to Protium Ratio

Dauphas, N., Robert, F., and Marty, B.

Icarus (2000) **148**, 508-512

Icarus 148, 508–512 (2000)
doi:10.1006/icar.2000.6489, available online at http://www.idealibrary.com on IDEAL®

The Late Asteroidal and Cometary Bombardment of Earth as Recorded in Water Deuterium to Protium Ratio

Nicolas Dauphas

Centre de Recherches Pétrographiques et Géochimiques, CNRS EP 2031, 15 rue Notre-Dame des Pauvres, B.P. 20, 54501 Vandœuvre-lès-Nancy Cedex, France
E-mail: dauphas@crpg.cnrs-nancy.fr

François Robert

Laboratoire de Minéralogie, CNRS URA 736, Muséum National d'Histoire Naturelle, 61 rue Buffon, 75005 Paris, France

and

Bernard Marty[1]

Centre de Recherches Pétrographiques et Géochimiques, CNRS EP 2031, 15 rue Notre-Dame des Pauvres, B.P. 20, 54501 Vandœuvre-lès-Nancy Cedex, France

Received November 3, 1998; revised May 19, 2000

The deuterium to protium (D/H) ratio of the deep mantle may be a remnant of the hydrogen isotopic composition of Earth forming planetesimals, which later evolved as a result of the late accretion of asteroids and comets. If so, the mass of asteroids and comets incident on Earth since the time of its accretion is estimated to be 4×10^{20}–2×10^{22} kg. The combined use of water D/H ratios, the lunar cratering record, and terrestrial mantle siderophiles would favor a rather low mass fraction of comets among impacting bodies ($\lesssim$0.01). Asteroids, comets, and the early Earth contributed to 0–0.5, 0–0.1, and 0.5–0.9 of Earth's water inventory, respectively. A two stage model is advocated in which escape to space of terrestrial volatiles predated the late accretion of extraterrestrial gases. We wish to emphasize that our interpretations and conclusions might evolve in the future when additional data on asteroids, comets, and Earth's interior become available.

Key Words: accretion; asteroids; atmospheres; evolution; comets; Earth.

1. INTRODUCTION

The surface density of lunar craters correlates with the age of the cratered surface, implying in turn that the Moon (and by extension Earth) endured a period of heavy bombardment by the remnants of planetary formation (Shoemaker and Hackman 1962). This late accretion of extraterrestrial matter is also recorded by highly siderophile elements (Ru, Rh, Pd, Re, Os, Ir, Pt, and Au) which are in chondritic proportion in Earth's mantle (Jagoutz *et al.* 1979) and are overabundant relative to that predicted in the case of equilibrium partitioning between the mantle and the core (Kimura *et al.* 1974). According to several heterogeneous accretion models, our planet received the bulk of its surface volatiles as a late accreting veneer. Conversely, the extreme ultraviolet radiation of the young evolving Sun (Zahnle and Walker 1982) could have driven a fractional loss of terrestrial volatiles. In the present contribution, an intermediate view is advocated in which escape to space of terrestrial volatiles predated the late accretion of extraterrestrial gases.

Mantle plumes sample a deep region of Earth (Bréger and Romanowicz 1998, Helmberger *et al.* 1998, Russel *et al.* 1998, Bijwaard and Spakman 1999, Goes *et al.* 1999, Ritsema *et al.* 1999), which offers the opportunity to study volatile elements trapped in our planet at the time of its accretion. The D/H ratio of the deep mantle (Deloule *et al.* 1991) may be a remnant of the hydrogen isotopic composition of Earth-forming planetesimals which later evolved to the present Earth value (Kyser and O'Neil 1984, Lécuyer *et al.* 1998) as a result of the late accretion of asteroids (Kerridge 1985) and comets (Balsiger *et al.* 1995, Eberhardt *et al.* 1995, Bockelée-Morvan *et al.* 1998, Meier *et al.* 1998). In consideration of water D/H ratios, the mass of asteroids and comets incident on Earth since the time of its accretion as well as the contributions of asteroids, comets, and early Earth to Earth's water inventory are estimated.

2. SETTING THE SCENE

The extraterrestrial flux to Earth ranges from a few micrometers up to several tens of kilometers. Melosh and Vickery (1989) and Vickery and Melosh (1990) constructed an analytical model of atmospheric erosion by impacts based on computer modeling.

[1] Also at: École Nationale Supérieure de Géologie, rue du Doyen Marcel Roubault, B.P. 40, 54501 Vandœuvre-lès-Nancy Cedex, France.

0019-1035/00 $35.00

They suggested that vapor plumes created by high-speed impacts might eject part or the entire air mass above the plane tangent to the point of impact. Recent analytical and computational modeling of impact induced erosion led Newman *et al.* (1999) to conclude that impact events (at least those up to K/T) would not remove significant atmospheric gases. As a first approximation, we shall consider that Earth retained all incident volatiles.

Despite the observation that ~4% of meteorite falls are carbonaceous chondrites (Sears and Dodd 1988), there is strong evidence that the accretion tail consisted of organic rich matter. Indeed, carbon-rich asteroids (Gaffey *et al.* 1993) dominate the asteroid belt population (Gradie *et al.* 1989), most xenoliths in meteorite regolithic breccias resemble carbonaceous chondrites (Anders 1978, Wasson and Wetherill 1979, Lipschutz *et al.* 1989), the lunar regolith is known to contain 1–2% of carbonaceous debris (Keays *et al.* 1970), and micrometeorites which represent the major extraterrestrial flux to Earth share similarities with carbonaceous chondrites (Kurat *et al.* 1994, Engrand and Maurette 1998). On the whole, we shall assume that our planet owes its water to Earth forming planetesimals (early Earth) and a late accreting veneer (asteroids similar to CI–CM chondrites and comets). It is worthwhile to note that recent papers (Delsemme 1999, Pavlov *et al.* 1999) address the late addition of water to Earth in a manner different from that which we advocate.

3. WATER IN ASTEROIDS, COMETS, AND EARTH

Literature data are compiled in Table I. Kerridge (1985) measured water concentrations and D/H ratios in some carbonaceous chondrites. The mean water concentrations of CI and CM are 0.0032 ± 0.0003 and 0.0038 ± 0.0002 mol g^{-1}, respectively. The mean D/H ratios of CI and CM are $181 \pm 10 \times 10^{-6}$ and $159 \pm 10 \times 10^{-6}$, respectively. Water concentrations in cometary ice and dust are 0.041 ± 0.009 and 0.025 ± 0.005 mol g^{-1}, respectively (Delsemme 1988, Jessberger *et al.* 1988). The ratio dust/ice is poorly known but may vary in the range 0.5–1.3 (Delsemme 1988). Measurements of D/H ratios in Halley 1P/1982 U1 (Balsiger *et al.* 1995, Eberhardt *et al.* 1995), Hale–Bopp C/1995 O1 (Meier *et al.* 1998), and Hyakutake C/1996 B2 (Bockelée-Morvan *et al.* 1998) yielded consistent results centered around $311 \pm 13 \times 10^{-6}$. The early Earth D/H ratio is consistently higher than the lowest ratio measured so far in undifferentiated meteorites ($\gtrsim 128 \times 10^{-6}$, Kerridge 1985) and is necessarily lower than the inferred deep mantle ratio ($\lesssim 136 \times 10^{-6}$, Deloule *et al.* 1991). Lécuyer *et al.* (1998) estimated the amount and D/H ratio of water stored at Earth's surface (oceans, ice sheets, organic matter, metamorphic rocks, shales, sandstones, continental carbonates, evaporites, marine clays, and marine carbonates) to be ca. 9.4×10^{22} mol and 153×10^{-6}, respectively. Measurements of water concentrations in nominally anhydrous minerals led Bell and Rossman (1992) to propose that at most ca. 6.6×10^{22} mol of water could be accommodated in the whole mantle. The mean mantle D/H ratio is ca. 143×10^{-6} (Kyser and O'Neil 1984).

4. FORMAL REASONING

If we assume that Earth retained all incident volatiles and that the late accreting veneer consisted of asteroids similar to CI–CM carbonaceous chondrites and comets, then it is straightforward to draw up mass balance equations (Javoy 1997, 1998, Dauphas *et al.* 1998) for H and D between asteroids (A), comets (C), the early Earth (E), and the present Earth (P).

$$M[(1-\alpha)C_A + \alpha C_C] + M_\oplus C_E = M_\oplus C_P$$
$$M[(1-\alpha)C_A R_A + \alpha C_C R_C] + M_\oplus C_E R_E = M_\oplus C_P R_P,$$

where M is the mass of asteroids similar to carbonaceous chondrites and comets incident on Earth since the time of its accretion, α is the mass fraction of comets among impacting bodies, C and R stand for concentration and isotopic ratio (respectively), and $M_\oplus$ denotes the mass of Earth. There are two mass-balance equations (H and D) in three unknowns (M, α, and C_E), so that one must fix a parameter to compute the remaining two (Figs. 1 and 2).

5. THE LATE BOMBARDMENT AND THE ORIGIN OF WATER ON EARTH

Results of the calculations are displayed in Figs. 1 and 2. The mass of asteroids and comets incident on Earth since the time of its accretion (Fig. 1) is estimated to be 4×10^{20}–2×10^{22} kg, which compares well with independent calculations based on the

TABLE I
Literature Data

	Asteroids	Comets	Early Earth	Present Earth
H_2O (10^{-3} mol g^{-1})	3.2 ± 0.3–3.8 ± 0.2	32 ± 5–36 ± 6	—	0.016–0.027
D/H (10^{-6})	159 ± 10–181 ± 10	311 ± 13	128–136	149–153

Note. $x - y$ and $x \pm y$ uncertainties were simulated as uniform and gaussian random variables (respectively) in Monte-Carlo error propagations (Anderson 1976). Some uncertainties are correlated (see text). References: Asteroids—Kerridge (1985). Comets—Delsemme (1988), Jessberger *et al.* (1988), Balsiger *et al.* (1995), Eberhardt *et al.* (1995), Bockelée-Morvan *et al.* (1998), Meier *et al.* (1998). Early Earth—Kerridge (1985), Deloule *et al.* (1991). Present Earth—Kyser and O'Neil (1984), Bell and Rossman (1992), Lécuyer *et al.* (1998).

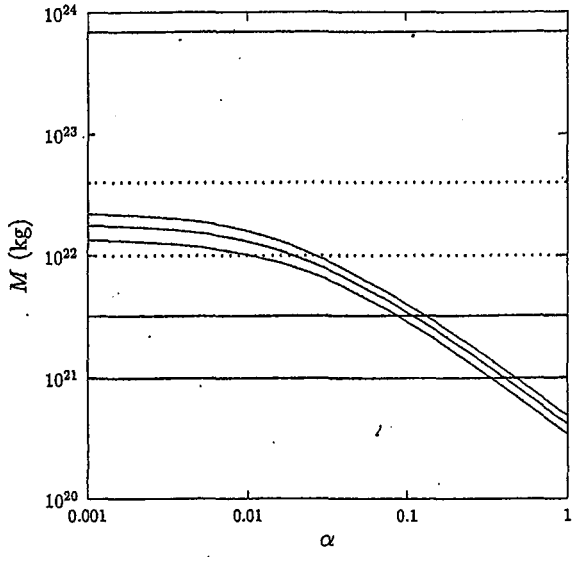

FIG. 1. Mass of asteroids and comets incident on Earth since the time of its accretion (M) as a function of the mass fraction of comets among impacting bodies (α). Light curves are based on water deuterium to protium ratios (uncertainties are depicted as 1σ and were propagated by means of Monte-Carlo simulations; Anderson 1976), heavy lines are derived from the lunar impact record (9.9×10^{20}, 3.2×10^{21}, and 6.9×10^{23} kg; Chyba 1990), and dotted lines are based on terrestrial mantle siderophiles (1×10^{22}–4×10^{22} kg; Chyba 1991).

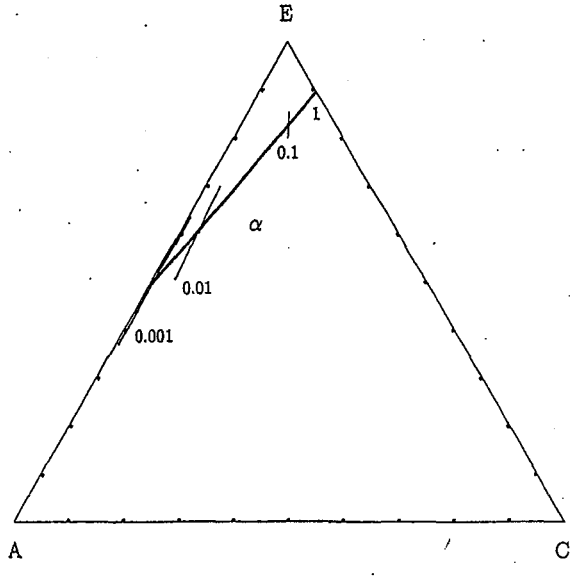

FIG. 2. Contributions of asteroids, comets, and the early Earth (ACE) to Earth's water inventory as a function of the mass fraction of comets among impacting bodies (α). Under the closure condition $x + y + z = 1$, x, y, and z are conveniently represented in an equilateral triangle. Uncertainties are depicted as 1σ and were propagated by means of Monte-Carlo simulations (Anderson 1976).

lunar impact record (9.9×10^{20}, 3.2×10^{21}, and 6.9×10^{23} kg; Chyba 1990) and terrestrial mantle siderophiles (1×10^{22}–4×10^{22} kg; Chyba 1991). As discussed previously, there is strong evidence that the late accreting veneer consisted of organic rich matter. In such a case, the combined use of water D/H ratios, the lunar impact record, and terrestrial mantle siderophiles would favor a rather low mass fraction of comets among impacting bodies ($\lesssim$0.01). Asteroids, comets, and early Earth contributed to 0–0.5, 0–0.1, and 0.5–0.9 of Earth's water inventory, respectively (Fig. 2).

6. THE CASE OF RARE GASES

The concentrations and isotopic compositions of rare gases ranging in mass from neon to xenon integrate all events the terrestrial atmosphere suffered, which makes these elements very important when addressing the origin of Earth's volatiles. We shall focus our discussion on neon and xenon because these elements play a peculiar role in geochemistry. Indeed, the near solar (Benkert *et al.* 1993) neon isotopic composition of the mantle (Honda *et al.* 1991) is different from that of the atmosphere (Ozima and Podosek 1983), and the xenon isotopic composition of air (Ozima and Podosek 1983) is fractionated by 0.03 per amu (atomic mass unit) relative to solar and meteoritic xenon (Pepin and Phinney, unpublished preprint, 1978).

Mazor *et al.* (1970) measured rare gas concentrations in some carbonaceous chondrites. The mean ^{20}Ne concentrations of CI and CM are $1.6 \pm 0.2 \times 10^{-11}$ and $2.5 \pm 0.9 \times 10^{-11}$ mol g^{-1}, respectively. The mean ^{130}Xe concentrations of CI and CM are $5.0 \pm 0.7 \times 10^{-14}$ and $3.0 \pm 0.5 \times 10^{-14}$ mol g^{-1}, respectively. Cometary rare gas isotopic compositions and concentrations are not known (Krasnopolsky *et al.* 1997) but by laboratory experiments aimed at reproducing the poorly known conditions that prevailed when water ice formed (Bar-Nun and Owen 1998). The present-day atmosphere contains 2.91×10^{15} mol of ^{20}Ne and 6.26×10^{11} mol of ^{130}Xe (Ozima and Podosek 1983).

If the late accreting veneer consisted of asteroids similar to carbonaceous chondrites only ($\alpha = 0$), then the amount of ^{20}Ne brought to Earth (ca. 4×10^{14} mol) would have been much lower than the global ^{20}Ne inventory at the surface of our planet (2.91×10^{15} mol). It implies that the gross isotopic disequilibrium of neon isotopes between the mantle and the atmosphere would not result from such late addition of carbonaceous material. Consequently, such an isotopic disequilibrium would have to predate these impacting events, a possibility in agreement with models calling for isotopic fractionation of neon isotopes during early atmospheric escape to space (Hunten *et al.* 1987, Zahnle *et al.* 1990, Pepin 1991, Ozima and Zahnle 1993, Tolstikhin and Marty 1998). The isotopic composition of xenon sets another important constraint on processes and sources having contributed atmospheric rare gases. Indeed, the 0.03 per amu mass fractionation observed in the present-day atmosphere relative to the Sun or meteorites cannot be the result of the contribution of a meteoritic or a solar component. The origin of such a fractionation

is unclear, but could result as well as from escape of a primitive atmosphere (Hunten *et al.* 1987, Sasaki and Nakazawa 1988, Pepin 1991, Tolstikhin and Marty 1998). The amount of ^{130}Xe contributed by impacting bodies is ca. 8×10^{11} mol, roughly similar to that present in the atmosphere (6.26×10^{11} mol). Although the contrast is less evident than for neon, it still allows the possibility that xenon isotope fractionation predated the extraterrestrial contribution considered in this model. If the late veneer comprised comets ($\alpha > 0$), then one cannot discuss further the origin of terrestrial rare gases.

7. CONCLUSIONS

Based on water deuterium to protium ratios, the mass of asteroids and comets incident on Earth since the time of its accretion is estimated to be 4×10^{20}–2×10^{22} kg. The mass fraction of comets among impacting bodies might have been lower than ~0.01. Asteroids, comets, and early Earth contributed to 0–0.5, 0–0.1, and 0.5–0.9 of Earth's water inventory, respectively. A two-stage model is advocated in which escape to space of terrestrial volatiles predated the late accretion of extraterrestrial gases. We wish to emphasize that our interpretations and conclusions might evolve in the future when additional data on asteroids, comets, and Earth's interior become available.

ACKNOWLEDGMENTS

We acknowledge three anonymous referees for their constructive and thorough reviews. We are grateful to C. F. Chyba for advice and encouragement during preparation of this paper. The support and interest of K. Hashizume, S. Léon-Hirtz, and J.-C. Royant were of great value. N. Dauphas was supported by a grant from the French space agency (Centre National d'Études Spatiales). This research has made use of NASA's Astrophysics Data System Abstract Service. This is CRPG contribution 1472.

REFERENCES

Anders, E. 1978. Most stony meteorites come from the asteroid belt. In *Asteroids: An Exploration Assessment* (D. Morrison and W. C. Wells, Eds.), pp. 57–75. NASA, Chicago.

Anderson, G. M. 1976. Error propagation by the Monte Carlo method in geochemical calculations. *Geochim. Cosmochim. Acta* **40**, 1533–1538.

Balsiger, H., K. Altwegg, and J. Geiss 1995. D/H and $^{18}O/^{16}O$ ratio in the hydronium ion and in neutral water from in situ ion measurements in Comet Halley. *J. Geophys. Res.* **100**, 5827–5834.

Bar-Nun, A., and T. Owen 1998. Trapping of gases in water ice and consequences to comets and the atmospheres of the inner planets. In *Solar System Ices* (B. B. Schmitt, C. de Bergh, and M. Festou, Eds.), pp. 353–366. Kluwer Academic, Dordrecht.

Bell, D. R., and G. R. Rossman 1992. Water in Earth's mantle: The role of nominally anhydrous minerals. *Science* **255**, 1391–1397.

Benkert, J.-P., H. Baur, P. Signer, and R. Wieler 1993. He, Ne, and Ar from the solar wind and solar energetic particles in lunar ilmenites and pyroxenes. *J. Geophys. Res.* **98**, 13147–13162.

Bijwaard, H., and W. Spakman 1999. Tomographic evidence for a narrow whole mantle plume below Iceland. *Earth Planet. Sci. Lett.* **166**, 121–126.

Bockelée-Morvan, D., D. Gautier, D. C. Lis, K. Young, J. Keene, T. Phillips, T. Owen, J. Crovisier, P. F. Goldsmith, E. A. Bergin, D. Despois, and A. Wootten 1998. Deuterated water in Comet C/1996 B2 (Hyakutake) and its implications for the origin of comets. *Icarus* **133**, 147–162.

Bréger, L., and B. Romanowicz 1998. Three-dimensional structure at the base of the mantle beneath the central pacific. *Science* **282**, 718–720.

Chyba, C. F. 1990. Impact delivery and erosion of planetary oceans in the inner Solar System. *Nature* **343**, 129–133.

Chyba, C. F. 1991. Terrestrial mantle siderophiles and the lunar impact record. *Icarus* **92**, 217–233.

Dauphas, N., F. Robert, and B. Marty 1998. Hydrogen, nitrogen, and neon elemental and isotopic constraints on cometary and meteoritic fluxes. *Meteorit. Planet. Sci.* **33**, A38–A39.

Deloule, E., F. Albarède, and S. M. F. Sheppard 1991. Hydrogen isotope heterogeneities in the mantle from ion probe analysis of amphiboles from ultramafic rocks. *Earth Planet. Sci. Lett.* **105**, 543–553.

Delsemme, A. H. 1988. The chemistry of comets. *Phil. Trans. R. Soc. London* **A325**, 509–523.

Delsemme, A. H. 1999. The deuterium enrichment observed in recent comets is consistent with the cometary origin of seawater. *Planet. Space Sci.* **47**, 125–131.

Eberhardt, P., M. Reber, D. Krankowsky, and R. R. Hodges 1995. The D/H and $^{18}O/^{16}O$ ratios in water from Comet P/Halley. *Astron. Astrophys.* **302**, 301–316.

Engrand, C., and M. Maurette 1998. Carbonaceous micrometeorites from Antartica. *Meteoritics Planet. Sci.* **33**, 565–580.

Gaffey, M. J., T. H. Burbine, and R. P. Binzel 1993. Asteroid spectroscopy: Progress and perspectives. *Meteoritics* **28**, 161–187.

Goes, S., W. Spakman, and H. Bijwaard 1999. A lower mantle source for central european volcanism. *Science* **286**, 1928–1931.

Gradie, J. C., C. R. Chapman, and E. F. Tedesco 1989. Distribution of taxonomic classes and the compositional structure of the asteroid belt. In *Asteroids II* (R. P. Binzel, T. Gehrels, and M. S. Matthews, Eds.), pp. 316–335. Univ. Arizona Press, Tucson.

Helmberger, D. V., L. Wen, and X. Ding 1998. Seismic evidence that the source of the Iceland hotspot lies at the core-mantle boundary. *Nature* **396**, 251–255.

Honda, M., I. McDougall, D. B. Patterson, A. Doulgeris, and D. A. Clague 1991. Possible solar noble-gas component in Hawaiian basalts. *Nature* **349**, 149–151.

Hunten, D. M., R. O. Pepin, and J. C. G. Walker 1987. Mass fractionation in hydrodynamic escape. *Icarus* **69**, 532–549.

Jagoutz, E., H. Palme, H. Baddenhausen, K. Blum, M. Cendales, G. Dreibus, B. Spettel, V. Lorenz, and H. Wänke 1979. The abundances of major, minor and trace elements in the Earth's mantle as derived from primitive ultramafic nodules. *Proc. Lunar Planet. Sci. Conf.* 10th, 2031–2050.

Javoy, M. 1997. The major volatile elements of the Earth: Their origin, behavior, and fate. *Geophys. Res. Lett.* **24**, 177–180.

Javoy, M. 1998. The birth of the Earth's atmosphere: The behaviour and fate of its major elements. *Chem. Geol.* **147**, 11–25.

Jessberger, E. K., A. Christoforidis, and J. Kissel 1988. Aspects of the major element composition of Halley's dust. *Nature* **332**, 691–695.

Keays, R. R., R. Ganapathy, J. C. Laul, E. Anders, G. F. Herzog, and P. M. Jeffery 1970. Trace elements and radioactivity in lunar rocks: Implications for meteorite infall, solar-wind flux, and formation conditions of moon. *Science* **167**, 490–493.

Kerridge, J. F. 1985. Carbon, hydrogen and nitrogen in carbonaceous chondrites: Abundances and isotopic compositions in bulk samples. *Geochim. Cosmochim. Acta* **49**, 1707–1714.

Kimura, K., R. S. Lewis, and E. Anders 1974. Distribution of gold and rhenium between nickel–iron and silicate melts: Implications for the abundance of siderophile elements on the Earth and Moon. *Geochim. Cosmochim. Acta* **38**, 683–701.

Krásnopolsky, V. A., M. J. Mumma, M. Abbott, B. C. Flynn, K. J. Meech, D. K. Yeomans, P. D. Feldman, and C. B. Cosmovici.1997. Detection of soft X-rays and a sensitive search for noble gases in Comet Hale–Bopp (C/1995 O1). *Science* 277, 1488–1491.

Kurat, G., C. Koeberl, T. Presper, F. Brandstätter, and M. Maurette 1994. Petrology and geochemistry of Antartic micrometeorites. *Geochim. Cosmochim. Acta* 58, 3879–3904.

Kyser, T. K., and J. R. O'Neil 1984. Hydrogen isotope systematics of submarine basalts. *Geochim. Cosmochim. Acta* 48, 2123–2133.

Lécuyer, C., P. Gillet, and F. Robert 1998. The hydrogen isotope composition of seawater and the global water cycle. *Chem. Geol.* 145, 249–261.

Lipschutz, M. E., M. J. Gaffey, and P. Pellas 1989. Meteoritic parent bodies: Nature, number, size and relation to present-day asteroids. In *Asteroids II* (R. P. Binzel, T. Gehrels, and M. S. Matthews, Eds.), pp. 740–777. Univ. Arizona Press, Tucson.

Mazor, E., D. Heymann, and E. Anders 1970. Noble gases in carbonaceous chondrites. *Geochim. Cosmochim. Acta* 34, 781–824.

Meier, R., T. C. Owen, H. E. Matthews, D. C. Jewitt, D. Bockelée-Morvan, N. Biver, J. Crovisier, and D. Gautier 1998. A determination of the HDO/H_2O ratio in Comet C/1995 O1 (Hale–Bopp). *Science* 279, 842–844.

Melosh, H. J., and A. M. Vickery 1989. Impact erosion of the primordial atmosphere of Mars. *Nature* 338, 487–489.

Newman, W. I., E. M. D. Symbalisty, T. J. Ahrens, and E. M. Jones 1999. Impact erosion of planetary atmospheres: Some surprising results. *Icarus* 138, 224–240.

Ozima, M., and F. A. Podosek 1983. *Noble Gas Geochemistry*. Cambridge Univ. Press, Cambridge.

Ozima, M., and K. Zahnle 1993. Mantle degassing and atmospheric evolution: Noble gas view. *Geochem. J.* 27, 185–200.

Pavlov, A. A., A. K. Pavlov, and J. F. Kasting 1999. Irradiated interplanetary dust particles as a possible solution for the deuterium/hydrogen paradox of Earth's oceans. *J. Geophys. Res.* 104, 30725–30728.

Pepin, R. O. 1991. On the origin and early evolution of terrestrial planet atmospheres and meteoritic volatiles. *Icarus* 92, 2–79.

Ritsema, J., H. J. van Heijst, and J. H. Woodhouse 1999. Complex shear wave velocity structure imaged beneath Africa and Iceland. *Science* 286, 1925–1928.

Russell, S. A., T. Lay, and E. J. Garnero 1998. Seismic evidence for small-scale dynamics in the lowermost mantle at the root of the Hawaiian hotspot. *Nature* 396, 255–258.

Sasaki, S., and K. Nakazawa 1988. Origin of isotopic fractionation of terrestrial Xe: Hydrodynamic fractionation during escape of the primordial H_2–He atmosphere. *Earth Planet. Sci. Lett.* 89, 323–334.

Sears, D. W. G., and R. T. Dodd 1988. Overview and classification of meteorites. In *Meteorites and the Early Solar System* (J. F. Kerridge and M. S. Matthews, Eds.), pp. 3–31. Univ. Arizona Press, Tucson.

Shoemaker, E. M., and R. J. Hackman 1962. Stratigraphic base for a lunar time scale. In *The Moon* (Z. Kopal and Z. K. Mikhailov, Eds.), pp. 289–300. Academic Press, London.

Tolstikhin, I. N., and B. Marty 1998. The evolution of terrestrial volatiles: A view from helium, neon, argon and nitrogen isotope modelling. *Chem. Geol.* 147, 27–52.

Vickery, A. M., and H. J. Melosh 1990. Atmospheric erosion and impactor retention in large impacts with applications to mass extinctions. In *Global Catastrophes in Earth History* (V. L. Sharpton and P. O. Ward, Eds.), pp. 289–300. Geological Society of America, Boulder, CO.

Wasson, J. T., and G. W. Wetherill 1979. Dynamical, chemical and isotopic evidence regarding the formation locations of asteroids and meteorites. In *Asteroids* (T. Gehrels, Ed.), pp. 926–974. Univ. Arizona Press, Tucson.

Zahnle, K., J. F. Kasting, and J. B. Pollack 1990. Mass fractionation of noble gases in diffusion-limited hydrodynamic hydrogen escape. *Icarus* 84, 502–527.

Zahnle, K. J., and J. C. G. Walker 1982. The evolution of solar ultraviolet luminosity. *Rev. Geophys. Space Phys.* 20, 280–292.

3 Early Earth, Geological Society Special Publications, in press

Formation and Early Evolution of the Atmosphere

Marty, B., and Dauphas, N.,.

Early Earth, Geological Society Special Publications, in press

Formation and early evolution of the atmosphere

Bernard Marty[1,2] & Nicolas Dauphas[1]

[1] Centre de Recherches Pétrographiques et Géochimiques,
Rue Notre-Dame des Pauvres,
B.P. 20
54501 Vandoeuvre Lès Nancy Cedex, France
bmarty@crpg.cnrs-nancy.fr

and

[2] Ecole Nationale Supérieure de Géologie
Avenue du Doyen Roubault
54501 Vandoeuvre Lès Nancy Cedex, France

Revised version, June 2nd, 2001

Abstract

The tectonic activity of the Earth allowed exchange of volatile elements (H, C, N, rare gases) between the surface of the Earth (atmosphere, crust, sediments, oceans) and the mantle. However, some of these elements still present elemental and isotopic heterogeneities which allow to reconstruct the volatile composition of the terrestrial mantle. The protosolar nebula supplied a significant fraction of helium and neon, which were presumably trapped during the major phase of the Earth's accretion and were possibly hosted by accreting dust and/or small porous planetesimals. Surprisingly, volatile elements are in chondritic proportion despite their drastic (10^{-3}) depletion in the mantle relative to chondrites, in a way that recalls the case of highly siderophile elements. From stable isotope systematics, we find that the contribution of comets to the volatile inventory of the Earth was very limited. The integrated flux of chondritic-like material necessary to provide water, carbon and nitrogen is consistent with that required for the formation of the Lunar craters as well as that necessary to account for the inventory of siderophile elements in the mantle. A consequence of this scenario is that the Earth's surface was oxidised very early. Alternatively, volatile and siderophile elements of the mantle could be the remnant of small patches of chondritic material that did not equilibrate with the core nor drastically degas.

1- Introduction

The development of life required adequate environmental conditions at the Earth's surface during the Hadean. Investigating these conditions and by consequence the origin and early evolution of the atmosphere is necessary to understand which chemical path and metabolism had been favoured during this period. Due to Earth's tectonics, the geological record during the Hadean has been completely erased, and most of our knowledge on atmospheric evolution is indirect. Volatile elements present in the present-day atmosphere have elemental and isotopic compositions (those of live and extinct radioactivity products) which bear information on the timing of atmospheric evolution. The mantle contains volatile elements which were trapped during Earth's accretion and which might have been preserved since then. However, this reservoir exchanged volatile elements with the atmosphere through volcanism and subduction (Figure 1) and only few elements still keep a record of the volatile component trapped in accreting silicates. Independently, the analysis of extraterrestrial bodies and of solar wind allows to infer the composition of potential contributors and to compare it with compositions observed in terrestrial reservoirs. One of the problems of this comparative approach is that the knowledge of these precursors is still limited. For example, the composition of comets is mainly known through remote sensing and in few instances through direct measurements (and possibly through the analysis of interplanetary dust particles -IDPs- but the origin of these objects remains to be established firmly). Other extremely important sources of information are the compositions of planetary atmospheres. The composition of the Jovian, Martian, and Venusian atmospheres have been already measured and there is no doubt that missions planned for the next two decades will allow significant advances in this field. In this contribution we focus on the case of the Earth and its early environment.

The terrestrial atmosphere cannot derive directly from the protosolar nebula (hereafter labelled PSN) : (i) the abundance of atmospheric rare gases (normalised to a non-volatile element like Si) is 6 to 10 orders of magnitude lower than Solar (Brown, 1952), and (ii) the isotopic compositions of rare gases (e.g., Ozima and Podosek, 1983) and nitrogen (Hashizume et al. 2000) are drastically different from those of solar gases. The depletion of rare gases in the Earth resulted in high parent/daugther ratios (where the parent element is a non-volatile element and the daughter is a rare gas isotope), allowing to use natural radioactivity products to quantify the evolution of the terrestrial atmosphere. The first significant observation in the field was done by Von Weisacker who proposed in 1931 the decay of ^{40}K ($T_{1/2}$ = 1.25 Ga) to ^{40}Ar to explain the relatively high content of

argon in the atmosphere (0.934 %) compared to other rare gases (e.g., 0.0016 % Ne). Since the major reservoir of terrestrial potassium is the silicate Earth (mantle + crust), this observation implies transfer of radiogenic ^{40}Ar from the K-bearing silicates to the atmosphere through time by magmatism and metamorphism. Rubey (1951) showed that the alteration of rocks at the Earth's surface could not account for the budget of atmospheric gases and, noting that the composition of volatiles present at the Earth's surface (atmosphere + sediments + oceans) resembled to that of volcanic gases, proposed that the atmosphere was formed by volcanic degassing. This view is fully consistent with the potassium-argon budget of the Earth : approximately half of radiogenic argon produced by the decay of ^{40}K is now in the atmosphere. The timing of this transfer was investigated when the analysis of oceanic basalts, presumably derived from the convective mantle, showed that the radioactive/primordial, $^{40}Ar/^{36}Ar$ ratio of the mantle was much higher than that of the atmosphere. In order to get such high isotopic ratio in the mantle relative to that of the atmosphere, it is necessary to transfer primordial ^{36}Ar from the mantle to the atmosphere "before" significant radiogenic in-growth of ^{40}Ar in the mantle from the decay of ^{40}K. Models quantifying this observation led to the concept of "catastrophic" degassing early in the Earth's history, a major event that was thought to have occurred in the Hadean and which might have been linked with the formation of the core (Alexander and Schwartzman, 1976; Allègre et al., 1983; Ozima, 1975; Ozima and Podosek, 1983; Sarda et al., 1985).

Another major advance in the field was the discovery of ^{129}Xe excess (relative to Xe isotopic composition of the atmosphere) in few CO_2-rich natural gases (Phinney et al., 1978; Zartman et al., 1961) and in mantle-derived, mid-ocean ridge basalts (MORB) (Marty, 1989; Staudacher and Allègre, 1982; Staudacher et al., 1989). ^{129}Xe is the radioactive daugther of ^{129}I ($T_{1/2}$ = 17 Ma), a now extinct radioactive isotope that was synthesised before formation of the solar system. Assuming that the atmosphere was derived from the mantle, $^{129}Xe/^{130}Xe$ ratios (where ^{130}Xe is a non-radiogenic Xe isotope used as a reference) higher in the mantle than in the atmosphere implied that the catastrophic degassing of the Earth occurred before ^{129}I of the mantle was completely decayed, that is, within few half lives of ^{129}I. The study of xenon isotopes ("terrestrial xenology") allowed to compute model ages of the atmosphere within the range 0.1-0.2 Ga after the start of condensation in the solar system (Allègre et al., 1987; Pepin, 1991; Staudacher and Allègre, 1982; Tolstikhin and Marty, 1998). It is important to note that the concept of rapid atmospheric formation is still valid even though the starting assumptions have proven to fail to reproduce all rare gas observations.

The first problem with the concept of catastrophic degassing as a source of atmospheric gases came from other radioactive decays having produced Xe isotopes. $^{131-136}Xe$ are produced by two radioactivities, the spontaneous fission of still alive ^{238}U ($T_{1/2}$ = 4.46 Ga), and that of ^{244}Pu ($T_{1/2}$ = 82 Ma). These two decays produce Xe isotopes in proportions that are quite close but precise analysis of Xe isotopes of natural gases and of MORB has allowed to compute the fraction of fissiogenic Xe in the mantle produced by Plutonium-244 (Kunz et al., 1998; Ozima et al., 1985) and therefore the $^{129}Xe^*/^{136}Xe^*_{Pu}$ ratio (where star means radiogenic/fissiogenic, ^{136}Xe is taken as an example among the $^{131-136}Xe$ isotopes) resulting from the decays of ^{129}I and ^{244}Pu in the mantle (Marty, 1989). The atmosphere contains also Xe isotopes produced by extinct radioactivities and the $^{129}Xe^*/^{136}Xe^*_{Pu}$ ratio of the atmospheric source could also be computed (Igarashi, 1986; Pepin and Phinney, 1979). It turned out that there was more plutonium-derived Xe relative to iodine-derived Xe in the atmosphere than in the mantle (Marty, 1989; Ozima et al., 1985). Degassing of the atmosphere after formation of the mantle would have predicted the opposite situation since the half life of ^{244}Pu is longer than that of ^{129}I. This comparison was at odds with the classical view of simple derivation of atmospheric gases from the mantle reservoir early in the Earth's history : for a common I-Pu geochemical source, the atmosphere as a geochemical reservoir would have been formed before the mantle which is logically absurd. A way to turn the problem is to consider that the hypothesis of a common I-Pu geochemical source is not adequate and that two different geochemical sources contributed xenon in the mantle and in the atmosphere, respectively (Marty, 1989). It implied either (i) heterogeneous accretion of bodies with contrasted compositions having different I/Pu ratios (Marty, 1989) and/or (ii) active exchange between atmosphere and mantle while atmospheric xenon was fractionated during escape to space (Pepin, 1991; Tolstikhin and Marty, 1998). It must be noted however that the identification of xenon components in the Earth-atmosphere is not yet definitive since the isotopic composition of primitive Xe that was presumably trapped during Earth's formation has not been measured directly in extraterrestrial samples but has been inferred from a statistical treatment of meteoritic data (Igarashi, 1986; Pepin and Phinney, 1979), making the terrestrial budget of $^{129}Xe^*$ and $^{136}Xe^*_{Pu}$ model-dependent. Moreover, the non-radiogenic isotopic composition of xenon in the mantle, necessary to compute these two values, is not precisely known, although CO_2-well gas studies suggest that there exists a non-atmospheric Xe component in the Earth (Caffee et al. 1999).

The aim of this contribution is to identify the volatile (H, C, N, rare gases) components present at the Earth's surface and in its interior. Then we use such compositions to infer the potential contributing sources and processes having settled the surface and the mantle inventory of volatile elements.

2- Reservoirs and potential contributors

Identification of volatile components in the Earth-Atmosphere

Due to plate tectonics, plume activity and volcanism, volatile elements are continuously exchanged between the surface and the mantle. The efficiency of these homogenising processes is illustrated in Figure 1, which compares the "mean degassing duration" (MDD) of the atmosphere for several volatile elements with the efficiency of recycling at arcs. The former is defined as the surface inventory (the total amount of a given volatile element, whatever its chemical state, in the crust, the sediments, the oceans and the atmosphere) divided by its degassing rate from the mantle, thought to occur mainly at mid-ocean ridges (degassing at plumes is minor compared to ridges, see for example, Marty and Tolstikhin, 1998). MDD lower than the age of the Earth would imply fast recycling whereas MDD greater than the age of the Earth suggest either decreasing degassing rate with time, the occurrence of a volatile component at the Earth's surface not derived from the mantle, or both. The y-axis of Figure 1 is the ratio F_{ARC}/F_{SUB} between the volatile flux through arc volcanism and the amount of volatiles carried by plates towards subduction zones (F_{ARC}/F_{SUB} values close to 1 imply no recycling). The correlation between F_{ARC}/F_{SUB} and MDD strongly suggest a recycling and mantle-atmosphere exchange efficiency decreasing from sulfur (MDD ~ 200 Ma), carbon (MDD ~ 4 Ga), H_2O, N and finally rare gases. The isotopic compositions of these volatiles between the mantle and the surface follow nicely this logic as both S and C isotopic ratios are similar in the mantle and in the surface inventory, whereas both water (δD ~ -80 ‰ relative to ocean water in the upper mantle), nitrogen ($\delta^{15}N$ ~ - 4 ‰ in the upper mantle relative to atmospheric N , e.g., Marty and Humbert, 1997) and neon ($\delta^{22}Ne \leq$ -200 ‰ relative to atmospheric N, e.g., Sarda et al., 1988) present isotopic heterogeneities that probably represent different volatile sources that were not fully homogenised. Hence it is possible to distinguish partly a mantle reservoir from the "atmosphere" (surface inventory) one and to explore the origins of both.

The potential components which might have delivered volatile elements to the Earth are the PSN (the major reservoir in the solar system) and solid matter bodies like

meteorites and comets. The composition of meteoritic volatiles is thought to have been derived from the PSN through elemental and isotopic fractionation. Contributions from sources outside the solar system like pre-solar grains or species affected by interstellar chemistry is attested by the discovery of pre-solar grains in primitive meteorites on one hand, and by the large variation of the D/H ratio in the solar system on another hand, but the extent of them is a matter of debate. A comparison of the abundances of He , Ne, Ar, C and N between cosmochemical potential precursors (PSN and chondrites) and terrestrial reservoirs (the atmosphere and the mantle source of MORB) is given in Figure 2. Volatile abundances are normalised to ^{20}Ne and the Sun, which, in this Figure, results in a flat pattern for the solar abundance. The reason to use neon for normalisation is its isotopic (non radiogenic) composition in the mantle which is clearly different from that of the atmosphere (see below).

Meteorites

Figure 2 illustrates the large difference in abundance pattern between primitive meteorites and the PSN which presumably reflects different trapping efficiency during condensation of the solar system material and further exchange between gas and solid in the forming solar system. The chondritic excesses of C and N relative to solar may have resulted from preferential trapping of C and N compounds which were stable in the reducing conditions of the hydrogen-rich PSN. The origin of these compounds is unclear : the large heterogeneity of the nitrogen isotopic composition among solar system objects (Kerridge and Swindle, 1988) is not compatible with a single homogeneous source like a well-mixed solar nebula, but rather suggests mixing between different components (Hashizume et al., 2000). It is likely that a major fraction of H, N (and C by analogy, although in this case the isotope argument is less straightforward) were incorporated as compounds and that the ultimate origin of these elements could be partly interstellar. Notably, rare gases are also fractionated in meteorites and the origin of such fractionation is a matter of debate (Ozima et al., 1998; Pepin, 1991).

Terrestrial mantle

The analysis of rare gases together with C and N of mantle-derived samples allows to investigate the volatile composition of the mantle. However, data need to be corrected for surficial processes such as partial melting, fractional crystallisation, degassing and atmospheric contamination, and we have developed in the past few years analytical and correction techniques which allow to reconstruct the elemental and isotopic composition of the mantle for He, C, N and Ar (Marty, 1995; Marty and Humbert, 1997; Marty and

Jambon, 1987; Marty and Zimmermann, 1999). The data used to build Figure 1 are summarised in Marty and Zimmermann (1999) and, for heavy rare gases, we have also used the best available estimates of the upper mantle composition (Moreira et al., 1998).

The mantle displays a chondritic pattern, and this similarity bears important information on the process of delivery as it suggests that the bulk fraction of these volatiles was delivered with minimal fractionation to the Earth by chondritic-like material. In fact it is very surprising that such chondritic pattern could have been preserved despite severe fractionating processes which are likely to have occurred during formation of the Earth, like impact degassing, core formation, or atmospheric escape. Indeed the Earth's mantle is extremely depleted in volatile elements, by a factor of 10^{-3} relative to carbonaceous chondrites in the case of nitrogen (1± 0.4 ppm N for the mantle, based on K-Ar-N systematics; (Dauphas and Marty, 1999; Marty, 1995), compared to about 1-3 x 10^3 ppm for carbonaceous chondrites). The situation resembles in fact to that of highly siderophile elements for which a chondritic pattern is found in the mantle despite drastic depletion (e.g., Righter and Drake, 1997). These elements should have been largely partitioned into the core, leaving the mantle much more depleted then presently observed, and largely fractionated relative to chondritic. The late addition of a chondritic veener (after core formation) is frequently advocated for siderophile elements (see Section 5). Could it be also the case for volatile elements ? We discuss this possibility later in this contribution for H and possibly C and N, but it seems doubtful that rare gases could have been preserved in silicates during late impact shocks. The observation that volatile element seem to be in chondritic proportion (and isotopic ratios for at least H, N and Ar) despite their drastic depletion is enigmatic at present and will certainly put strong constraints in future models of volatile geochemistry.

There are two notable exceptions to the chondrite analogy. First, carbon is enriched in the mantle relative to other cosmochemical reservoirs, and this difference is likely to reflect preferential recycling of carbon from the surface since carbon at the Earth's surface is manly present in sediments as carbonates and organic matter (Javoy et al., 1986). This view is consistent with the first-order homogeneity of C isotopes in the mantle and at the Earth's surface, as mentioned above (part of surface nitrogen has been probably recycled also and its fate will be discussed later). Second, the He/Ne ratio of the mantle is similar to the solar ratio within a factor of two (Honda and McDougall, 1997; Marty et al., 1998; Moreira et al., 1998), strongly suggesting that a major fraction of light rare gases in the mantle are derived from the PSN with limited fractionation.

The possibility that light rare gases originated partly from the PSN is confirmed by Ne isotopic ratios in mantle-derived rocks (Figure 3). In the now classical three-isotope diagram for neon ($^{20}Ne/^{22}Ne$ vs. $^{21}Ne/^{22}Ne$) the mantle differs from atmospheric neon by excesses of ^{20}Ne and ^{21}Ne relative to ^{22}Ne (Hiyagon et al., 1992; Honda et al., 1991; Honda et al., 1993a; Honda et al., 1993b; Marty, 1989; Marty et al., 1998; Moreira et al., 1998; Sarda et al., 1988; Staudacher et al., 1989). In this diagram format, mixing between two Ne components translates into a straight line joining dots representing these components. Excesses of ^{21}Ne result from nuclear reactions such as neutron activation of oxygen in the mantle or spallation reactions by cosmic rays and is not a primordial character. In contrast high $^{20}Ne/^{22}Ne$ ratios in the mantle relative to the air composition require the presence of a primordial Ne component different from that present in the atmosphere since no known nuclear process can produce the observed excesses of ^{20}Ne. $^{20}Ne/^{22}Ne$ ratios observed for some of the mantle-derived rocks analysed so far are higher than those of neon-Q ($^{20}Ne/^{22}Ne = 10.7$), a meteoritic component thought to characterise best rare gases trapped in chondrites (Wieler et al., 1992), or SEP neon ($^{20}Ne/^{22}Ne = 11.2$) (e.g., Ozima et al., 1998), a high energy component of the solar corpuscular emission. Therefore, mantle samples display Ne isotope variations which are best explained by mixing between atmospheric neon ($^{20}Ne/^{22}Ne = 9.80$) and a ^{20}Ne-rich component such as neon ($^{20}Ne/^{22}Ne = 13.8$ as measured in solar-wind irradiated lunar soils, (e.g., Ozima et al., 1998). The observation that the abundance pattern of volatiles normalised to ^{20}Ne reproduces a chondritic pattern despite a presumably solar origin for Ne is not problematic. Indeed, neon in the mantle seems to include also a meteoritic-like component (Trieloff et al., 2000). These authors remarked that very few, if any, Ne isotope data with good accuracy have $^{20}Ne/^{22}Ne$ higher than 12.5 and proposed that neon in the mantle was not exactly solar but included a component of the type found in some gas-rich chondrites. In addition, since the solar pattern of rare gases is highly enriched in He and Ne relative to chondritic, mixing of the two results in He/Ne ratio close to Solar together with a near chondritic-like Ar/N ratio. The fact that the N/Ne ratio is also chondritic is the result of the extreme relative depletion of nitrogen in the solar composition (N/Ne = 0.8) relative to chondritic ($N/Ne \sim 10^7$)

The case of trapping light rare gases in the terrestrial mantle from the PSN with little fractionation requires the presence of the PSN and gas-dust exchange during the early stage of accretion of terrestrial planets. The process of trapping is unclear and could be adsorption on accreting dust. However, such process would probably result in elemental

He-Ne fractionation (although the lack of adsorption data for light rare gases prevents quantitative evaluation of this possibility). PSN gases could also have been occluded in pores of accreting material, a process which would have been able to prevent elemental fractionation. Further compaction would have then resulted in occlusion of pores and subsequent trapping into mantle-forming silicates. Another possibility is gas exchange between the PSN and the Earth in a molten stage, for example, during episodes of magma ocean in presence of a thick proto-atmosphere derived from the PSN (Abe and Matsui, 1986). Equilibrium dissolution of rare gases into silicate melts would have resulted in He-Ne fractionation by a factor of ~2 (e.g., Jambon et al., 1986), which is within the uncertainty of the mantle He/Ne ratio.

Atmosphere and volatile recycling

The atmosphere presents a fractionated rare gas pattern somewhat similar to that of chondrites, but there are also wo major differences. First, C and N are under-abundant relative to chondritic (Figure 2). We have advocated recycling through time for carbon and possibly for nitrogen as a net sink for surface C and N. For carbon, this would make the mantle and "atmosphere" patterns converge towards the shaded zone representing the field of chondrites. A similar effect is also expected for nitrogen. The "atmosphere" reservoir and the mantle reservoir contain approximately the same amount of nitrogen (Marty, 1995), equivalent to 1 ppm when normalised to the mass of the mantle. Contrary to the case of carbon, the two reservoirs differ isotopically by approximately 5 ‰, which is significant for the Earth, but not for extraterrestrial reservoirs. Therefore, we postulate that nitrogen was exchanged actively between the surface and the mantle, but not to a point erasing isotopic differences (the isotopic difference may alternatively result from isotopic fractionation, a possibility that will be discussed in another paper). It must be emphasised that most of nitrogen recycling must have taken place before ~ 3 Ga ago, since both mid-ocean-ridge basalts, sampling the present-day upper mantle, and diamonds (Cartigny et al., 1997), having sampled the ancient (for some of them Archean) sub-continental lithospheric mantle present a similar distribution of $\delta^{15}N$ values centred around - 4 ‰. A further argument for nitrogen recycling is based on the N_2/Ar ratio of the upper mantle (Marty, 1995). The $N_2/^{40}Ar$ ratio of this reservoir is comparable to that of the atmosphere and, since ^{40}Ar is produced by ^{40}K, this similarity suggests a similar behaviour of N and K. Nitrogen can substitutes to K^+ under the form of NH_4^+, which make these two elements potentially recyclable at similar rates. In contrast, the $N_2/^{36}Ar$ ratio of the mantle is two orders of magnitude higher than that of the atmosphere, exactly what is expected if nitrogen is recycled and ^{36}Ar is not.

Apart from the case of recycling as a source of atmosphere alteration, the isotopic compositions of atmospheric neon (and xenon, see introduction) do not support a mantle origin. An important feature of the atmosphere is its $^{20}Ne/^{22}Ne$ ratio of 9.8 much lower than that of the mantle. Assuming that atmospheric Ne was also solar-like initially, its present-day value requires extensive isotopic fractionation, which might have taken place either in precursors, or in the atmosphere itself during early evolution (Zanhle et al., 1988). In the first possibility, late accreting material would have released a low $^{20}Ne/^{22}Ne$ component (Marty, 1989). Indeed $^{20}Ne/^{22}Ne$ ratios as low as 8 are observed in bulk chondrites (Mazor et al., 1970) and are thought to result from mixing between a nucleosynthetic ^{22}Ne-rich end-member and the well characterised trapped Ne-Q component (Wieler et al., 1992) and/or solar Ne. Alternatively, atmospheric neon could have been isotopically fractionated by hydrodynamic escape of a thick proto-atmosphere (Zanhle et al., 1988). Early models required an extremely thick hydrogen-rich atmosphere to start with (Hunten et al., 1987; Sasaki and Nakasawa, 1988), which faced a serious problem with conventional models of planetary formation in the terrestrial feeding zone. In this type of scenario, an hydrogen-rich atmosphere, either a remnant of the PSN, or the result of strong reduction of water by molten iron, possibly ionised by an enhanced solar UV flux, is escaping from the terrestrial gravitational field and is entraining other volatile species following a distillation process which greatly fractionates isotopes according to their mass difference. Subsequent works showed the role of other atmospheric constituents such as CO, CO_2 and H_2O to increase significantly the efficiency of isotopic fractionation during escape (Ozima and Zahnle, 1993), which lifted the need of a very thick proto-atmosphere. Model calculations show that, depending on the atmospheric composition, Ne can be fractionated from the solar composition to the atmospheric composition with limited Ne loss (Ozima and Zahnle, 1993). Further models advocated giant impacts to blow off partially the early atmosphere of the Earth (Pepin, 1997), but it is not yet clear if such events would have resulted in extensive isotopic fractionation (Melosh and Vickery, 1989). Atmospheric escape could also account for the underabundance of C and N in the atmosphere relative to Ne (Figure 2), provided that these elements were in the forms of species lighter than ^{20}Ne in order to be lost more efficiently than neon. The best candidates for these are methane (m =16) and ammonia (m = 17), implying escape when the atmosphere was strongly reducing (a detailed scenario for isotope fractional loss of nitrogen is developed by Tolstikhin and Marty (1998).

Atmospheric xenon is also isotopically unique among Xe components in the solar system (with the possible exception of Martian atmospheric Xe, e.g., Swindle, 1995) as it is fractionated by 3 % per amu. In addition, atmospheric xenon is depleted relative to the chondritic or solar patterns : the Kr/Xe ratio of air is 25 times the mean ratio of chondrites (Figure 2). The depletion of xenon is not consistent with its isotopic fractionation since, in the first case the heavy element (Xe) is depleted relative to the lighest one (Kr) and, in the second case, the light isotopes (e.g., ^{124}Xe) are depleted relative to the heavy ones (e.g., ^{136}Xe). The elemental depletion of Xe could be due to xenon trapping in a terrestrial reservoir, but possibilities exclude ice or sediments which cannot explain the 25 fold depletion (Bernatowicz et al., 1985; Podosek et al., 1981). Preferential subduction of Xe trapped in sediments could account qualitatively for it, but is not yet documented.

3-Timing

In this section we review briefly chronological constraints relevant to atmospheric evolution. The onset of condensation and accretion of the solar system is well dated at 4.556 Ga from the analysis of primitive meteorites (Allègre et al., 1995). Recent accretion models propose that the duration to get Mars-sized planets would have been quite short, less than 10 Ma (see for example, (Chambers and Wetherhill, 1998)) . The typical time interval indicated by extinct radioactivities to differentiate primitive meteorite parent bodies into metal and silicates is also short, of the order of few Ma (e.g., (Lee and Halliday, 1995; Wetherill, 1975). The formation of the giant planets would have also been a relatively (< 10 Ma) short process, but the process of accretion of terrestrial planets would have slowed down given the decreasing availability of bodies in the inner solar system. Recent models postulate a time duration of 50-80 Ma to get a terrestrial planet of the size of the Earth (Vityazev et al., 1990; Weidenschilling et al., 1997). Some models postulate that, due to the presence of giant planets, gravitational forces would have deflected bodies formed in colder regions of the solar system and therefore richer in volatiles to the inner solar system (e.g., (Chambers and Wetherhill, 1998; Petit et al., 1999). Periodic gravitational forces produced by Jupiter and Saturn could move bodies from the asteroidal belt located in specific narrow zones known as orbital resonances into elongated orbits crossing the terrestrial region. The efficiency of such process is so high that such zones would have become quickly exhausted and, recently, (Vokrouhlicky and Farinella, 2000) have proposed that such zones could be continuously refuelled in meteoritic fragments due to the drag exerted by emission of thermal radiation from objects assymetrically exposed to the Sun. Linking the efficiency of terrestrial bombardment with

the solar radiation presents the exciting possibility to modulate the bombardment of the Earth with Solar activity.

The life duration of the PSN, which presence is required to feed solar-type Ne in the terrestrial matter forming the mantle, is thought to have not exceeded 10-20 Ma (Montmerle, 1999). Hence it is conceivable that, if solar-like light rare gases now seen in the mantle were trapped directly from the PSN during accretion or during exchanges between the proto-mantle and a PSN-rich atmosphere, these processes could not have lasted more than a few tensof Ma and that both waning of the PSN and increasing rate of degassing of bodies impacting on the growing Earth would have prevented further delivery of rare gases to the interior of the Earth. The Hf-W chronometer allows to propose a time interval of 10-60 Ma to form the core (Lee and Halliday, 1995), depending on which type of model (e.g., continuous accretion and differentiation vs. single stage differentiation) is adopted. As stated above, the duration to grow the Earth to its present-day mass is ≤ 100 Ma, and such duration is in agreement with the lead isotope record of the mantle (Allègre et al., 1995). Notably, the age of the Moon-forming event is on the order of 4.46 Ga (e.g., (Heiken et al., 1991), and the use of coupled ^{146}Sm-^{147}Sm system allows to constrain the initial mantle differentiation yielding the first crustal reservoir to 4.47 Ga (Jacobsen and Harper, 1996). Finally, evidence has been reported from zircon analysis that a continental crust existed 4.4 Gyr ago (Wilde et al., 2001), and that liquid water was present 4.3 Gyr ago (Mojzsis et al., 2001).

We postulate in the view of these constraints that rare gases were delivered to the Earth and fractionated in the atmosphere mainly within the first 100 Ma possibly within 50 Ma when most of terrestrial accretion took place. During this period, atmosphere and proto-mantle rare gases were actively exchanged and rare gas fractionation took place following a combination of impact degassing, atmospheric escape and mantle-atmosphere exchange during magma ocean stages (Pepin, 1997; Sasaki and Nakasawa, 1988; Tolstikhin and Marty, 1998). Rare gas modelling of mantle-atmosphere differentiation suggests that these reservoirs might have remained "open", that is, might have continued to exchange their volatiles between them or with the outer space during a longer period reaching 100 Ma, but they also predict that the corresponding fluxes would have decreased dramatically with time (Pepin, 1991; Tolstikhin and Marty, 1998).

4- Rare gas models

The fractionation of rare gases in the atmosphere cannot be explained in a straightforward manner and calls for selective fractionation processes. Several sophisticated models have been developed in which each rare gas is affected selectively by a combination of mixing and isotope fractionation during atmospheric escape events. Pepin (Pepin, 1991; Pepin, 1997) assumed a two-stage hydrodynamic atmospheric escape. In the first one, a H_2-rich proto-atmosphere containing CO, N_2 and the noble gases in proportions found in primitive chondrites was driven by intense extreme-ultraviolet (EUV) radiation from the young evolving Sun starting at a solar age of ~50 Ma. This episode was followed by a long (~80 Ma) period of quiescence, followed by abrupt degassing of remnant H_2, CO_2 and N_2 from the mantle and of light rare gases trapped deep in the Earth having a solar composition. Hydrodynamic escape resumed with the available H_2 in a waning but still potent EUV flux. Atmospheric volatiles remaining at the end of this second stage, 4.2 Ga ago, formed the bulk of the present-day atmosphere. The role of atmospheric erosion by giant impacts was further considered but did not change the essence of this two-stage scenario (Pepin, 1997). Tolstikhin and Marty (Tolstikhin and Marty, 1998) attempted to integrate in a global model the formation of the Earth, the differentiation of the mantle, and the formation of the atmosphere. They proposed a combination of isotopic fractionation during hydrodynamic atmospheric escape and mantle-atmosphere exchange, with significant differences from Pepin's models. A gradual, single-stage process in which solar-like rare gases and chondritic N were contributed by impacts in the presence of the PSN was postulated. The selective fractionation of each rare gas took place during ocean magma episodes when rare gases were sorted according to their respective solubilities in basaltic melt during vigorous magma convection. The timing of these processes was derived from the I-Pu-Xe systematics and the model predicted that the atmosphere was settled for its rare gases and nitrogen > 4.3 Ga ago. Pepin (1991)'s and Tolstikhin and Marty (1998)' models agree on several important predictions : (i) both the PSN and chondritic-type material contributed terrestrial volatiles, (ii) during the first tensof Ma the forming mantle and atmosphere exchanged volatiles, (iii) the atmosphere (and the mantle) were closed early in the Earth's history around 4.3 ago and the atmospheric composition (but not its chemistry) experienced little change since then, and (iv) they require intense yet decreasing EUV during a long period, e.g., 100-200 Ma. It also poses the problem of penetration of the EUV radiation in an initially dense region. These models call for very specific conditions and processes which will need close examination to confirm, or refute them. It may also be possible that we still ignore the composition of the contributing sources, and with this respect comets deserve a special attention since the process of rare gas trapping at low temperature in their ice might have resulted in specific fractionation that remains to be documented. The recent discovery that comet C/1995 O1 (Hale Bopp)

contains argon in solar proportion (Stern et al., 2001) suggests however that fractionation of heavy rare gases in comets is unlikely.

5-The case of major volatiles

The case of major volatiles deserves a special attention since these elements are in fact those which shaped the early terrestrial environment necessary for the development of life. A direct derivation of major volatile elements from the PSN is not supported by abundance data and H, N isotopic ratios which rather favour a chondritic origin (Figure 2).

The D/H ratio of solar system reservoirs presents variations over a factor of 30 (Figure 4) which are thought to result from mixing of PSN-type H_2 and D-rich compounds (Geiss and Gloecker, 1998; Robert et al., 2000). The deuterium enrichment of the latter is attributed to trapping of hydrogen-bearing molecules that experienced low temperature fractionation in molecular clouds during ion-molecule exchanges. This makes the hydrogen isotopic composition a good diagnostic tracer of sources and mixings among solar system objects (Robert et al., 2000). Hydrogen in water of terrestrial oceans is enriched by a factor of 6 relative to solar (pre-deuterium burning) hydrogen (Figure 4) and cannot be derived from the PSN directly. It is possible however that hydrodynamic escape of PSN hydrogen would have favoured preferential escape of hydrogen, leaving residual hydrogen rich in deuterium. However the terrestrial D/H ratio is within the range of values found in primitive meteorites, and this similarity strongly suggests a chondritic origin for terrestrial water. It is also important to note that the terrestrial D/H ratio is clearly different from those of comets as far as the few available data are representative of these objects. Therefore hydrogen isotopic data favour a derivation of terrestrial hydrogen from chondrite-like bodies, with limited, if any, fractionation.

A similar scenario emerges from N isotope systematics. Most planetary objects display $^{15}N/^{14}N$ ratios around the terrestrial atmospheric value within 50 ‰. These objects include the Earth, Venus (Mars constitutes an exception as its atmosphere is enriched by > 600 ‰ in ^{15}N, presumably as a result of fractional loss of nitrogen, e.g., Yung and DeMore, 1999), carbonaceous chondrites, and notably enstatite chondrites which constitute a building material of reference since their oxygen isotopic composition lie on the terrestrial fractionation line (Javoy et al., 1986). Recently, (Hashizume et al., 2000) proposed that solar wind nitrogen is in ^{15}N relative to the terrestrial atmosphere ($\delta^{15}N \leq$ 240 ‰) based on ion probe analysis of lunar soil grains and (Owen et al., 2001) proposed a

solar N composition of $\delta^{15}N$ = -370±80 ‰ from Galileo data for the atmosphere of Jupiter. Thus it is conceivable that nitrogen in the solar system is the result of mixing between gaseous nitrogen of the PSN and a ^{15}N-rich component carried by solid phases and mostly present in planetary bodies. The incorporation of solar nitrogen would have resulted in ^{15}N-poor nitrogen which is not seen at the Earth's surface, but a remnant of it could be still present in the deep Earth (although the N/Ne ratio of the mantle does not support this possibility). Interestingly, mid-ocean ridge lavas are slightly depleted in ^{15}N by 5 ‰ relative to atmospheric N. There are however other possibilities such as Enstatite-type nitrogen which is depleted by 20-40 ‰ in ^{15}N relative to atmospheric N (Javoy et al., 1986).

6-The late bombardment of the Earth.

The term late generally refers to addition of material to the growing Earth once its differentiation was completed. It does not quantify any time interval but is termed late because it is thought to have occurred once the Earth had reached a "significant" size allowing differentiation and internal evolution. Hence material added after the major building period was not in chemical equilibrium with the bulk Earth. Planets formed from the accretion of planetary material and this process is still going on at present but at a much lower rate than 4.56 Ga ago. The density of lunar craters increases with the age of the exposed surface in a manner indicative of an overall decline with time of the bombardment intensity (e.g., (Chyba, 1990; Heiken et al., 1991). It is interesting to note that this idea was first stated based on the superposition principle cherished by field geologists seven years before the first lunar samples were collected and brought back to Earth (Shoemacker and Hackman, 1962). It is estimated from the lunar impact record that the mass of asteroids and comets that fell lately on our planet lies within 1×10^{21} - 7×10^{23} kg with a preferred value of 3.2×10^{21} kg as derived from fitting of the cumulative crater density versus age curve (Chyba, 1990).

Additional evidence that remnants of planetary formation impacted Earth at a much higher rate in the Hadean than at present comes from highly siderophile elements (Ru, Rh, Pd, Re, Os, Ir, Pt, and Au). When the core segregated from the mantle, highly siderophile elements should have been partitioned into the core, leaving the mantle depleted and fractionated. The concentrations of highly siderophile elements in the mantle are much higher that those predicted in the case of equilibrium partitioning between metal and silicate. In addition, the highly siderophile elements abundance pattern of the mantle is almost unfractionated relative to potential Earth forming material (e.g., (Righter and Drake,

1997)). A straightforward interpretation is that a late veneer brought highly siderophile elements into the mantle after the core formed. It has been suggested that highly siderophile elements were not in chondritic proportion in the Earth's mantle and that highly siderophile elements were carried by non-chondritic extraterrestrial material or by the entrainment of core material by plumes. (Alard et al., 2000) measured highly siderophile elements in mantle sulphides and they concluded that non-chondritic highly siderophile elements abundance patterns directly reflect processes occurring in the upper mantle and are not evidence for the addition of core material or exotic meteoritic components. The mass of extraterrestrial matter necessary to account for the budget of siderophile elements in the mantle is (1-4) x 10^{22} kg (Chyba, 1991).

Several observations suggest that our planet was impacted by volatile-rich bodies. Carbonaceous asteroids are overwhelmingly the most abundant type in the main belt. Whether pieces of C-type asteroids are present in meteorite collections is debatable but it seems that their reflectance spectra best match that of the carbonaceous chondrites, specifically of the CI-CM types (Gaffey et al., 1993). The extraterrestrial flux to Earth is dominated by carbonaceous micrometeorites (Engrand and Maurette, 1998). They lack strict equivalent among macroscopic samples but their closest analogues are CM carbonaceous chondrites (Kurat et al., 1994). Most xenoliths in meteorite regolithic breccias share affinities with carbonaceous chondrites, which implies that asteroids were embedded in a swarm of carbonaceous material (Anders, 1978). The lunar regolith is enriched in trace elements relative to indigeneous lunar rocks. The trace element pattern of this enriched compound best match that of carbonaceous chondrites, implying in turn that the lunar regolith contains 1-2 % of carbonaceous debris (Keays et al., 1970).

When an asteroid or a comet impacts the Earth, part of it and of Earth's atmosphere might be ejected back into space. Recent analytical and computational modelling of impact induced erosion led (Newman et al., 1999) to conclude that impact events would not remove significant atmospheric gases. As discussed earlier, the isotopic ratio of hydrogen supports the contribution of carbonaceous chondrites for the origin of water on Earth. Recent observations indicate that comets are enriched in deuterium relative to the oceans by a factor of two, which prevents the possibility that comets contributed a significant fraction of Earth's hydrosphere (< 10 %) unless one calls on hypothetical comets. It is noteworthy that all the three comets so far measured originate in the Oort cloud, and the scientific community is in need of the determination of the D/H ratio in Kuiper belt objects in order to ascertain the idea that comets did not significantly contributed to Earth's oceans. Delsemme (1989) calculated the composition of comets and we give an updated version of this compilation where uncertainties were propagated rigorously and the dust composition

was modified according to (Jessberger et al., 1988b). The D/H ratio of the deep mantle is much lower than that of Earth's surface (Deloule et al., 1991). An appealing possibility is that the D/H ratio of the deep mantle is a remnant of the hydrogen isotopic composition of Earth forming planetesimals which later evolved as a result of the late accretion of asteroids and comets. Thus, the mass of asteroids and comets incident on Earth since the time of its accretion required to balance the low D/H ratio of the deep mantle is estimated to be 4 x 10^{20} - 2 x 10^{22} kg (Dauphas et al., 2000). It is worthwhile to note that fractionation of D/H within the Earth might explain the isotopic heterogeneity of Earth but we wish to emphasise that the few elements for which there exists an isotopic heterogeneity are those which are not efficiently recycled, those which are prone to record the heterogeneous accretion of the Earth.

It is worthwhile to note that the estimates based on the Lunar cratering record, highly siderophile elements, and water deuterium to protium (D/H) ratios integrate the late bombardment of Earth over timescales that are not necessarily identical. In the case of the lunar cratering record, time zero corresponds to the moment when the Moon formed. In the case of highly siderophile elements, time zero corresponds to the moment when the Earth's core formed. In the case of water deuterium to protium ratios, time zero corresponds to the moment when the bulk Earth had a D/H ratio lower than that of the present deep mantle. One might see the remarkably good agreement between the various approaches as merely coincidental. Alternatively, it means that the Moon, highly siderophile elements, and water D/H ratios recorded the late heavy bombardment over the same period of time. If so, the mass of extraterrestrial matter that fell on Earth throughout its history must be the same from all point of views. The only locus where the mass of extraterrestrial matter incident on Earth is the same from all point of views is for low mass fractions of comets among impacting bodies (<1 %). This inference is highly speculative because it relies on the assumption that all three approaches integrated the late bombardment of Earth over the same period of time but if it was proven to be right, then it would have strong implications on cometary dynamics and organics delivery to Earth.

It was suggested based on water D/H ratios that the late veneer consisted predominantly of carbonaceous asteroids and that the mass of extraterrestrial bodies incident on Earth since the time of its accretion was ~ 2 x 10^{22} kg. The carbon and nitrogen concentrations of carbonaceous chondrites are 1.5 x 10^{-3} and 4.2 x 10^{-5} mol/g. If a late veneer supplied Earth with the water required to balance the low D/H of the deep mantle, then it should have contributed Earth with ~ 3 x10^{22} and 8 x 10^{20} mol of carbon and nitrogen, respectively. The Earth's surface (atmosphere+sediments+igneous crust) has 9 x 10^{21} and 3.5 x10^{20} moles of carbon and nitrogen, respectively . These estimates are in

surprisingly good agreement with the inferred contributions of late bombardment for carbon and nitrogen (3×10^{22} mol 8×10^{20} mol, respectively) if one considers that a significant fraction of carbon and possibly nitrogen has been recycled into the mantle through time. It implies that carbonaceous asteroids might have contributed a significant fraction of hydrogen, carbon, and nitrogen on Earth presumably in the form of prebiotic molecules such as amino acids and heterocycles.

6- Conclusions

The major conclusion of this work is that there exists a chondritic-like component for volatile elements in the terrestrial mantle, not only for elements presenting a chemical affinity for silicates or metal such as C and N, but also for chemically inert gases. A chondritic, rather than solar, origin for volatile elements is consistent with the stable isotope composition of H, C and N, and eliminates in the case of H a major contribution from comets. However, a major fraction of He and Ne may be derived from the protosolar nebula and this contribution can only be seen for these two elements due to their high abundance in the PSN. Despite their chondritic chracteristics, the absolute abundances of volatiles in the mantles are three orders of magnitude lower than those of chondrites, as are also strongly siderophile elements. It may well be possible that the growing Earth did not fully equilibrate with the forming proto-atmosphere and the core and preserved minor (10-3) fractions undifferentiated and later incorporated in the convection of the mantle.

Acknowledgements

This study was funded by the INSU:CNRS program "Interieur de la Terre". We thank the organisers of the Fermor meeting for the nice opportunity to present and discuss this work and numerous colleagues for fruitful discussions, among them Francis Albarède, Allessandro Morbidelli, Minoru Ozima, François Robert, Franck Selsis, Igor Tolstikhin, Kevin Zahlne. The paper benefited from constructive comments by two anonymous reviewers. CRPG contribution # 1526.

References

Abe Y. and Matsui T. (1986) Early evolution of the Earth: accretion, atmosphere formation, and thermal hystory. *J. Geophys.Res. Proc. 17-th Lunar Planet. Sci.* **91**, E291-E302.

Alard O., Griffin W. L., Lorand J. P., Jackson S. E., and O'Reilly S. Y. (2000) Non-chondritic distribution of the siderophile elements in mantle sulphides. *Nature* **407**, 891-894.

Alexander E. C. and Schwartzman D. W. (1976) Argon isotopic evolution of upper mantle. *Nature* **259**, 104-108.

Allard P. (1992) Global emmissions of helium-3 by subaerial volcanism. *geophys. Res. Lett.* **19**, 1478-1481.

Allègre C. J., Manhès G., and Göpel C. (1995) The age of the Earth. *Geochim. Cosmochim. Acta* **59**, 1445-1457.

Allègre C. J., Staudacher T., and Sarda P. (1987) Rare gas systematics : formation of the atmosphere, evolution and structure of the Earth's mantle. *Earth Planet. Sci. Lett.* **81**, 127-150.

Allègre C. J., Staudacher T., Sarda P., and Kurz M. (1983) Constraints on evolution of Earth's mantle from rare gas systematics. **303**, 762-766.

Anders E. (1978) Most stony meteorites come from the asteroid belt. In *Asteroids: An Exploration Assesment* (ed. D. M. W. C. Wells), pp. 57-75. NASA.

Anders E. and Grevesse N. (1989) Abundances of the elements : meteoritic and solar. *Geochim. Cosmochim. Acta* **53**, 197-214.

Bernatowicz T. J., Kennedy B. M., and Podosek F. A. (1985) Xe in glacial ice and the atmospheric inventory of noble gases. *Geochim. Cosmochim. Acta* **49**, 2561-2564.

Brown H. (1952) *The atmospheres of the Earth and Planets*. Univ. Chicago Press.

Caffee M. W., Hudson G. B., Velsko C., Huss G., Alexander Jr. E. C., and Chivas A. R. (1999) Primordial nobel gases from the Earth's mantle : Identification of a primitive volatile component. *Science*.

Cartigny P., Boyd S. R., Harris J. W., and Javoy M. (1997) Nitrogen isotopes in peridotitic diamonds from Fuxian, China : the mantle signature. *Terra Nova* **9**, 175-179.

Chambers J. E. and Wetherhill G. W. (1998) Making the terrestrial planets : N-body integrations of planetary embryos in three dimensions. *Icarus* **136**, 304-327.

Chyba C. (1990) Impact delivery and erosion of planetary oceans in the inner solar system. *Nature* **343**, 129-133.

Chyba C. F. (1991) Terrestrial mantle siderophiles and the Lunar impact record. *Icarus* **92**, 217-233.

Craig H., Clarke W. B., and Beg M. A. (1975) Excess 3He in deep water on the East Pacific rise. *Earth Planet. Sci. Lett.* **26**, 125-132.

Dauphas N. and Marty B. (1999) Heavy nitrogen in carbonatites of the Kola Peninsula : a possible signature of the deep mantle. *Science* **286**, 2488-2490.

Dauphas N., Robert F., and Marty B. (2000) The late asteroidal and cometary bombardment of the Earth as recorded in water deuterium to protium ratio. *Icarus* **148**, 508-512

Deloule E., Albarède F., and Sheppard S. M. F. (1991) Hydrogen isotope heterogeneities in the mantle from ion probe analysis of amphiboles from ultramafic rocks. *Earth Planet. Sci. Lett.* **105**, 543-553.

Delsemme A. H. (1988) The chemistry of comets. *Phil. Trans. R. Soc. London* **A325**, 509-523.

Engrand C. and Maurette M. (1998) Carbonaceous micrometeorites from Antartica. *Meteorit. Planet. Sci.* **33**, 565-580.

Gaffey M. J., Burbine T. H., and Binzel R. P. (1993) Asteroid spectroscopy : Prospects and perspectives. *Meteoritics* **28**, 161-187.

Geiss J. and Gloecker G. (1998) Abundances of deuterium and helium in the protosolar cloud. *Space Sci. Rev.* **84**, 239-250.

Hashizume K., Chaussidon M., Marty B., and Robert F. (2000) Solar wind record on the Moon: Deciphering presolar from planetary nitrogen. *Science* **290**, 1142-1145.

Heiken G. H., Vaniman D. T., and French B. V. (1991) *Lunar sourcebook.* Cambridge University Press.

Hiyagon H., Ozima M., Marty B., Zashu S., and Sakai H. (1992) Noble gases in submarine glasses from mid-oceanic ridge and Loihi Seamount: constraints on early history of the Earth. *Geochim. Cosmochim. Acta* **56**.

Honda M. and McDougall I. (1997) Primordial helium and neon in the Earth : A speculation on early degassing. *Seventh Annual Goldschmidt Conf.*, 98-99, LPI Contrib. n° 921, Lunar Planet. Inst. , Houston.

Honda M., McDougall I., Patterson D. B., Doulgeris A., and Clague D. A. (1991) Possible solar noble-gas component in Hawaiian basalts. *Nature* **349**, 149-151.

Honda M., McDougall I., Patterson D. B., Doulgeris A., and Clague D. A. (1993a) Noble gases in submarine pillow basalt glasses from Loihi and Kilauea, Hawaii : A solar component in the Earth. *Geochim. Cosmochim. Acta* **57**, 859-874.

Honda M., Patterson D. B., McDougall I., and Falloon T. J. (1993b) Noble gases in submarine pillow basalt glasses from the Lau Basin: detection of a solar component in back-arc basalts. *Earth Planet. Sci. Lett.* **120**, 135-148.

Hunten D. M., Pepin R. O., and Walker J. C. B. (1987) Mass fractionation in hydrodynamic escape. *Icarus* **69**, 532-549.

Igarashi G. (1986) Components of xenon in carbonaceous chondrites and fission component in the terrestrial atmosphere. *Japan U. S. Seminar on Terrestrial Noble Gases*, Abstr. 20-23.

Jacobsen S. B. and Harper C. L. J. (1996) Accretion and early differentiation history of the Earth based on extinct radionuclides. In *Earth processes : Reading the isotopic code*, Vol. Geophys. Monograph 95 (ed. S. H. A. Basu), pp. 47-74. Amer. Geophys. Union.

Jambon A., Weber H., and Braun O. (1986) Solubilities of He, Ne, Ar, Kr and Xe in a basalts melt in the range 1250-1600°C: Geochemical implications. *Geochim. Cosmochim. Acta* **50**, 401-408.

Javoy M., Pineau F., and Delorme H. (1986) Carbon and nitrogen isotopes in the mantle. *Chem. Geol.* **57**, 41-62.

Jessberger E. K., Christoforidis A., and Kissel J. (1988a) Aspects of the major element composition of Halley's dust. *Nature* **332**, 691-695.

Jessberger E. K., Cristoforidis A., and Kissel J. (1988b) Aspects of the major elemental composition of Halley's dust. *Nature* **332**, 691-695.

Keays R. R., Ganapathy R., Laul J. C., Anders E., Herzog G. F., and Jeffery P. M. (1970) Trace elements and radioactivity in Lunar rocks : Implications for meteorite infall, solar-wind flux, and formation conditions of Moon. *Science* **167**, 490-493.

Kerridge J. F. and Swindle T. D. (1988) *Meteorites and the Early Solar System.* Univ. Arizona Press.

Kunz J., Staudacher T., and Allègre C. J. (1998) Plutonium-fission xenon found in the Earth's mantle. *Science* **280**, 877-880.

Kurat G., Koeberl C., Presper T., Brandstätter F., and Maurette M. (1994) Petrology and geochemistry of Antartic micrometeorites. *Geochim. Cosmochim. Acta* **58**, 3879-3904.

Le Guern F. (1982) Les débits de CO_2 et de SO_2 volcaniques dans l'atmosphère. *Bull. Volc.* **45**, 197-202.

Lee D. C. and Halliday A. (1995) Hafnium-Tungsten chronometry and the timing of terrestrial core formation. *Nature* **378**, 771-774.

Marty B. (1989) Neon and xenon isotopes in MORB : implications for the earth-atmosphere evolution. *Earth Planet. Sci. Lett.* **94**, 45-56.

Marty B. (1992) Volcanic fluxes of volatiles. Preliminary estimates based on rare gas and major volatile calibration. *International Atomic Energy Agency.*

Marty B. (1995) Nitrogen content of the mantle inferred from N2-Ar correlation in oceanic basalts. *Nature* **377**, 326-329.

Marty B. and Humbert F. (1997) Nitrogen and argon isotopes in oceanic basalts. *Earth Planet. Sci. Lett.* **152**, 101-112.

Marty B. and Jambon A. (1987) C/^{3}He in volatile fluxes from the solid Earth : Implications for carbon geodynamics. *Earth Planet. Sci. Lett.* **83**, 16-26.

Marty B. and Tolstikhin I. N. (1998) CO2 fluxes from Mid-Ocean Ridges, Arcs and Plumes. *Chem. Geol.* **145**, 233-248.

Marty B., Tolstikhin I. N., Kamensky I. L., Nivin V., Balaganskaya E., and Zimmermann J. L. (1998) Plume-derived rare gases in 380 Ma carbonatites from the Kola region (Russia) and the argon isotopic composition in the deep mantle. *Earth Planet. Sci. Lett. 164, 179-192.*

Marty B. and Zimmermann J. L. (1999) Volatiles (He, C, N, Ar) in mid-ocean ridge basalts: Assesment of shallow-level fractionation and characterization of source composition. *Geochim. Cosmochim. Acta* **63**, 3619-3633.

Matsuo S., Suzuki M., and Mizutani Y. (1978) Nitrogen to argon ratio in volcanic gases. In *Terrestrial rare gases* (ed. E. C. J. Alexander and M. Ozima), pp. 17-25. Japan Sci. Soc. Press.

Mazor E., Heymann D., and Anders E. (1970) Noble gases in carbonaceous chondrites. *Geochim. Cosmochim. Acta* **34**, 781-824.

Melosh H. J. and Vickery A. M. (1989) Impact erosion of the primordial atmosphere of Mars. *Nature* **338**, 487-489.

Mojzsis S. J., Harrisson T. M., and Pidgeon R. T. (2001) Oxygen-isotope evidence from ancient zircons for liquid water at the Erth's surface 4,300 Myr ago. *Nature* **409**, 178-181.

Montmerle T. (1999) La formation des étoiles de type solaire; des conditions aux limites pour l'origine de la vie ? *L'Environnement de la Terre Primitive et l'Origine de la Vie*, CI-1.

Moreira M., Kunz J., and Allègre C. J. (1998) Rare gas systematics in Popping Rock : Isotopic and elemental compositions in the upper mantle. *Science* **279**, 1178-1181.

Newman W. I., Symbalisty E. M. D., Ahrens, T.J., and Jones E. M. (1999) Impact erosion of planetary atmospheres: Some surprising results. *Icarus* **138**, 224-240.

Owen T., Mahaffy P. R., Niemann H. B., Atreya S., and Wong M. (2001) Protosolar nitrogen. *Astrophys. J.* **553**, L77-L79.

Ozima M. (1975) Ar isotopes and Earth-atmosphere evolution models. *Geochim. Cosmochim. Acta* **39**, 1127-1140.

Ozima M. and Podosek F. A. (1983) *Noble gas geochemistry*. Cambridge University Press.

Ozima M., Podosek F. A., and Igarashi G. (1985) Terrestrial xenon isotope constraints on the early history of the Earth. *Nature* **315**, 471-474.

Ozima M., Wieler R., Marty B., and Podosek F. A. (1998) Comparative studies of solar, Q-gases and terrestrial noble gases, and implications on the evolution of the solar nebula. *Geochim. Cosmochim. Acta* **62**, 301-314.

Ozima M. and Zahnle K. (1993) Mantle degassing and atmospheric evolution: Noble gas view. *Geochem. J.*, 185-200.

Pepin R. O. (1991) On the origin and early evolution of terrestrial planetary atmospheres and meteoritic volatiles. *Icarus* **92**, 1-79.

Pepin R. O. (1997) Evolution of Earth's noble gases: Consequences of assuming hydrodynamic loss driven by giant impact. *Icarus* **126**, 148-156.

Pepin R. O. and Phinney D. (1979) Components of xenon in the solar system, mytical unpublished ms. .

Petit J. M., Morbidelli A., and Valsecchi G. B. (1999) Large scattered planetesimals and the excitation of the small body belts. *Icarus* **141**, 367-387.

Phinney D., Tennyson J., and Frick U. (1978) Xenon in the CO_2-well gas revisited. *J. Geophys. Res.* **83**, 2313-2319.

Podosek F. A., Bernatowicz T. J., and Kramer F. E. (1981) Adsorption of xenon and krypton on shales. *Geochim. Cosmochim. Acta* **45**, 2401-2415.

Rea D. K. and Ruff L. J. (1996) Composition and mass flux of sediments entering the world's subduction zones: Implications for global sediment budgets, great earthquakes and volcanism. *Earth Planet. Sci. Lett.* **140**, 1-12.

Righter K. and Drake M. J. (1997) Metal/silicate equilibrium in an homogeneous accreting Earth: New results for Re. *Earth Planet. Sci. Lett.* **146**, 541-553.

Robert F., Gautier D., and Dubrulle B. (2000) The solar system D/H ratio: Observations and theories. *Space Sci. Rev.* **92**, 201-224.

Rubey W. W. (1951) Geologic history of sea water. *Geol. Soc. Amer. Bull.* **62**, 1111-1148.

Sano Y. and Williams S. N. (1996) Fluxes of mantle and subducted carbon along convergent plate boundaries. *Geophys. Res. Lett.* **23**, 2749-2752.

Sarda P., Staudacher T., and Allègre C. J. (1985) 40Ar/36Ar in MORB glases : Constraints on atmosphere and mantle evolution. *Earth Planet. Sci. Lett.* **72**, 357-375.

Sarda P., Staudacher T., and Allègre C. J. (1988) Neon isotopes in submarine basalts. *Earth Planet. Sci. Lett.* **91**, 73-88.

Sasaki S. and Nakasawa K. (1988) Origin of isotopic fractionation of terrestrial Xe, hydrodynamic fractionation during escape of the primordial H_2-He atmosphere. *Earth Planet. Sci. Lett.* **89**, 323-334.

Shoemacker E. M. and Hackman R. J. (1962) Stratigraphic base for a lunar time scale. In *The Moon* (ed. Z. K. Z. K. Mikhailov), pp. 289-300. Academic Press.

Staudacher T. and Allègre C. J. (1982) Terrestrial xenololy. *Earth Planet. Sci. Lett.* **60**, 389-405.

Staudacher T. and Allègre C. J. (1988) Recycling of oceanic crust and sediments : the noble gas subduction barrier. *Earth Planet. Sci. Lett.* **89**, 173-183.

Staudacher T., Sarda P., Richardson S. H., Allègre C. J., Sagna I., and Dmitriev L. V. (1989) Noble gases in basalt glasses from a Mid-Atlantic Rdige topographic high at 14°N : geodynamic consequences. *Earth Planet. Sci. Lett.* **96**, 119-133.

Staudigel H., Hart S. R., Schmincke H. U., and Smith B. M. (1989) Cretaceous ocean crust at DSDP sites 417 and 418: Carbon uptake from weathering versus loss by magmatic outgassing. *Geochim. Csomochim. Acta* **53**, 3091-3094.

Stern S. A., Slater D. C., Festou M. C., Parker J. W., Glastone G. R., Hearn M. F. A., and Wilkinson E. (2001) The discovery of argon in comet C/1995 01 (Hale Bopp). *Astrophys. J.* in press.

Swindle T. D. (1995) How many Martian noble gas reservoirs have we sampled ? *AIP Congr.*, 175-185.

Tolstikhin I. N. and Marty B. (1998) The evolution of terrestrial volatiles : A view from helium, neon, argon and nitrogen isotope modelling. *Chem. Geol.* **147**, 27-52.

Trieloff M., Kunz J., Clague D. A., Harrisson C. J., and Allègre C. J. (2000) The nature of pristine noble gases in mantle plumes. *Science* **288**, 1036-1038.

Vityazev A. V., Pechernikova G. V., and Safronov V. S. (1990) *Planets of the Earth's group.* Nauka.

Vokrouhlicky D. and Farinella P. (2000) Efficient delivery of meteorites to the Earth from a wide range of asteroid parent bodies. *Nature* **407**, 606-608.

Weidenschilling S. J., Spaute D., Davies D. R., Marzari F., and Ohtsuki K. (1997) Accretional evolution of a planetary swarm. *Icarus* **128**, 429-438.

Wetherill G. W. (1975) Radiometric chronology of the early solar system. *Annu. Rev. Nucl. Sci* **25**, 283-328.

Wieler R., Anders E., Baur H., Lewis R. S., and Signer P. (1992) Characterization of Q-gases and other noble gas components in the Murchison meteorite. *Geochim. Cosmochim. Acta* **56**, 2907-2921.

Wilde S. A., Valley J. W., Peck W. H., and Graham C. M. (2001) Evidence from detrital zircons for the existence of continental crust and oceans on the Earth 4.4 Gyr ago. *Nature* **409**, 175-178.

Yung Y. L. and DeMore W. D. (1999) . In *Photochemistry of Planetary atmospheres*. Oxford University press.

Zanhle K. J., Kasting J. F., and Pollack J. B. (1988) Evolution of a steam atmsophere during Earth's accretion. *Icarus* **74**, 62-97.

Zartman R. E., Wasserburg G. J., and Reynolds J. H. (1961) Helium, argon and carbon in some natural gases. *J. Geophys. Res.* **66-1**, 277-306.

Table 1 : Elemental composition of comets. Dust composition is from (Jessberger et al., 1988a), gas composition is from (Delsemme, 1988). Bulk abundances were calculated assuming that the dust/gas ratio of typical comets is within 0.5-1.3 (Delsemme, 1988). Uncertainties were propagated accordingly.

	Dust		Gas		Bulk	
	$mol.g^{-1}$		$mol.g^{-1}$		$mol.g^{-1}$	
H	0.050	+/- 0.010	0.081	+/- 0.017	0.067	+/- 0.010
C	0.020	+/- 0.003	0.009	+/- 0.002	0.014	+/- 0.002
N	0.0010	+/- 0.0003	0.0045	+/- 0.0022	0.0029	+/- 0.0012
O	0.022	+/- 0.002	0.045	+/- 0.002	0.034	+/- 0.002
Na	0.00025	+/- 0.00015		-	0.00012	+/- 0.00007
Mg	0.0025	+/- 0.0002		-	0.0012	+/- 0.0002
Al	0.00017	+/- 0.00004		-	0.000079	+/- 0.000023
Si	0.0046	+/- 0.0005		-	0.0021	+/- 0.0004
S	0.0018	+/- 0.0006	0.00045	+/- 0.00022	0.0011	+/- 0.0003
K	0.0000050	+/- 0.0000025		-	0.0000023	+/- 0.0000012
Ca	0.00016	+/- 0.00005		-	0.000073	+/- 0.000025
Ti	0.000010	+/- 0.000005		-	0.000005	+/- 0.0000025
Cr	0.000022	+/- 0.000005		-	0.000010	+/- 0.000003
Mn	0.000012	+/- 0.000005		-	0.0000061	+/- 0.0000026
Fe	0.0013	+/- 0.0002		-	0.00060	+/- 0.00014
Co	0.0000074	+/- 0.0000050		-	0.0000034	+/- 0.0000024
Ni	0.00010	+/- 0.00005		-	0.00005	+/- 0.000025

Figure Caption

Figure 1 : Recycling of volatile elements in the Earth. The x-axis is the ratio of the surface (atmosphere, oceans, crust, sediments) inventory divided by the present-day flux at ridges. The y-axis is the amount of volatile elements carried by the oceanic crust and sediments to subduction zones by the volcanic flux at arcs. Neon is not represented because its volcanic flux is not known. Data sources : Allard (1992), Craig et al. (1975), Le Guern (1982), Marty (1995, 1992), Marty and Tolstikhin (1998), Marty and Zimmermann (1999), Matsuo et al. (1978), Rea and Ruff (1996), Sano and Williams (1996), Staudacher and Allègre (1988), Staudigel et al. (1989) and refs. therein.

Figure 2 : Comparison of volatile abundance data in Proto-Solar Nebula (PSN), primitive chondrites, terrestrial mantle and "atmosphere" (atmosphere sensu stricto, crust, sediments, oceans). Data are normalised to ^{20}Ne and PSN, so that the PSN pattern is flat. The choice of ^{20}Ne as a normalising isotope is based on the observation that recycling of atmospheric neon in the mantle is limited as indicated by its isotopic composition. Data source : Anders and Grevesse, (1989), Marty and Jambon (1987), Marty and Zimmermann (1999), Mazor et al. (1970), Moreira et al. (1998), Ozima et al. (1998), Pepin (1991).

Figure 3 : Three neon isotope diagram. In this format, mixings between end-members are represented by straight lines. Top : overall variations of Ne isotopes in Nature. ^{21}Ne and ^{22}Ne are produced significantly by natural nuclear reactions such as neutron activation of oxygen and fluorine, and spallation by cosmic rays. The PSN component is represented by the analysis of solar wind and displays the highest $^{20}Ne/^{22}Ne$ ratio measured so far. Neon-Q is an ubiquitous rare gas component trapped in primitive meteorites (Wieler et al., 1992), neon-A, often called planetary neon, is another meteoritic end-member but it is not clear if it represents a single, well individualised component or a mixture between other neon components, neon-E is almost pure ^{22}Ne of nucleosynthetic origin. Note that atmospheric neon presents a $^{20}Ne/^{22}Ne$ ratio intermediate between Solar and Ne-A. Dashed lines between Ne-A, Solar and nucleogenic Ne represent the field of values observed in meteorites. Bottom : Ne isotope variations in mantle-derived samples. Mid-ocean ridge basalts (MORB) are thought to derived directly from the convective mantle driving plate tectonics and is represented by an array between atmospheric neon and a mantle component enriched in both ^{20}Ne and ^{21}Ne (Sarda et al., 1988). The latter enrichment is accounted by production and accumulation of nucleogenic neon in the mantle whereas the ^{20}Ne enrichment is regarded as representing the occurrence of solar-type neon in the mantle.

A similar situation is observed for samples linked with mantle plumes such as Hawaii (Loihi Seamount is the youngest volcano of the Hawaiian chain; (Hiyagon et al., 1992; Honda et al., 1991) or carbonates and associated minerals from the Kola Peninsula (data points are represented to illustrate their spread and uncertainties; (Marty et al., 1998). The slopes of the plume-related data are steeper than that of the MORB correlation because the plume sources have apparently lower parent/daughter ratios than that of MORB. In both cases Ne isotopic variations point to the occurrence of a high $^{20}Ne/^{22}Ne$ ratio at depth diagnostic of a solar Ne component in the terrestrial mantle.

Figure 4 : Isotopic variations of hydrogen in the solar system (adapted from (Robert et al., 2000). The deuterium/hydrogen ratio of different components is normalised to the D/H ratio of the Sun (as it was before deuterium burning) which is thought to represent H_2 in the proto-solar nebula. Numbers along the y-axis represent the numbers of cases. Terrestrial hydrogen is enriched in deuterium by a factor of ~ 6 relative to Solar. Among solar system objects analysed so far, carbonaceous chondrites, Antarctic micrometeorites (Engrand and Maurette, 1998) and chondrules from LL3 chondrites present a distribution of D/H values that center around the terrestrial D/H ratio. Notably, comets analysed so far (Halley, Hale-Bopp and Hyakutake, refs. in (Dauphas et al., 2000) present D/H values about two times higher than the terrestrial value.

Figure 5 : The mass (M) of asteroids and comets that fell on Earth is reported as a function of the mass fraction (f) of comets among impacting bodies. Lunar cratering record (Chyba, 1990); highly siderophile elements (Chyba, 1991); water deuterium to protium ratios (Dauphas et al., 2000). If these three approaches recorded the late bombardment over the same period of time, then $M \sim 2 \times 10^{22}$ kg and $f \leq 0.01$. Actually, the mass of asteroids and comets evaluated by the lunar cratering record and highly siderophile elements depend on the mass fraction of comets. Given the level of uncertainty on all these estimates (M and f are reported in a log-log plot), taking this effect into account would not affect our conclusions.

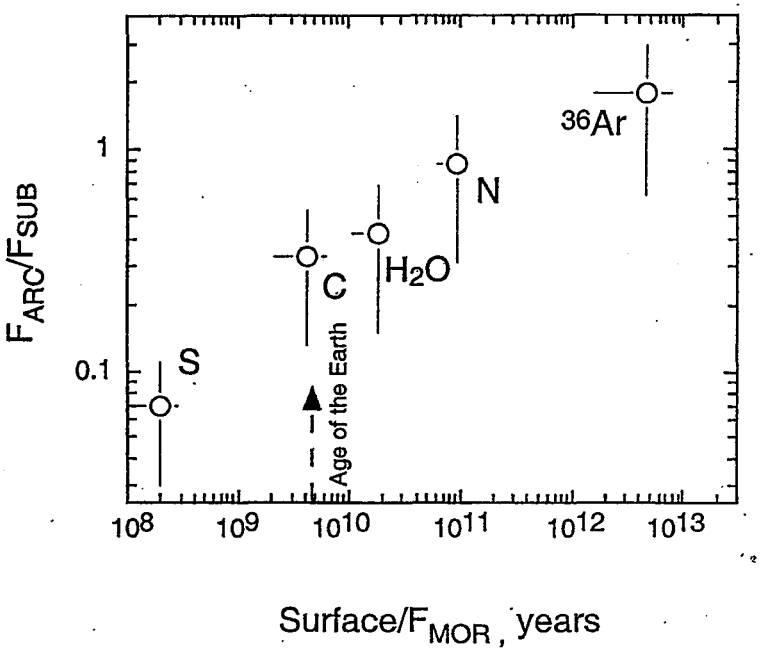

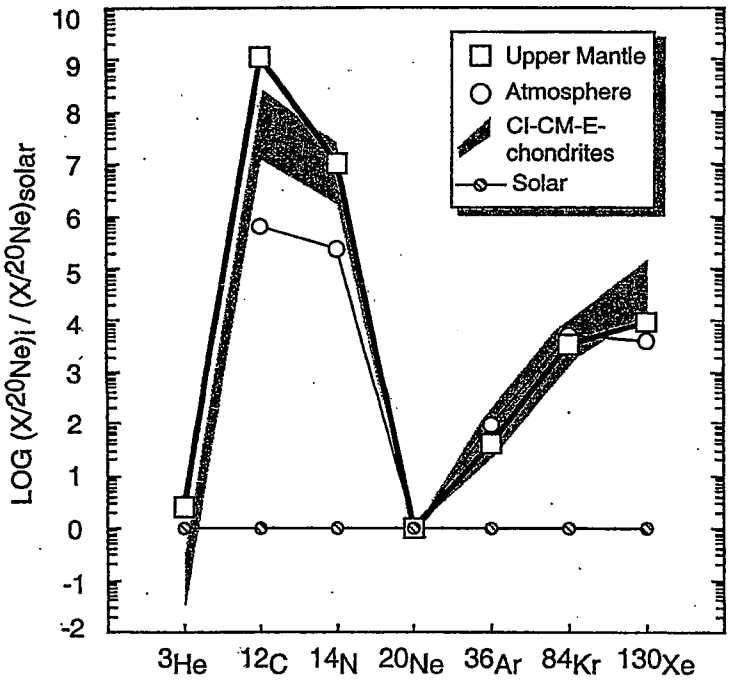
Upper Mantle
Atmosphere
CI-CM-E-chondrites
Solar
LOG (X/20Ne)i / (X/20Ne)solar
3He 12C 14N 20Ne 36Ar 84Kr 130Xe

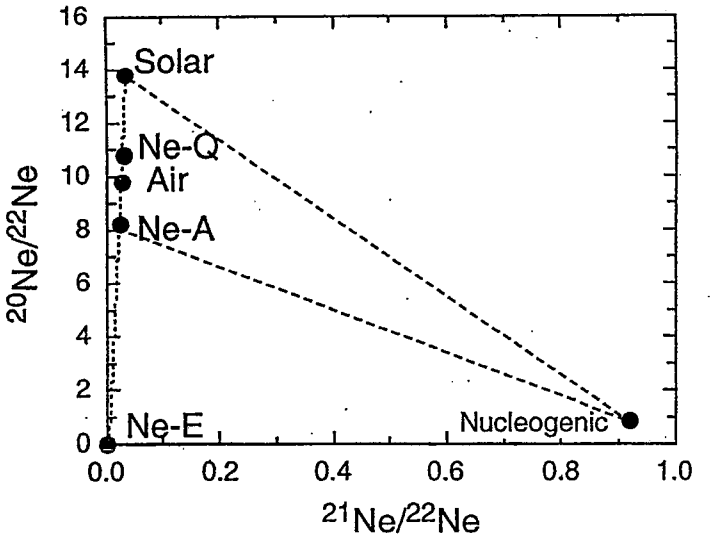
Solar
Ne-Q
Air
Ne-A
Ne-E
Nucleogenic
20Ne/22Ne
21Ne/22Ne

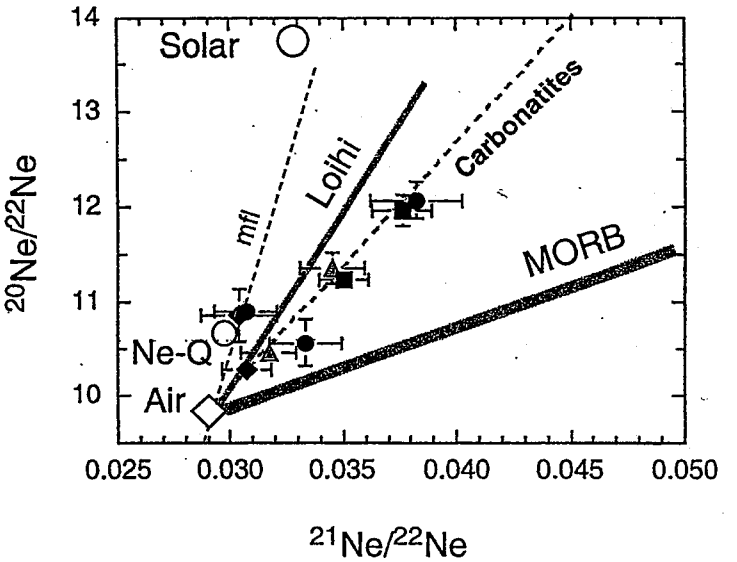
Solar
mfl
Loihi
Carbonatites
MORB
Ne-Q
Air
20Ne/22Ne
21Ne/22Ne

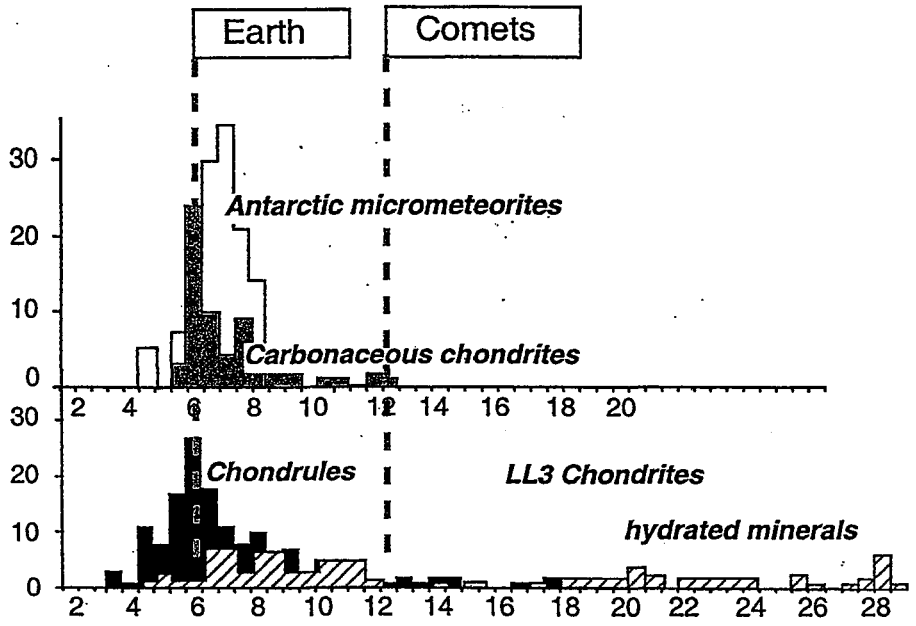
Earth
Comets
Antarctic micrometeorites
Carbonaceous chondrites
Chondrules
LL3 Chondrites
hydrated minerals

$$f = (D/H)_{H_2O} / (D/H)_{H_2}$$

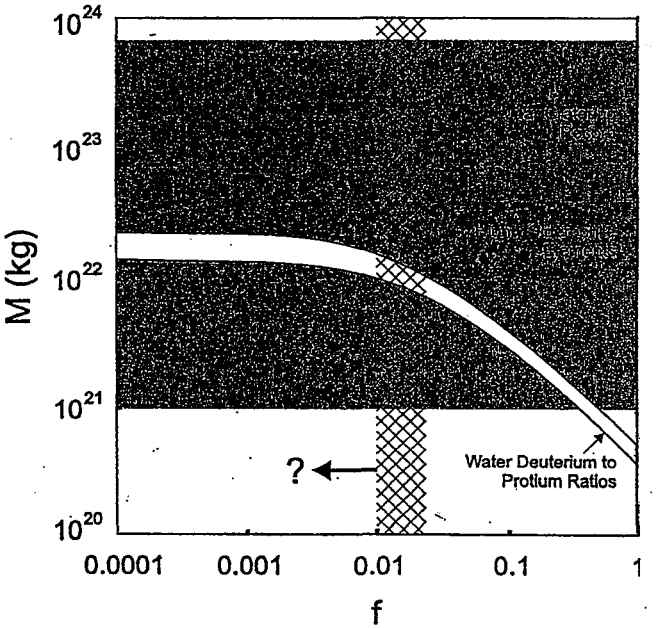
M (kg)
f
?
Water Deuterium to Protium Ratios

4 J. Geophys. Res., in press

Inference on the Nature and the Mass of Earth's Late Veneer from Noble Metals and Gases

Dauphas, N., and Marty, B.

Journal of Geophysical Research, in press

Journal of Geophysical Research, in press.

Inference on the Nature and the Mass of Earth's Late Veneer from Noble Metals and Gases

Nicolas Dauphas and Bernard Marty [1]
Centre de Recherches Pétrographiques et Géochimiques, CNRS UPR 2300, Vandœuvre-lès-Nancy, France.

Abstract

Noble metals and gases are very sensitive to the late accretion to the Earth of asteroids and comets. We present mass balance arguments based on these elements that indicate that $0.7 - 2.7 \times 10^{22}$ kg of extraterrestrial bodies struck the Earth after core formation and that comets comprised less than 10^{-3} by mass of the impacting population. These results imply that the dynamics of asteroids and comets changed with time and that biogenic elements and prebiotic molecules were not delivered to the Earth by comets but rather by carbonaceous asteroids.

1. Introduction

The first recognizable microfossils are 3.5 Ga old and there is isotopic evidence that life was present on our planet before 3.8 Ga ago [*Schopf*, 1993; *Mojzsis et al.*, 1996]. The chain of events that led to the emergence of self-replicating organisms is poorly known but the late heavy bombardment of Earth by remnants of planetary formation might have played a vital role. The asteroidal and cometary battering that scarred the lunar surface had an ambivalent effect on the emergence and early evolution of life. On the one hand, large impacts caused global trauma of the biosphere but on the other hand, they contributed biogenic elements and prebiotic molecules.

Approximately 65 Ma ago, a carbonaceous asteroid [*Kyte*, 1998] struck our planet at Chicxulub [*Hildebrand et al.*, 1991]. This impact probably caused the Cretaceous-Tertiary mass extinction [*Alvarez et al.*, 1980] and deposited intact organic molecules in sediments [*Zhao and Bada*, 1989]. Large impacts such as the K/T event imposed selection pressure on the biosphere [*Maher and Stevenson*, 1988; *Sleep et al.*, 1989] and drove the evolutionary course from abiogenesis to the emergence of conciousness. Abiogenesis occured early in Earth's history [*Schopf*, 1993; *Mojzsis et al.*, 1996] while our planet was pummelled by an intense rain of carbonaceous asteroids and comets [*Chyba*, 1990, 1991; *Dauphas et al.*, 2000]. This late accreting veneer might have delivered biogenic elements and prebiotic molecules to the surface of Earth [*Chyba and Sagan*, 1992]. The lunar cratering record [*Chyba*, 1990], highly siderophile elements [*Chyba*, 1991], and water deuterium to protium ratios [*Dauphas et al.*, 2000] impose constraints on the mass of the late veneer (M is the mass of asteroids and comets that struck the Earth in a late accretionary stage). What remains unanswered is whether the Earth was struck by stony or icy planetesimals (α is defined as the mass fraction of comets among impacting bodies). There is a stark contrast between the rare gas chemistry of asteroids and comets (Figure 1), which raises the possibility that these elements can be used to address this question. In the present contribution, we show that noble metals and gases place indeed stringent restrictions on the mass (M) and the nature (α) of the late accreting veneer.

There are many pieces of evidence that, in the late accretionary stage, the Earth was impacted mostly by volatile-rich bodies. (*i*) At present, the short-term accretion rate is dominated by sub-millimeter dust particles [*Love and Brownlee*, 1993]. Petrological and geochemical investigations conducted on micrometeorites indicate that the majority are carbonaceous [*Kurat et al.*, 1994; *Engrand and Maurette*, 1998]. (*ii*) Earth crossers, which dominate the long-term accretion rate, comprise a significant fraction of carbonaceous asteroids and comets [*Shoemaker et al.*, 1990]. (*iii*) Spectroscopic surveys of minor planets suggest that carbonaceous asteroids are overwhelmingly the most abundant type in outer regions of the main belt [*Gradie et al.*, 1989]. (*iv*) The debris found in regolith breccias might represent a faithful time-integrated sampling of the asteroid belt population. The majority of these debris are carbonaceous [*Lipschutz et al.*, 1989]. (*v*) Dynamical modelling of the early solar system evolution indicates that Earth's feeding zone extended with time to larger heliocentric distances, so that during the late accretionary stage our planet was impacted mostly by carbonaceous asteroids and comets [*Morbidelli et al.*, 2000]. For these reasons, we shall assume that the late veneer can be described as a binary mixture of carbonaceous asteroids and comets.

It is sometimes suggested that the osmium isotopic composition of the primitive upper mantle precludes direct filiation between mantle highly siderophile elements and carbonaceous chondrites [*Meisel et al.*, 1996; *Meisel et al.*, 2001; *Walker et al.*, 2001]. Core formation resulted in a fractionated noble metal pattern in the residual mantle. If a late carbonaceous veneer was mixed with this fractionated residue, then the osmium signature of the mantle is reconciliable with a carbonaceous late veneer [*Dauphas et al.*, 2002]. Note however that our conclusions do not rely heavily on this assumption.

2. Noble Metals

On Earth, geological processes such as erosion and tectonism obliterate impact structures so that the terrestrial cratering record does not exceed $\sim$ 2 Ga [*Grieve*, 1991]. The earlier bombardment history of our planet can be inferred by examining the crater record of the Moon. The density of lunar craters increases with the age of the exposed surface in a manner indicative of an overall decline with time of the bombardment intensity [*Shoemaker and Hackman*, 1962; *BVSP*, 1981]. After scaling the lunar cratering record to Earth's gravitational cross section, it is estimated that $9.9 \times 10^{20} - 6.9 \times 10^{23}$ kg of extraterrestrial bodies impacted our planet after the Moon formed [*Chyba*, 1990]. The lunar cratering record pro-

vides direct evidence for a decrease with time of the bombardment intensity but reliable quantification is difficult.

Additional evidence that asteroids and comets impacted our planet at a much higher rate in the Hadean than at present comes from water. The deuterium to protium ratio of the deep mantle [*Deloule et al.*, 1991] may be a remnant of the hydrogen isotopic composition of Earth forming planetesimals, which later evolved to the present terrestrial value as a result of the late accretion of volatile-rich matter [*Kokubu et al.*, 1961; *Dauphas et al.*, 2000]. If so, $4\times10^{20}-2\times10^{22}$ kg of asteroids and comets must have struck the Earth in a late accretionary stage [*Dauphas et al.*, 2000]. Note that this estimate depends on the mass fraction of comets among impacting bodies. Water deuterium to protium ratio provides a tighter estimate of the bombardment intensity than the lunar cratering record but the time interval over which integration holds is not very well constrained.

The late bombardment of Earth by remnants of planetary formation left also its imprint in highly siderophile elements (Ru, Rh, Pd, Re, Os, Ir, Pt, and Au). When our planet differentiated, highly siderophile elements should have been partitioned almost completely into the core, leaving the mantle depleted and fractionated. This view is inconsistent with highly siderophile element abundances in mantle rocks [*Kimura et al.*, 1974; *Jagoutz et al.*, 1979]. A widely held opinion is that highly siderophile elements were delivered to the mantle by a late accreting veneer after metal/silicate differentiation [*Morgan*, 1986]. Thus, noble metals integrate the late bombardment of Earth over a time interval extending between core formation and present. Core formation is estimated from lead isotopes and ^{182}Hf $-^{182}$ W systematics to have occurred approximately 100 Ma after collapse of the protosolar cloud [*Allègre et al.*, 1995; *Galer and Goldstein*, 1996; *Lee and Halliday*, 1995; *Halliday et al.*, 1996]. Knowing the inventory of the silicate Earth for noble metals, it is then straightforward to calculate the mass of impacting bodies (M) required to explain the observed concentrations as a function of the mass fraction of comets (α),

$$M = \frac{M_{\oplus}C_{\oplus}}{\alpha C_{\circ} + (1-\alpha)C_{\bullet}},$$

where $C_{\oplus}$, $C_{\circ}$, and $C_{\bullet}$ are the concentrations of the silicate Earth, comets, and asteroids, respectively.

We focus our discussion on osmium because its geochemistry is better known than that of other noble metals (Table 1). It has recently been suggested on the basis of the osmium isotopic composition of the mantle that there might be a concentration contrast for noble metals between the deep and the shallow mantle, the upper mantle being a factor of 3 ± 2 richer than the lower mantle [*Dauphas et al.*, 2002]. The osmium concentration of the upper mantle is estimated to be 0.018×10^{-9} mol.g^{-1} [*McDonough and Sun*, 1995], hence the osmium concentration of the deep mantle should be approximately 0.006×10^{-9} mol.g^{-1} and there should be $3-7\times10^{16}$ mol of osmium in the whole mantle. A conservative estimate of the osmium content of the mantle [*Chyba* 1991] can also be derived assuming that (*i*) highly siderophile elements are homogeneously distributed in the whole mantle or (*ii*) the deep mantle is devoid of noble metals. It is thus calculated that there should be $1.8-7.2\times10^{16}$ mol of osmium in the mantle.

The osmium concentration of carbonaceous chondrites ranges from 2.6×10^{-9} to 4.3×10^{-9} mol.g^{-1} and encompasses the range observed in other undifferentiated meteorite groups [*Wasson and Kallemeyn*, 1988]. Thus, the total mass of extraterrestrial matter accreted by the Earth after core formation must have been $0.7-2.7\times10^{22}$ kg. Note that *Chyba* [1991] estimated that the mass accreted by the Earth after core formation must have been $1-4\times10^{22}$ kg, in complete agreement with the value we infer.

These estimates rely on the assumption that the Earth was impacted by stony planetesimals. If the Earth was impacted by comets, then the total mass of extraterrestrial matter incident on Earth required to deliver the mantle inventory of noble metals would have been higher because the concentration of noble metals in comets must be lower than that of asteroids. Assuming that the cometary dust has chondritic composition [*Jessberger et al.*, 1988], we estimate that the osmium concentration in comets must be $0.8-2.6\times10^{-9}$ mol.g^{-1}. Thus, the mass of extraterrestrial matter accreted by the Earth after core formation calculated on the basis of noble metals must increase along with the mass fraction of comets among impacting bodies (Figure 2). Among the three approaches discussed so far, noble metals provide the tightest and most reliable estimate of M.

3. Noble Gases

Krypton and xenon have high masses and high boiling points, so they are robust against atmospheric loss and their concentrations in comets are not sensi-

tive to the trapping temperature. For these reasons, we shall focus our discussion on these elements.

The net contribution of asteroids and comets to Earth's atmosphere is a balance between impact delivery and erosion [*Chyba,* 1990]. Detailed analytical and computational modeling of impact induced erosion indicate that impact events on Earth did not remove significant quantities of atmospheric gases [*Newman et al.,* 1999; *Shuvalov and Artemieva,* 2000]. It is sometimes suggested that rare gases were lost to space early in Earth's history as a result of an intense flux of extreme ultraviolet radiation from the young evolving sun [*Zahnle and Walker,* 1982]. The timing of such a phenomenon is not precisely known but it seems that Earth's atmosphere would have been retentive for krypton and xenon $\sim$ 100 Ma after collapse of the protosolar nebula [*Hunten et al.,* 1987; *Tolstikhin and Marty,* 1998]. As discussed previously, noble metals record the late bombardment of Earth beginning with core formation, which is thought to have occured $\sim$ 100 Ma after formation of the solar system [*Allègre et al.,* 1995; *Galer and Goldstein,* 1996; *Lee and Halliday,* 1995; *Halliday et al.,* 1996]. Thus, it is reasonable to assume that during the accretionary stage investigated in the present contribution (after metal/silicate differentiation), the atmosphere was retentive for krypton and xenon.

If heavy noble gases were not lost to space by either impact erosion or hydrodynamic hydrogen escape after core formation, then the simplest mass balance requirement that the late veneer must meet is that it cannot deliver more than the terrestrial volatile inventory [*Swindle and Kring,* 1997, 2001]. This statement has strong implications on both the mass of asteroids and comets incident on Earth and the mass fraction of comets among impacting bodies. It is noteworthy that this mass balance holds even if Earth-forming planetesimals contributed a significant fraction of the terrestrial volatile inventory. The mass-balance equation derived in the case of noble metals can be applied to noble gases as well. Thus, the noble gas inventory of the Earth provides an independent upper-limit on M (mass of the late veneer) as a function of α (nature of the late veneer). Reliable estimates of noble gas concentrations are required before discussing further the mass and the nature of the late accreting veneer (Table 2).

Carbonaceous chondrites are the closest spectral analogs available in laboratory of the carbonaceous asteroids that impacted our planet during the Hadean eon [*Gaffey et al.,* 1993]. In these meteorites, the ^{84}Kr and ^{130}Xe concentrations lie within $2.2 - 4.5 \times 10^{-13}$ and $2.9 - 5.0 \times 10^{-14}$ mol.g^{-1}, respectively [*Mazor et al.,* 1970].

The appropriate cometary concentration to use is a bit more difficult to determine. Dynamical modeling of the early solar system evolution indicates that comets from the trans-Uranian region dominated the cometary flux in the neighborhood of Earth [*Morbidelli et al.,* 2000]. The ultimate source region of Oort cloud comets is uncertain but it might lie somewhere between the orbits of Uranus and Neptune [*Fernandez and Ip,* 1981]. In that case, the formation temperature of Oort cloud comets is relevant to the late bombardment of Earth. The inferred condensation temperatures of comets derived from observations are contradictory. The ortho-para ratios of water [*Crovisier et al.,* 1997] and ammonia [*Kawakita et al.,* 2001], and the cosmic Ar/O ratio measured in C/1995 O1 [*Stern et al.,* 2000] would favor formation near 30 K. This temperature is at odds with the volatile composition of C/1999 S4 [*Mumma et al.,* 2001] and the low Ar/O ratio measured in C/2001 A2 [*Feldman et al.,* 2001]. At present, the formation temperature of typical Oort cloud comets is difficult to assess but it may have been in the range 30-70 K.

As discussed previously, simulation of the early solar system evolution suggests that comets originating beyond the orbit of Uranus dominated the cometary flux in the neighborhood of Earth [*Morbidelli et al.,* 2000]. Models of the protosolar nebula [*Yamamoto,* 1985] indicate that at such distances, the temperature would have been lower than 70 K.

The formation temperature of the comets that impacted the Earth can be derived from rare gas abundances [*Owen et al.,* 1992; *Bar-Nun and Owen,* 1998; *Owen and Bar-Nun,* 2000]. In a Ar/Xe-Kr/Xe diagram, terrestrial and martian samples align along a mixing line extending between internal and external volatile reservoirs [*Owen et al.,* 1992]. The intersection between this line and the correlation defined by gases trapped in amorphous ice in laboratory experiments [*Bar-Nun et al.,* 1988] permits the determination of the trapping temperature of rare gases. It is thus estimated that the comets that impacted the Earth in a late accretionary stage formed at a temperature of 50 K [*Owen and Bar-Nun,* 2000].

Thus, it is reasonable to assume that comets in the late veneer had formation temperatures of 50 ± 20 K. In this temperature range, helium and neon are not retained, argon is partially trapped, and krypton and xenon are quantitatively condensed. The noble gas

concentration in comets can be inferred from laboratory experiments [*Bar-Nun et al.*, 1988; *Bar-Nun and Owen*, 1998]. In the temperature range 30-70 K, laboratory experiments indicate that the Kr/O and Xe/O are almost unfractionated relative to solar. Using the oxygen abundance and dust/gas ratio measured in comets [*Jessberger et al.*, 1988; *Delsemme*, 1988], it is then straightforward to compute the rare gas concentrations. The cometary ^{84}Kr and ^{130}Xe concentrations are thus estimated to be $2.1 - 3.2 \times 10^{-8}$ and $0.4 - 2.6 \times 10^{-10}$ mol.g^{-1}, respectively.

The remaining piece of information required for calculation is the total ^{84}Kr and ^{130}Xe content of the Earth. For the sake of simplicity, we shall consider a layered mantle comprising the shallow mantle feeding mid-ocean ridges and the deep mantle feeding ocean islands, though we recognize that the true mantle structure may be considerably more complex [*Tackley*, 2000]. The shallow–deep mantle boundary lies somewhere between the transition zone and the D" layer. The concentration of helium in the shallow mantle is calculated based on the observed flux at mid-ocean ridges [*Craig et al.*, 1975], the estimated rate of ocean crust formation [*Crisp*, 1984], and the inferred degree of partial melting [*Klein and Langmuir*, 1987]. The argon concentration in the shallow mantle is computed using isotopic and elemental ratios indexed to helium [*Moreira et al.*, 1998; *Marty and Zimmermann*, 1999]. Following the procedure outlined by *Allègre et al.* [1996], the radiogenic argon produced in Earth since 4.5 Ga by the decay of potassium is calculated [*McDonough and Sun*, 1995] and the amounts residing both in the shallow mantle and at the surface of Earth are then substracted in order to estimate the deep mantle ^{40}Ar content. Using deep mantle ^{40}Ar/^{36}Ar ratios, it is then straightforward to calculate the deep mantle ^{36}Ar content [*Valbracht et al.*, 1997; *Marty et al.*, 1998; *Trieloff et al.*, 2000]. Earth's core is thought to contain a negligible amount of argon [*Matsuda et al.*, 1993]. We can then derive the ^{36}Ar content of the Earth. Uncertainties were propagated in the calculation by means of Monte-Carlo simulations [*Anderson*, 1976]. The ^{36}Ar concentration of the bulk Earth is thus estimated to be $9.5 - 10.4 \times 10^{-13}$ mol.g^{-1}. It is worthwhile to note that the argon inventory of the Earth is not plagued by large uncertainty because most ^{36}Ar resides in the atmosphere. Simply stated, approximately 50 % of the ^{40}Ar produced in Earth by the decay of potassium resides in the mantle [*Allègre et al.*, 1996]. The ^{40}Ar/^{36}Ar of the silicate Earth (> 3000) is at least a factor of ten higher than that of the atmosphere (~ 300) [*Valbracht et al.*, 1997; *Marty et al.*, 1998; *Trieloff et al.*, 2000], so that at most 10 % of the terrestrial ^{36}Ar inventory resides in the mantle. Knowing the ^{36}Ar content of the mantle, it is then straightforward to compute the ^{84}Kr and ^{130}Xe abundances. The ^{84}Kr/^{36}Ar and ^{130}Xe/^{36}Ar ratios of the mantle are not precisely known but we can reasonably assume that they are in the range defined by the sun and meteorites (Table 2). The ^{36}Ar inventory in the mantle is estimated to be lower than 7×10^{14} mol. Thus, there should be at most 7×10^{12} mol of ^{84}Kr and 9×10^{11} mol of ^{130}Xe in the whole mantle. After addition of the atmosphere inventory, it is thus estimated that the ^{84}Kr and ^{130}Xe concentration in the Earth are $2.0 - 2.1 \times 10^{-14}$ and $1.1 - 2.6 \times 10^{-16}$ mol.g^{-1}, respectively. The uncertainties are small because a significant share of ^{84}Kr and ^{130}Xe resides in the atmosphere.

The atmophile inventories compiled in Table 2 were computed in a similar manner to that detailed in the case of krypton and xenon.

The mass balance requirement on noble gases dictates that only a limited region of the $\alpha - M$ space is admissible (hatched region labelled Noble Gases in Figure 2). Outside this region, too much krypton or xenon would have been delivered to the Earth. As discussed earlier, noble metals provide independent constraints on M (hatched region labelled Noble Metals). Combining these two admissible locii, the mass of asteroids and comets incident on Earth after core formation must have been $0.7 - 2.7 \times 10^{22}$ kg and comets must have represented less than 10^{-3} by mass of the impacting population (cross hatched region). Note that *Swindle and Kring* [2001] also reached the conclusion that comets represented a minor fraction of Earth's late veneer by similar lines of argument. They rely on argon but its abundance in comets is very sensitive to the formation temperature [*Bar-Nun et al.*, 1988; *Bar-Nun and Owen*, 1998] and measurements of cometary Ar/O ratios are contradictory [*Stern et al.*, 2000; *Feldman et al.*, 2001].

4. Perspectives

At present, comets comprise a significant fraction of Earth's impacting population, at least on the order of a few percent [*Shoemaker et al.*, 1990]. On the contrary, our results indicate that comets represented a very small fraction of the extraterrestrial bodies that impacted our planet in a late accretionary stage.

Thus, the dynamics of asteroids and comets might have changed with time, which calls for theoretical confirmation.

The mass fraction of comets among impacting bodies is so small that they could not have contributed significant quantities of biogenic elements and prebiotic molecules to Earth (Table 3). In constrast, carbonaceous asteroids [*Kerridge,* 1985] could have delivered a significant fraction of the present surface inventory [*Schlesinger,* 1997] of hydrogen, carbon, and nitrogen (Table 3). These biogenic elements might have been delivered in the form of prebiotic molecules and might also have been reprocessed by impact shockwaves into organic molecules [*Chyba and Sagan,* 1992].

The finding that the mass of asteroids and comets incident on Earth after core formation was $0.7-2.7\times 10^{22}$ kg and that comets represented less than 10^{-3} by mass of the impacting population has important implications for both early solar system dynamics and the emergence and early evolution of life on Earth. Further investigations must be conducted on comets, specifically on their rare gas chemistry, in order to obtain a clearer picture of the origin of planetary atmospheres and Earth's biosphere.

Acknowledgments. We acknowledge an anonymous reviewer and P.G. Lucey for constructive comments. We thank T.C. Owen, V.V. Shuvalov, L. Reisberg, and F. Robert for stimulating discussions. This research has made use of NASA's Astrophysics Data System Abstract Service. This is CRPG contribution 1560.

References

Allègre, C.J., A. Hofmann, and K. O'Nions, The argon constraints on mantle structure, *Geophys. Res. Lett., 23,* 3555-3557, 1996.

Allègre, C.-J., G. Manhès, and C. Göpel, The age of the Earth, *Geochim. Cosmochim. Acta, 59,* 1445-1456, 1995.

Alvarez, L.W., W. Alvarez, F. Asaro, and H.V. Michel, Extraterrestrial cause for the Cretaceous-Tertiary extinction, *Science, 208,* 1095-1108, 1980.

Anders, E., and N. Grevesse, Abundances of the elements: meteoritic and solar, *Geochim. Cosmochim. Acta, 53,* 197-214, 1989.

Anderson, G.M. Error propagation by the Monte Carlo method in geochemical calculations, *Geochim. Cosmochim. Acta, 40,* 1533-1538, 1976.

Bar-Nun, A., I. Kleinfeld, and E. Kochavi, Trapping of gas mixtures by amorphous water ice, *Phys. Rev. B., 38,* 7749-7754, 1988.

Bar-Nun, A., and T. Owen, Trapping of gases in water ice and consequences to comets and the atmospheres of the inner planets, in *Solar System Ices,* edited by B.B. Schmitt, C. De Bergh, and M. Festou, pp. 353-366, Kluwer Academic, Dordrecht, 1998.

Basaltic Volcanism Study Project (BVSP) *Basaltic Volcanism on the Terrestrial Planets,* 1286 pp., Pergamon Press, New York, 1981.

Chyba, C.F., Impact delivery and erosion of planetary oceans in the early inner Solar System, *Nature, 343,* 129-133, 1990.

Chyba, C.F., Terrestrial mantle siderophiles and the lunar impact record, *Icarus, 92,* 217-233, 1991.

Chyba, C.F., and C. Sagan, Endogenous production, exogenous delivery and impact-shock synthesis of organic molecules: an inventory for the origins of life, *Nature, 355,* 125-132, 1992.

Craig, H., W.B. Clarke, and M.A. Beg, Excess ^{3}He in deep water on the East Pacific Rise, *Earth Planet. Sci. Lett., 26,* 125-132, 1975.

Crisp, J.A., Rates of magma emplacement and volcanic output, *J. Volcanol. Geotherm. Res., 20,* 177-211, 1984.

Crovisier, J., K. Leech, D. Bockelée-Morvan, T.Y. Brooke, M.S. Hanner, B. Altieri, H.U. Keller, and E. Lellouch, The spectrum of Comet Hale-Bopp (C/1995 O1) observed with the Infrared Space Observatory at 2.9 AU from the sun, *Science, 275,* 1904-1907, 1997.

Dauphas, N., and B. Marty, Heavy nitrogen in carbonatites of the Kola peninsula: a possible signature of the deep mantle, *Science, 286,* 2488-2490, 1999.

Dauphas, N., L. Reisberg, and B. Marty, An alternative explanation for the distribution of highly siderophile elements in Earth, *Submitted to Geochem. J.,* 2002.

Dauphas, N., F. Robert, and B. Marty, The late asteroidal and cometary bombardment of Earth as recorded in water deuterium to protium ratio, *Icarus, 148,* 508-512, 2000.

Deloule, E., F. Albarède, and S.M.F. Sheppard, Hydrogen isotope heterogeneities in the mantle from ion probe analysis of amphiboles from ultramafic rocks, *Earth Planet. Sci. Lett., 105,* 543-553, 1991.

Delsemme, A.H., The chemistry of comets, *Phil. Trans. R. Soc. Lond., A325,* 509-523, 1988.

Engrand, C., and M. Maurette, Carbonaceous micrometeorites from Antarctica, *Meteorit. Planet. Sci., 33,* 565-580, 1998.

Feldman, P.D., H.A. Weaver, and E.B. Burgh, Comet C/2001 A2 (LINEAR), *IAU Circular* 7681, 2001.

Fernandez, J.A., and W.H. Ip, Dynamical evolution of a cometary swarm in the outer planetary region, *Icarus, 47,* 470-479, 1981.

Gaffey, M.J., T.H. Burbine, and R.P. Binzel, Asteroid spectroscopy: progress and perspectives, *Meteoritics, 28,* 161-187, 1993.

Galer, S.J.G., and S.L. Goldstein, Influence of accretion

on lead in the Earth, in *Earth Processes: Reading the Isotopic Code, Geophysical Monograph 95,* edited by A. Basu, and S. Hart, pp. 75-98, American Geophysical Union, Washington, 1996.

Gradie, J.C., C.R. Chapman, and E.F. Tedesco, Distribution of taxonomic classes and the compositional structure of the asteroid belt, in *Asteroids II,* edited by R.P. Binzel, T. Gehrels, and M.S. Matthews, pp. 316-335, The University of Arizona Press, Tucson, 1989.

Grieve, R.A.F., Terrestrial impact: the record in the rocks, *Meteoritics, 26,* 175-194, 1991.

Halliday, A., M. Rehkämper, D.-C. Lee, and W. Yi, Early evolution of the Earth and Moon: new constraints from Hf-W isotope geochemistry, *Earth Planet. Sci. Lett., 142,* 75-89, 1996.

Hildebrand, A.R., G.T. Penfield, D.A. Kring, M. Pilkington, A. Camargo-Zanoguera, S.B. Jacobsen, and W.V. Boynton, Chicxulub Crater: a possible Cretaceous/Tertiary boundary impact crater on the Yucatan Peninsula, Mexico, *Geology, 19,* 867-871, 1991.

Hunten, D.M., R.O. Pepin, and J.C.G. Walker, Mass fractionation in hydrodynamic escape, *Icarus, 69,* 532-549, 1987.

Jagoutz, E., H. Palme, H. Baddenhausen, K. Blum, M. Cendales, G. Dreibus, B. Spettel, V. Lorenz, and H. Wänke, The abundances of major, minor and trace elements in the Earth's mantle as derived from primitive ultramafic nodules, *Proc. Lunar Planet. Sci. Conf., X,* 2031-2050, 1979.

Jambon, A., and J.-L. Zimmermann, Water in oceanic basalts: evidence for dehydration of recycled crust, *Earth Planet. Sci. Lett., 101,* 323-331, 1990.

Jessberger, E.K., A. Christoforidis, and J. Kissel, Aspects of the major element composition of Halley's dust, *Nature, 332,* 691-695, 1988.

Kawakita, H., J.-I. Watanabe, H. Ando, W. Aoki, T. Fuse, S. Honda, H. Izumiura, T. Kajino, E. Kambe, S. Kawanomoto, K. Noguchi, K. Okita, K. Sadakane, B. Sàto, M. Takada-Hidai, Y. Takeda, T. Usuda, T. Watanabe, and M. Yoshida, The spin temperature of NH_3 in comet C/1999S4 (LINEAR), *Science, 294,* 1089-1091, 2001.

Kerridge, J.F., Carbon, hydrogen and nitrogen in carbonaceous chondrites: abundances and isotopic compositions in bulk samples, *Geochim. Cosmochim. Acta, 49,* 1707-1714, 1985.

Kimura, K., R.S. Lewis, and E. Anders, Distribution of gold and rhenium between nickel-iron and silicate melts: implications for the abundance of siderophile elements on the Earth and Moon, *Geochim. Cosmochim. Acta, 38,* 683-701, 1974.

Klein, E.M., and C.H. Langmuir, Global correlations of ocean ridge basalt chemistry with axial depth and crustal thickness, *J. Geophys. Res., 92,* 8089-8115, 1987.

Kokubu, N., T. Mayeda, and H.C. Urey, Deuterium content of minerals, rocks and liquid inclusion from rocks, *Geochim. Cosmochim. Acta, 21,* 247-256, 1961.

Krasnopolsky, V.A., M.J. Mumma, M. Abbott, B.C. Flynn, K.J. Meech, D.K. Yeomans, P.D. Feldman, and C.B. Cosmovici, Detection of soft X-rays and a sensitive search for noble gases in Comet Hale-Bopp (C/1995 O1), *Science, 277,* 1488-1491, 1997

Kurat, G., C. Koeberl, T. Presper, F. Brandstätter, and M. Maurette, Petrology and geochemistry of Antarctic micrometeorites, *Geochim. Cosmochim. Acta, 58,* 3879-3904, 1994.

Kyte, F.T., A meteorite from the Cretaceous/Tertiary boundary, *Nature, 396,* 237-239, 1998.

Lee, D.-C., and A.N. Halliday, Hafnium-tungsten chronometry and the timing of terrestrial core formation, *Nature, 378,* 771-774, 1995.

Lipschutz, M.E., M.J. Gaffey, and P. Pellas, Meteoritic parent bodies: nature, number, size and relation to present-day asteroids, in *Asteroids II,* edited by R.P. Binzel, T. Gehrels, and M.S. Matthews, pp. 741-777, The University of Arizona Press, Tucson, 1989.

Love, S.G., and D.E. Brownlee, A direct measurement of the terrestrial mass accretion rate of cosmic dust, *Science, 262,* 550-553, 1993.

Maher, K.A., and D.J. Stevenson, Impact frustration of the origin of life, *Nature, 331,* 612-614, 1988.

Marty, B., and I.N. Tolstikhin, CO_2 fluxes from mid-ocean ridges, arcs and plumes, *Chem. Geol., 145,* 233-248, 1998.

Marty, B., I. Tolstikhin, I.L. Kamensky, V. Nivin, E. Balaganskaya, and J.-L. Zimmermann, Plume-derived rare gases in 380 Ma carbonatites from the Kola region (Russia) and the argon isotopic composition in the deep mantle, *Earth Planet. Sci. Lett., 164,* 179-192, 1998.

Marty, B., and L. Zimmermann, Volatiles (He, C, N, Ar) in mid-ocean ridge basalts: Assesment of shallow-level fractionation and characterization of source composition, *Geochim. Cosmochim. Acta, 63,* 3619-3633, 1999.

Matsuda, J., M. Sudo, M. Ozima, K. Ito, O. Ohtaka, and E. Ito, Noble gas partitioning between metal and silicate under high pressures, *Science, 259,* 788-790, 1993.

Mazor, E., D. Heymann, and E. Anders, Noble gases in carbonaceous chondrites, *Geochim. Cosmochim. Acta, 34,* 781-824, 1970.

McDonough, W.F., and S.-S. Sun, The composition of the Earth, *Chem. Geol., 120,* 223-253, 1995.

Meisel, T., R.J. Walker, A.J. Irving, and J.-P. Lorand, Osmium isotopic compositions of mantle xenoliths: a global perspective, *Geochim. Cosmochim. Acta, 65,* 1311-1323, 2001.

Meisel, T., R.J. Walker, and J.W. Morgan, The osmium isotopic composition of the Earth's primitive upper mantle, *Nature, 383,* 517-520, 1996.

Michael, P.J. The concentration, behavior and storage of H_2O in the suboceanic upper mantle: implications for mantle metasomatism, *Geochim. Cosmochim. Acta,*

52, 555-566, 1988.

Mojzsis, S.J., G. Arrhenius, K.D. McKeegan, T.M. Harrison, A.P. Nutman, and C.R.L. Friend, Evidence for life on Earth before 3,800 million years ago, *Nature, 384,* 55-59, 1996.

Morbidelli, A., J. Chambers, J.I. Lunine, J.M. Petit, F. Robert, G.B. Valsecchi, and K.E. Cyr, Source regions and timescales for the delivery of water to Earth, *Meteorit. Planet. Sci., 35,* 1309-1320, 2000.

Moreira, M., J. Kunz, and C. & Allègre, Rare gas systematics in popping rock: isotopic and elemental compositions in the upper mantle, *Science, 279,* 1178-1181, 1998.

Morgan, J.W., Ultramafic xenoliths: clues to Earth's late accretionary history, *J. Geophys. Res., 91,* 12375-12387, 1986.

Mumma, M.J., N. Dello Russo, M.A. DiSanti, K. Magee-Sauer, R.E. Novak, S. Brittain, T. Rettig, I.S. McLean, D.C. Reuter, and L.-H. Xu, Organic composition of C/1999 S4 (LINEAR): A comet formed near Jupiter?, *Science, 292,* 1334-1339, 2001.

Newman, W.I., E.M.D. Symbalisty, T.J. Ahrens, and E.M. Jones, Impact erosion of planetary atmospheres: some surprising results, *Icarus, 138,* 224-240, 1999.

Owen, T.C., and A. Bar-Nun, Volatile contributions from icy planetesimals, in *Origin of the Earth and Moon,* edited by R.M. Canup, and K. Righter, pp. 459-471, The University of Arizona Press, Tucson, 2000.

Owen, T., A. Bar-Nun, and I. Kleinfeld, Possible cometary origin of heavy noble gases in the atmospheres of Venus, Earth and Mars, *Nature, 358,* 43-46, 1992.

Ozima, M., and F.A. Podosek *Noble Gas Geochemistry,* 367 pp., Cambridge University Press, Cambridge, 1983.

Schlesinger, W.H. *Biogeochemistry,* 588 pp., Academic Press, San Diego, 1997.

Schopf, J.W., Microfossils of the Early Archean Apex chert: new evidence of the antiquity of life, *Science, 260,* 640-646, 1993.

Shoemaker, E.M. and R.J. Hackman, Stratigraphic base for a lunar time scale, in *The Moon,* edited by Z. Kopal, and Z.K. Mikhailov, pp. 289-300, Academic Press, London, 1962.

Shoemaker, E.M., R.F. Wolfe, and C.S Shoemaker, Asteroid and comet flux in the neighborhood of Earth, in *Global Catastrophes in Earth History,* edited by V.L. Sharpton, and P.O. Ward, pp. 155-170, Geological Society of America, Boulder, 1990.

Shuvalov, V.V., and N.A. Artemieva, Atmospheric erosion and radiation impulse induced by impacts, *LPI Contribution, 1053,* #3060, 2000.

Sleep, N.H., K.J. Zahnle, J.F. Kasting, and H.J. Morowitz, Annihilation of ecosystems by large asteroid impacts on the early Earth, *Nature, 342,* 139-142, 1989.

Stern, S.A., J.C. Green, W. Cash, and T.A. Cook, Helium and argon abundance constraints and the thermal evolution of comet Austin (1989c1), *Icarus, 95,* 157-161, 1992.

Stern, S.A., D.C. Slater, M.C. Festou, J.W. Parker, G.R. Gladstone, M.F. A'Hearn, and E. Wilkinson, The discovery of argon in comet C/1995 O1 (Hale-Bopp), *Astrophys. J., 544,* L169-L172, 2000.

Swindle, T.D., and D.A. Kring, Implications of small comets for the noble gas inventories of Earth and Mars, *Geophys. Res. Lett., 24,* 3113-3116, 1997.

Swindle, T.D., and D.A. Kring, Cataclysm+cold comets=lots of asteroid impacts, *Lunar Planet. Sci., XXXII,* #1466, 2001.

Tackley, P.J., Mantle convection and plate tectonics: toward an integrated physical and chemical theory, *Science, 288,* 2002-2007, 2000.

Tolstikhin, I.N., and B. Marty, The evolution of terrestrial volatiles: a view from helium, neon, argon and nitrogen isotope modelling, *Chem. Geol., 147,* 27-52, 1998.

Trieloff, M., J. Kunz, D.A. Clague, D. Harrison, and C.J. Allègre, The nature of pristine noble gases in mantle plumes, *Science, 288,* 1036-1038, 2000.

Valbracht, P.J., T. Staudacher, A. Malahoff, and C.J. Allègre, Noble gas systematics of deep rift zone glasses from Loihi Seamount, Hawaii, *Earth Planet. Sci. Lett., 150,* 399-411, 1997.

Walker, R.J., M.F. Horan, J.W. Morgan, and T. Meisel, Osmium isotopic compositions of chondrites and Earth's primitive upper mantle: constraints on the late veneer, *Lunar Planet. Sci., XXXII,* #1152, 2001.

Wasson, J.T., and G.W. Kallemeyn, Compositions of chondrites, *Phil. Trans. R. Soc. London, A325,* 535-544, 1988.

Yamamoto, T., Formation environment of cometary nuclei in the primordial solar nebula, *Astron. Astrophys., 142,* 31-36, 1985.

Zahnle, K.J., and J.C.G. Walker, The evolution of solar ultraviolet luminosity, *Rev. Geophys. Space Phys., 20,* 280-292, 1982.

Zhao, M., and J.L. Bada, Extraterrestrial amino acids in Cretaceous/Tertiary boundary sediments at Stevns Klint, Denmark, *Nature, 339,* 463-465, 1989.

N. Dauphas and B. Marty, Centre de Recherches Pétrographiques et Géochimiques, CNRS UPR 2300, 15 rue Notre-Dame des Pauvres, BP 20, 54501 Vandœuvre-lès-Nancy Cedex France. (e-mail: dauphas@crpg.cnrs-nancy.fr; bmarty@crpg.cnrs-nancy.fr)

[1]Also at École Nationale Supérieure de Géologie, rue du doyen Marcel Roubault, B.P. 40, 54501 Vandœuvre-lès-Nancy Cedex France.

This preprint was prepared with AGU's LaTeX macros v5.01. File dauphasms formatted January 7, 2002.

Figure 1. Concentrations of hydrogen, helium, carbon, nitrogen, neon, argon, krypton, and xenon in asteroids (•), comets (○), and Earth (⊕) are normalized to cosmic abundances of the elements (⊙). Values and references are compiled in Table 2.

Figure 2. The mass of asteroids and comets that struck the Earth after core formation (M) is reported as a function of the mass fraction of comets among impacting bodies (α). The admissible locii from the points of view of noble metals and gases are indicated as hatched regions. The admissible region for both noble metals and gases is the intersection of these two fields (cross hatched). Thus, we estimate that the mass of asteroids and comets incident on Earth after core formation was $0.7 - 2.7 \times 10^{22}$ kg and that comets represented less than 10^{-3} by mass of the impacting population (see text for details).

Table 1. Siderophile Inventories

		Osmium
Cosmic		1.7(-11)
Asteroids	{	2.6(−9) 4.3(−9)
Comets	{	0.8(−9) 2.6(−9)
Silicate Earth	{	5.0(−12) 1.2(−11)

Concentrations are expressed in $mol.g^{-1}$ and power of ten multipliers are in parentheses. The mantle concentration is reported *per* gram of the Earth (5.98×10^{27} g). Cosmic – *Anders and Grevesse,* 1989. Asteroids – *Wasson and Kallemeyn,* 1988. Comets – *Delsemme,* 1988; *Wasson and Kallemeyn,* 1988. Earth – *Dauphas et al.,* 2002; *McDonough and Sun,* 1995.

Table 2. Atmophile Inventories

		^{1}H	^{3}He	^{12}C	^{14}N	^{20}Ne	^{36}Ar	^{84}Kr	^{130}Xe
Cosmic		7.0(-1)	9.6(-6)	2.5(-4)	7.8(-5)	8.0(-5)	2.1(-6)	6.5(-10)	5.2(-12)
Asteroids	{	2.8(−4)	7.0(−14)	2.9(−4)	2.0(−6)	1.8(−12)	2.3(−11)	2.2(−13)	2.9(−14)
	{	8.1(−3)	2.7(−12)	3.1(−3)	1.1(−4)	2.8(−11)	6.2(−11)	4.5(−13)	5.0(−14)
Comets (50 ± 20 K)	{	5.7(−2)	< 4(−8)	1.2(−2)	1.7(−3)	< 1(−4)	1(−8)	2.1(−8)	0.4(−10)
	{	7.7(−2)		1.6(−2)	4.1(−3)		1(−4)	3.2(−8)	2.6(−10)
Earth	{	3.2(−5)	4.3(−15)	3.5(−5)	7.2(−8)	4.8(−13)	9.5(−13)	2.0(−14)	1.1(−16)
	{	2.2(−4)	3.7(−14)	3.5(−4)	1.3(−7)	5.5(−13)	1.1(−12)	2.1(−14)	2.6(−16)

Concentrations are expressed in mol.g^{-1} and power of ten multipliers are in parentheses. The terrestrial composition is reported *per* gram of the Earth (5.98×10^{27} g). The concentrations of argon, krypton, and xenon in comets were derived from laboratory experiments assuming a trapping temperature of 50 ± 20 K. Cosmic – *Anders and Grevesse,* 1989. Asteroids – *Kerridge,* 1985; *Mazor et al.,* 1970. Comets – *Bar-Nun et al.,* 1988; *Bar-Nun and Owen,* 1998; *Delsemme,* 1988; *Jessberger et al.,* 1988; *Krasnopolsky et al.,* 1997; *Stern et al.,* 1992. Earth – *Allègre et al.,* 1996; *Craig et al.,* 1975; *Crisp,* 1984; *Dauphas and Marty,* 1999; *Jambon and Zimmermann,* 1990; *Klein and Langmuir,* 1987; *McDonough and Sun,* 1995; *Marty and Tolstikhin,* 1998; *Marty et al.,* 1998; *Marty and Zimmermann,* 1999; *Michael,* 1988; *Moreira et al.,* 1998; *Ozima and Podosek,* 1983; *Schlesinger,* 1997; *Trieloff et al.,* 2000; *Valbracht et al.,* 1997.

Table 3. Contributions of the Late Veneer

		^{1}H	^{12}C	^{14}N
Asteroids	{	2.0(21)	2.0(21)	1.4(19)
		2.2(23)	8.4(22)	3.0(21)
Comets		< 2.1(21)	< 4.3(20)	< 1.1(20)
Earth	{	1.9(23)	2.1(23)	4.3(20)
		1.3(24)	2.1(24)	7.8(20)

Amounts are expressed in mol and power of ten multipliers are in parentheses. See text and Table 2 for further references.

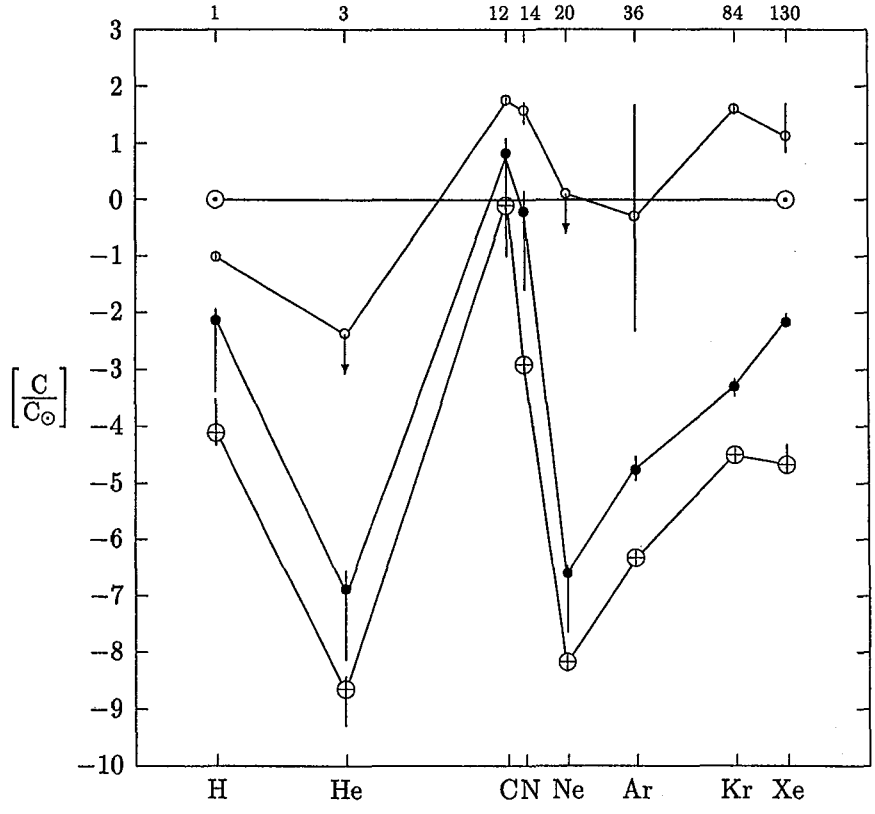
1
3
12 14 20
36
84 130
3
2
1
0
−1
−2
−3
−4
−5
−6
−7
−8
−9
−10
$\left[\frac{C}{C_\odot}\right]$
H
He
CN Ne
Ar
Kr Xe

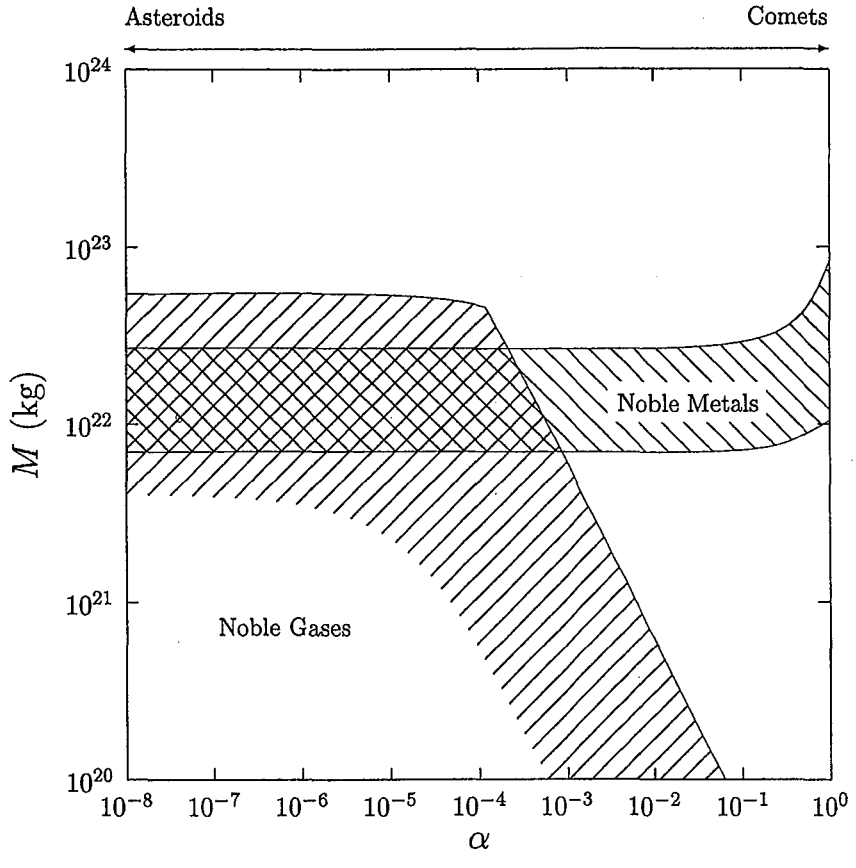
Asteroids
Comets
10^{24}
10^{23}
10^{22}
10^{21}
10^{20}
M (kg)
Noble Metals
Noble Gases
10^{-8} 10^{-7} 10^{-6} 10^{-5} 10^{-4} 10^{-3} 10^{-2} 10^{-1} 10^{0}
α

5 Geochem. J., in press

An Alternative Explanation for the Distribution of Highly Siderophile Elements in Earth

Dauphas, N., Reisberg, L., and Marty, B.

Geochemical Journal, in press

An Alternative Explanation for the Distribution of Highly Siderophile Elements in the Earth

Nicolas Dauphas[1*]
Laurie Reisberg[1]
Bernard Marty[1,2]

[1]Centre de Recherches Pétrographiques et Géochimiques, CNRS UPR 2300, 15 rue Notre-Dame des Pauvres, BP 20, 54501 Vandœuvre-lès-Nancy Cedex France.
[2]École Nationale Supérieure de Géologie, rue du doyen Marcel Roubault, BP 40, 54501 Vandœuvre-lès-Nancy Cedex France.
*To whom correspondence should be adressed. E-mail: dauphas@crpg.cnrs-nancy.fr

Submitted to
Geochemical Journal
9/10/2001

Revised version
27/ 2/ 2002

Keywords: Highly siderophile elements, osmium isotopes, mantle, late veneer, partition coefficients

Running title: Highly siderophile elements in the mantle

Abstract

The presence of highly siderophile elements (Ru, Rh, Pd, Re, Os, Ir, Pt, and Au) in the mantle has been a long standing enigma in the Earth sciences. Highly siderophile elements exhibit extremely low silicate/metal partition coefficients and so should have partitioned into the core, leaving the mantle depleted and fractionated compared with precursor material. Late accretion of undifferentiated material after completion of core formation may have overprinted the residue inherited from metal-silicate equilibrium partitioning. Here, we present a model based on the osmium isotopic composition of the mantle that sheds new light on the distribution of highly siderophile elements in Earth. As the Earth grew from the accretion of chondritic material of unspecified nature, gravitational and radioactive heating permitted early segregation of metal from silicate. This resulted in fractionation of highly siderophile element abundances in the residual mantle relative to chondritic abundances. After completion of core formation, the model supposes that a late carbonaceous veneer delivered biogenic and highly siderophile elements to the Earth. This late veneer was mixed inhomogeneously with the fractionated residue left over after core formation. Part of the deep mantle was isolated early from shallow convection and thus preserved primordial noble gas and highly siderophile element signatures. In this scenario, the contrast between the $^{187}Os/^{188}Os$ ratio of the carbonaceous late veneer and that of fertile lherzolites places strict constraints on the coupled silicate/metal partition coefficicents of Re and Os ($D^{Re} = 1.6 \pm 1.2 \times 10^{-4} + D^{Os}$). Similarly, the high $^{187}Os/^{188}Os$ and $^{186}Os/^{188}Os$ ratios observed in certain plumes impose restrictions on the coupled silicate/metal partition coefficients of Pt and Os ($D^{Pt} = 8.0 \pm 6.2 \times 10^{-4} + D^{Os}$).

Introduction

Metal/silicate differentiation was one of the most important events in early Earth history. However, we have a very poor understanding of the underlying mechanisms that governed this segregation (Stevenson, 1990). Low pressure experiments indicate that highly siderophile elements in the residual mantle left over after core formation should have been much more depleted and fractionated (Jones and Drake, 1986) than is observed (Kimura *et al.*, 1974; Jagoutz *et al.*, 1979; Allègre and Luck, 1980). This contradiction disappears (Morgan, 1986) if highly siderophile elements were delivered to the mantle by a late accreting veneer after completion of core formation (Morgan, 1986; Chyba, 1990; Dauphas *et al.*, 2000). Nevertheless, recent theoretical (Murthy, 1991) and experimental (Li and Agee, 1996; Righter and Drake, 1997; Cottrell and Walker, 2002) studies on the high pressure/high temperature partition coefficients of moderately and highly siderophile elements have revived discussion of the idea that the distribution of highly siderophile elements in Earth was governed by metal-silicate equilibrium partitioning in a magma ocean.

Osmium isotope abundances provide precise time-integrated information on Re/Os ($^{187}\mathrm{Re} \rightarrow ^{187}\mathrm{Os} + \mathrm{e}^- + \overline{\nu}_\mathrm{e}$, $\lambda = 1.666 \times 10^{-11}$ a^{-1}, Smoliar *et al.*, 1996) and Pt/Os ($^{190}\mathrm{Pt} \rightarrow ^{186}\mathrm{Os} + \alpha$, $\lambda = 1.477 \times 10^{-12}$ a^{-1}, Brandon *et al.*, 1999) ratios. Condensation processes in the protosolar nebula led to a subtle fractionation of the $^{187}\mathrm{Re}/^{188}\mathrm{Os}$ ratio which resulted in appreciable variation of the present $^{187}\mathrm{Os}/^{188}\mathrm{Os}$ ratio among the various meteorite classes. This implies that it may be possible to deduce the ultimate source of mantle osmium from its isotopic composition (Morgan, 1985; Meisel *et al.*, 1996; Walker *et al.*, 2001). Analysis of fertile lherzolites suggests that the $^{187}\mathrm{Os}/^{188}\mathrm{Os}$ ratio of the primitive upper mantle that has not experienced melt extraction is 0.1296 ± 0.0008 (Meisel *et al.*, 2001). This value, first proposed by Meisel *et al.* (1996), has been confirmed by numerous recent studies of lithospheric peridotite suites (McBride *et al.*, 1996; Handler *et al.*, 1997; Peslier *et al.*, 2000; Reisberg *et al.*, 2000; Snow *et al.*, 2000; Meisel *et al.*, 2001; Reisberg *et al.*, 2001) and thus represents a firm estimate of the primitive upper mantle osmium composition. The $^{187}\mathrm{Os}/^{188}\mathrm{Os}$ ratio of carbonaceous chondrites averages 0.1260 ± 0.0021 (Walker *et al.*, 2001). Some have argued that this difference indicates that the highly siderophile elements in the mantle were not derived from carbonaceous chondrites (Meisel *et al.*, 1996; Meisel *et al.*, 2001; Walker *et al.*, 2001). However, dynamical modelling of early solar system evolution (Morbidelli *et al.*, 2000) indicates that Earth's feeding zone extended with time to larger heliocentric distances, so that during the late accretionary stage our planet was impacted mostly by carbona-

ceous asteroids and comets. Knowing whether the Earth was impacted by ordinary or enstatite chondrites (Meisel *et al.*, 2001; Walker *et al.*, 2001; Morgan *et al.*, 2001) rather than carbonaceous chondrites is crucial to our understanding of the emergence and early evolution of life on Earth (Chyba, 1992; Dauphas and Marty, 2002). If the Earth was impacted by carbonaceous asteroids and comets, then biogenic elements and prebiotic molecules could have been delivered to the Earth by the late accreting veneer (Chyba and Sagan, 1992; Dauphas and Marty, 2002). Otherwise, they must have been inherited from Earth forming planetesimals. This latter possibility poses a difficulty as oxygen (Clayton *et al.*, 1984), chromium (Shukolyukov and Lugmair, 1998), and molybdenum (Dauphas *et al.*, 2002) isotopic data suggest that these planetesimals shared similarities with enstatite chondrites (Javoy, 1998). Material of this composition could not provide the volatile content currently observed on Earth. In the present contribution, our main aim is to show that the osmium signature of the mantle is reconcilable with a carbonaceous late veneer.

Results and Discussion

If carbonaceous chondrites are representative of the late veneer, then why does the fertile upper mantle have a slightly but significantly different Os isotopic ratio? An appealing possibility (Walker *et al.*, 1997a; Walker *et al.*, 1997b; O'Neill and Palme, 1998) is that the late carbonaceous veneer was mixed with the fractionated residue left over after core-mantle segregation (Fig. 1). The two mass-balance equations that formalize this idea are $[X]_m = [X]_r + [X]_l$ and $[X]_r = [X]_\oplus D^X/x$ (Appendix), where $[X]_m$ corresponds to the present concentration of nuclide X in the mantle, $[X]_r$ is the concentration remaining immediately after core formation, $[X]_l$ is the concentration derived from the late veneer, $[X]_\oplus$ is the concentration of the bulk Earth, D^X is the silicate/metal partition coefficient, and x is the mass fraction of metal in the Earth. This model imposes stringent constraints on the coupled silicate/metal partition coefficients of rhenium (D^{Re}) and osmium (D^{Os}). If we assume that the shallow mantle behaved as a closed system since the time of its formation then it is straightforward to demonstrate, applying the mass-balance equations at the time of core formation for both ^{187}Re and ^{188}Os, that there must be a relationship between D^{Re} and D^{Os} of the form (Appendix),

$$D^{Re'} = x\,[Os]_s^* f_s^{Re} + D^{Os}. \qquad (1)$$

Subscript s denotes the shallow mantle, $[Os]_s^*$ represents the normalized non-radiogenic Os concentration $[Os]_s/[Os]_\oplus$, and f_s^{Re} is the Re/Os fractionation factor after addition of the late veneer $(^{187}Re/^{188}Os)_s/(^{187}Re/^{188}Os)_l - 1$ (Appendix). Note that this and

all further fractionation factors are defined relative to the composition of the late veneer. The proportion of metal in Earth x is 0.32. The osmium concentrations of the shallow mantle and of the bulk Earth are estimated to be $0.018 \pm 0.005 \times 10^{-9}$ mol.g^{-1} (McDonough and Sun, 1995) and $4.3 \pm 0.2 \times 10^{-9}$ mol.g^{-1} (Allègre *et al.*, 2001) respectively, so that the normalized osmium concentration of the shallow mantle $[Os]_s^*$ must be 0.0042 ± 0.0013. The $^{187}Os/^{188}Os$ ratio of the shallow mantle is taken as 0.1296 ± 0.0008 (Meisel et al., 2001), the $^{187}Os/^{188}Os$ ratio of carbonaceous chondrites averages 0.1260 ± 0.0021 (Walker *et al.*, 2001), and the initial solar system $^{187}Os/^{188}Os$ ratio is 0.0953 ± 0.0013 (Chen *et al.*, 1998), thus the Re/Os fractionation factor f_s^{Re} of the shallow mantle after addition of the late veneer, assumed to occur soon after core formation at ~ 4.5 Ga (Allègre *et al.*, 1995), is calculated to be 0.12 ± 0.08. Combining all of these estimates results in the following relationship between D^{Re} and D^{Os} (uncertainty is 2σ and was calculated using Monte-Carlo simulation),

$$D^{Re} = 1.6 \pm 1.2 \times 10^{-4} + D^{Os}. \qquad (2)$$

D^{Os} is necessarily positive implying that D^{Re} must be higher than $\sim 0.7 \times 10^{-4}$.

The distribution of highly siderophile elements in the silicate Earth is not uniform as shown by the variable osmium isotopic compositions of mantle rocks. Much of the variation in $^{187}Os/^{188}Os$ ratios of mantle volcanics is undoubtedly caused by the recycling of ancient oceanic crust (Hauri and Hart, 1993). However, in certain plumes, the high $^{187}Os/^{188}Os$ ratios are coupled with high $^{186}Os/^{188}Os$ ratios, reflecting a source with long-term elevated Re/Os and Pt/Os ratios (Walker *et al.*, 1997a; Brandon *et al.*, 1998; Brandon *et al.*, 1999). Unrealistically high proportions of oceanic crust would be required to explain the highest $^{186}Os/^{188}Os$ ratios (Brandon *et al.*, 1999). Furthermore, recycling is unlikely to produce the observed correlation between $^{187}Os/^{188}Os$ and $^{186}Os/^{188}Os$ ratios (Brandon *et al.*, 1999).

Several authors have proposed a different explanation for the high $^{186}Os/^{188}Os$ ratios, namely that they reflect Os added to the lower mantle from the evolved outer core. This reservoir is thought to have a high Pt/Os ratio, and thus a high $^{186}Os/^{188}Os$ ratio (Walker *et al.*, 1995; Walker *et al.*, 1997a; Brandon *et al.*, 1998; Brandon *et al.*, 1999). This model, though intriguing, may also present some difficulties. Addition of outer core material may shift the Pb isotopic composition away from the northern hemisphere regression line, which is not observed (Widom and Shirey, 1996). Simple addition of metal from the outer core would raise the PGE content of the lower mantle to unrealistically high levels (Puchtel and Humayun, 2000) and would be expected to lead to high Re/Yb

ratios, which again are not observed (Hauri and Hart, 1997; Righter and Hauri, 1998). Simple addition of metallic iron also may not be compatible with the f_{O_2} of the lower mantle (Righter and Hauri, 1998). None of these objections is fatal to the core-derived Os model. For example, the effect of core addition on the Pb budget depends on the Pb concentration of the core, which is model dependent (Widom and Shirey, 1996; Allègre *et al.*, 2001). In order to get around the problem of overly high PGE contents, Puchtel and Humayun (2000) suggested that the Os isotopic composition of the outer core is imprinted on the lower mantle by Os isotopic equilibration at the core-mantle boundary, rather than by simple physical admixture. Thus, mechanisms may exist for getting Os from the outer core into the deep mantle. However, these mechanisms are complex, leading us to wonder whether a simpler alternative exists.

In line with the interpretation we advocated for the shallow mantle, we propose an alternative explanation for the coupled enrichment in ^{187}Os and ^{186}Os of certain plumes (Fig. 1). Rare gas systematics indicate that parts of the deep mantle have remained largely isolated since very early in Earth history (Kurz *et al.*, 1982; Honda *et al.*, 1991; Marty *et al.*, 1998). It seems likely that such regions would have assimilated smaller proportions of the late veneer than the shallow mantle, and thus may have partially retained the fractionated highly siderophile element pattern inherited from the metal/silicate segregation event (Walker *et al.*, 1997a; Walker *et al.*, 1997b; O'Neill and Palme, 1998). This view is in accord with recent "lava lamp" models of the Earth's mantle (Kellogg *et al.*, 1999), in which convective isolation of deep and shallow mantle reservoirs is stabilized by a minor density difference. For the sake of simplicity, we shall consider that the highly siderophile element contribution of the residual mantle left over after core formation $[X]_r$ is constant although we realize that this may not be true because partition coefficients vary with pressure and temperature. We consider instead that the contribution of the late veneer $[X]_l$ varies between the deep and shallow mantle. If we assume that the deep mantle behaved as a closed system since the time of its formation then it is straightforward to demonstrate, applying mass-balance equations at the time of core formation for ^{187}Re and ^{188}Os in the shallow mantle and for ^{187}Re, ^{188}Os, and ^{190}Pt in the deep mantle, that there must be a relationship between D^{Pt} and D^{Os} of the form (Appendix),

$$D^{Pt} = x\,[Os]_s^* f_s^{Re} f_d^{Pt} / f_d^{Re} + D^{Os}. \qquad (3)$$

Subscript d denotes the deep mantle and f_d^{Pt} is the Pt/Os fractionation factor after addition of the late veneer $(^{190}Pt/^{188}Os)_d/(^{190}Pt/^{188}Os)_l - 1$. The ^{186}Os/^{188}Os and ^{187}Os/^{188}Os ratios of the deep mantle are taken to be 0.1198500 ± 0.0000068 and

0.1364758±0.0000095 respectively from the most extreme sample (Hualali) of the Hawaiian trend (Brandon *et al.*, 1999), the $^{186}Os/^{188}Os$ ratio of carbonaceous chondrites is estimated to be 0.119831 ± 0.0000061 (Allende meteorite) (Walker *et al.*, 1997a), and the $^{190}Pt/^{188}Os$ ratio of Allende is 0.0016 ± 0.0001 (Jochum, 1996), thus the Re/Os and Pt/Os fractionation factors after addition of the late veneer f_d^{Re} and f_d^{Pt} are calculated to be 0.3 ± 0.1 and 1.8 ± 0.9, respectively. Note that the ratio f_d^{Pt}/f_d^{Re} depends on the slope of the $^{187}Os/^{188}Os$ – $^{186}Os/^{188}Os$ correlation rather than the exact composition of the plume end-member. Therefore, any point lying along the observed trend will yield the same final result. Combining all these estimates results in the following relationship between D^{Pt} and D^{Os} (uncertainty is 2σ and was calculated using Monte-Carlo simulation),

$$D^{Pt} = 8.0 \pm 6.2 \times 10^{-4} + D^{Os}. \quad (4)$$

D^{Os} is necessarily positive implying that D^{Pt} must be higher than $\sim 3.5 \times 10^{-4}$.

Our model makes some specific predictions about the HSE concentrations in the deep mantle source of basalts with high $^{186}Os/^{188}Os$ ratios. Assuming that the residue left by core formation contained essentially no ^{188}Os, and that the ^{187}Re concentration of the residue was uniform, the relative concentrations in the deep and shallow mantle reservoirs can be calculated from the difference in their $^{187}Os/^{188}Os$ ratios relative to that of carbonaceous chondrites. We assume here that some fraction of the late veneer has been added directly to the deep mantle, but the final conclusions will be identical if an uncontaminated residue is mixed with shallow mantle material prior to basalt generation. For the shallow mantle, the ratio of ^{187}Os derived from radioactive decay of Re in the residue relative to ^{188}Os (all from the late veneer) is 0.0036 (0.1296-0.1260). For the deep mantle, assuming a present day $^{187}Os/^{188}Os$ ratio similar to that of Hualali, this ratio is 0.0105 (0.1365-0.1260), about three times higher than that of the upper mantle. Since the concentrations of ^{187}Os derived from ^{187}Re in the fractionated residue is assumed to be the same thoughout the mantle, this difference implies that the ^{188}Os concentration of the deep mantle is about 3 times lower than that of the upper mantle. Expressed formally, $[^{188}Os]_s/[^{188}Os]_d = f_d^{Re}/f_s^{Re} = 3^{+3}_{-1}$. Why then, do OIBs derived from the deep mantle usually have Os concentrations considerably higher than those of MORBs (Schiano *et al.*, 1997)? A simple answer is that core formation depleted the residual silicate Earth in sulfur, as well as in HSE (Morgan, 1986; Li and Agee, 2001a). The shallow mantle would have been largely refertilized in S by the late veneer, while the deep mantle would have received about a third as much of this component. Since sulfides are the dominant host of PGEs in the mantle, loss of this phase during partial

melting would greatly decrease the $D^{sol/liq}$ partition coefficients for these elements. Thus basalts with Os concentrations of 200 or 300 ppt could be produced from a deep source region with only about 1 ppb Os, while the upper mantle, with about 3 ppb Os but a higher sulfide content, would produce MORBs with the much lower concentrations observed. Rhenium, being a less thiophile element, would be much less strongly affected by the loss of sulfides. The generally lower Re concentrations of OIBs (Hauri and Hart, 1997) would then reflect the lower Re concentration of their deep source region. Thus, our model makes prediction about the Os and Re concentrations of basalts that are in excellent agreement with the observations.

Conclusions

Based on the osmium isotopic composition of the mantle, we estimated that D^{Re} and D^{Pt} must be higher than 0.7×10^{-4} and 3.5×10^{-4}, respectively. Recent experimental studies do not favor such high values for D^{Re} (Ertel *et al.*, 2001) and D^{Pt} (Holzheid *et al.*, 2000) compared with D^{Os} (Borisov and Walker, 2000) but further experimental work is needed before a definitive answer can be given to this long-standing problem. Indeed, it was recently suggested that the abundance of moderately siderophile elements in Earth's mantle was set by equilibrium partitioning at model pressures (40 to 60 Gpa) and temperatures (2000 to 4000 K) much higher (Gessmann and Rubie, 2000; Li and Agee, 2001b) than those investigated by partitioning experiments of highly siderophile elements (Borisov and Walker, 2000; Holzheid *et al.*, 2000; Ertel *et al.*, 2001). One might also question whether metal segregated from silicate at uniform pressure and temperature. If not, HSEs partition coefficients must be integrated over the complete liquid column and knowledge of HSE behavior at all pressures and temperatures existing between the surface and the core-mantle boundary is necessary. One particular problem complicating the interpretation of experimental results is the frequent presence of HSE micronuggets in the silicate glass phase. While some authors (Ertel *et al.*, 2001) view these as experimental artifacts that must be avoided, a very recent study (Cottrell and Walker, 2002) suggests that these micronuggets may in fact be quench products. If true, then the silicate/metal partition coefficient of platinum and rhenium may be several orders of magnitude higher than conventionally assumed. Finally, it must be stressed that the behavior of HSEs in multicomponent natural systems is extremely complex and poorly understood, and trace phases, HSE molecular clusters (Tredoux *et al.*, 1995), and non-equilibrium partitioning may play important roles (Ballhaus and Sylvester, 2000).

The late accreting veneer probably contributed a significant fraction of the hydrogen, carbon, nitrogen, sulphur, selenium, and tellurium in our planet because the level of

depletion of these elements in Earth's shallow mantle relative to carbonaceous chondrites is comparable within a factor of ten to that of highly siderophile elements (McDonough and Sun, 1995; Dauphas and Marty, 2002). If the late veneer was not fully homogenized in the whole mantle, then isotopic and elemental stratification of the silicate Earth for some of these elements should be observable, which seems to be the case (Deloule *et al.*, 1991; Dauphas and Marty, 1999).

Thus fractionation of highly siderophile element ratios in the silicate Earth by core formation, followed by inhomogeneous addition of a carbonaceous late veneer, may explain many aspects of the siderophile and volatile budget of the mantle. This model makes specific predictions about Re, Os, and Pt partition coefficients. These predictions will become testable as our knowledge of core formation conditions increases, and as experiments capable of predicting highly siderophile element behavior under those conditions become possible. Given our current level of understanding of HSE partitioning behavior, the osmium isotope systematics of the mantle does not preclude the possibility that the late veneer was composed mainly of material similar in composition to carbonaceous chondrites.

Acknowledgements

We are grateful to K. Suzuki and an anonymous referee for constructive reviews of the manuscript. This work benefited from fruitful comments by T. Meisel and A.D. Brandon as well as discussions with M. Toplis and A.J. Naldrett. This is CRPG contribution 1566.

References

Allègre, C.J. and Luck, J.-M. (1980) Osmium isotopes as petrogenetic and geological tracers. *Earth Planet. Sci. Lett.* **48**, 148-154.

Allègre, C.J., Manhès, G. and Göpel, C. (1995) The age of the Earth. *Geochim. Cosmochim. Acta* **59**, 1445-1456.

Allègre, C., Manhès, G. and Lewin, E. (2001) Chemical composition of the Earth and the volatility control on planetary genetics. *Earth Planet. Sci. Lett.* **185**, 49-69.

Ballhaus, C. and Sylvester, P. (2000) Noble metals enrichment processes in the Merensky Reef, Bushveld Complex. *J. Petrol.* **41**, 545-561.

Borisov, A. and Walker, R.J. (2000) Os solubility in silicate melts: New efforts and results. *Am. Mineral.* **85**, 912-917.

Brandon, A.D., Walker, R.J., Morgan, J.W., Norman, M.D. and Prichard H.M. (1998) Coupled ^{186}Os and ^{187}Os evidence for core-mantle interaction. *Science* **280**, 1570-1573.

Brandon, A.D., Norman, M.D., Walker, R.J. and Morgan, J.W. (1999) ^{186}Os $-^{187}$ Os systematics of Hawaiian picrites. *Earth Planet. Sci. Lett.* **174**, 25-42.

Chen, J.H., Papanastassiou, D.A. and Wasserburg, G.J. (1998) Re-Os systematics in chondrites and the fractionation of the platinum group elements in the early solar system. *Geochim. Cosmochim. Acta* **62**, 3379-3392.

Chyba, C.F. (1990) Impact delivery and erosion of planetary oceans in the early inner Solar System. *Nature* **343**, 129-133.

Chyba, C. and Sagan, C. (1992) Endogenous production, exogenous delivery and impact-shock synthesis of organic molecules: an inventory for the origins of life. *Nature* **355**, 125-132.

Clayton, R.N., Mayeda, T.K. and Rubin, A.E. (1984) Oxygen isotopic compositions of enstatite chondrites and aubrites. *J. Geophys. Res* **89**, C245-C249.

Cottrell, E.A. and Walker, D. (2002) A new look at Pt solubility in silicate liquid. *Lunar Planet. Sci.* **XXXIII**, #1274.

Dauphas, N. and Marty, B. (1999) Heavy nitrogen in carbonatites of the Kola peninsula: a possible signature of the deep mantle. *Science* **286**, 2488-2490.

Dauphas, N., Robert, F. and Marty, B. (2000) The late asteroidal and cometary bombardment of Earth as recorded in water deuterium to protium ratio. *Icarus* **148**, 508-512.

Dauphas, N. and Marty, B. (2002) Inference on the nature and the mass of Earth's late veneer from noble metals and gases. *J. Geophys. Res.*, in press.

Dauphas, N., Marty, B. and Reisberg L. (2002) Inference on terrestrial genesis from molybdenum isotope systematics. *Geophys. Res. Lett.*, in press.

Deloule, E., Albarède, F. and Sheppard, S.M.F. (1991) Hydrogen isotope heterogeneities in the mantle from ion probe analysis of amphiboles from ultramafic rocks. *Earth Planet. Sci. Lett.* **105**, 543-553.

Ertel, W., O'Neill, H.St.C., Sylvester, P.J., Dingwell, D.B. and Spettel, B. (2001) The solubility of rhenium in silicate melts: Implications for the geochemical properties of rhenium at high temperatures. *Geochim. Cosmochim. Acta* **65**, 2161-2170.

Gessmann, C.K. and Rubie, D.C. (2000) The origin of the depletions of V, Cr and Mn in the mantles of the Earth and Moon. *Geochim. Cosmochim. Acta* **184**, 95-107.

Handler, M.R., Bennett, V.C. and Esat, T.M. (1997) The persistence of off-cratonic lithospheric mantle: Os isotopic systematics of variably metasomatised southeast Australian xenoliths. *Earth Planet. Sci. Lett.* **151**, 61-75.

Hauri, E.H. and Hart, S.R. (1993) Re-Os isotope systematics of HIMU and EMII oceanic island basalts from the South Pacific Ocean. *Earth Planet. Sci. Lett.* **114**, 353-371.

Hauri, E.H. and Hart, S.R. (1997) Rhenium abundances and systematics in oceanic basalts. *Chem. Geol.* **139**, 185-205.

Holzheid, A., Sylvester, P., O'Neill, H. St C., Rubie, D.C., and Palme, H. (2000) Evidence for a late chondritic veneer in the Earth's mantle from high-pressure partitioning of palladium and platinum. *Nature* **406**, 396-399.

Honda, M., McDougall, I., Patterson, D.B., Doulgeris, A. and Clague D.A. (1991) Possible solar noble-gas component in Hawaiian basalts. *Nature* **349**, 149-151.

Jagoutz, E., Palme, H., Baddenhausen, H., Blum, K., Cendales, M., Dreibus, G., Spettel, B., Lorenz, V. and Wänke, H. (1979) The abundances of major, minor and trace elements in the Earth's mantle as derived from primitive ultramafic nodules. *Proc. Lunar Planet. Sci. Conf.* **X**, 2031-2050.

Javoy, M. (1998) The birth of the Earth's atmosphere: the behaviour and fate of its major elements. *Chem. Geol.* **147**, 11-25.

Jochum, K.P. (1996) Rhodium and other platinum-group elements in carbonaceous chondrites. *Geochim. Cosmochim. Acta* **60**, 3353-3357.

Jones, J.H. and Drake, M.J. (1986) Geochemical constraints on core formation in the Earth. *Nature* **322**, 221-228.

Kellogg, L.H., Bradford, H.H. and van der Hilst, R.D. (1999) Compositional stratification in the deep mantle. *Science* **283**, 1881-1884.

Kimura, K., Lewis, R.S. and Anders, E. (1974) Distribution of gold and rhenium between nickel-iron and silicate melts: implications for the abundance of siderophile elements on the Earth and Moon. *Geochim. Cosmochim. Acta* **38**, 683-701.

Kurz, M.D., Jenkins, W.J. and Hart, S.R. (1982) Helium isotopic systematics of oceanic islands and mantle heterogeneity. *Nature* **297**, 43-47.

Li, J. and Agee, C.B. (1996) Geochemistry of mantle-core differentiation at high pressure. *Nature* **381**, 686-689.

Li, J. and Agee, C.B. (2001a) Element partitioning constraints on the light element composition of the Earth's core. *Geophys. Res. Lett.* **28**, 81-84.

Li, J. and Agee, C.B. (2001b) The effect of pressure, temperature, oxygen fugacity and composition on partitioning of nickel and cobalt between liquid Fe-Ni-S alloy and liquid silicate: implications for the Earth's core formation. *Geochim. Cosmochim. Acta* **65**, 1821-1832.

Marty, B., Tolstikhin, I.N., Kamensky, I.L., Nivin, V., Balaganskaya, E. and Zimmermann, J.L. (1998) Plume-derived rare gases in 380 Ma carbonatites from the Kola region (Russia) and the argon isotopic composition in the deep mantle. *Earth Planet. Sci. Lett.* **164**, 179-192.

McBride, J.S., Lambert, D.D., Creig, A. and Nicholls, I.A. (1996) Multistage evolution of Australian subcontinental mantle: Re-Os isotopic constraints from Victorian mantle xenoliths. *Geology* **24**, 631-634.

McDonough, W.F. and Sun, S.-s. (1995) The composition of the Earth. *Chem. Geol.* **120**, 223-253.

Meisel, T., Walker, R.J. and Morgan, J.W. (1996) The osmium isotopic composition of the Earth's primitive upper mantle. *Nature* **383**, 517-520.

Meisel, T., Walker, R.J., Irving, A.J. and Lorand, J.-P. (2001) Osmium isotopic compositions of mantle xenoliths: a global perspective. *Geochim. Cosmochim. Acta* **65**, 1311-1323.

Morbidelli, A., Chambers, J., Lunine, J.I., Petit, J.M., Robert, F., Valsecchi, G.B. and Cyr, K.E. (2000) Source regions and timescales for the delivery of water to the Earth. *Meteoritics Planet. Sci.* **35**, 1309-1320.

Morgan, J.W.(1985) Osmium isotope constraints on Earth's late accretionary history. *Nature* **317**, 703-705.

Morgan, J.W. (1986) Ultramafic xenoliths: clues to Earth's late accretionary history. *J. Geophys. Res.* **91**, 12375-12387.

Morgan J.W., Walker, R.J., Brandon, A.D. and Horan, M.F. (2001) Siderophile ele-

ments in Earth's upper mantle and lunar breccias: Data synthesis suggests manifestations of the same late influx. *Meteoritics Planet. Sci.*, **36**, 1257-1276.

Murthy, V.R. (1991) Early differentiation of the Earth and the problem of mantle siderophile elements: a new approach. *Science* **253**, 303-306; corrections **253**, 1467.

O'Neill, H.St.C. and Palme, H. (1998) Composition of the silicate Earth: implications for accretion and core formation. *The Earth's Mantle: Structure, Composition and Evolution* (Jackson, I., ed.), 3-126, Cambridge Univ. Press, Cambridge.

Peslier, A., Reisberg, L., Ludden, J. and Francis, D. (2000) Os isotopic systematics in mantle xenoliths; age constraints on the Canadian Cordillera lithosphere. *Chem. Geol.* **166**, 85-101.

Puchtel, I. and Humayun, M. (2000) Platinum group elements in Kostomuksha komatiites and basalts: Implications for oceanic crust recycling and core-mantle interaction. *Geochim. Cosmochim. Acta* **64**, 4227-4242.

Reisberg, L., Lorand, J.-P., Bedini, R. and Bodinier, J.-L. (2000) Os isotopic and PGE results from spinel peridotites of the East African Rift. *J. Conf. Abs.* **5**, 837.

Reisberg, L., Zhi, X., Peng, Z., Wagner, C. and Sun, W. (2001) The mantle lithosphere beneath eastern China: trace element and Os isotopic results from spinel peridotite xenoliths from Jiangsu Province. *J. Conf. Abs.* **6**, 355.

Righter, K. and Drake, M.J. (1997) Metal-silicate equilibrium in a homogeneously accreting earth: new results for Re. *Earth Planet. Sci. Lett.* **146**, 541-553.

Righter, K. and Hauri, E.H. (1998) Compatibility of rhenium in garnet during mantle melting and magma genesis. *Science* **280**, 1737-1741.

Schiano, P., Birck, J.-L. and Allègre C.-J. (1997) Osmium-strontium-neodymium-lead isotopic covariations in mid-ocean ridge basalt glasses and the heterogeneity of the upper mantle. *Earth Planet. Sci. Lett.* **150**, 363-379.

Shukolyukov, A. and Lugmair, G.W. (1998) The ^{53}Mn-^{53}Cr isotope system in the Indarch EH4 chondrite: a further argument for ^{53}Mn heterogeneity in the early solar system. *Lunar Planet. Sci.* **XXIX**, #1208.

Smoliar, M.I., Walker, R.J. and Morgan, J.W. (1996) Re-Os ages of group IIA, IIIA, IVA, and IVB iron meteorites. *Science* **271** 1099-1102.

Snow, J.E., Schmidt, G. and Rampone, E. (2000) Os isotopes and highly siderophile elements (HSE) in the Ligurian ophiolites, Italy. *Earth Planet. Sci. Lett.* **175**, 119-132.

Stevenson, D.J. (1990) Fluid dynamics of core formation. *Origin of the Earth* (Newsom, H.E. and Jones, J.H., eds.), 231-249, Oxford Univ. Press, Oxford.

Tredoux, M., Lindsay, N.M., Davies, G. and McDonald, I. (1995) The fractionation

of platinum-group elements in magmatic systems, with the suggestion of a novel causal mechanism. *S. Afr. J. Geol.* **98**, 157-167.

Walker, R.J., Morgan, J.W. and Horan, M.F. (1995) Osmium-187 enrichment in some plumes: evidence for core-mantle interaction? *Science* **269**, 819-825.

Walker, R.J., Morgan, J.W., Beary, E.S., Smoliar, M.I., Czamanske, G.K. and Horan, M.F. (1997a) Applications of the $^{190}Pt - ^{186}Os$ isotope system to geochemistry and cosmochemistry. *Geochim. Cosmochim. Acta* **61**, 4799-4807.

Walker, R.J., Morgan, J.W., Hanski, E.J. and Smolkin, V.F. (1997b) Re-Os systematics of Early Proterozoic ferropicrites, Pechenga Complex, northwestern Russia: evidence for ancient ^{187}Os-enriched plumes. *Geochim. Cosmochim. Acta* **61**, 3145-3160.

Walker, R.J., Horan, M.F., Morgan, J.W. and Meisel, T. (2001) Osmium isotopic compositions of chondrites and Earth's primitive upper mantle: constraints on the late veneer. *Lunar Planet. Sci.* **XXXII**, #1152.

Widom, E. and Shirey, S.B. (1996) Os isotope systematics in the Azores: implications for mantle plume sources. *Earth Planet. Sci. Lett.* **142**, 451-465.

A Appendix

The late veneer was mixed with the fractionated residue left over after core-mantle segregation. The two mass balance equations that formalize this idea are,

$$[\mathrm{X}]_m = [\mathrm{X}]_r + [\mathrm{X}]_l, \tag{A.1}$$

$$[\mathrm{X}]_\oplus = [x/\mathrm{D}^\mathrm{X} + (1-x)][\mathrm{X}]_r, \tag{A.2}$$

where $[\mathrm{X}]_m$ corresponds to the present concentration of nuclide X in the mantle, $[\mathrm{X}]_r$ is the concentration remaining immediately after core formation, $[\mathrm{X}]_l$ is the concentration derived from the late veneer, $[\mathrm{X}]_\oplus$ is the concentration of the bulk Earth prior to late veneer addition, D^X is the silicate/metal partition coefficient, and x is the mass fraction of metal in the Earth. In the case of highly siderophile elements, $1-x$ is negligible compared with x/D^X, so equation (A.2) reduces to $[\mathrm{X}]_\oplus \simeq (x/\mathrm{D}^\mathrm{X})[\mathrm{X}]_r$.

Shallow Mantle

In the case of the shallow mantle, mass-balance equations (A.1, A.2) can be applied to $^{187}\mathrm{Re}$ and $^{188}\mathrm{Os}$ after core formation and late veneer addition,

$$\left(\frac{^{187}\mathrm{Re}}{^{188}\mathrm{Os}}\right)_s [^{188}\mathrm{Os}]_s = [^{187}\mathrm{Re}]_r + \left(\frac{^{187}\mathrm{Re}}{^{188}\mathrm{Os}}\right)_l [^{188}\mathrm{Os}]_l, \tag{A.3}$$

$$[^{188}\mathrm{Os}]_s = [^{188}\mathrm{Os}]_r + [^{188}\mathrm{Os}]_l, \tag{A.4}$$

$$[^{187}\mathrm{Re}]_r = [^{187}\mathrm{Re}]_\oplus \frac{\mathrm{D}^\mathrm{Re}}{x}. \tag{A.5}$$

$$[^{188}\mathrm{Os}]_r = [^{188}\mathrm{Os}]_\oplus \frac{\mathrm{D}^\mathrm{Os}}{x}, \tag{A.6}$$

The subscript s denotes shallow mantle. There are four mass-balance equations (A.3-A.6) in five unknowns $[^{187}\mathrm{Re}]_r$, $[^{188}\mathrm{Os}]_r$, $[^{188}\mathrm{Os}]_l$, D^Re, and D^Os, so that one must fix a parameter to compute the remaining four. Combining equations (A.3-A.6) results in,

$$\left(\frac{^{187}\mathrm{Re}}{^{188}\mathrm{Os}}\right)_s [^{188}\mathrm{Os}]_s = [^{187}\mathrm{Re}]_\oplus \frac{\mathrm{D}^\mathrm{Re}}{x} + \left(\frac{^{187}\mathrm{Re}}{^{188}\mathrm{Os}}\right)_l \left([^{188}\mathrm{Os}]_s - [^{188}\mathrm{Os}]_\oplus \frac{\mathrm{D}^\mathrm{Os}}{x}\right). \tag{A.7}$$

The Re/Os fractionation factor in the shallow mantle after core formation and late veneer addition is defined as,

$$f_s^\mathrm{Re} = \left(\frac{^{187}\mathrm{Re}}{^{188}\mathrm{Os}}\right)_s \Big/ \left(\frac{^{187}\mathrm{Re}}{^{188}\mathrm{Os}}\right)_l - 1. \tag{A.8}$$

This factor can be calculated using osmium isotopes,

$$f_s^{\mathrm{Re}} = \left[\left(\frac{^{187}\mathrm{Os}}{^{188}\mathrm{Os}}\right)_s - \left(\frac{^{187}\mathrm{Os}}{^{188}\mathrm{Os}}\right)_l\right] / \left[\left(\frac{^{187}\mathrm{Os}}{^{188}\mathrm{Os}}\right)_l - \left(\frac{^{187}\mathrm{Os}}{^{188}\mathrm{Os}}\right)_i\right], \qquad (A.9)$$

where the subscript i denotes *initial*.

The late veneer Re/Os ratio was nearly equal to that of the bulk Earth,

$$[^{187}\mathrm{Re}]_\oplus = \left(\frac{^{187}\mathrm{Re}}{^{188}\mathrm{Os}}\right)_l [^{188}\mathrm{Os}]_\oplus, \qquad (A.10)$$

so that equation (A.7) can be rewritten as,

$$f_s^{\mathrm{Re}}[^{188}\mathrm{Os}]_s = [^{188}\mathrm{Os}]_\oplus \frac{\mathrm{D}^{\mathrm{Re}}}{x} - [^{188}\mathrm{Os}]_\oplus \frac{\mathrm{D}^{\mathrm{Os}}}{x}. \qquad (A.11)$$

The normalized non-radiogenic Os concentration is defined as,

$$[\mathrm{Os}]_s^* = \frac{[^{188}\mathrm{Os}]_s}{[^{188}\mathrm{Os}]_\oplus} \simeq \frac{[\mathrm{Os}]_s}{[\mathrm{Os}]_\oplus}. \qquad (A.12)$$

Thus, there must be a relationship between D^{Re} and D^{Os} of the form,

$$\mathrm{D}^{\mathrm{Re}} = x\,[\mathrm{Os}]_s^* f_s^{\mathrm{Re}} + \mathrm{D}^{\mathrm{Os}}. \qquad (A.13)$$

Deep Mantle

For the sake of simplicity, we shall consider that the highly siderophile element contribution of the residual mantle left over after core formation $[\mathrm{X}]_r$ was constant while the contribution of the late veneer $[\mathrm{X}]_l$ varied between the deep and shallow mantle. In the case of the deep mantle, mass-balance equations (A.1, A.2) can be applied to $^{187}\mathrm{Re}$, $^{188}\mathrm{Os}$, and $^{190}\mathrm{Pt}$ after core formation and late veneer addition,

$$\left(\frac{^{187}\mathrm{Re}}{^{188}\mathrm{Os}}\right)_d [^{188}\mathrm{Os}]_d = [^{187}\mathrm{Re}]_r + \left(\frac{^{187}\mathrm{Re}}{^{188}\mathrm{Os}}\right)_l [^{188}\mathrm{Os}]_l, \qquad (A.14)$$

$$[^{188}\mathrm{Os}]_d = [^{188}\mathrm{Os}]_r + [^{188}\mathrm{Os}]_l, \qquad (A.15)$$

$$\left(\frac{^{190}\mathrm{Pt}}{^{188}\mathrm{Os}}\right)_d [^{188}\mathrm{Os}]_d = [^{190}\mathrm{Pt}]_r + \left(\frac{^{190}\mathrm{Pt}}{^{188}\mathrm{Os}}\right)_l [^{188}\mathrm{Os}]_l, \qquad (A.16)$$

using the expression for D^{Re} given by equation (A.13),

$$[^{187}Re]_r = [^{187}Re]_\oplus \left([Os]_s^* f_s^{Re} + \frac{D^{Os}}{x} \right), \tag{A.17}$$

$$[^{188}Os]_r = [^{188}Os]_\oplus \frac{D^{Os}}{x}, \tag{A.18}$$

$$[^{190}Pt]_r = [^{190}Pt]_\oplus \frac{D^{Pt}}{x}. \tag{A.19}$$

There are six mass-balance equations (A.14-A.19) in seven unknowns $[^{187}Re]_r$, $[^{188}Os]_d$, $[^{188}Os]_r$, $[^{188}Os]_l$, D^{Os}, and D^{Pt}, so that one must fix a parameter to compute the remaining six. The Re/Os fractionation factor in the deep mantle after core formation and late veneer addition is defined as,

$$f_d^{Re} = \left(\frac{^{187}Re}{^{188}Os} \right)_d / \left(\frac{^{187}Re}{^{188}Os} \right)_l - 1. \tag{A.20}$$

As discussed in the case of the shallow mantle (A.9), this factor can be calculated using osmium isotopes,

$$f_d^{Re} = \left[\left(\frac{^{187}Os}{^{188}Os} \right)_d - \left(\frac{^{187}Os}{^{188}Os} \right)_l \right] / \left[\left(\frac{^{187}Os}{^{188}Os} \right)_l - \left(\frac{^{187}Os}{^{188}Os} \right)_i \right]. \tag{A.21}$$

Equation (A.11) holds for rhenium in the deep mantle as well,

$$f_d^{Re}[^{188}Os]_d = [^{188}Os]_\oplus \frac{D^{Re}}{x} - [^{188}Os]_\oplus \frac{D^{Os}}{x}. \tag{A.22}$$

D^{Re} is related to D^{Os} through equation (A.13) so that equation (A.22) can be rewritten as,

$$f_d^{Re}[^{188}Os]_d = [^{188}Os]_\oplus [Os]_s^* f_s^{Re}. \tag{A.23}$$

The Pt/Os fractionation factor in the deep mantle after core formation and late veneer addition is defined as,

$$f_d^{Pt} = \left(\frac{^{190}Pt}{^{188}Os} \right)_d / \left(\frac{^{190}Pt}{^{188}Os} \right)_l - 1. \tag{A.24}$$

This factor can be calculated using osmium isotopes and the chondritic Pt/Os ratio,

$$f_d^{Pt} \simeq \left[\left(\frac{^{186}Os}{^{188}Os} \right)_d - \left(\frac{^{186}Os}{^{188}Os} \right)_l \right] / \left[\left(\frac{^{190}Pt}{^{188}Os} \right)_l \lambda_{190} T \right], \tag{A.25}$$

where λ_{190} is the decay constant of ^{190}Pt and T is the age of the Earth.

Equations (A.11, A.22) hold for Pt in the deep mantle as well,

$$f_d^{\mathrm{Pt}}[^{188}\mathrm{Os}]_d = [^{188}\mathrm{Os}]_\oplus \frac{\mathrm{D}^{\mathrm{Pt}}}{x} - [^{188}\mathrm{Os}]_\oplus \frac{\mathrm{D}^{\mathrm{Os}}}{x}. \qquad \text{(A.26)}$$

Combining equations (A.23, A.26), it is straightforward to demonstrate that there must be a relationship between D^{Pt} and D^{Os} of the form,

$$\mathrm{D}^{\mathrm{Pt}} = x\,[\mathrm{Os}]_s^* f_s^{\mathrm{Re}} f_d^{\mathrm{Pt}} / f_d^{\mathrm{Re}} + \mathrm{D}^{\mathrm{Os}}. \qquad \text{(A.27)}$$

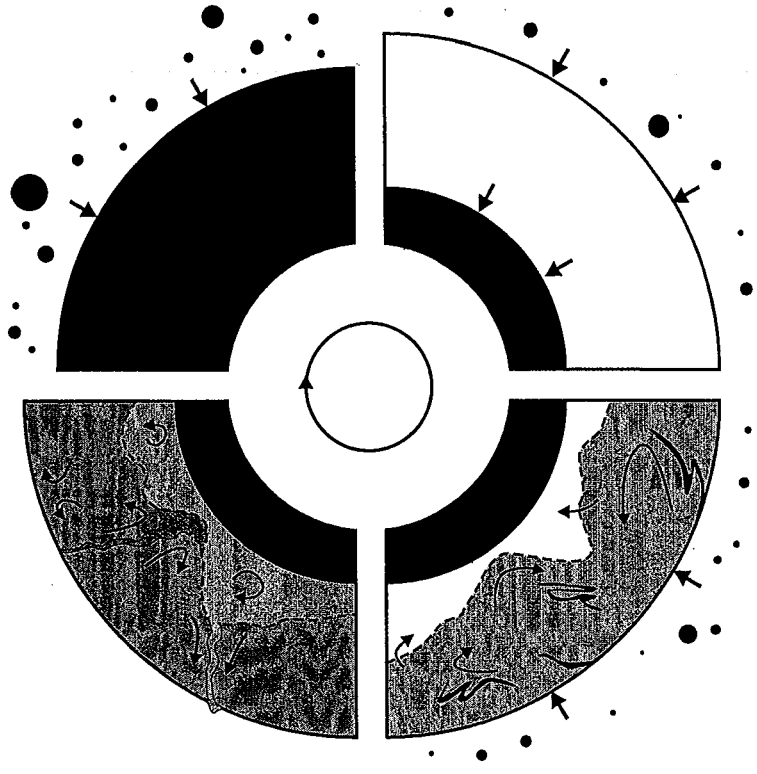

Figure 1: Evolution of the silicate Earth through time. Upper left quarter - The Earth accreted from material of unspecified nature. Upper right quarter - Metal segregated from silicate. Highly siderophile elements in the residual mantle were depleted and strongly fractionated. Lower right quarter - The Earth continued to accrete undifferentiated material after the completion of core formation. This late carbonaceous veneer was mixed with the fractionated residue left over after core formation. Part of the deep mantle was isolated early from shallow convection and thus preserved primordial noble gas and highly siderophile element signatures. Lower left quarter - Some mantle plumes sample distinct portions of the deep mantle that bear highly siderophile element signatures different from that of the shallow mantle because the contribution of the late carbonaceous veneer was not identical in the two regions.

Bibliographie

[1] A.N. Halliday, D.-C. Lee, J.N. Christensen, M. Rehkämper, W. Yi, X. Luo, C.M. Hall, C.J. Ballentine, T. Pettke, and C. Stirling. Applications of multiple collector-ICPMS to cosmochemistry, geochemistry, and paleoceanography. *Geochimica et Cosmochimica Acta*, 62 :919–940, 1998.

[2] N.N. Greenwood and A. Earnshaw. *Chemistry of the Elements.* Pergamon Press, Oxford, 1984.

[3] E. Anders and N. Grevesse. Abundances of the elements : meteoritic and solar. *Geochimica et Cosmochimica Acta*, 53 :197–214, 1989.

[4] N. Dauphas, L. Reisberg, and B. Marty. Solvent extraction, ion chromatography, and mass spectrometry of molybdenum isotopes. *Analytical Chemistry*, 73 :2613–2616, 2001.

[5] S. Amari, R.S. Lewis, and E. Anders. Interstellar grains in meteorites : I. Isolation of SiC, graphite, and diamond ; size distributions of SiC and graphite. *Geochimica et Cosmochimica Acta*, 58 :459–470, 1994.

[6] G.K. Nicolussi, M.J. Pellin, R.S. Lewis, A.M. Davis, S. Amari, and R.N. Clayton. Molybdenum isotopic composition of individual presolar silicon carbide grains from the Murchison meteorite. *Geochimica et Cosmochimica Acta*, 62 :1093–1104, 1998.

[7] G.K. Nicolussi, M.J. Pellin, R.S. Lewis, A.M. Davis, R.N. Clayton, and S. Amari. Zirconium and molybdenum in individual circumstellar graphite grains : new isotopic data on the nucleosynthesis of heavy elements. *The Astrophysical Journal*, 504 :492–499, 1998.

[8] M.J. Pellin, A.M. Davis, R.S. Lewis, S. Amari, and R.N. Clayton. Molybdenum isotopic composition of single silicon carbide grains from supernovae. *Lunar and Planetary Science*, XXX :#1969, 1999.

[9] M.J. Pellin, A.M. Davis, W.F. Calaway, R.S. Lewis, R.N. Clayton, and S. Amari. Zr and Mo isotopic constraints on the origins of unusual types of presolar SiC grains. *Lunar and Planetary Science*, XXXI :#1934, 2000.

[10] Q.Z. Yin, K. Yamashita, and S.B. Jacobsen. Mo and Zr isotopic signatures in the "haystack" : evidence for presolar silicates of supernova origin ? *Lunar and Planetary Science*, XXXI :#1920, 2000.

[11] F.A. Podosek and R.H. Nichols Jr. Short-lived radionuclides in the solar nebula. In T.J. Bernatowicz and E. Zinner, editors, *CP402, Astrophysical Implications of the Laboratory Study of Presolar Materials*, pages 617–647. AIP, Woodbury, 1997.

[12] M. Wadhwa and S.S. Russell. Timescales of accretion and differentiation in the early solar system : the meteoritic evidence. In A.P. Boss and S.S. Russell, editors, *Protostars and Planets IV*, pages 995–1018. The University of Arizona Press, Tucson, 2000.

[13] Q.Z. Yin and S.B. Jacobsen. The ^{97}Tc $-^{97}$ Mo chronometer and its implications for timing of terrestrial accretion and core formation. *Lunar and Planetary Science*, XXIX :#1802, 1998.

[14] D.W. Mittlefehldt, T.J. McCoy, C.A. Goodrich, and A. Kracher. Non-chondritic meteorites from asteroidal bodies. In J.J. Papike, editor, *Planetary Materials, Reviews in Mineralogy 36*, pages 4.1–4.195. Mineralogical Society of America, Washington, 1998.

[15] M. Liu and M.E. Fleet. Partitioning of siderophile elements (W, Mo, As, Ag, Ge, Ga, and Sn) and Si in the Fe-S system and their fractionation in iron meteorites. *Geochimica et Cosmochimica Acta*, 65 :671–682, 2001.

[16] B. Fegley, Jr. and H. Palme. Evidence for oxidizing conditions in the solar nebula from Mo and W depletions in refractory inclusions in carbonaceous chondrites. *Earth and Planetary Science Letters*, 72 :311–326, 1985.

[17] V.R. Murthy. Elemental and isotopic abundances of molybdenum in some meteorites. *Geochimica et Cosmochimica Acta*, 27 :1171–1178, 1963.

[18] G.W. Wetherill. Isotopic composition and concentration of molybdenum in iron meteorites. *Journal of Geophysical Research*, 69 :4403–4408, 1964.

[19] N. Dauphas, B. Marty, and L. Reisberg. Molybdenum evidence for inherited planetary scale isotope heterogeneity of the protosolar nebula. *The Astrophysical Journal*, 565 :640–644, 2002.

[20] N. Dauphas, B. Marty, and L. Reisberg. Inference on terrestrial genesis from molybdenum isotope systematics. *Geophysical Research Letters, in press*, 2002.

[21] N. Dauphas, B. Marty, and L. Reisberg. Molybdenum Nucleosynthetic Dichotomy Revealed in Primitive Meteorites. *The Astrophysical Journal Letters, in press*, 2002.

[22] N. Dauphas, T. Rauscher, H. Schatz, B. Marty, and L. Reisberg. Short-lived p-nuclides in the early solar system, bridging the gap between galactic chemical evolution and solar system formation. *The Astrophysical Journal, submitted*, 2002.

[23] M. Nomura, K. Kogure, and M. Okamoto. Isotopic abundance ratios and atomic weight of zirconium. *International Journal of Mass Spectrometry and Ion Physics*, 50 :219–227, 1983.

[24] M. Huang and A. Masuda. Measurement of the atomic weight of ruthenium by negative ionization mass spectrometry. *Analytical Chemistry*, 69 :1135–1139, 1997.

[25] I.H. Qureshi, L.T. Clendon, and P.D. LaFleur. Exraction studies of the group IIIB-VIIB elemnts and the lanthanides utilizing bis(2-ethyl-hexyl)orthophosphoric acid. *Radiochimica Acta*, 12 :107–111, 1969.

[26] Guide to Ion Exchange. Technical Report 140-9997, BIO-RAD.

[27] A.J.P. Martin and R.L.M. Synge. A new form of chromatogram employing two liquid phases. 1. A theory of chromatography. 2. Application to the micro-determination of the higher monoamino-acids in proteins. *Biochemical Journal*, 35 :1358–1368, 1941.

[28] B. Trémillon. *Les Séparations par les Résines Échangeuses d'Ions*. Gauthier-Villars, Paris, 1965.

[29] K.A. Kraus, F. Nelson, and G.E. Moore. Anion exchange studies. XVII. Molybdenum(VI), tungsten(VI) and uranium(VI) in HCl and HF-HCl solutions. *Journal of the American Chemical Society*, 77 :3972–3977, 1955.

[30] I. Szabo. New optical devices utilizing oscillatory electric fields. I. principles of operation and analytical theory of multipole devices with two-dimensional electric fields. *International Journal of Mass Spectrometry and Ion Processes*, 73 :197–235, 1986.

[31] A.N. Krutchinsky, I.V. Chernushevich, V.L. Spicer, W. Ens, and K.G. Standing. Collisional damping interface for an electrospray ionization time-of-flight mass spectrometer. *Journal of the American Society for Mass Spectrometry*, 9 :569–579, 1998.

[32] D.W.G. Sears and R.T. Dodd. Overview and classification of meteorites. In J.F. Kerridge and M.S. Matthews, editors, *Meteorites and the early solar system*, pages 3–31. The University of Arizona Press, Tucson, 1989.

[33] A.J. Brearley and R.H. Jones. Chondritic meteorites. In J.J. Papike, editor, *Planetary Materials, Reviews in Mineralogy 36*, pages 3.1–3.398. Mineralogical Society of America, Washington, 1998.

[34] R.N. Clayton. Oxygen isotopes in meteorites. *Annual Reviews of Earth and Planetary Sciences*, 21 :115–149, 1993.

[35] C. Arlandini, F. Käppeler, K. Wisshak, R. Gallino, M. Lugaro, M. Busso, and O. Straniero. Neutron capture in low-mass asymptotic giant branch stars : cross sections and abundance signatures. *The Astrophysical Journal*, 525 :886–900, 1999.

[36] S. Van Eck, A. Jorissen, S. Udry, M. Mayor, and B. Pernier. The HIPPARCOS Hertzsprung-Russell diagram of S stars : probing nucleosynthesis and dredge-up. *Astronomy and Astrophysics*, 329 :971–985, 1998.

[37] D.D. Clayton. *Principles of Stellar Evolution and Nucleosynthesis.* The University of Chicago Press, Chicago, 1983.

[38] T. Rauscher, A. Heger, S.E. Woosley, and R.D. Hoffman. Nuclear aspects of the s- and n-processes in massive stars. In *Proc. 9th Int. Sem. Interactions of Neutrons With Nuclei (ISINN-9), in press*, 2001.

[39] E. Anders and E. Zinner. Interstellar grains in primitive meteorites : diamond, silicon carbide, and graphite. *Meteoritics*, 28 :490–514, 1993.

[40] E. Zinner. Presolar material in meteorites : an overview. In T.J. Bernatowicz and E. Zinner, editors, *CP402, Astrophysical Implications of the Laboratory Study of Presolar Materials*, pages 3–26. AIP, Woodbury, 1997.

[41] Y. Kashiv, Z. Cai, B. Lai, S.R. Sutton, R.S. Lewis, A.M. Davis, R.N. Clayton, and M.J. Pellin. Synchrotron X-ray fluorescence : a new approach for determining trace element concentrations in individual presolar SiC grains. *Lunar and Planetary Science*, XXXII :#2192, 2001.

[42] R. Gallino, M. Lugaro, C. Arlandini, M. Busso, and O. Straniero. Isotopic composition of zirconium and molybdenum in single silicon carbide presolar grains : asymptotic giant branch model prediction and measurements. *Meteoritics and Planetary Science*, 33 :A54, 1998.

[43] T. Bernatowicz, P. Swan, S. Messenger, R. Walker, and S. Amari. Comparative morphology of pristine and chemical-dissolution presolar SiC from Murchison. *Lunar and Planetary Science*, XXXI :#1238, 2000.

[44] T. Lee, D.A. Papanastassiou, and G.J. Wasserburg. Demonstration of ^{26}Mg excess in Allende and evidence for ^{26}Al. *Geophysical Research Letters*, 3 :109–113, 1976.

[45] G.J. MacPherson, A.M. Davis, and E.K. Zinner. The distribution of aluminum-26 in the early Solar System - a reappraisal. *Meteoritics*, 30 :365–386, 1995.

[46] A.E. Rubin. Mineralogy of meteorite groups. *Meteoritics and Planetary Science*, 32 :231–247, 1997.

[47] M.E. Wieser and J.R. De Laeter. Stable isotope dilution analyses of molybdenum in meteorites. *Fresenius' Journal of Analytical Chemistry*, 368 :303–306, 2000.

[48] Qi-Lu and A. Masuda. High accuracy measurement of isotope ratios of molybdenum in some terrestrial molybdenites. *Journal of the American Society for Mass Spectrometry*, 3 :10–17, 1992.

[49] Qi-Lu and A. Masuda. Rapid, high-purity chemical separation of molybdenum from iron meteorites for isotopic analysis by using thermal ionization mass spectrometry. *Analyst*, 117 :869–872, 1992.

[50] Qi-Lu and A. Masuda. The isotopic composition and atomic weight of molybdenum. *International Journal of Mass Spectrometry and Ion Processes*, 130 :65–72, 1994.

[51] Z. Šulcek and P. Povondra. *Methods of decomposition in inorganic analysis.* CRC Press, Boca Raton, 1989.

[52] J. Coca, F.V. Diez, and M.A. Moris. Solvent extraction of molybdenum and tungsten by Alamine 336 and DEHPA. *Hydrometallurgy*, 25 :125–135, 1990.

[53] J.N. Wilson. A theory of chromatography. *Journal of the American Chemical Society*, 62 :1583–1591, 1940.

[54] D. DeVault. The theory of chromatography. *Journal of the American Chemical Society*, 65 :532–540, 1943.

[55] J. Bear. *Dynamics of Fluids in Porous Media.* Elsevier, New-York, 1972.

[56] A.A. Pupyshev, V.N. Muzgin, and A.K. Lutsak. Thermochemical processes and ion transport in inductively coupled plasma mass spectrometry : theoretical description and experimental confirmation. *Journal of Analytical Atomic Spectrometry*, 14 :1485–1492, 1999.

[57] C. Trassy and J.M. Mermet. *Les Applications Analytiques des Plasmas HF.* Lavoisier, Paris, 1984.

[58] P.J. Turner, T.O. Merren, J. Speakman, R.C. Haines, Z. Palacz, and S. Meffan-Main. Ion optics of multi-collector ICP-MS systems for precise and accurate isotope ratio measurements. Technical Report 403, Micromass, 2000.

[59] D.J. Douglas and J.B. French. Collisional focusing effects in radio frequency quadrupoles. *Journal of the American Society for Mass Spectrometry*, 3 :398–408, 1992.

[60] D.J. Douglas. Some current perspectives on ICP-MS. *Canadian Journal of Spectroscopy*, 34 :38–49, 1989.

[61] J.T. Rowan and R.S. Houk. Attenuation of polyatomic ion interferences in inductively coupled plasma mass spectrometry by gas-phase collisions. *Applied Spectroscopy*, 43 :976–980, 1989.

[62] C. Hägg and I Szabo. New ion-optical devices utilizing oscillatory electric fields. II. Stability of ion motion in a two-dimensional hexapole field. *International Journal of Mass Spectrometry and Ion Processes*, 73 :237–275, 1986.

[63] C.N. Maréchal, P. Télouk, and F. Albarède. Precise analysis of copper and zinc isotopic compositions by plasma-source mass spectrometry. *Chemical Geology*, 156 :251–273, 1999.

[64] W.R. Van Schmus and J.A. Wood. A chemical-petrologic classification for chondritic meteorites. *Geochimica et Cosmochimica Acta*, 31 :747–765, 1967.

[65] D. Stöffler, K. Keil, and E.R.D. Scott. Shock metamorphism of ordinary chondrites. *Geochimica et Cosmochimica Acta*, 55 :3845–3867, 1991.

[66] F. Wlotzka. A weathering scale for the ordinary chondrites. *Meteoritics*, 28 :460, 1993.

[67] M.H. Thiemens. Mass-independent isotope effects in planetary atmospheres and the early solar system. *Science*, 283 :341–345, 1999.

[68] F. Robert and C. Camy-Peyret. Ozone isotopic composition : an angular effect in scattering processes? *Annales Geophysicae*, 19 :229–244, 2001.

[69] K. Mauersberger, B. Erbacher, D. Krankowsky, J. Günther, and R. Nickel. Ozone isotope enrichment : isotopomer-specific rate coefficients. *Science*, 283 :370–372, 1999.

[70] Y.Q. Gao and R.A. Marcus. Strange and unconventional isotope effects in ozone formation. *Science*, 293 :259–263, 2001.

[71] P.W. Merrill. Spectroscopic observations of stars of calss S. *The Astrophysical Journal*, 116 :21–26, 1952.

[72] E.M. Burbidge, G.R. Burbidge, W.A. Fowler, and F. Hoyle. Synthesis of the elements in stars. *Reviews of Modern Physics*, 29 :547–650, 1957.

[73] A.G.W. Cameron. Nuclear reactions in stars and nucleogenesis. *Publications of the Astronomical Society of the Pacific*, 69 :201–222, 1957.

[74] S.J. Little, I.R. Little-Marenin, and W.H. Bauer. Additional late-type stars with technetium. *The Astronomical Journal*, 94 :981–990, 1987.

[75] V.V. Smith and D.L. Lambert. s-process-enriched cool stars with and without technetium : clues to asymptotic giant branch and binary star evolution. *The Astrophysical Journal*, 333 :219–226, 1988.

[76] J.A. Brown, V.V. Smith, D.L. Lambert, E. Dutchover, Jr., K.H. Hinkle, and H.R. Johnson. S stars without technetium : the binary star connection. *The Astronomical Journal*, 99 :1930–1940, 1990.

[77] S. Van Eck and A. Jorissen. The Henize sample of S stars. I. The technetium dichotomy. *Astronomy and Astrophysics*, 345 :127–136, 1999.

[78] P.A. Seeger, W.A. Fowler, and D.D. Clayton. Nucleosynthesis of heavy elements by neutron capture. *The Astrophysical Journal Supplement Series*, 11 :121–166, 1965.

[79] F. Käppeler, H. Beer, and K. Wisshak. s-process nucleosynthesis-nuclear physics and the classical model. *Reports on Progess in Physics*, 52 :945–1013, 1989.

[80] B.E.J. Pagel. *Nucleosynthesis and Chemical Evolution of Galaxies.* Cambridge University Press, Cambridge, 1997.

[81] D.D. Clayton. Galactic Chemical Evolution and Nucleocosmochronology : a standard model. In W.D. Arnett and J.W. Truran, editors, *Nucleosynthesis, Challenges and New Developments*, pages 65–88. The University of Chicago Press, Chicago, 1985.

[82] D.D. Clayton. Nuclear cosmochronology within analytic models of the chemical evolution of the solar neighbourhood. *Monthly Notices of the Royal Astronomical Society*, 234 :1–36, 1988.

[83] F.-K. Thielemann, P. Hauser, E. Kolbe, G. Martinez-Pinedo, T. Rauscher, K.-L. Kratz, B. Pfeiffer, S. Rosswog, M. Liebendörfer, and A. Mezzacappa. Heavy elements and age determinations. *Space Science Reviews, in press*, 2001.

[84] G.J. Wasserburg, M. Busso, and R. Gallino. Abundances of actinides and short-lived nonactinides in the interstellar medium : diverse supernova sources for the r-process. *The Astrophysical Journal*, 466 :L109–L113, 1996.

[85] Y.-Z. Qian, P. Vogel, and G.J. Wasserburg. Diverse supernova sources for the r-process. *The Astrophysical Journal*, 494 :285–296, 1998.

[86] J.W. Truran and A.G.W. Cameron. The p-process in explosive nucleosynthesis. *The Astrophysical Journal*, 171 :89–92, 1972.

[87] J. Audouze and J.W. Truran. p-process nucleosynthesis in postshock supernova envelope environments. *The Astrophysical Journal*, 202 :204–213, 1975.

[88] S.E. Woosley and W.M. Howard. The p-process in supernovae. *The Astrophysical Journal Supplement Series*, 36 :285–304, 1978.

[89] N. Prantzos, M. Hashimoto, M. Rayet, and M. Arnould. The p-process in SN 1987A. *Astronomy and Astrophysics*, 238 :455–461, 1990.

[90] W.M. Howard, B.S. Meyer, and S.E. Woosley. A new site for the astrophysical gamma-process. *The Astrophysical Journal*, 373 :L5–L8, 1991.

[91] S.E. Woosley and W.M. Howard. ^{146}Sm production by the gamma-process. *The Astrophysical Journal*, 354 :L21–L24, 1990.

[92] M. Rayet, N. Prantzos, and M. Arnould. The p-process revisited. *Astronomy and Astrophysics*, 227 :271–281, 1990.

[93] D.L. Lambert. The p-nuclei : abundances and origins. *The Astronomy and Astrophysics Review*, 3 :201–256, 1992.

[94] M. Rayet, M. Arnould, M. Hashimoto, N. Prantzos, and K. Nomoto. The p-process in type II supernovae. *Astronomy and Astrophysics*, 298 :517–527, 1995.

[95] V. Costa, M. Rayet, R.A. Zappalà, and M. Arnould. The synthesis of the light Mo and Ru isotopes : how now, no need for an exotic solution? *Astronomy and Astrophysics*, 358 :L67–L70, 2000.

[96] H. Schatz, L. Bildsten, A. Cumming, and M. Wiescher. The rapid proton process ashes from stable nuclear burning on an accreting neutron star. *The Astrophysical Journal*, 524 :1014–1029, 1999.

[97] H. Schatz, A. Aprahamian, V. Barnard, L. Bildsten, A. Cumming, M. Ouellette, T. Rauscher, F.-K. Thielemann, and M. Wiescher. The endpoint oft the rp process on accreting neutron stars. *Physical Review Letters*, 86 :3471–3474, 2001.

[98] T.J. Bernatowicz and E. Zinner, editors. *CP402, Astrophysical Implications of the Laboratory Study of Presolar Materials*. AIP, Woodbury, 1997.

[99] G.R. Huss. The survival of presolar grains in solar system bodies. In T.J. Bernatowicz and E. Zinner, editors, *CP402, Astrophysical Implications of the Laboratory Study of Presolar Materials*, pages 721–748. AIP, Woodbury, 1997.

[100] L.R. Nittler, C.M.O. Alexander, X. Gao, R.M. Walker, and E.K. Zinner. Interstellar oxide grains from the Tieschitz ordinary chondrite. *Nature*, 370 :443–446, 1994.

[101] L.R. Nittler, P. Hoppe, C.M.O. Alexander, S. Amari, P. Eberhardt, X. Gao, R.S. Lewis, R. Strebel, R.M. Walker, and E. Zinner. Silicon nitride from supernovae. *The Astrophysical Journal*, 453 :L25–L28, 1995.

[102] B.S. Meyer, D.D. Clayton, and L.-S. The. Molybdenum and zirconium isotopes from a supernova neutron burst. *The Astrophysical Journal, submitted*, 2001.

[103] A. Shukolyukov and G.W. Lugmair. Isotopic evidence for the Cretaceous-Tertiary impactor and its type. *Science*, 282 :927–929, 1998.

[104] F.A. Podosek, R.H. Nichols, Jr., J.C. Brannon, and J.R. Dougherty. Cr isotopic analyses of undifferentiated meteorites. *Lunar and Planetary Science*, XXX :#1307, 1999.

[105] A. Shukolyukov and G.W. Lugmair. Cr isotopic systematics in the pallasite Eagle Station : chronology and evidence for a genetic link to carbonaceous chondrites. *Lunar and Planetary Science*, XXXII :#1365, 2001.

[106] M. Javoy, F. Pineau, and H. Delorme. Carbon and nitrogen isotopes in the mantle. *Chemical Geology*, 57 :41–62, 1986.

[107] M. Javoy. The birth of the Earth's atmosphere : the behaviour and fate of its major elements. *Chemical Geology*, 147 :11–25, 1998.

[108] M. Javoy. The major volatile elements of the Earth : their origin, behavior, and fate. *Geophysical Research Letters*, 24 :177–180, 1997.

[109] M. Javoy. The integral enstatite chondrite model of the earth. *Geophysical Research Letters*, 22 :2219–2222, 1995.

[110] M. Javoy. Chemical earth models. *Comptes Rendus de l'Académie des Sciences*, 329 :537–555, 1999.

[111] D.-C. Lee and A.N. Halliday. Accretion of primitive planetesimals : Hf-W isotopic evidence from enstatite chondrites. *Science*, 288 :1629–1631, 2000.

[112] M. Rotaru, J.-L. Birck, and C.J. Allègre. Clues to early solar system history from chromium isotopes in carbonaceous chondrites. *Nature*, 358 :465–470, 1992.

[113] F.A. Podosek, Jr. R.H. Nichols, J.C. Brannon, B.S. Meyer, U. Ott, C.L. Jennings, and N. Luo. Potassium, stardust, and the last supernova. *Geochimica et Cosmochimica Acta*, 63 :2351–2362, 1999.

[114] A.G.W. Cameron and J.W. Truran. The supernova trigger for formation of the solar system. *Icarus*, 30 :447–461, 1977.

[115] A.G.W. Cameron. The first ten million years in the solar nebula. *Meteoritics*, 30 :133–161, 1995.

[116] A.G.W. Cameron, H. Vanhala, and P. Höflich. Some aspects of triggered star formation. In T.J. Bernatowicz and E. Zinner, editors, *CP402, Astrophysical Implications of the Laboratory Study of Presolar Materials*, pages 665–693. AIP, Woodbury, 1997.

[117] A.G.W. Cameron. Extinct radioactivities and the r-process jet. *Lunar and Planetary Science*, XXXII :#1035, 2001.

[118] K.D. McKeegan, M. Chaussidon, and F. Robert. Incorporation of short-lived ^{10}Be in a calcium-aluminum-rich inclusion from the Allende meteorite. *Science*, 289 :1334–1337, 2000.

[119] M. Gounelle, F.H. Shu, H. Shang, A.E. Glassgold, K.E. Rehm, and T. Lee. Extinct radioactivities and protosolar cosmic rays : self-shielding and light elements. *The Astrophysical Journal*, 548 :1051–1070, 2001.

[120] B.M. Tinsley. Nucleochronology and chemical evolution. *The Astrophysical Journal*, 198 :145–150, 1975.

[121] S. van den Bergh. The frequency of stars with different metal abundances. *The Astronomical Journal*, 67 :486–490, 1962.

[122] M. Schmidt. The rate of star formation. II. The rate of formation of stars of different mass. *The Astrophysical Journal*, 137 :758–769, 1963.

[123] M. Haywood. A revision of the solar neighbourhood metallicity distribution. *Monthly Notices of the Royal Astronomical Society*, 325 :1365–1382, 2001.

[124] B.P. Wakker, J.C. Howk, B.D. Savage, H. van Woerden, S.L. Tufte, U.J. Schwarz, R. Benjamin, R.J. Reynolds, R.F. Peletier, and P.M.W. Kalberla. Accretion of low-metallicity gas by the Milky Way. *Nature*, 402 :388–390, 1999.

[125] M. Schmidt. The rate of star formation. *The Astrophysical Journal*, 129 :243–258, 1959.

[126] J.P.E. Gerritsen and V. Icke. Star formation in N-body simulations. I. The impact of the stellar ultraviolet radiation on star formation. *Astronomy and Astrophysics*, 325 :972–986, 1997.

[127] Jr. R.C. Kennicutt. The global Schmidt law in star-forming galaxies. *The Astrophysical Journal*, 498 :541–552, 1998.

[128] H. Becker and R.J. Walker. The ^{98}Tc $-^{98}$ Ru and ^{99}Tc $-^{99}$ Ru chronometers : new results on iron meteorites and terrestrial Ru. *V.M. Goldschmidt Conference*, XI :#3047, 2001.

[129] Q.Z. Yin, S.B. Jacobsen, W.F. McDonough, I. Horn, M.I. Petaev, and J. Zipfel. Supernova sources and the ^{92}Nb $-^{92}$ Zr p-process chronometer. *The Astrophysical Journal*, 536 :L49–L53, 2000.

[130] C. Sanloup, J. Blichert-Toft, P. Télouk, P. Gillet, and F. Albarède. Zr isotope anomalies in chondrites and the presence of ^{92}Nb in the early solar system. *Earth and Planetary Science Letters*, 184 :75–81, 2000.

[131] C. Münker, S. Weyer, K. Mezger, M. Rehkämper, F. Wombacher, and A. Bischoff. ^{92}Nb $-^{92}$ Zr and the early differentiation history of planetary bodies. *Science*, 289 :1538–1542, 2000.

[132] Jr. C.L. Harper. Evidence for ^{92g}Nb in the early solar system and evaluation of a new p-process cosmochronometer from ^{92}Nb/^{92}Mo. *Science*, 222 :1015–1018, 1983.

[133] T. Hirata. Determination of Zr isotopic composition and U-Pb ages for terrestrial and extraterrestrial Zr-bearing minerals using laser ablation-inductively coupled plasma mass spectrometry : implications for Nb-Zr isotopic systematics. *Chemical Geology*, 176 :323–342, 2001.

[134] M. Schönbächler, M. Rehkämper, A.N. Halliday, D.-C. Lee, B. Zanda, M. Bourot-Denise, B. Hattendorf, and D. Günther. The initial ^{92}Nb/^{93}Nb of the solar system. *Meteoritics and Planetary Science*, 36 :A184–A185, 2001.

[135] A. Prinzhofer, D.A. Papanastassiou, and G.J. Wasserburg. The presence of ^{146}Sm in the early solar system and implications for its nucleosynthesis. *The Astrophysical Journal*, 344 :L81–L84, 1989.

[136] A. Prinzhofer, D.A. Papanastassiou, and G.J. Wasserburg. Samarium-neodymium evolution of meteorites. *Geochimica et Cosmochimica Acta*, 56 :797–815, 1992.

[137] G.W. Lugmair and K. Marti. Sm-Nd-Pu timepieces in the Angra dos Reis meteorite. *Earth and Planetary Science Letters*, 35 :273–284, 1977.

[138] L.E. Nyquist, B. Bansal, H. Wiesmann, and C.-Y. Shih. Neodymium, strontium and chromium isotopic studies of the LEW86010 and Angre dos Reis meteorites and the chronology of the angrite parent body. *Meteoritics*, 29 :872–885, 1994.

[139] S.B. Jacobsen and G.J. Wasserburg. Sm-Nd isotopic evolution of chondrites and achondrites, II. *Earth and Planetary Science Letters*, 67 :137–150, 1984.

[140] G.W. Lugmair and S.J.G. Galer. Age and isotopic relationships among the angrites Lewis Cliff 86010 and Angra dos Reis. *Geochimica et Cosmochimica Acta*, 56 :1673–1694, 1992.

[141] G.W. Lugmair, T. Shimamura, R.S. Lewis, and E. Anders. Samarium-146 in the early solar system : evidence from neodymium in the Allende meteorite. *Science*, 222 :1015–1018, 1983.

INSTITUT NATIONAL
POLYTECHNIQUE
DE LORRAINE

AUTORISATION DE SOUTENANCE DE THESE
DU DOCTORAT DE L'INSTITUT NATIONAL
POLYTECHNIQUE DE LORRAINE

o0o

VU LES RAPPORTS ETABLIS PAR :
Monsieur BIRCK Jean-Louis, Directeur de Recherche, Institut de Physique du Globe, Paris
Monsieur ROBERT François, Directeur de Recherche, Muséum National d'Histoire Naturelle, Paris

Le Président de l'Institut National Polytechnique de Lorraine, autorise :

Monsieur DAUPHAS Nicolas

à soutenir devant un jury de l'INSTITUT NATIONAL POLYTECHNIQUE DE LORRAINE, une thèse intitulée :

"Cosmochimie isotopique du molybdène"

en vue de l'obtention du titre de :

DOCTEUR DE L'INSTITUT NATIONAL POLYTECHNIQUE DE LORRAINE

Spécialité : « **Géosciences** »

NANCY BRABOIS
2, AVENUE DE LA
FORET-DE-HAYE
BOITE POSTALE 3
F - 5 4 5 0 1
VANDŒUVRE CEDEX

Fait à Vandoeuvre, le 10 janvier 2002
Le Président de l'I.N.P.L.,
L. SCHUFFENECKER

INSTITUT NATIONAL POLYTECHNIQUE DE LORRAINE - NANCY -

TEL. 33/03.83.59.59.59
FAX. 33/03.83.59.59.55

Résumé

Le système solaire est le résultat d'une maturation lente et complexe de la matière. La composition isotopique du molybdène mesurée dans des objets extraterrestres enregistre l'action des phénomènes qui ont contribué à la mise en place et au développement du système planétaire qui nous abrite. (*i*) Aucun fractionnement de masse n'est observé dans les météorites différenciées et primitives. (*ii*) Aucune preuve de la présence du radionucléide technétium-97 dans le système solaire n'est trouvée (^{97}Tc/^{98}Ru $< 4 \times 10^{-4}$). Ce résultat est cohérent avec l'abondance attendue dans le cas d'une nucléosynthèse des *p*-radionucléides éteints dans les supernovae de type II et un modèle d'évolution chimique ouvert non linéaire de la Galaxie. (*iii*) Des anomalies nucléosynthétiques héritées sont observées dans des objets différenciés et des fractions lessivées de météorites primitives. Deux pôles sont ainsi identifiés. Le spectre Mo-m est porté par des grains circumstellaires de carbure de silicium et est enrichi en produits du processus *s* tandis que le spectre Mo-w représente la signature homogène de la nébuleuse protosolaire et est appauvri en produits du processus *s*. La présence d'anomalies nucléosynthétiques à une échelle mégascopique permet de discuter les filiations entre corps planétaires et permet également d'étudier la distribution spatiale des grains circumstellaires dans la nébuleuse.

Mots-clés: Molybdène, isotopes, anomalies nucléosynthétiques, relations génétiques, grains circumstellaires, nucléosynthèse stellaire, technétium-97, radioactivités éteintes, évolution chimique de la Galaxie.

Abstract

The solar system represents the end-product of a complex and slow maturation of matter. The molybdenum isotopic composition measured in extraterrestrial samples bears information on the events that contributed to shaping the solar system we live in. (*i*) No mass fractionation is observed in primitive or differentiated meteorites. (*ii*) No evidence for the presence of live ^{97}Tc in the nascent solar system is found (^{97}Tc/^{98}Ru $< 4 \times 10^{-4}$). This result is consistent with the low ^{97}Tc abundance expected from production of extinct *p*-radionuclides in type II supernovae and chemical evolution of the Galaxy incorporating infall and non-linearity. (*iii*) Inherited nucleosynthetic anomalies are observed in both differentiated meteorites and leachate fractions of primitive chondrites. Thus, two nucleosynthetic poles are identified. The Mo-m spectrum is hosted by circumstellar carbide grains and is characterized by an enrichment in *s*-nuclides while the Mo-w spectrum represents the ambient isotopic signature of the nebula and is characterized by a deficit in *s*-nuclides. The presence of molybdenum nucleosynthetic anomalies at macroscopic scale is then used in order to discuss the genetic relationships between planetary bodies and investigate the spatial distribution of circumstellar dust in the nebula.

Keywords: Molybdenum, isotopes, nucleosynthetic anomalies, genetic relationships, circumstellar grains, stellar nucleosynthesis, technetium-97, extinct radionuclides, chemical evolution of the Galaxy.